UNIVERSITY OF CALIFORNIA
RIVERSIDE

Insights Into Predicting Secondary Organic Aerosol Formation from Anthropogenic Volatile Organic Compounds: Impact of Molecular Structure and NO_x Concentration

A Dissertation submitted in partial satisfaction
of the requirements for the degree of

Doctor of Philosophy

in

Chemical and Environmental Engineering

by

Lijie Li

June 2016

Dissertation Committee:
Dr. David R. Cocker III, Chairperson
Dr. Akua Asa-Awuku.
Dr. Roya Bahreini

The Dissertation of Lijie Li is approved:

Committee Chairperson

University of California, Riverside

Acknowledgements

I would like to express my sincere gratitude to many people for helping me along the road to obtaining my Ph.D. Without the people mentioned here, this dissertation would not be possible. I wish I had space in this dissertation to thank everyone. However, in order to finish my dissertation in the end of this quarter, I'd like to highlight the people who have had the greatest impact.

First and foremost, I owe a tremendous debt of gratitude to my academic advisor, Prefoessor David Cocker. He brings me to the atmospheric science world and provides me millions of opportunity to develop myself. His positive attitude and bright ideas inspired me to step forward on research and reveal the big picture of certain findings instead of stucking in trivial details. He always squezzed in some time out from his busy schedule when I need his advice on my research. He always tried to find time to talk to me on my paper and presentations and taught me how to better deliver my idea. He taught me things more than science, which are critical to my development as a scientist. I am extremely fortunate to have him as my mentor. I believe what I learned from him will be an invaluable treasure for my life.

I am very glad to be part of the chamber team and work together with many wonderful people. I would like to thank Dr. Ping Tang for training me patiently on how to operate the chamber facilities. I feel grateful to have the opportunity to continue the aromatic hydrocarbon work in the APL lab team after Dr. Ping Tang, Dr. Li Qi and Dr. Shunsuke

Nakao. I will not have that many accomplishments on SOA formation from aromatic hydrocarbons without the efforts from these former graduate students. I worked most closely with Dr. Chia-Li (Candice) Chen, Dr. Derek Price and Mary Kacarab over the past five years and learned a lot hands-on skills from them. I learned many techniques on instrument troubleshooting and maintenance by working together with Candice. Her kindness and patience makes me efficiently learn more about these state-of-art instruments. Derek is really helpful when I worked with the Selected Ion Flow Tube Mass Spectrometry (SIFT) and the continuous gas injection system of chamber. It is nice to work shoulder to shoulder with Mary for five years and we made great progress together to prepare ourselves to be better scientist. I am infectious by her responsibility to the lab and positive attitude toward research. Thanks also go out to to the youger APL chamber team members including Weihua Li, Paul Van Rooy, Xinze Peng and Weihan Peng, who aided in serveral final experiments.

I would also like to thank Dr. William Carter and Dr. Gookyoung Heo, who helped me on the SAPRC modeling. I enjoyed my discussion with these senior chemists to provide me important perspectives on kinetics and radical concentrations. I would like to thank my first year graduate advisor Dr. Sharon Walker. She is very helpful at the beginning of my graduate school by providing me opportunity to enhance myself. She made me feel that I was part of the big family in our department and get used to the new life here smoothly.

I am grateful to my committee members my advisory committee Dr. Akua Asa-Awuku and Dr. Roya Bahreini for their advice on my research. Dr. Xin Ge and Dr. Haizhou Liu gave me valuable comments during my proposal defense. In addition, thanks should be given to W.M. Keck Foundation, National Science Foundation, UCR- Department of Chemical and Environmental Engineering, California Air Resources Board, and William R. Pierson/Ford Graduate.

It was the help and love from my family and friend that make this dissertation a reality. Thanks Mom and Dad, who are always with me, support me and encourage me. Thanks grandma, who taught me independence and strongwill. She will always be in my heart and my memories of her will always be cherished. Thanks my friend Hua Peng and Chen Lin for providing statistician's point of view, especially when I analyze my data. I feel relaxed to hang out with you, movie, bowling, skiing, barbecue, dinner……. To my loved fiancé, Xiao (Eric), I should not be here writing the acknowledgement without your accompany all the way along. You gave more than joy and happiness to my life. You listened to me and tolerate everything of mine. You encouraged me when I failed in my experiements and spiritually assisted me to make progress on reaserch. Thanks for all the valuabe suggestions you gave to my work and life. Thanks for always be with me. I love you.

The text of this dissertation, in part, is a reprint of the material as is appears in Li et al. (Environ. Sci. Technol., doi: 10.1021/acs.est.5b05778, 2016), Li et al. (Atmos. Chem. Phys., 16, 2255-2272, 2016), Li et al. (Atmos. Chem. Phys. Discuss, doi:10.5194/acp-

2015-871, 2016), and Li et al. (Atmos. Environ. 119, 2015). The co-author listed in that publication directed and supervised the research which forms the basis for this dissertation.

ABSTRACT OF THE DISSERTATION

Insights Into Predicting Secondary Organic Aerosol Formation from Anthropogenic Volatile Organic Compounds: Impact of Molecular Structure and NO_x Concentration

by

Lijie Li

Doctor of Philosophy, Graduate Program in Chemical and Environmental Engineering
University of California, Riverside, June 2016
Dr. David R. Cocker, Chairperson

Understanding secondary organic aerosol (SOA) formation is of critical importance to public health and global climate. SOA formation from anthropogenic volatile organic compounds (VOCs) is influenced by NO, precursor molecular structure, oxidation conditions and other factors. This dissertation explores the impact of NO effect and molecular structure for two categories of VOCs at urban atmosphere relevant conditions by utilizing the state of art 90 m^3 UCR/CE-CERT chamber facilities.

Monocyclic aromatic hydrocarbons are the dominant anthropogenic SOA precursor in urban areas. The impact of instantaneous NO_x source is demonstrated by data mining of *m*-xylene photooxidation experiments, developing of new reaction scenario and SAPRC model prediction. The relationship of SOA growth rate to NO_2/NO ratio, instantaneous HC/NO, absolute NO concentration, peroxy radical reaction branching ratio and hydroxyl radical concentration are illustrated. It is found that NO at sub-ppb

level enhances ·OH formation by increasing HO_2· and RO_2· and therefore promotes SOA formation. Further, innovative SOA composition analysis methods normalizing aerosol yield and chemical composition on an aromatic ring basis are developed and utilized to explore aerosol formation from oxidation of 17 aromatic hydrocarbons. The yield normalization process demonstrates that the aromatic ring is a more significant driver of aerosol formation than alkyl substitute structure. More important, four oxygens per aromatic ring are observed in SOA chemical composition, regardless of the alkyl substitutes attached to the ring. The investigation on SOA formation from aromatic hydrocarbons provides new perspective on the complicated aromatic oxidation mechanisms.

Glycol ethers, from consumer products, are newly identified as SOA precursors in this dissertation. The impact of molecular structure on SOA formation from glycol ethers and relative ethers is investigated. The presence and location of –OH are found to be an important structure in ether precursor to SOA formation. Products with cyclic structure are observed in both gas and particle phase during the oxidation of ethers containing –OH. Further, intermolecular cyclization pathway is considered to determine SOA formation during ether oxidation, especially under atmospherically relevant NO_x conditions.

Table of Contents

List of Tables

List of Figures

1. Introduction

1.1 Introduction of Dissertation

An aerosol is defined as a suspension of liquid or solid particles in a gas, with particle diameters in the range of 10^{-9}-10^{-4} m (Seinfeld and Pandis, 2006). Atmospheric aerosols are of central importance for climate change (IPCC 2013), human health (Davidson, et al., 2005; Pöschl, 2005; Pope and Dockery, 2006; Brook, et al., 2010; Shiraiwa, et al., 2012; Pöschl and Shiraiwa, 2015) and visibility degradation (Cao, et al., 2012; Lin, et al., 2014). Organic aerosols (OA), which include primary OA (POA) and secondary OA (SOA), account for 20% - 90% of aerosol mass in the lower troposphere (Kanakidou, et al., 2005). OA emitted directly from sources are POA; while OA formed from oxidative processing of volatile organic compounds (VOCs), followed by gas-to-particle conversion are referred to as SOA. Approximately 70% of OA are SOA according to field observation and global model prediction (Lim and Turpin, 2002; Zhang, et al., 2005; Sullivan, et al., 2006; Lanz, et al., 2007; Hallquist, et al., 2009). SOA from biogenic sources is considered to dominate global SOA formation (Tsigaridis and Kanakidou, 2003; Hallquist, et al., 2009; Monks, et al., 2009). However, anthropogenic SOA is underestimated in current models by a factor up to 10 (Volkamer, et al. 2006; Matsui, et al., 2009; Woody et al. 2016) and is recently found to be more important to the global scale SOA budget than earlier model prediction (Henze, et al., 2008; De Gouw, et al. 2008; Farina, et al., 2010; Heald, et al., 2011; Spracklen, et al., 2011). An improvement in SOA prediction can be achieved by a further understanding of SOA formation mechanisms and a more comprehensive inventory of SOA precursors.

Traditional SOA yield is defined as a mass fraction of SOA formed per hydrocarbon reacted (Odum, et al., 1996). SOA yield, a fundamental input to SOA model prediction, is a function of multiple parameters such as gas phase components (e.g., NO_x concentration (Song, et al., 2005; Presto, et al., 2005; Ng, et al., 2007; Loza , et al., 2014; Xu, et al., 2014), ·OH exposure (Kang, et al., 2011; Henry and Donahue, 2012; Lambe, et al., 2015), coexisting VOC interaction effect (Huff Hartz, et al., 2007; Jaoui, et al., 2008; Hildebrandt, et al., 2011; Chen and Jang, et al., 2012; Emanuelsson, et al., 2013)), physical conditions (e.g., light intensity (Presto, et al., 2005; Warren, et al., 2008), temperature (Takekawa, et al., 2003; Saathoff, et al., 2009; Qi, et al., 2010; Denjean, et al., 2015), humidity (Warren, et al., 2009; Healy, et al., 2009; Zhang, et al, 2011; Lewandowski, et al., 2015), cloud processing (Lim, et al., 2010; Lim, et al., 2013; McNeill, et al., 2015) and mixing state (Asa-Awuku, et al., 2009; Gordon, et al., 2016; Ye, et al., 2016)) and chamber wall loss correction methods (e.g., particle (Cocker, et al., 2001) and gas phase product wall loss correction (Zhang, et al., 2014, 2015; La, et al., 2016)). There is an ongoing discussion on the importance of oligomerization (Gao, et al., 2004; Tolocka, et al., 2004; Kalberer, et al., 2004; Gross, et al., 2006; Sadezky, et al., 2008; Trump and Donahue, 2014) and small molecular VOCs uptake (Jang, et al., 2002; Kroll, et al., 2005; Liggio, et al., 2005; Nakao, et al., 2012;) to SOA formation. An increasing number of SOA components are identified with improvement in instrumentation (Chan, et al., 2013; Timkovsky, et al., 2015; Zhang, et al., 2015; Kroll, 2015) eventually enhancing SOA mechanisms understanding. Unveiling SOA formation mechanisms associated with these parameters improves global or regional models.

NO is an important anthropogenic emission (Aneja, et al., 2001; Jaeglé, et al., 2005; Seinfeld and Pandis, 2006) and strongly influences SOA formation mechanisms. Different NO and SOA yield relationships are found among different SOA precursors. SOA yield is found to increase with NO concentration during the oxidation of certain VOCs due to the formation of organic nitrate (eg. sesquiterpenes, longifolene and aromadendrene Ng, et al., 2007). Mostly, NO inhibits SOA formation when the reaction of NO with peroxy radical ($RO_2\cdot$or $HO_2\cdot$) competing with the reaction of $RO_2\cdot$and $HO_2\cdot$ (Kroll and Seinfeld, 2008). A recent study also observed a large enhancement in the heterogeneous oxidation rate of organic aerosols by hydroxyl radicals in the presence of NO (Richards-Henderson, et al., 2015). Aromatic hydrocarbons are major anthropogenic VOCs in urban area (Kanakidou, et al., 2005; Henze, et al., 2008; Derwent, et al., 2010; Freney, et al., 2014). NO is found to suppress SOA formation from aromatic hydrocarbons (Song, et al., 2005; Song, et al., 2007; Ng, et al., 2007). However, the relationship between NO and SOA formation relies on a pulse initial rejection of NO in a batch reactor system in previous studies (Song, et al., 2005; Song, et al., 2007; Ng, et al., 2007, include isoprene, terpene + NO as well). NO_x (NO and NO_2) is continuously emitted into atmosphere, especially in urban areas (Rattigan et al., 2010). It is valuable to a comprehensively understand of the impact of NO on SOA formation by investigating instantaneous NO_x impact on SOA formation.

Molecular structure of VOCs determines the oxidation mechanism of VOCs and therefore affects SOA formation from VOCs. Previous studies have observed increasing SOA yields from OH initiated alkane and alkene reactions as carbon chain length

increases and branched structure decreases (Lim and Ziemann, 2009; Matsunaga et al., 2009; Tkacik et al., 2012; Loza, et al., 2014). Also, the presence of cyclization in the parent alkane structure is found to increase SOA yields (Lim and Ziemann, 2009; Loza, et al., 2014). SOA yield from aromatics is found to decrease with the number of carbons by adding methyl groups to the aromatic ring (Odum et al., 1997a; Cocker III et al., 2001b; Sato et al., 2012). However, it is noted that previous studies on SOA formation in the presence of NO_x (e.g. Odum et al., 1997a; Cocker III et al., 2001b; Sato et al., 2012) have been conducted under high NO_x levels (100 ppb - 2000 ppb). Current NO_x concentration in urban atmosphere is normally below 150 ppb (Dunlea, et al., 2007; Geng, et al., 2008; Rattigan et al., 2010; Gaur, et al., 2014). It is important to explore molecular structure impact on SOA formation under more atmospherically relevant NO_x conditions (<150 ppb).

Gas-particle partitioning theory (Pankow, 1994) is a solid foundation for all current SOA models. The fundamental concept of the theory is that SOA comprises a mixture of semivolatile organic compounds that partition between the gas and particle phases. First, the two-product model, a simplified semi-empirical gas-particle partitioning model, is developed by Odum, et al. (1996) to simulate SOA yield by categorizing all oxidation products into two lumped semi-volatile products according to their gas-article phase partitioning coefficient ($K_{om,1}$ and $K_{om,2}$). Then, Donahue et al.(2006) proposed the volatility basis set (VBS), in which VOC oxidation products are assigned to volatility "bins", which spans across multiple ambient organic effective saturation mass concentrations (C^*). Several models have also been established based on the two product

and/or VBS model by adding tunable parameters that estimate chemical polarity, polymerization, fragmentation, functionalization and elemental ratio (Pankow, et al., 2009; Barsanti, et al., 2011; Donahue, et al.,2012; Cappa, et al., 2012). More complicated models are also developed considering explicit gas and particle phase reaction mechanisms (Aumont, et al., 2005; Valorso, et al,, 2011; Zhang, et al., 2013) and phase state impact (Zuend, et al., 2010; Shiraiwa, et al., 2012). The latest models, as mentioned above, improve the models by adding constraints and parameters. It should be noted that the beauty of the original two-product model is to provide a good estimation in SOA formation by using a simple model, which is fast in calculation and straightforward in physical meaning. A general mechanism summarized on top of complicated detailed mechanism should also be considered and approached to reduce redundant parameters.

More SOA precursors are newly identified to contribute to SOA formation recently. Small molecular VOCs, such as isoprene (Claeys, et al., 2004; Edney, et al., 2005), glyoxal (Volkamer, et al., 2007; Kroll, et al., 2007) and carbonyl species (Jang, et al., 2002) are found to contribute SOA formation by oxidation, oligomerization and heterogeneous reaction. The contribution of semivolatile compounds (semivolatile VOC (SVOC) or intermediate VOC (IVOC)) has been found in recent studies (Robinson, et al., 2007; Presto, et al., 2009; Chan, et al., 2009; Pye, et al., 2010). It is necessary to explore more new SOA precursors besides the well-known sources (e.g. engine exhaust, fuel evaporation, biomass burning and cooking), especially with with the availability of more advanced techniques and instruments (Goldstein and Galbally, 2007).

This study integrates state-of-the-art chamber facilities with unique analysis methods to provide insights into SOA formation form anthropogenic VOCs including aromatic hydrocarbons and glycol ethers. Sub-ppb NO effects on SOA formation from aromatic hydrocarbons is explored by data mining classic environmental chamber studies and was verified by developing advanced reaction scenarios simulating continuous NO_x in urban areas. The role of molecular structure on SOA formation from aromatic hydrocarbons is comprehensively investigated according to the SOA yield and elemental ratio trend of aromatic hydrocarbons. Alkyl substitute dilution conjecture is proposed to demonstrate the contribution of alkyl substitute SOA composition. Novel approaches developed on aromatic ring basis successfully unify SOA yield and chemical composition among all aromatic hydrocarbons. A much higher extent of oxidation in aromatic ring carbon than that of alkyl substitute is further explored by isotope labeled aromatic hydrocarbon photooxidation. This suggests that aromatic ring is a driving force for SOA formation from aromatic hydrocarbons. Moreover, the importance of cyclization to SOA formation from glycol ethers is demonstrated by scrutinizing gas phase and particle phase mass spectrum.

Chapter 2 advances the understating of NO impact on SOA formation from aromatic hydrocarbons. The relationship between SOA growth rate with the concentrations of NO, NO_2, precursor and radical is illustrated. Enhanced SOA formation is observed when low NO levels (<1 ppb) are artificially maintained by continuous or step-wise injection. This chapter implies that SOA yields from aromatic hydrocarbon and low NO_x photooxidation

is previously underestimated due to the differences between traditional environmental chamber experiments and atmospheric reactivity.

Chapter 3 comprehensively demonstrates the role of methyl group number on SOA formation from aromatic hydrocarbons photooxidation under low NO_x conditions. SOA formation from pentamethylbenzene and hexamethylbenzene are reported for the first time. A decreasing SOA yield with increasing number of methyl groups is observed. Linear trends are found in both f_{44} vs. f_{43} and O/C vs. H/C for SOA from aromatic hydrocarbons with zero to six methyl groups. Methyl group dilution theory is proposed to explain the role of methyl group in SOA formation form aromatic hydrocarbons. This chapter suggests that, as more methyl groups are attached on the aromatic ring, SOA products from these aromatic hydrocarbons become less oxidized per mass/carbon on the basis of SOA yield or chemical composition.

Chapter 4 extends the impact of molecular structure on SOA formation from aromatic hydrocarbons under low NO_x conditions. Major focus in this chapter is toward the differences in SOA yield and chemical composition among C_8 and C_9 isomers. The ortho position is found to promote aromatic oxidation and therefore SOA formation while the para position suppresses both of them. Meta containing alkyl substitutes are more readily participate into oxidation products with low volatility leading to a slight different SOA chemical composition compared with the ortho and para substituted aromatic hydrocarbon. Further, carbon dilution conjecture is derived based on methyl dilution

theory in Chapter 3 to determine that longer alkyl substitute is more readily oxidized than the methyl substitue.

Chapter 5 provides an innovative perspective on SOA formation from aromatic hydrocarbons. Ring normalized approaches are first developed to evaluate SOA yield and elemental ratio. Ring normalized SOA yields of all aromatic hydrocarbons are similar to SOA mass based yield of benzene. Ring normalized SOA elemental ratio suggests that the bulk SOA chemical composition could be generalized as $C_{6+n}H_{6+2n}O_4$, where n is the number of non-aromatic carbons, during the photooxidation of aromatic hydrocarbons. The key point is that four oxygens per aromatic ring are observed in SOA, regardless of the alkyl substitutes attached to the ring. The normalization of yield and composition to the aromatic ring clearly demonstrate the great significance of aromatic ring carbons compared with alkyl carbon substituents in determining SOA formation and composition.

Chapter 6 further confirms the difference in oxidation between alkyl substitute and aromatic ring carbon during the photooxidation of aromatic hydrocarbons. Methyl carbon labeled aromatic hydrocarbons (($^{13}C_2$) *m*-xylene and ($^{13}C_2$) *p*-xylene) are applied in the aromatic hydrocarbon photooxidation experiment to track the pathway of alkyl substitute oxidation. A larger portion of methyl group carbon is found in gas phase than particle phase as a result of ring opening reactions. Also, carbon in methyl group is observed to be less oxidized in particle phase than aromatic ring carbons. This chapter supports the similarity in the SOA formation from aromatic hydrocarbons regardless of the alkyl substitutes as found in Chapter 5.

Chapter 7 explores SOA formation from newly identified anthropogenic SOA precursor-glycol ethers- representative low vapor pressure-VOC (LVP-VOC) from consumer products. The photooxidation of glycol ethers and ethers with similar molecular structure is investigated under low NO_x and H_2O_2 only conditions. –OH is found to be a critical functional groupto SOA formation from ethers. The formation of cyclic products is observed during the oxidation of several ethers based on gas phase and particle mass spectrometry. It is proposed that the formation of cyclization products during oxidation prevents the cleavage of ether carbon bonds and therefore lowering the volatility of oxidation products leading to an increase in SOA formation. This chapter sheds lights on the SOA formation from missing aerosol precursors.

Chapter 8 summarizes the results of the dissertation studies along with providing suggestion for future research.

1.2 References

Aneja, V. P., Roelle, P. A., Murray, G. C., Southerland, J., Erisman, J. W., Fowler, D., Asman, W. A., and Patni, N.: Atmospheric nitrogen compounds II: emissions, transport, transformation, deposition and assessment, Atmos. Environ., 35(11), 1903-1911, 2001.

Asa-Awuku, A., Miracolo, M. A., Kroll, J. H., Robinson A. L., and Donahue N. M.: Mixing and phase partitioning of primary and secondary organic aerosols, Geophys. Res. Lett., 36(15), 2009.

Aumont, B.; Szopa, S., and Madronich, S.: Modelling the evolution of organic carbon during its gas-phase tropospheric oxidation: development of an explicit model based on a self generating approach, Atmos. Chem. Phys., 5(9), 2497-2517, 2005.

Barsanti, K. C.; Smith, J. N., and Pankow, J. F.: Application of the np+mP modeling approach for simulating secondary organic particulate matter formation from α-pinene oxidation, Atmos. Environ., 45(37), 6812-6819, 2011.

Brook, R. D., Rajagopalan, S., Pope, C. A., Brook, J. R., Bhatnagar, A., Diez-Roux, A. V., Holguin, F., Hong, Y., Luepker, R. V., Mittleman, M. A., Peters. A., Siscovick. D., Smith., S. C., Whitsel, L. and Kaufman, J. D.: Particulate matter air pollution and cardiovascular disease an update to the scientific statement from the American Heart Association, Circulation 121,(21), 2331-2378, 2010.

Cao, J., Wang, Q., Chow, J. C., Watson, J. G., Tie, X., Shen, Z., Wang, P., and An, Z.: Impacts of aerosol compositions on visibility impairment in Xi'an, China, Atmos. Environ., 59, 559-566, 2012.

Cappa, C. D. and K. R. Wilson: Multi-generation gas-phase oxidation, equilibrium partitioning, and the formation and evolution of secondary organic aerosol, Atmos. Chem. Phys., 12, 20, 9505-9528, 2012.

Chan, A. W., Isaacman, G., Wilson, K. R., Worton, D. R., Ruehl, C. R., Nah, T., Gentner, D. R., Dallmann, T. R., Kirchstetter, T. W. and Harley, R. A.: Detailed chemical characterization of unresolved complex mixtures in atmospheric organics: Insights into emission sources, atmospheric processing, and secondary organic aerosol formation, , J. Geophys. Res. Atmos., 118(12), 6783-6796, 2013.

Chan, A. W. H., Kautzman, K. E., Chhabra, P. S., Surratt, J. D., Chan, M. N., Crounse, J. D., Kürten, A., Wennberg, P. O., Flagan, R., and Seinfeld, J. H..: Secondary organic aerosol formation from photooxidation of naphthalene and alkylnaphthalenes: implications for oxidation of intermediate volatility organic compounds (IVOCs), Atmos. Chem. Phys., 9(9): 3049-3060, 2009.

Chen, T. and Jang M.: Secondary organic aerosol formation from photooxidation of a mixture of dimethyl sulfide and isoprene, Atmos. Environ., 46: 271-278, 2012.

Claeys, M., Graham, B., Vas, G., Wang, W., Vermeylen, R., Pashynska, V., Cafmeyer, J., Guyon, P., Andreae, M. O., Artaxo, P., and Maenhaut., W.: Formation of secondary organic aerosols through photooxidation of isoprene, Science, 303, 5661, 1173-1176, 2004.

Cocker III, D. R., Flagan, R. C. and Seinfeld, J. H.: State-of-the-art chamber facility for studying atmospheric aerosol chemistry, Environ. Sci. Technol., 35(12), 2594-2601, 2001a.

Cocker III, D. R., Mader, B. T., Kalberer, M., Flagan, R.C. and Seinfeld, J. H.: The effect of water on gas–particle partitioning of secondary organic aerosol: II. *m*-xylene and 1, 3, 5-trimethylbenzene photooxidation systems, Atmos. Environ., 35(35), 6073-6085, 2001b.

Davidson, C. I., Phalen, R. F., and Solomon, P. A.: Airborne particulate matter and human health: A review, Aerosol Sci. Tech., 39(8), 737-749, 2005.

De Gouw, J. A., Brock, C. A., Atlas, E. L., Bates, T. S., Fehsenfeld, F. C., Goldan, P. D., Holloway, J. S., Kuster, W. C., Lerner, B. M., Matthew, B. M., Middlebrook, A. M., Onasch, T. B., Peltier, R. E., Quinn, P. K., Senff, C. J., Stohl, A., Sullivan, A. P., Trainer, M., Warneke, C., Weber, R. J. andWilliams, E. J.: Sources of particulate matter in the northeastern United States in summer: 1. Direct emissions and secondary formation of organic matter in urban plumes, J. Geophys. Res. Atmos., 113(D8), D08301, 2008.

Denjean, C., Formenti, P., Picquet-Varrault, B., Camredon, M., Pangui, E., Zapf, P., Katrib, Y., Giorio, C., Tapparo, A., Temime-Roussel, B., Monod, A., Aumont1, B., and Doussin., J. F.: Aging of secondary organic aerosol generated from the ozonolysis of α-pinene: effects of ozone, light and temperature, Atmos. Chem. Phys.,15(2), 883-897, 2015.

Derwent, R. G., Jenkin, M. E., Utembe, S. R., Shallcross, D. E., Murrells, T. P., and Passant, N. R.: Secondary organic aerosol formation from a large number of reactive man-made organic compounds. Sci. Total. Environ., 408(16), 3374-3381, 2010.

Donahue, N. M.; Kroll, J.; Pandis, S. N., and Robinson, A. L. A two-dimensional volatility basis set–Part 2: Diagnostics of organic-aerosol evolution. Atmos. Chem. Phys., 12, (2), 615-634, 2012.

Dunlea, E. J., Herndon, S. C., Nelson, D. D., Volkamer, R. M., San Martini, F., Sheehy, P. M., Zahniser, M. S., Shorter, J. H., Wormhoudt J. C., Lamb, B. K., Allwine, E. J., Gaffney, J. S., Marley, N. A., Grutter, M., Marquez, C., Blanco, S., Cardenas, B., Retama, A., Ramos Villegas, C. R., Kolb, C. E., Molina, L. T., and Molina, M. J.:

Evaluation of nitrogen dioxide chemiluminescence monitors in a polluted urban environment, Atmos. Chem. Phys., 7(10), 2691-2704, 2007.

Edney, E. O., Kleindienst, T. E., Jaoui, M., Lewandowski, M., Offenberg, J., Wang, W., and Claeys, M.: Formation of 2-methyl tetrols and 2-methylglyceric acid in secondary organic aerosol from laboratory irradiated isoprene/NO_X/SO_2/air mixtures and their detection in ambient PM 2.5 samples collected in the eastern United States, Atmos. Environ., 39(29), 5281-5289, 2005.

Emanuelsson, E., Hallquist, M., Kristensen, K., Glasius, M., Bohn, B., Fuchs, H., Kammer, B., Kiendler-Scharr, A., Nehr, S. and Rubach, F.: Formation of anthropogenic secondary organic aerosol (SOA) and its influence on biogenic SOA properties, Atmos. Chem. Phys., 13(5), 2837-2855, 2013.

Farina, S. C., Adams, P. J., and Pandis, S. N.: Modeling global secondary organic aerosol formation and processing with the volatility basis set: Implications for anthropogenic secondary organic aerosol. J. Geophys. Res.-Atmos., 115(D9), 2010.

Freney, E. J.; Sellegri, K.; Canonaco, F.; Colomb, A.; Borbon, A.; Michoud, V.; Doussin, J.-F.; Crumeyrolle, S.; Amarouche, N.; Pichon, J.-M. Bourianne, T.; Gomes, L.; Prevot, A. S. H.; Beekmann, M. and Schwarzenböeck, A.: Characterizing the impact of urban emissions on regional aerosol particles: airborne measurements during the MEGAPOLI experiment. Atmos. Chem. Phys., 14, (3), 1397-1412, 2014.

Gao, S., Keywood, M., Ng, N. L., Surratt, J., Varutbangkul, V., Bahreini, R., Flagan, R. C. and Seinfeld, J. H.: Low-molecular-weight and oligomeric components in secondary organic aerosol from the ozonolysis of cycloalkenes and α-pinene, J. Phys. Chem. A, 108(46), 10147-10164, 2004.

Gaur, A., Tripathi, S. N., Kanawade, V. P., Tare, V. and Shukla, S. P.: Four-year measurements of trace gases (SO_2, NO_x, CO, and O_3) at an urban location, Kanpur, in Northern India, J. Atmos. Chem., 71(4), 283-301, 2014.

Geng, F., Tie, X., Xu, J., Zhou, G., Peng, L., Gao, W., Tang, X. and Zhao. C.: Characterizations of ozone, NO_x, and VOCs measured in Shanghai, China, Atmos. Environ., 42(29), 6873-6883, 2008.

Goldstein, A. H. and Galbally I. E.: Known and unexplored organic constituents in the earth's atmosphere, Environ. Sci. Technol., 41(5), 1514-1521, 2007.

Gordon, C. A., Ye, J., and Chan, A. W. H.: Secondary Organic Aerosol Formation Enhanced by Organic Seeds of Similar Polarity at Atmospherically Relative Humidity, STEM Fellowship Journal, 1(2), 6-10, 2016.

Gross, D. S., Gälli, M. E., Kalberer, M., Prevot, A. S., Dommen, J., Alfarra, M. R., Duplissy, J., Gaeggeler, K., Gascho A., Metzger, A., Baltensperger U.: Real-time measurement of oligomeric species in secondary organic aerosol with the aerosol time-of-flight mass spectrometer, Anal. Chem., 78(7), 2130-2137, 2006.

Hallquist, M., Wenger, J. C., Baltensperger, U., Rudich, Y., Simpson, D., Claeys, M., Dommen, J., Donahue, N. M., George, C., Goldstein, A. H., Hamilton, J. F., Herrmann, H., Hoffmann, T., Iinuma, Y., Jang, M., Jenkin, M. E., Jimenez, J. L., Kiendler-Scharr, A., Maenhaut, W., McFiggans, G., Mentel, Th. F., Monod, A., Prévôt, A. S. H., Seinfeld, J. H., Surratt, J. D., Szmigielski, R. and Wildt, J.: The formation, properties and impact of secondary organic aerosol: current and emerging issues, Atmos. Chem. Phys., 9(14), 5155-5236, 2009.

Heald, C. L., Coe, H., Jimenez, J. L., Weber, R. J., Bahreini, R., Middlebrook, A. M., Russell, L. M., Jolleys, M., Fu, T.-M., Allan, J. D., Bower, K. N., Capes, G., Crosier, J., Morgan, W. T., Robinson, N. H., Williams, P. I., Cubison, M. J., DeCarlo, P. F., and Dunlea, E. J.,: Exploring the vertical profile of atmospheric organic aerosol: comparing 17 aircraft field campaigns with a global model, Atmos. Chem. Phys., 11(24), 12673-12696, 2011.

Healy, R. M., Temime, B., Kuprovskyte, K. and Wenger, J. C.: Effect of relative humidity on gas/particle partitioning and aerosol mass yield in the photooxidation of *p*-xylene, Environ. Sci. Technol., 43(6), 1884-1889, 2009.

Henry, K. M. and Donahue, N. M.: Photochemical aging of α-pinene secondary organic aerosol: effects of OH radical sources and photolysis, J. Phys. Chem. A., 116(24): 5932-5940, 2012.

Henze, D. K., Seinfeld, J. H., Ng, N. L., Kroll, J. H., Fu, T-M., Jacob, D. J., Heald, C. L.: Global modeling of secondary organic aerosol formation from aromatic hydrocarbons: high-vs. low-yield pathways, Atmos. Chem. Phys., 8(9), 2405-2421, 2008.

Hildebrandt, L., Henry, K. M., Kroll, J. H., Worsnop, D. R., Pandis, S. N. and Donahue, N. M.: Evaluating the mixing of organic aerosol components using high-resolution aerosol mass spectrometry, Environ. Sci. Technol., 45(15): 6329-6335, 2011.

Huff Hartz, K. E., Weitkamp, E. A., Sage, A. M., Donahue, N. M. and Robinson, A. L.: Laboratory measurements of the oxidation kinetics of organic aerosol mixtures using a relative rate constants approach, J. Geophys. Res. Atmos., 112(D4), 2007.

Intergovernmental Panel on Climate Change (2013), Climate change 2013, in The Physical Science Basis. Contribution of Working Group I to the Fifth Assessment Report of the Intergovernmental Panel on Climate Change, edited by T. F. Stocker et al., Cambridge University Press,Cambridge, U. K., and New York

Jaeglé, L., Steinberger, L., Martin, R. V., and Chance, K.: Global partitioning of NO_x sources using satellite observations: Relative roles of fossil fuel combustion, biomass burning and soil emissions, Faraday. Discuss., 130: 407-423, 2005.

Jang, M., Czoschke, N. M., Lee, S., and Kamens, R. M.: Heterogeneous atmospheric aerosol production by acid-catalyzed particle-phase reactions, Science, 298(5594), 814-817, 2002.

Jaoui, M., Edney, E. O., Kleindienst, T. E., Lewandowski, M., Offenberg, J. H., Surratt, J. D. and Seinfeld, J. H.: Formation of secondary organic aerosol from irradiated α - pinene/toluene/NOx mixtures and the effect of isoprene and sulfur dioxide, J. Geophys. Res. Atmos., 113(D9), 2008.

Kalberer, M., Paulsen, D., Sax, M., Steinbacher, M., Dommen, J., Prevot, A. S. H., Fisseha, R., Weingartner, E., Frankevich, V. and Zenobi, R.: Identification of polymers as major components of atmospheric organic aerosols, Science, 303(5664), 1659-1662, 2004.

Kanakidou, M., Seinfeld, J. H., Pandis, S. N., Barnes, I., Dentener, F. J, Facchini, M. C., Van Dingenen, R., Ervens, B., Nenes, A., Nielsen, C. J., Swietlicki, E., Putaud, J. P., Balkanski, Y., Fuzzi, S., Horth, J., Moortgat, G. K., Winterhalter, R., Myhre, C. E. L., Tsigaridis, K., Vignati, E., Stephanou, E. G., and Wilson, J.: Organic aerosol and global climate modelling: a review, Atmos. Chem. Phys., 5(4), 1053-1123, 2005.

Kang, E., Toohey D. W. and Brune, W. H.: Dependence of SOA oxidation on organic aerosol mass concentration and OH exposure: experimental PAM chamber studies, Atmos. Chem. Phys., 11(4), 1837-1852, 2011.

Kroll, J.: Comprehensive Characterization of Atmospheric Organic Carbon using Multiple High-Resolution Mass Spectrometric Instruments, 2015 AGU Fall Meeting, AGU, 2015.

Kroll, J. H., Chan, A.W. H., Ng, N. L., Flagan, R. C. and Seinfeld, J. H.: Reactions of semivolatile organics and their effects on secondary organic aerosol formation. Environ. Sci. Technol., 41(10), 3545-3550, 2007.

Kroll, J. H., Ng, N. L., Murphy, S. M., Varutbangkul, V., Flagan, R. C. and Seinfeld, J. H.: Chamber studies of secondary organic aerosol growth by reactive uptake of simple carbonyl compounds, J. Geophys. Res. Atmos. (1984–2012), 110(D23), 2005.

Kroll, J. H. and Seinfeld, J. H.: Chemistry of secondary organic aerosol: Formation and evolution of low-volatility organics in the atmosphere, Atmos. Environ., 42(16), 3593-3624, 2008.

La, Y. S., Camredon, M., Ziemann, P. J., Valorso, R., Matsunaga, A., Lannuque, V., Lee-Taylor, J., Hodzic, A., Madronich, S., and Aumont, B.: Impact of chamber wall loss of gaseous organic compounds on secondary organic aerosol formation: explicit modeling of SOA formation from alkane and alkene oxidation, Atmos. Chem. Phys., 16(3), 1417-1431, 2016.

Lambe, A. T., Chhabra, P. S., Onasch, T. B., Brune, W. H., Hunter, J. F., Kroll, J. H., Cummings, M. J., Brogan, J. F., Parmar, Y., Worsnop, D. R., Kolb, C. E., and Davidovits, P.: Effect of oxidant concentration, exposure time, and seed particles on secondary organic aerosol chemical composition and yield, Atmos. Chem. Phys., 15(6), 3063-3075 2015

Lanz, V., Alfarra, M., Baltensperger, U., Buchmann, B., Hueglin, C., and Prévôt, A.: Source apportionment of submicron organic aerosols at an urban site by factor analytical modelling of aerosol mass spectra, Atmos. Chem. Phys., 7(6): 1503-1522, 2007.

Lewandowski, M., Jaoui, M., Offenberg, J. H., Krug, J. D. and Kleindienst, T., Atmospheric oxidation of isoprene and 1, 3-butadiene: influence of aerosol acidity and relative humidity on secondary organic aerosol, Atmos. Chem. Phys., 15(7): 3773-3783, 2015.

Liggio, J., Li, S. M., and McLaren, R.: Reactive uptake of glyoxal by particulate matter, J. Geophys. Res.-Atmos., (1984–2012), 110(D10), 2005.

Lim, H. J. and Turpin, B. J.: Origins of primary and secondary organic aerosol in Atlanta: Results of time-resolved measurements during the Atlanta supersite experiment, Environ. Sci. Technol., 36(21): 4489-4496, 2002.

Lim, Y. B., Tan, Y., Perri, M. J., Seitzinger, S. P., and Turpin, B. J.: Aqueous chemistry and its role in secondary organic aerosol (SOA) formation, Atmos. Chem. Phys., 10, 10521–10539, 2010.

Lim, Y. B., Tan, Y., and Turpin, B. J.: Chemical insights, explicit chemistry, and yields of secondary organic aerosol from OH radical oxidation of methylglyoxal and glyoxal in the aqueous phase, Atmos. Chem. Phys., 13(17), 8651-8667, 2013.

Lim, Y. B. and Ziemann, P. J.: Effects of molecular structure on aerosol yields from OH radical-initiated reactions of linear, branched, and cyclic alkanes in the presence of NO_x, Environ. Sci. Technol., 43(7): 2328-2334, 2009.

Lin, Y., Huang, K., Zhuang, G., Fu, S. J., Wang, Q., Liu, T., Deng, C., and Fu, Q.: A multi-year evolution of aerosol chemistry impacting visibility and haze formation over an Eastern Asia megacity, Shanghai, Atmos. Environ., 92, 76-86, 2014.

Loza, C. L., Craven, J. D., Yee, L. D., Coggon, M. M., Schwantes, R. H., Shiraiwa, M., Zhang, X., Schilling, K. A, Ng, N. L., Canagaratna, M. R., Ziemann, P. J., Flagan, R. C., and Seinfeld, J. H.: Secondary organic aerosol yields of 12-carbon alkanes. Atmos. Chem. Phys., 14(3), 1423-1439, 2014.

Matsui, H., Koike, M., Takegawa, N., Kondo, Y., Griffin, R., Miyazaki, Y., Yokouchi, Y., and Ohara, T.: Secondary organic aerosol formation in urban air: Temporal variations and possible contributions from unidentified hydrocarbons, J. Geophys. Res.-Atmos, 114(D4), D04201, 2009.

Matsunaga, A., Docherty, K. S., Lim, Y. B. and Ziemann, P. J.: Composition and yields of secondary organic aerosol formed from OH radical-initiated reactions of linear alkenes in the presence of NO_x: Modeling and measurements, Atmos. Environ., 43(6), 1349-1357, 2009.

McNeill, V. F.: Aqueous organic chemistry in the atmosphere: Sources and chemical processing of organic aerosols, Environ. Sci. Technol., 49(3): 1237-1244, 2015.

Monks, P. S., Granier, C., Fuzzi, S., Stohl, A., Williams, M. L., Akimoto, H., Amann, M., Baklanov, A., Baltensperger, U., Bey, I., Blake, N., Blake, R. S., Carslaw, K., Cooper, O.R., Dentener, F., Fowler, D., Fragkou, E., Frost, G. J., Generoso, S., Ginoux, P., Grewe, V., Guenther, A., Hansson, H. C., Henne, S., Hjorth, J., Hofzumahaus, A., Huntrieser, H. Isaksen, I. S.,A., Jenkin, M. E., Kaiser, J., Kanakidou, M., Klimont, Z., Kulmala, M., Laj, P. and Lawrence, M.G.: Atmospheric composition change–global and regional air quality, Atmos. Environ., 43(33): 5268-5350, 2009.

Nakao, S., Liu, Y., Tang, P., Chen, C.-L., Zhang, J. and Cocker III, D. R.: Chamber studies of SOA formation from aromatic hydrocarbons: observation of limited glyoxal uptake, Atmos. Chem. Phys., 12(9), 3927-3937, 2012.

Ng, N. L., Chhabra, P. S., Chan, A. W. H., Surratt, J., Kroll, J. H., A. Kwan, McCabe, D. C., Wennberg, P. O., Sorooshian, A., Murphy, S. M., Dalleska, N. F., Flagan, R. C., and J. H. Seinfeld: Effect of NOx level on secondary organic aerosol (SOA) formation from the photooxidation of terpenes, Atmos. Chem. Phys., 7(4): 10131-10177, 2007.

Ng, N. L., Kroll, J. H., Chan, A. W. H., Chhabra, P. S., Flagan, R. C. and Seinfeld, J. H.: Secondary organic aerosol formation from *m*-xylene, toluene, and benzene, Atmos. Chem. Phys., 7(14), 3909-3922, 2007.

Odum, J. R., Hoffmann, T., Bowman, F., Collins, D., Flagan, R. C. and Seinfeld, J. H.: Gas/particle partitioning and secondary organic aerosol yields, Environ. Sci. Technol., 30(8), 2580-2585, 1996.

Odum, J. R., Jungkamp, T., Griffin, R. J., Forstner, H., Flagan, R. C. and Seinfeld, J.H.: Aromatics, reformulated gasoline, and atmospheric organic aerosol formation, Environ. Sci. Technol., 31(7), 1890-1897, 1997.

Pöschl, U.: Atmospheric aerosols: Composition, transformation, climate and health effects, Angew. Chem. Int. Edit., 44(46), 7520-7540, 10.1002/anie.200501122, 2005.

Pankow, J. F., and Barsanti, K. C.: The carbon number-polarity grid: A means to manage the complexity of the mix of organic compounds when modeling atmospheric organic particulate matter, Atmos. Environ., 43, (17), 2829-2835, 2009.

Pope III, C. A. and Dockery, D. W.: Health effects of fine particulate air pollution: lines that connect, J. Air. Waste. Manage., 56(6), 709-742, 2006.

Pöschl, U. and Shiraiwa M: Multiphase Chemistry at the Atmosphere–Biosphere Interface Influencing Climate and Public Health in the Anthropocene, Chem. Rev. 115(10), 4440-4475, 2015.

Presto, A. A., Huff Hartz, K. E. and Donahue, N. M.: Secondary organic aerosol production from terpene ozonolysis. 2. Effect of NOx concentration, Environ. Sci. Technol., 39(18): 7046-7054, 2005.

Presto, A. A., Miracolo, M. A., Kroll, J. H., Worsnop, D. R., Robinson A. L. and Donahue, N. M.: Intermediate-volatility organic compounds: A potential source of ambient oxidized organic aerosol, Environ. Sci. Technol., 43(13), 4744-4749, 2009.

Pye, H. O. and Seinfeld, J. H.: A global perspective on aerosol from low-volatility organic compounds, Atmos. Chem. Phys., 10(9), 4377-4401, 2010.

Qi, L., Nakao, S., Tang, P. and Cocker III, D. R.: Temperature effect on physical and chemical properties of secondary organic aerosol from *m*-xylene photooxidation, Atmos. Chem. Phys., 10(8), 3847-3854, 2010b.

Rattigan, O.V., Dirk Felton, H., Bae, M.-S., Schwab, J.J. and Demerjian, K.L: Multi-year hourly PM2.5 carbon measurements in New York: Diurnal, day of week and seasonal patterns, Atmos. Environ., 44(16), 2043-2053, 2010.

Richards-Henderson, N. K., Goldstein, A. H. and Wilson, K. R.: Large Enhancement in the Heterogeneous Oxidation Rate of Organic Aerosols by Hydroxyl Radicals in the Presence of Nitric Oxide, J. Phys. Chem. Lett., 6(22), 4451-4455, 2015.

Robinson, A. L., Donahue, N. M., Shrivastava, M. K., Weitkamp, E. A., Sage, A. M., Grieshop, A. P., Lane, T. E., Pierce, J. R. and Pandis, S. N.: Rethinking organic aerosols: Semivolatile emissions and photochemical aging, Science, 315(5816), 1259-1262, 2007.

Saathoff, H., Naumann, K.-H., Möhler, O., Jonsson, Å. M., Hallquist, M., Kiendler-Scharr, A., Mentel, T. F., Tillmann, R. and Schurath, U.: Temperature dependence of yields of secondary organic aerosols from the ozonolysis of α-pinene and limonene, Atmos. Chem. Phys., 9(5), 1551-1577, 2009.

Sadezky, A., Winterhalter, R., Kanawati, B., Römpp, A., Spengler, B., Mellouki, A., Le Bras, G., Chaimbault, P. and Moortgat, G.: Oligomer formation during gas-phase ozonolysis of small alkenes and enol ethers: new evidence for the central role of the Criegee Intermediate as oligomer chain unit, Atmos. Chem. Phys., 8(10), 2667-2699, 2008.

Sato, K., Takami, A., Kato, Y., Seta, T., Fujitani, Y., Hikida, T., Shimono, A. and Imamura, T. 2012. AMS and LC/MS analyses of SOA from the photooxidation of benzene and 1, 3, 5-trimethylbenzene in the presence of NO_x: effects of chemical structure on SOA aging, Atmos. Chem. Phys., 12, 4667-4682, 2012.

Seinfeld, J. and Pandis, S.: Atmospheric chemistry and physics: from air pollution to climate change. John Wiley & Sons Publications, Hoboken, New Jersey, US, 2006.

Shiraiwa, M., Pfrang, C., Koop, T. and Pöschl, U.: Kinetic multi-layer model of gas-particle interactions in aerosols and clouds (KM-GAP): linking condensation, evaporation and chemical reactions of organics, oxidants and water, Atmos. Chem. Phys., 12, (5), 2777-2794, 2012.

Shiraiwa, M., Selzle K. and Pöschl U.: Hazardous components and health effects of atmospheric aerosol particles: reactive oxygen species, soot, polycyclic aromatic compounds and allergenic proteins, Free Radical Res., 46(8), 927-939, 2012.

Song, C., Na, K. and Cocker III, D. R.: Impact of the hydrocarbon to NO_x ratio on secondary organic aerosol formation, Environ. Sci. Technol., 39(9), 3143-3149, 2005.

Song, C., Na, K., Warren, B., Malloy, Q. and Cocker III, D. R.: Secondary organic aerosol formation from m-xylene in the absence of NO_x. Environ. Sci. Technol., 41(21), 7409-7416, 2007.

Spracklen, D., Jimenez, J. L., Carslaw, K. S., Worsnop, D. R., Evans, M. J., Mann, G. W., Zhang, Q., Canagaratna, M. R., Allan, J., Coe. H., McFiggans, G. , Rap, A. and Forster P.:Aerosol mass spectrometer constraint on the global secondary organic aerosol budget, Atmos. Chem. Phys., 11(23), 12109-12136, 2011.

Sullivan, A. P., Peltier, R. E., Brock, C. A., De Gouw, J. A., Holloway, J. S., Warneke, C., Wollny A. G., and Weber R. J.: Airborne measurements of carbonaceous aerosol soluble in water over northeastern United States: Method development and an

investigation into water-soluble organic carbon sources, J. Geophys. Res. Atmos., 111(D23), D23S46, 2006.

Takekawa, H., Minoura, H. and Yamazaki, S.: Temperature dependence of secondary organic aerosol formation by photo-oxidation of hydrocarbons, Atmos. Environ., 37(24), 3413-3424, 2003.

Timkovsky, J., Chan, A. W. H., Dorst, T., Goldstein, A. H., Oyama, B. and Holzinger: Comparison of advanced offline and in situ techniques of organic aerosol composition measurement during the CalNex campaign, Atmos. Meas. Tech., 8(12), 5177-5187, 2015

Tkacik, D. S., Presto, A. A., Donahue, N. M. and Robinson, A. L.: Secondary organic aerosol formation from intermediate-volatility organic compounds: cyclic, linear, and branched alkanes, Environ. Sci. Technol., 46(16), 8773-8781, 2012.

Tolocka, M. P., Jang, M., Ginter, J. M., Cox, F. J., Kamens, R. M., and Johnston, M. V.: Formation of oligomers in secondary organic aerosol, Environ. Sci. Technol., 38(5), 1428-1434, 2004.

Trump, E. and Donahue N. M.: Oligomer formation within secondary organic aerosols: equilibrium and dynamic considerations, Atmos. Chem. Phys., 14(7), 3691-3701, 2014.

Tsigaridis, K. and M. Kanakidou: Global modelling of secondary organic aerosol in the troposphere: a sensitivity analysis, Atmos. Chem. Phys., 3(5), 1849-1869, 2003.

Valorso, R., Aumont, B., Camredon, M., Raventos-Duran, T., Mouchel-Vallon, C., Ng, N. L., Seinfeld, J. H., Lee-Taylor, J. and Madronich, S.: Explicit modelling of SOA formation from α-pinene photooxidation: sensitivity to vapour pressure estimation, Atmos. Chem. Phys., 11(14), 6895-6910, 2011.

Volkamer, R., Jimenez, J. L., San Martini, F., Dzepina, K., Zhang, Q., Salcedo, D., Molina, L. T., Worsnop, D. R., and Molina, M. J.: Secondary organic aerosol formation from anthropogenic air pollution: Rapid and higher than expected, Geophys. Res. Lett., 33, (17), L17811, 2006.

Volkamer, R., San Martini, F., Molina, L. T., Salcedo, D., Jimenez, J. L. and Molina, M.J.: A missing sink for gas‐phase glyoxal in Mexico City: Formation of secondary organic aerosol, Geophys. Res. Lett., 34(19), 2007.

Warren, B., Malloy, Q. G., Yee, L. D. and Cocker III, D. R.: Secondary organic aerosol formation from cyclohexene ozonolysis in the presence of water vapor and dissolved salts, Atmos. Environ., 43(10), 1789-1795, 2009.

Warren, B., Song, C. and Cocker III, D. R.: Light intensity and light source influence on secondary organic aerosol formation for the m-xylene/NOx photooxidation system, Environ. Sci. Technol., 42(15), 5461-5466, 2008.

Woody, M. C., K. R. Baker, P. L. Hayes, J. L. Jimenez, B. Koo and H. O. Pye.: Understanding sources of organic aerosol during CalNex-2010 using the CMAQ-VBS, Atmos. Chem. Phys., 16(6), 4081-4100.10, 2016.

Xu, L., Kollman, M. S., Song, C., Shilling, J. E. and Ng, N. L.: Effects of NOx on the volatility of secondary organic aerosol from isoprene photooxidation, Environ. Sci. Technol., 48(4), 2253-2262, 2014.

Ye, J., Gordon C. A., and Chan, A. W. H.: Enhancement in Secondary Organic Aerosol Formation in the Presence of Preexisting Organic Particle, Environ. Sci. Technol., 50 (7), 3572–3579, 2016

Zhang, H., Surratt, J., Lin, Y., Bapat J. and Kamens. R.: Effect of relative humidity on SOA formation from isoprene/NO photooxidation: enhancement of 2-methylglyceric acid and its corresponding oligoesters under dry conditions, Atmos. Chem. Phys., 11(13), 6411-6424, 2011.

Zhang, H., Worton, D. R., Shen, S., Nah, T., Isaacman-VanWertz, G., Wilson, K. R. and A. H. Goldstein: Fundamental Time Scales Governing Organic Aerosol Multiphase Partitioning and Oxidative Aging, Environ. Sci. Technol., 49(16), 9768-9777, 2015.

Zhang, Q., Worsnop, D. R, Canagaratna, M. R., and Jimenez, J. L.: Hydrocarbon-like and oxygenated organic aerosols in Pittsburgh: insights into sources and processes of organic aerosols, Atmos. Chem. Phys., 5, 3289-3311, 2005

Zhang, X., Cappa, C. D., Jathar, S. H., McVay, R. C., Ensberg, J. J., Kleeman, M. J. and Seinfeld, J. H.: Influence of vapor wall loss in laboratory chambers on yields of secondary organic aerosol, Proc. Natl. Acad. Sci. U.S.A. 111(16), 5802-5807, 2014.

Zhang, X., Schwantes, R. H., McVay, R. C., Lignell, H., Coggon, M. M., Flagan, R. C., and Seinfeld, J. H.: Vapor wall deposition in Teflon chambers, Atmos. Chem. Phys., 15(8), 4197-4214, 2015.

Zhang, X. and Seinfeld J. H.: A functional group oxidation model (FGOM) for SOA formation and aging, Atmos. Chem. Phys.,13(12), 5907-5926, 2013.

Zuend, A., Marcolli, C., Peter, T. and Seinfeld, J. H.: Computation of liquid-liquid equilibria and phase stabilities: implications for RH-dependent gas/particle partitioning of organic-inorganic aerosols., Atmos. Chem. Phys., 10, (16), 7795-7820, 2010.

2. Instantaneous nitric oxide effect on secondary organic aerosol formation from *m*-xylene photooxidation

2.1 Introduction

Aromatic hydrocarbons are major anthropogenic SOA precursors (Calvert, et al., 2002; Kanakidou, et al., 2005) contributing upto 50-70% of SOA formation in urban areas (Na, et al., 2004). However, the mechanism of SOA formation from aromatic hydrocarbons is not explicitly understood (Hallquist, et al., 2009; Calvert, et al., 2002). Previous papers report that SOA formation from aromatic hydrocarbon photooxidation is highly sensitive to the nitric oxide (NO) level during environmental chamber simulations (e.g., Hurley et al., 2001; Johnson et al., 2005; Martín-Reviejo and Wirtz, 2005; Song et al., 2005). Previous chamber studies demonstrate that higher initial NO_x concentration lowers aromatic SOA yields (Song, et al., 2005; Ng, et al., 2007).

It is generally accepted that the NO concentration determines the branching ratio of peroxy radical ($RO_2\cdot$) reaction with NO and the hydroxperoxy radical ($HO_2\cdot$) impacting SOA formation and volatility (Kroll and Seinfeld, 2008). Hurley et al. (2001) suggest that SOA yield decreases when O_3 and nitrate radical ($NO_3\cdot$) are suppressed by high NO concentration. Cao and Jang (2008) assert that NO_x directly reacts with intermediate radicals, thus increasing organic nitrate formation and leading to less SOA formation. Song et al. (2005) suggest that NO_x concentration also affects the ring-opening and ring-retaining oxidation pathways of aromatics. Ng et al. (2007) further argue that NO would

not reduce SOA formation if sufficient hydroxyl radical (·OH) was available. Chan et al. (2010) propose that the RO_2·+NO_2 pathway of unsaturated aldehyde photooxidation serves as an additional important route for SOA formation from aromatics.

The atmospheric relevance of laboratory studies is critical for development of accurate SOA models. First, ambient-like chamber conditions are preferable to best mimic intermediate and radical concentrations. NO concentrations in recent chamber experiments are much closer to ambient conditions compared with earlier studies (Izumi and Fukuyama, 1990; Odum et al., 1996; Song et al., 2005; White et al., 2014). It should be pointed out that SOA precursors, NO_x (e.g. NO, NO_2 and HONO) and radical sources are typically injected before photooxidation begins (e.g. Forstner et al., 1997; Hurly et al., 2001; Ng et al., 2007). Experiments with only initial precursor and NO or H_2O_2 injection will be referred to as "classic experiments" within this work. Chemical components including SOA precursors, NO, NO_2, O_3, ·OH, HO_2· and NO_3· dramatically change during classic SOA formation experiments (Warren et al., 2008). In a classic low initial NO concentration experiment (e.g., Ng, et al., 2007), NO decreases from dozens of ppb to below detection limit (~0.2 ppb), the SOA precursor exponentially decays, and the instantaneous O_3 production rate (Sillman, 1999) and accumulated O_3 concentration change (Fig. S2.1). However, the ambient atmosphere usually has continuous NO and NO_2 sources, especially in urban areas with heavy traffic (Rattigan et al., 2010) where average NO concentrations exceed 0.2 ppb (Cusack et al., 2013). Excess NO has been used in a previous study to suppress O_3 and NO_3· formation during photoxidation (Hurly et al., 2001). However, the high initial NO_x (>250 ppb) and hydrocarbon concentrations

(>2 ppm) still do not accurately mimic the ambient condition. Hence, more field relevant experimental scenarios are needed to improve the reliability of atmospheric model inputs.

Further, reliable methodologies of data interpretation, in view of the differences between laboratory and ambient conditions, are needed to more accurately explore aerosol formation processes directly applicable to the atmosphere. Traditional SOA yield curves (Odum et al., 1996) rely on smog chamber experiments conducted under a variety of conditions and are extensively used in current atmospheric models (e.g., Binkowski and Roselle, 2003; Jenkin et al., 2003). It is worth noting that final fractional aerosol yield (Odum et al., 1996), an averaged SOA growth potential throughout a chamber oxidation process, is currently used to generate SOA yield curves (Ng et al., 2006). However, the average $[\cdot OH]/[HO_2\cdot]$ ratio in traditional chamber experiments are lower than typical atmospheric conditions with the exception of the initial $[\cdot OH]/[HO_2\cdot]$ ratio (Kanaya et al., 2012). The initial $[\cdot OH]/[HO_2\cdot]$ ratio is driven by the high initial NO concentration, which promotes ·OH concentration from the NO-O_3-NO_2 photolytic cycle. It indicates that continuous NO_x injection scenarios during photooxidation could improve the similarity between chamber experiments and the atmosphere. Further, changes to the SOA growth curve induction period or time to the onset of aerosol formation in a classic chamber experiment (Hurley et al., 2001; Ng et al., 2007), directly influences the measured overall SOA yield. It is also useful to incorporate instantaneous SOA growth curves into analyses of SOA formation in order to improve model mechanisms. In this work, we use SOA growth curves of 56 classic *m*-xylene photooxidation experiments to investigate the instantaneous NO_x effect on SOA growth. Stepwise and continuous NO_x

injection scenarios are also utilized during chamber photooxidation experiments to simulate continuous NO_x sources in urban areas and to bridge the NO influence principle from laboratory observations to the atmosphere. The main goal of the study is to shed insight on the mechanism of NO effect on SOA formation from aromatic hydrocarbons.

2.2 Method

2.2.1 Environmental chamber

The UC Riverside/CE-CERT indoor dual 90 m^3 environmental chambers were used in this study and are described in detail elsewhere (Carter et al., 2005). Experiments were all conducted at dry conditions (RH<0.1%), in the absence of inorganic seed aerosol, and with temperature controlled to 27±1°C. Two movable top frames were slowly lowered during each experiment to maintain a slight positive differential pressure (~0.02" H_2O) between the reactors and enclosure to minimize dilution and/or contamination of the reactors. 276 115 W Sylvania 350BL blacklights are used as light sources for photooxidation.

2.2.2 Gas-phase analysis

Decay of *m*-xylene was measured by a pair of Agilent 6980 (Palo Alto, CA) gas chromatographs (GC) equipped with flame ionization detectors (FID). A Thermal Environmental Instruments Model 42C chemiluminescence NO_x analyzer was used to monitor NO, NO_y-NO and NO_y. O_3 was monitored by a Dasibi Environmental Corp. Model 1003-AH O_3 analyzer.

2.2.3 Particle phase analysis

Aerosol growth was measured using an in-house built scanning mobility particle sizer (SMPS). The differential mobility analyzer is located inside the chamber enclosure to ensure that aerosol sizing was conducted at a temperature identical to the chamber temperature. Particle volume was corrected for particle wall loss assuming a first order wall loss decay as described in Cocker et al (2001).

2.2.4 Radical Analysis

The gas-phase reaction model SAPRC-11 developed by Carter and Heo (2012) was utilized to predict radical concentrations (·OH, HO_2·, RO_2· and NO_3·). SAPRC-11 uses updated chemical mechanisms designed to address NO_x impacts on aromatic photooxidation. The model accurately simulated data within the UCR/CE-CERT environmental chamber experiments within acceptable biases (Carter and Heo, 2012) for 14 different types of aromatic hydrocarbons and for a variety of reactant concentrations and NO_x levels.

2.2.5 Data mining

Data mining was conducted on 56 previous classic *m*-xylene photooxidation experiments conducted in the UCR/CE-CERT environmental chamber with blacklights (k_1=0.13 min^{-1} Warren et al., 2008) and initial HC/NO ranging from 1.3 to 591.2 (ppbC:ppb) (Table S2.1).

2.2.6 Reaction scenarios

Five reaction scenarios (RS) were used to study the NO influence on SOA formation: 1) Classic RS; 2) H_2O_2 RS; 3) Stepwise HONO RS; 4) Stepwise or continuous NO RS and 5) Stepwise NO_2 RS (Table 2.1). NO and *m*-xylene were initially injected in all five scenarios. H_2O_2 was also injected initially in RS2, RS4 and RS5. In RS4 and RS5, NO or NO_2 was injected at 5-15 ppb·hr^{-1} either stepwise (once per hour) or continuously. HONO was injected at ~20-60 ppb·hr^{-1}injected stepwise in RS3. *m*-Xylene, NO, NO_2 and hydrogen peroxide (H_2O_2) injection followed previous work (Song, et al., 2005; Qi et al., 2010; Nakao et al., 2011a). Nitrous acid (HONO) was prepared by adding 1 wt % aqueous $NaNO_2$ dropwise or by syringe (250 μl) into 20 mL of 10 wt % sulfuric acid in a glass bulb (Kautzman et al., 2009) and flushed into chamber with ~2 LPM nitrogen for 15 minutes each time along with the NO and NO_2 side products formed as part of the HONO preparation. Perfluorohexane was used as an inert tracer for each experiment to monitor reactor dilution. Dilution of the inert tracer was observed to be <2% during the course of all experiments.

2.3 Results

2.3.1 NO effect on SOA growth curve during classic *m*-xylene photoxidation

The traditional SOA growth curve (ΔM_0 vs. ΔHC) is used to represent SOA formation (Kroll and Seinfeld, 2005). The slope of the SOA growth curve provides instantaneous SOA growth rates as reactivity conditions evolve. SOA growth curves for 56 classic *m*-

xylene photooxidation experiments (black lights, k_1=0.13 min^{-1}; SOA density = 1.4 g cm^{-3} (Song et al., 2007b, Ng et al., 2007, Malloy et al., 2009)) with initial HC/NO_x ranging from 1.3 to 591.2 (ppbC:ppb) are displayed in Fig. S2.2.

The induction period, measured in this work as the amount of aerosol precursor consumed between lights on and initial aerosol formation, varies widely for the 56 experiments. The hydrocarbon consumption during the induction period directly affects SOA yield (aerosol mass formed/hydrocarbon reacted) calculations (Henze et al., 2008; Kroll et al., 2007). Hurley et al. (2001) previously shifted the x-axis (hydrocarbon consumed) of their SOA growth curve by a fixed fraction of the initial hydrocarbon ($[HC]_i$) to remove the induction period and group their SOA growth curves. However, in the current study, $[HC]_i$ alone cannot explain variations in the induction period length for experiments with similar $[HC]_i$ and different NO (e.g. 368A and 368B) and therefore NO concentration is considered critical to induction period. By defining significant SOA growth as instantaneous SOA yield (Jiang, 2003) higher than 0.01, experimental parameters including initial HC concentration, instantaneous SOA yield, [NO], $[NO_2]/[O_3]$, $[NO_2]/([NO]*[\cdot OH])$ and$[NO_2]/([NO]*[HC])$) were correlated to induction period (Table S2.2) with NO_2/NO ratio identified as the best indicator of induction-period length. Therefore, the experimental hydrocarbon consumed is offset (Fig. S4) in this work by the hydrocarbon consumed when NO_2/NO=70 (first of three consecutive 10-minute average measurements above threshold) based on the statistical analysis (Table S2.2) for the 56 classic *m*-xylene experiments with initial NO ranging from 0-433 ppb. ΔHC' represents the hydrocarbon decay after the NO_2/NO threshold is achieved (Fig.

S2.3 a) and b)). ΔHC' is zero if the threshold is never achieved, which occurs for experiments with extreme low initial NO_x (NO_x<1ppb) or HC/NO_x. The curve color (Fig. S2.4) corresponds to the fraction of hydrocarbon consumption at threshold (f_1=ΔHC'/ΔHC_f). ΔHC_f stands for the total hydrocarbon decay during photooxidation.

M_0-M_0' (new Y-axis) is then defined as the SOA formed only after crossing the NO_2/NO threshold (Fig. S2.3c). It is obtained by subtracting the minimal aerosol formation (M_o') at the time the NO_2/NO threshold is reached. The modified SOA growth curves of the 56 classic experiments are shown (Fig. 2.1). Violet curves (154A, 223A, 223B and 820B) located in the lower right region of the figure are experiments that did not reach the NO_2/NO threshold. These four experiments have initial HC/NO_x lower than 3 ppbC:ppb and the lowest SOA formation rate among all 56 experiments and will not be further discussed in this section. Three regions (Region 1, 2 and 3) are used to categorize the remaining 52 curves (Fig. 2.1, Table S2.1; the four experiments that never reached the NO_2/NO threshold are marked as Region 4). Different regions suggest different SOA growth rates since all curves are modified to start from the origin of new coordinate M_0-M_0' vs. ΔHC-ΔHC' and have approximately linear trends.

Green and blue curves (Fig. 2.1) in Regions 1 and 2 are sandwiched by red and orange curves in Regions 2 and 3 indicating that factors other than NO_2/NO ratio also affect SOA growth rate. Therefore, the HC/NO ratio, NO and NO_2 influence on SOA growth rate are also investigated. Table S2.1 lists HC/NO ratio, NO and NO_2 concentration at the time the NO_2/NO threshold is reached. The relationship between SOA growth rate and

NO_2 or HC/NO concentration are shown in Fig. 2.2. Curves in Region 1 have NO_2 concentrations below 20.6 ppb when the NO_2/NO threshold are reached. Region 3 curves are related to smaller HC/NO (<164 ppbC: ppb) at the NO_2/NO threshold. Curves in Region 2 (Fig. 2.1) with medium NO_2 concentration and high HC/NO ranks at the top in SOA growth rate among the three regions. This indicates that low NO or NO_2 concentration promotes SOA formation (comparing Region 2 with Region 1) particularly when the NO is below ppb level. Since curve colors are well organized red to blue from higher to lower SOA growth rate, it is also possible that the fraction of hydrocarbon consumption before the threshold or the average ·OH concentration related to hydrocarbon consumption also affects SOA growth rate after the threshold (see Section 2.4.1). Second, it is demonstrated that sub-ppb level NO promotion of aerosol growth rate depends on instantaneous HC/NO when comparing curves in Region 3 to Region 2. For example, experiments (e.g. 247A and 247B) that start with high initial NO and hydrocarbon concentrations have significant SOA formation even for relatively high NO concentrations (5.80 and 5.02 ppb). Significant SOA formation is attributed to the high HC/NO ratios (32.2 and 36.6 ppb: ppb) at elevated NO concentrations thus confirming the importance of instantaneous HC/NO.

2.3.2 Radical analysis of classic *m*-xylene photoxidation experiments

HO_2· plus RO_2· reaction has been considered as a major pathway of SOA formation under low NO_x conditions (Kroll and Seinfeld, 2008). Instantaneous relationships between SOA growth rate, fraction of RO_2· reacting with HO_2· and ·OH concentration

are studied by using the modified SOA growth curve (Section 2.3.1). First, it is assumed that $RO_2\cdot$ reacts only with $HO_2\cdot$ and NO (Kroll and Seinfeld, 2008). The fraction of $RO_2\cdot$ reacting with $HO_2\cdot$ is then defined as f_2 (eq. 3-1)

$$f_2 = k_3[HO_2\cdot]/(k_3[HO_2\cdot]+k_1[NO\cdot]). \quad \text{Eq 3-1}$$

where k_3 (7.63×10^{-12} $cm^3\cdot molecules^{-1}\cdot s^{-1}$) and k_1 (9.23×10^{-12} $cm^3\cdot molecules^{-1}\cdot s^{-1}$) are the reaction rates of $RO_2\cdot$ with $HO_2\cdot$ and NO, respectively (Carter, 2010; Carter and Heo, 2013). $[HO_2\cdot]$ is predicted by SAPRC-11 with $[\cdot OH]$ calculated from *m*-xylene decay. Modified SOA growth curves of 52 classic *m*-xylene photooxidation experiments are colored by f_2 (Fig. 2.3a). $HO_2\cdot$ and $RO_2\cdot$ reaction and SOA formation are insignificant for experiments with initial HC/NO_x lower than 3 ppbC:ppb. A color gradient of increasing f_2 is observed with increasing SOA growth (Fig. 2.3a). When NO_2/NO ratios are lower than 70, $HO_2\cdot$ is unable to compete with NO for $RO_2\cdot$ resulting in insignificant SOA formation. It is observed that the medial f_2 value (green color, $0.25 < f_2 < 0.5$, Fig. 2.3a) exists in the initial part of Region 1, end part of Region 3 and most of Region 2. The medial f_2 value represents the value for which the SOA formation mechanism transitions from NO suppression to $HO_2\cdot$ dominant. The large medial f_2 in Region 2 indicates SOA formation peaks when NO and $HO_2\cdot$ are in similar concentration rather than when NO is completely depleted. Assuming that SOA originates from $RO_2\cdot$ and $HO_2\cdot$ reactions, it will be shown later (Section 2.4.2) that $RO_2\cdot$ and $HO_2\cdot$ concentrations can be promoted by NO (especially under sub-ppb NO concentration range). Several red and orange curves in Fig. 2.1 of Region 2 and Region 3 show lower initial f_2 (blue in Fig. 2.3a) after

the threshold compared with others. Low HC/NO ratio in Region 3 inhibits $RO_2\cdot$ and $HO_2\cdot$ reaction by reducing peroxy radical concentration (Fig. 2.8a). Further, higher initial NO_x concentrations in Region 3 increase yields of higher volatility organic nitrate species thereby lowering the overall SOA yield. The lower f_2 in Region 2 compared to Region 1 (Fig. 2.3a) corresponds to the highest SOA growth rate indicating a boundary $[NO]/[HO_2\cdot]$ condition that promotes SOA formation.

The ·OH effect on SOA formation is studied by coloring the modified growth curves with the hydrocarbon decay rate (R_{HC}) (Fig. 2.3b). By assuming *m*-xylene only reacts with ·OH (Martín-Reviejo and Wirtz, 2005), R_{HC} (min^{-1}) is described by eq. 3-2

$$R_{HC} = \frac{\Delta(HC_i)}{[HC_i]\times\Delta t} = k \times [\cdot OH] \qquad \text{Eq 3-2}$$

where k (7.86 $m^3\cdot\mu g^{-1}\cdot min^{-1}$ or 2.31 x 10^{-11} ($cm^3\cdot molecule^{-1}\cdot s^{-1}$) (Calvert, et al., 2002) is the reaction rate constant of the hydrocarbon with ·OH, $[HC_i]$ and [·OH] are the mass concentration ($\mu g\cdot m^{-3}$) of parent hydrocarbon and ·OH at time *t,* respectively, Δt is the time change (min) and $\Delta(HC_i)$ is the change of hydrocarbon mass concentration ($\mu g\cdot m^{-3}$) during (t, $t+\Delta t$). Since *m*-xylene predominantly reacts with ·OH (Atkinson 1989; Calvert, et al., 2002) faster hydrocarbon decay indicates higher ·OH concentration. High ·OH concentration is mainly observed in Regions 2 and 3, which have higher NO or NO_2 compared with Region 1. NO enhances ·OH formation by reaction of NO with $HO_2\cdot$ to form more ·OH and therefore higher $R\cdot$ and $RO_2\cdot$ (Fig. 2.8a). The change in $[RO_2\cdot]$, $[HO_2\cdot]$ and $[HO_2\cdot]/[RO_2\cdot]$ with [·OH] directly influences SOA growth rate. SOA growth

rate is still low in Region 3 despite high ·OH concentration due to competition between NO promotion and inhibition effects on SOA.

2.3.3 SOA formation of *m*-xylene photoxidation for five reaction scenarios

Overall aerosol yield (OAY) defined by Odum et al. (1996) and instantaneous aerosol yield (IAY) introduced by Jiang (2003) are both applied to describe SOA formation. Fig. S2.5 shows linear SOA growth after an induction period ($r^2 > 0.97$ after $M_o > 0.5$ $\mu g \cdot m^{-3}$) for each reaction scenario suggesting that oxidation of first generation products are the rate-determining step (Kroll and Seinfeld, 2008; Ng et al., 2006) for SOA formation consistent with Ng et al. (2007). Modified SOA growth curves for each injection scenario (Fig. 2.4) illustrate IAY differences between scenarios. Hydrocarbon consumption when aerosol mass reaches 2 $\mu g \cdot m^{-3}$ is used to offset the X-axis and the Y-axis offset is 2 $\mu g \cdot m^{-3}$. SOA growth curves (Fig. 2.4) are categorized into two groups: with initial H_2O_2 injection (RS2, RS4 and RS5) and without H_2O_2 (RS1 and RS3). The scenarios including H_2O_2 have higher IAY (>0.24) and OAY (>0.11) compared with the schemes without H_2O_2 (IAY<0.22, OAY<0.08) ((Table S2.3).

RS1: RS1 is the classic chamber photooxidation experiments with only hydrocarbon and low initial NO. OAYs obtained in this work are similar to previous studies (Song, et al., 2005; Tang, et al., in preparation, a).

RS2, RS4&RS5 (w/ H_2O_2)**:** RS2 initially injects H_2O_2 and NO with measured IAY and OAY higher than RS1 or OAY from H_2O_2 only experiments (Song, et al., 2005; Tang, et

al., in preparation, b). Song et al. (2007b) performed a *m*-xylene photoxidation experiment (521B) where ~20 ppb of NO was injected in the middle of an H_2O_2 oxidation experiment and observed higher OAY (0.27) than RS2 in this work (1795B, OAY = 0.11) even though the same total amount of NO was injected. This indicates that the induction period resulting from initial NO injection (RS2) lowers OAY. It is also observed in RS2 (Table S2.3) that higher initial NO (HC/NO = 13.0±2.4 ppbC/ppb vs. HC/NO = 38.2± 10.3 ppbC/ppb) may lead to higher IAY (IAY = 0.35±0.04 vs. IAY = 0.32 ± 0.07).

Increases in IAY over RS2 is found when NO is injected step-wise or continuously in RS4. This is consistent with Martín-Reviejo and Wirtz (2005) where continuously injected HONO/NO_x experiments (benzene photooxidation) also yielded higher SOA yields than NO-free H_2O_2 experiments. Similar SOA growth is observed in the current study when NO_2 (vs. NO) was injected stepwise (RS5) as the NO_2/NO ratio in the chamber was rapidly re-established with little impact on the overall reactivity of the system. Higher OAYs in RS4 and RS5 are associated with shorter induction periods than the bulk NO_x injection of RS2.

Changes to OAY and IAY (RS4&RS5 vs. RS2) are observed for experiments commencing with similar initial NO_x levels and induction periods. Generally, IAYs are greater for RS4 than RS2 and monotonically increase for decreasing NO injection rates (NO_x injection rates < 15 ppb·hr^{-1}) (1885A<1868A<1867A<1863A). However, lower IAYs are observed when the stepwise NO concentration is raised to ~15 ppb·hr^{-1}

(1778A). Similarly, increasing IAY and OAY is observed for RS5 compared to RS2 for stepwise small NO_2 injections (1849A and 1872A, NO_2 5 ppb·hr^{-1}) with IAY decreasing relative to RS2 when NO_2 is injected at 10 ppb·hr^{-1} (1885B). Inhibition of SOA formation at higher NO_x injection rates is consistent with observations in Song et al. (2007b) (NO injection of 50 ppb midway through *m*-xylene photoxidation experiment). Initial hydrocarbon concentration is also found to affect the impact of continuous NO_x injection on SOA formation (Table S2.3). The IAY increases relative to RS2 discussed above are not observed in RS4 (1858A) or RS5 (1859A and 1801A) experiments with higher initial hydrocarbon concentration (similar NO_x as before). The induction period for the high initial hydrocarbon experiments is shorter due to the higher initial HC/NO ratio (Song, et al., 2005).

RS3: HONO (along with ~10% NO plus NO_2 impurity, Becker et al., 1996) were continually injected in RS3 to investigate the NO effect while increasing the ·OH radical source. The HONO injection rate determines SOA growth rate: compared with RS1, small amounts of HONO injected (1774B, ~20 ppb·hr^{-1}) raises IAY and OAY, while large HONO injection (1748B, ~60 ppb·hr^{-1}) suppresses IAY and OAY. The impacts of HONO on SOA formation parallels observations made for RS4 and RS5 providing further evidence that NO has a two-edged effect on SOA growth.

No vertical trends (Ng, et al., 2006) or sharp turns (Song, et al., 2007b) are observed in the SOA growth curves during continuous or step wise injections indicating that HONO (RS3), NO (RS4) and NO_2 (RS5) did not instantaneously react with intermediate

photooxidation products (e.g. phenol) to immediately form SOA. Therefore, we hypothesize that radical kinetics are changing with injection scenario thereby influencing SOA yield.

Additional seeded experiments were conducted in the dual UC Riverside/CE-CERT chamber to assess the impact of wall-loss of semi-volatile species. *m*-Xylene and NO_x were injected and mixed thoroughly between the chambers. Next, dry $(NH_4)_2SO_4$ seeds (~10,000 cm^{-3} with diameter of 30-50 nm) were injected to one side of the bag. No measurable differences were observed in SOA formation (amount or timing) between the non-seeded and seeded experiments indicating that wall loss of semivolatile compounds did not significantly impact measured SOA formation from *m*-xylene photooxidation.

2.3.4 Relating NO-radical chemistry to SOA formation

2.3.4.1 NO impacts on radical kinetics

NO increases are typical in the atmosphere in the morning and late afternoon (Guicherit, 1975; Williams et al., 1988). Conventional (RS1) chamber experiments commence with high NO, which is rapidly converted to NO_2 resulting in very low residual NO concentrations during SOA formation. Step-wise or continuous NO_x injection scenarios are used in this work to simulate the NO increase in the daytime urban atmosphere.

RS1: $HO_2\cdot$ and $RO_2\cdot$ sharply increases at the start of an experiment and then dramatically decreases when NO is depleted to sub-ppb levels in classic chamber photooxidation experiments (RS1) (Fig. 2.5).

RS2: Experiments with initial H_2O_2 injection (RS2) have higher $HO_2\cdot$ and $RO_2\cdot$ peak concentrations for longer periods of time (order of tens of minutes) than RS1. (Fig. 2.5 RS2).

RS4&RS5: The RS4 $HO_2\cdot$ and $RO_2\cdot$ peak concentrations is extended relative to RS2 by a couple hours, which is more similar to the urban atmosphere $HO_2\cdot$ and $RO_2\cdot$ trends (Dusanter et al., 2009; Handisides et al., 2003; Ren et al., 2003). $HO_2\cdot$ and $RO_2\cdot$ drop further in RS4 than RS2 after their peak radical concentrations due to the lack of hydrocarbon available for further reaction (Fig. 2.5). The longer peak radical concentrations in RS4 indicates that the continual presence of low NO concentrations maintains $RO_2\cdot$ and $HO_2\cdot$ concentration at elevated levels (while sufficient hydrocarbons are available to react) due to RS4 maintaining higher ·OH concentrations. RS5 has a similar $RO_2\cdot$ and $HO_2\cdot$ profile to RS4 (Fig. 2.8). It is generally observed (Fig. 2.5) that $RO_2\cdot$ and $HO_2\cdot$ level depends on ·OH concentration since steep decays in their concentration correspond to changing ·OH levels. Fig. 2.5 supports the hypothesis (Section 2.3.3) that NO promotion of $RO_2\cdot$ and $HO_2\cdot$ radical results from increasing the rate of ·OH - aromatic reaction. It should also be noted that $HO_2\cdot$ formation from H_2O_2 and ·OH reaction can happen together with photolytic $HO_2\cdot$ production. The ratio of $HO_2\cdot$ from H_2O_2 + ·OH to the photolytic cycle can be described by $1.62*[H_2O_2]/2.31*$ [*m*-xylene] (Keyser, 1980; Calvert, et al., 2002). $HO_2\cdot$ levels are similar in RS2, RS4 and RS5 as initial $[H_2O_2]$ and [*m*-xylene] are similar in these reaction schemes. Therefore, $HO_2\cdot$ increase by H_2O_2 + ·OH reaction in RS2, RS4, and RS5 may enhance SOA formation from the increasing ·OH driven by continuous NO injection.

Slight and temporary peroxy radical decreases are observed immediately after each step wise NO_x injection (RS4 and RS5). The decreases are positively correlated with NO injection rate and are smaller in RS5. This is due to instantly higher NO/HC after NO_x injection. The decreases are smaller during the initial period when sufficient hydrocarbon is available to minimize the peroxy radical decrease. The temporary decreases are avoided continuous NO injections are performed (Fig. 2.5 RS4-2:1867A). Additionally, NO/HC (or initial hydrocarbon) impacts on radical concentration are observed (Fig. 2.5 RS5-2:1801A and 1858A) with higher initial hydrocarbon leading to higher average $RO_2\cdot$ and $[RO_2\cdot][HO_2\cdot]$ but not average $HO_2\cdot$.

High NO_x injection effect: The consistently high NO_x injection rate (>7.5 ppb·hr^{-1}) in RS4 (Fig. 2.5 RS4-3:1778A and 1885A) and RS5 (1885B) leads to "higher" NO (e.g. 0.5-2ppb in 1778A) constraining peroxy radicals to low concentrations and therefore lowering SOA yields. This observation is consistent with the suggestion by Ng et al. (2007) that NO suppresses nonvolatile hydroperoxides formation from the $RO_2\cdot$ and $HO_2\cdot$reaction resulting in a lower SOA yield. However, if the high NO injection occurs after maximum peroxy radical concentrations (Fig. 2.5, RS4-4), the NO_x inhibition effect on SOA formation is not observed.

2.3.4.2 Linking SOA formation to average radical parameters

Average radical concentrations (Table S2.3) were calculated using the SAPRC-11 model with ·OH adjusted by the measured *m*-xylene decay (Carter and Heo, 2013).
Average ·OH and $RO_2\cdot$ concentration ranges within the chamber (2.22-10.61×10^6

molecules·cm^{-3} and 4.97-29.58 ×10^{8} molecules·cm^{-3}) are within typical daytime urban atmospheric levels (1.2-20×10^{6} molecules·cm^{-3} and 5-15 ×10^{8} molecules·cm^{-3}) while average $HO_2\cdot$ concentrations (11.9-560×10^{8} molecules·cm^{-3}) are at or above the reported maximum level of the urban atmosphere (0.4-10×10^{8} molecules·cm^{-3}) (Dusanter et al., 2009; Emmerson et al., 2005; Emmerson et al., 2007; Lee et al., 2006; Ren et al., 2003). While H_2O_2 injections may be expected to enhance $HO_2\cdot$ concentrations, NO/$HO_2\cdot$ ratios for RS2, RS4, and RS5 0.11-1.18, Table S2.4) after nucleation remain similar to classic (RS1) experiments (Section 2.3.2, Fig. 2.3a). The average [·OH]/[HO_2·] ratio in RS1 is 1.91-11 ×10^{-3} and approaches atmospheric conditions (Kanaya et al., 2012) as initial NO/HC increases. Experiments in RS2, RS4 and RS5 have higher [·OH]/[HO_2·] ratios compared with classic H_2O_2 only experiments (Fig. 2.6, Table S2.5) due to NO_x injection but lower ratios compared with RS1 as a result of higher $HO_2\cdot$ concentration originating from H_2O_2 injection. Higher NO_x injection rates within this work are used to increase the [·OH]/[HO_2·] ratio among experiments with H_2O_2 injection.

OAY and radical parameters: High correlation is observed between OAY and [·OH]/[HO_2·], HO_2·and RO_2·(Table 2. 2), which is mostly driven by H_2O_2 injection. Average ·OH, $HO_2\cdot$ and RO_2·concentrations in RS2, RS4 and RS5 are higher than those of RS1 (Table S2.3). An extra ·OH source from H_2O_2 decomposition for RS2, RS4 and RS5 leads to higher $R\cdot$ and therefore RO_2·. Once most of NO is converted (sub-ppb level), $HO_2\cdot$ is no longer suppressed leading to higher SOA formation from reaction of RO_2·with HO_2·.

IAY and radical parameters: It is also found that IAY is well correlated with [·OH] and $[HO_2\cdot]/[RO_2\cdot]$. There is no significant $[HO_2\cdot]/[RO_2\cdot]$ difference between RS2 and RS1 indicating H_2O_2 injection enhances $HO_2\cdot$ and $RO_2\cdot$ on a comparable scale. It also indicates that the high correlation between IAY and $[HO_2\cdot]/[RO_2\cdot]$ is caused by the NO_x injection. ·OH concentrations in RS1 are similar for the range of H_2O_2 only experiments (RS8 in Table S2.5) and the RS2 experiments further demonstrating the importance of NO to ·OH concentration particularly for the reaction schemes that include H_2O_2. It confirms that NO influence on SOA formation is related to ·OH concentration consistent with previous studies (Nakao et al., 2011a; Ng et al., 2007). Also, a high correlation (0.822, p-value=0) between ·OH and $[HO_2\cdot]/[RO_2\cdot]$ implies that NO influences $[HO_2\cdot]/[RO_2\cdot]$ through ·OH . The positive relationship between IAY and $[HO_2\cdot]/[RO_2\cdot]$ is consistent with high $[RO_2\cdot]$ in the high initial hydrocarbon experiments having lower yields.

$\Delta M_0'$ and radical parameter: Average radical concentrations for the 175 $\mu g\cdot m^{-3}$ hydrocarbon consumption after M_0>2 $\mu g\cdot m^{-3}$ are analyzed to explore relationships between SOA growth rate and radical concentrations after the induction period. $\Delta M_0'$ (M_0-M_0') is the particle concentration increase after M_0'=2 $\mu g\cdot m^{-3}$ until ΔHC-$\Delta HC'$=175 $\mu g\cdot m^{-3}$. $\Delta HC'$ (Section 2.3.1) uses M_0'=2 $\mu g\cdot m^{-3}$ as a threshold. $\Delta M_0'$ at ΔHC-$\Delta HC'$=175 $\mu g\cdot m^{-3}$ (Fig. 2.4) is used as an indicator for average SOA growth rate after the induction period. Average radical parameters (e.g. $[HO_2\cdot]/[RO_2\cdot]$ and [·OH]) are calculated by dividing integrated radical parameters from the induction period threshold (M_0'=2 $\mu g\cdot m^{-3}$) to ΔHC-$\Delta HC'$=175$\mu g\cdot m^{-3}$. Fig. 2.7 shows a relationship between $\Delta M_0'$ and $[HO_2\cdot]/[RO_2\cdot]$

colored by [·OH]/[HO_2·] and sized with NO_x injection rate. A general increasing ΔM_0' trend with [HO_2·]/[RO_2·] is found (Fig. 2.7) with a high correlation factor (0.724, p-value=0) suggesting that a higher [HO_2·]/[RO_2·] ratio leads to higher SOA formation. It is also found (Fig. 2.7) that [·OH]/[HO_2·] is positively correlated to ΔM_0' for both points below (high NO_x injection rate; SOA suppression regime) or above (low NO_x injection rate; SOA enhancement regime) the points describing the RS2 experiments. This is explained by high ·OH concentrations facilitating production of the HO_2· and RO_2· radicals through the reaction cycles shown in Fig. 2.8. Further, [RO_2·] [HO_2·] is negatively correlated to ΔM_0' (Fig. S2.6) when only RS2, RS4 and RS5 are considered. The negative correlation is attributed to increasing RO_2· (lower [HO_2·]/[RO_2·]) leading to a higher fraction of NO reacting with RO_2· instead of HO_2·; this results in higher molecular fragmentation thereby lowering aerosol yields. Kroll et al. (2006) suggests that SOA growth rate increases as [NO]/[HO_2·] decreases. Correlations in this work are also observed among [NO]/[HO_2·]; however, the correlation is weaker than the radical parameter mentioned above (Table 2. 2). The lower [NO]/[HO_2·] correlation results from differences in NO_x injection methods used in this work. For example, similar amounts of hydrocarbon and NO_x are injected into RS4 (1867A) and RS2 (1867B) using different injection scenarios leading to similar [NO]/[HO_2·] but differing yields, which provides further evidence that the NO_x effect on SOA yields depends on how NO_x is injected.

RS3: Radical concentrations are not predicted in RS3 since HONO injection is not readily quantifiable. Generally, HONO serves as a source of ·OH to accelerate the initial ·OH attack on the precursor aromatic during photooxidation. It is expected that

more $RO_2\cdot$ is formed from the increased OH radical concentration. However, the coexistence of "high" NO concentrations results from HONO synthesis (Becker et al., 1996). Therefore, large quantities of HONO injection are observed to inhibit SOA formation in this work. Smaller HONO injections did not show this inhibition.

Organic nitrate from either NO or NO_2 reaction with $RO_2\cdot$ (Atkinson, 2000; Koch et al., 2007) are not significantly correlated with yields. Similar fractions of peroxy radical are consumed by NO_x in all experiments (9.34%-12.24%) to form organic nitrate based on SAPRC-11 (Table S2.3, RO_2XC/RO_2).

2.4 Discussion

2.4.1 Implication of modified SOA growth curve on relationships between SOA formation and NO_x

The modified SOA growth curve (using NO_2/NO=70 threshold) for classic *m*-xylene photooxidation experiments fall into three regions (Fig. 2.1). Regions 1, 2, and 3 are experiments with moderate SOA formation, those where NO promotes SOA, and those where NO suppresses SOA, respectively.

An *m*-xylene photooxidation mechanism is illustrated in Fig. S2.7 (Carter et al., 2012; Carter and Heo, 2012; Nehr et al., 2012; Zhao et al., 2005). Lower energy intermediate radical products are used to describe the aromatic-OH adduct pathway (·OH adduct between two methyl groups). NO_2 reaction with the *m*-xylene adduct (dashed line, Fig. S2.7) is not considered since NO_x levels in all experiments are below ppm level

(Atkinson & Arey, 2007). Three reaction pathways in addition to the induction period are used to explain the NO effect on SOA formation (Fig. 2.8a). All experiments in Fig. 2.1 experience an induction period for SOA formation due to chemical kinetics and gas-particle partitioning (Martín-Reviejo and Wirtz, 2005). During the induction period, NO reacts with the bicyclic peroxy radical to form alkoxy radicals and hence $HO_2\cdot$, α-dicarbonyls and monounsaturated dicarbonyls. These products from *m*-xylene include glyoxal, methylglyoxal, unsaturated 1,4-dicarbonyls and methyl unsaturated 1,4-dicarbonyls (Andino et al., 1996; Atkinson and Arey, 2007; Carter and Heo, 2013; Forstner et al., 1997; Nehr et al., 2012), which are more volatile compared with ring-retaining reaction products (Kroll et al., 2005; Volkamer et al., 2007). These dicarbonyls yield $HO_2\cdot$ and ·OH (Talukdar et al., 2011) leading to an increase in $RO_2\cdot$. Dicarbonyl yields are not influenced by NO_x concentration (NO_x <100 ppb) (Nishino et al., 2010). Experiments in Region 2 consume more *m*-xylene and form larger amounts of dicarbonyls during the induction period than those in Region 1 (Fig. S2.4), potentially contributing to the higher SOA growth rate observed for Region 2 experiments after the induction period. Aerosol formation during the induction period may be attributed to production of semi-volatile products (e.g. benzoquinone and *m*-tolualdehyde) formed in the presence of NO by P2P and to H-atom abstraction (Fig. S2.7) (Chan et al., 2007; Kroll et al., 2007; Kroll and Seinfeld, 2005).

Several aerosol growth pathways are observed as the reaction proceeds (Fig. 2.8a). Initially, when NO_2/NO is low, the NO competes with $HO_2\cdot$ inhibiting particle formation. As NO_2/NO increases, an intermediate phase is achieved where the presence of NO

enhances SOA formation through rapid recycling of ·OH (Pathway II). Finally, NO depletes (NO_2/NO rises) to levels where existing HO_2· prefers to react with RO_2· to form additional SOA. The relative contribution of each pathway varies based on instantaneous HC/NO loadings. The contributions for each region (Fig. 2.1) relative to the length of the induction period are schematically shown in Fig. 2.8b. The HC/NO range for aerosol promotion is observed to be 200-450 ppbC: ppb (Fig. 2.9, green dash line). Instantaneous HC/NO is above, near, and below the promotion range when NO_2/NO reaches 70 for Regions 1, 2 and 3, respectively.

Pathway I: NO competes with HO_2· for RO_2·in this step (P1 vs P3, P1P vs P2P in Fig. S2.7). NO leads to more fragmentation by P3 (Song et al., 2005) and less phenol-like compounds by P2P. Initial HC/NO_x ratio determines the time spent following Pathway I in classic photooxidation experiments.

Pathway II: Pathway II domination depends on instantaneous HC/NO ratio. HC/NO around 200 ppbC: ppb serves as a boundary value for Pathway II domination. As shown in Fig. 2.8a (dashed line) the concentration of RO_2· and HO_2· could increase for low NO concentrations provided there is sufficient hydrocarbon available. HO_2· and RO_2· reaction rate peaks for HC/NO ratios of~200-450 ppbC: ppb(Fig. 2.9). It is proposed that peroxy radical formation is not significantly affected by NO concentration above the upper limit of this range while NO suppresses peroxy radical formation below that range. Red to blue trends (decreasing HC consumption during induction period) in Regions 1 and 2 (Fig. 2.1) shows higher SOA growth rates for decreasing HC:NO ratios

for experiments with similar NO levels. This implies increased SOA formation as lowering HC/NO promotes further oxidation by the $RO_2\cdot$ plus $HO_2\cdot$ pathway (Fig. 2.8a). $HO_2\cdot$ and $RO_2\cdot$concentration increasing for lower HC/NO is further supported by the larger observed SOA growth rates during stepwise or continuous NO_x injection (Section 2.3.3, RS4 and RS5). Experiments with similar initial HC/NO_x are located in different regions (Fig. 2.1) because of differences between hydrocarbon decay and NO conversion rates (Stroud et al., 2004).

NO "free" phase: The NO "free" phase commences when HC/NO increases to >450 ppbC: ppb where $RO_2\cdot$ and $HO_2\cdot$ reaction dominates.

Most classic photooxidation experiments with initial NO will progress through the three phases leading to the slope changes observed in the SOA growth curves (Fig. 2.1). The rates of change of NO_2/NO and HC/NO determine the length of each phase (Fig. 2.8b and Fig. 2.9). However, the HC/NO and NO_2/NO threshold for experiments will differ under atmospheric conditions. Therefore, ambient atmospheric conditions must be simulated to study the atmospheric NO effect on SOA formation.

H_2O_2 with initial NO (RS2) and step wise or continuous NO_x injection (RS4 and RS5) are methods that improve the atmospheric relevance of chamber experiments (Section 2.3.4). Linear SOA growth curve trends are found in these modified NO injection scenario experiments (after the induction period) indicating that the experiment is remaining within a single dominant SOA pathway rather than progressing through each pathway (Fig. 2.8b) as occurs during traditional (RS1) photooxidation experiments.

2.4.2 NO impacts on SOA formation

Overall, NO exerts a two-edge impact on SOA formation defined instantaneously by radical concentrations. The two-edge NO effect explains observations in 3.1 that curves in Region 2 (Fig. 2.1) with medium initial NO have higher SOA growth rates than those in Region 1 and Region 3. It is the NO levels in Region 2 that increases ·OH concentration without significantly suppressing SOA formation. The f_2 value used in Section 2.3.2 only considers the NO and HO_2· competition while ignoring ·OH concentration. Further, previous *m*-xylene photooxidation experiments with CO (RS6) or propene (RS7) (Song et al., 2007a) show lower SOA yield and growth rate compared those without CO or propene because ·OH concentration is suppressed (Table S2.5).

The NO effect on SOA formation from *m*-xylene also depends on instantaneous HC/NO. Fig. 2.8a illustrates the relationship between NO and peroxy radicals on SOA formation pathways. Although organic peroxides (ROOR) from self or cross reaction of RO_2· is a potential SOA source (Ziemann, 2002), RO_2· reaction with NO_2 and RO_2· self and cross reaction are not included in Fig. 2.8a due to their low reactivity in this study (Atkinson and Arey, 2007; Ng et al., 2007; Ziemann and Atkinson, 2012). The NO inhibition effect dominates when initial NO concentration (e.g HC/NO_x<3 ppbC:ppb) or pulse NO injection (e.g.1778A) is high. NO competes with HO_2· for RO_2· depressing hydroxperoxide (ROOH) formation, which is a major SOA component (Bonn et al., 2004). More volatile compounds are formed when NO reacts with RO_2· (Johnson et al., 2005; Kroll et al., 2006; Presto et al., 2005). NO suppression gradually ceases when NO

is sufficiently converted to NO_2 (below sub-ppb level (Kroll and Seinfeld, 2008)). In this study, $NO_2/NO>70$ is identified as a threshold for adequate NO conversion to form SOA from classic *m*-xylene photooxidation chamber experiments with initial HC/NO_x higher than 3 ppbC: ppb. However, typical 12 hour daytime average concentration ratio of NO_2/NO in atmosphere is only 10 (Seinfeld and Pandis, 2006). In this study, higher SOA formation and instantaneous NO_2/NO ranging from 4.1-10.2 was achieved during stepwise NO injection. This indicates SOA yields from classic *m*-xylene photooxidation experiments may underestimate SOA formation for typical atmospheric conditions.

It is further demonstrated that increasing SOA formation rates not only depend on the NO concentration but also on the HC/NO ratio. As revealed by Fig. 2.8a, the reaction of $RO_2\cdot$ and $HO_2\cdot$ is suppressed directly (pathway I) and enhanced indirectly (pathway II) by NO. The net effect of NO on the rate of $RO_2\cdot$ and $HO_2\cdot$ formation are described by eq. 4-1 and eq. 4-2. Further, eq. 4-3 and eq. 4-4 describe the condition for $RO_2\cdot$ and $HO_2\cdot$ to increase, respectively. The NO concentration must therefore be in the range given by eq. 4-5 to promote $HO_2\cdot$ and $RO_2\cdot$ reaction. It is observed that higher available $RO\cdot$ and $RO_2\cdot$ widens the NO concentration range that increases SOA formation.

$$\frac{d[RO_2\cdot]}{dt} = k_5[O_2][R\cdot] - k_1[RO_2\cdot][NO] \qquad \text{Eq 4-1}$$

$$\frac{d[HO_2\cdot]}{dt} = k_6[O_2][RO\cdot] - k_2[HO_2\cdot][NO] \qquad \text{Eq 4-2}$$

$$[NO] < k_5[O_2][R\cdot]/k_1[RO_2\cdot] = M \qquad \text{Eq 4-3}$$

$$[NO] < k_6[O_2][RO\cdot]/k_2[HO_2\cdot] \ = N \quad \text{Eq 4-4}$$

$$A < [NO] < [M, N] \quad \text{Eq 4-5}$$

By assuming [RO_2·] and [HO_2·] are on the order of 10^{-2} ppb, NO should be 4 ×10^6 times and 2 ×10^8 times lower than [R·] and [RO·], respectively. The maximum [R·] and [RO·] can be estimated (eq.4-7 and eq.4-9) by assuming [RH] = 50 ppb, [·OH] = 0.1ppt, [NO_2] = 30 ppb, [RO_2·] = 50 ppt and [NO] = 1ppb. [R·] and [RO·] are estimated as 2.7 ×10^{-7} ppb and 2.8 ×10^{-7} ppb, respectively, suggesting that NO should be below 1.1 ppb under atmospheric conditions to promote HO_2· and RO_2· reaction.

$$\frac{d[R\cdot]}{dt} = k_4[RH][HO\cdot] - k_5[O_2][R\cdot] \quad \text{Eq 4-6}$$

$$[R\cdot]_{max} = \ k_4[RH][HO\cdot]/k_5[O_2] \quad \text{Eq 4-7}$$

$$\frac{d[RO\cdot]}{dt} = k_1[RO_2\cdot][NO] - k_6[O_2][RO\cdot] - \ k_7[NO_2][RO\cdot] \quad \text{Eq 4-8}$$

$$[RO\cdot]_{max} = \ k_1[\mathrm{RO_2}\cdot][NO]/(k_6[O_2] + k_7[NO_2 \quad \text{Eq 4-9}$$

The NO promotion will disappear (Fig. 2a) when NO concentration becomes less than 300ppt as occurs in traditional chamber experiments. However, NO increases in the morning and late afternoon (Guicherit, 1975; Williams et al., 1988) make it possible to enhance SOA formation in an urban atmosphere, especially when HC/NO is above 200 ppbC: ppb.

Dry conditions were used in this work to specifically concentrate on the NO impact on SOA formation. An increase trend of SOA formation with increasing RH from aromatic photooxidation has been reported in previous studies (Zhou et al., 2011; Kamens et al., 2011; Parikh et al., 2011). Healy, et al. (2009) suggests that increasing humidity contributes to higher ·OH concentrations leading to greater oxidation of the aromatic precursor. Based on the current work, increasing ·OH concentrations would be expected to promote SOA formation. The impact of ·OH concentration due to increased humidity is likely to be much smaller than the influence of NOx documented in this work.

2.5 Conclusion

Instantaneous NO effects on SOA formation from *m*-xylene under different atmospheric activities are observed from data mining 10 years of aromatic hydrocarbon chamber experiments conducted in the UCR/CE-CERT chamber. A two-edged NO effect on SOA formation is found in this study indicating that NO could promote SOA formation from $RO_2\cdot$ and $HO_2\cdot$ at low concentration (<5ppb) with sufficient hydrocarbon (HC/NO >400 ppbC: ppb) present. Traditional chamber experiments with HC and NO_x only injected at the start of the experiment progresses through multiple pathways and may not be as atmospherically relevant when considered as a whole. This study suggests that continuous NO injection into environmental chamber experiments could improve such chamber simulations. Better NO injection scenarios avoiding NO suppression on SOA while raising $[\cdot OH]/[HO_2\cdot]$ ratio should be explored in future studies in order to improve

urban atmosphere characterization with coexistence of NO, NO_2, VOC and SOA. Moreover, the modified SOA growth curve is identified as a valuable tool to compare the instantaneous SOA growth rate of different experiments. While this modified approach is challenging and in its infancy, the trend of incorporating instantaneous NO_2/NO into SOA formation analysis is expected to continue since it provides more detailed SOA growth information at the sub-ppb NO levels generally ignored by previous models. Further experiments and analyses are needed to more precisely define the boundary condition for NO promotion of SOA formation from other hydrocarbon precursors.

2.6 Reference

Andino, J. M., Smith, J. N., Flagan, R. C., Goddard, W. A. and Seinfeld, J. H.: Mechanism of atmospheric photooxidation of aromatics: A theoretical study, J. Phys. Chem., 100(26), 10967-10980, 1996.

Atkinson, R.: Atmospheric chemistry of VOCs and NOx, Atmos. Environ., 34(12-14), 2063-2101, 2000.

Atkinson, R.: Kinetics and mechanisms of the gas-phase reactions of the hydroxyl radical with organic compounds, J. Phys. Chem. Ref. Data Monogr., 1, 1–246, 1989.

Atkinson, R. and Arey, J.: Mechanisms of the gas-phase reactions of aromatic hydrocarbons and PAHs with OH and NO_3 radicals, Polycycl. Aromat. Compd., 27(1), 15-40, 2007.

Becker, K. H., Kleffmann, J., Kurtenbach, R., and Wiesen, P.: Solubility of nitrous acid (HONO) in sulfuric acid solutions, J. Phys. Chem., 100(36), 14984-14990, 1996.

Binkowski, F. S., and Roselle, S. J.: Models-3 Community Multiscale Air Quality (CMAQ) model aerosol component 1. Model description, J. Geophys. Res. Atmos., 108(D6), 2003.

Bonn, B., von Kuhlmann, R., and Lawrence, M. G.: High contribution of biogenic hydroperoxides to secondary organic aerosol formation, Geophys. Res. Lett., 31, L10108, 2004.

Calvert, J. G., Atkinson, R., Becker, K. H., Kamens, R. M., Seinfeld, J. H., Wallington, T. J., and Yarwood, G.: The mechanisms of atmospheric oxidation of aromatic hydrocarbons, Oxford University Press New York, 2002.

Cao, G., and Jang, M.: Secondary organic aerosol formation from toluene photooxidation under various NO_x conditions and particle acidity, Atmos. Chem. Phys. Discuss, 8, 14467-14495, 2008.

Carter, W. P.: Development of the SAPRC-07 chemical mechanism, Atmos. Environ., 44(40), 5324-5335, 2010.

Carter, W. P., Cocker III, D. R., Fitz, D. R., Malkina, I. L., Bumiller, K., Sauer, C. G., Pisano, J.T., Bufalino, C. and Song, C.: A new environmental chamber for evaluation of gas-phase chemical mechanisms and secondary aerosol formation, Atmos. Environ., 39(40), 7768-7788, 2005.

Carter, W. P. L., and Heo, G.: Development of revised SAPRC aromatics mechanisms, Atmos. Environ., 77, 404-414, 2013.

Carter, W. P. L., Heo, G., Cocker III, D. R. and Nakao, S.: SOA Formation: Chamber Study and Model Development, Final report to CARB, Contract 08-326, 2012.

Carter, W. P. L. and Heo, G.: Development of Revised SAPRC Aromatics Mechanisms, Report to the California Air Resources Board Contracts 07-730, 2012.

Chan, A. W. H., Chan, M. N., Surratt, J. D., Chhabra, P. S., Loza, C. L., Crounse, J. D., Yee, L. D., Flagan, R. C., Wennberg, P. O. and Seinfeld, J. H.: Role of aldehyde chemistry and NO_x concentrations in secondary organic aerosol formation, Atmos. Chem. Phys., 10(15), 7169-7188, 2010.

Chan, A. W. H., Kroll, J. H., Ng, N. L. and Seinfeld, J. H.: Kinetic modeling of secondary organic aerosol formation: effects of particle-and gas-phase reactions of semivolatile products, Atmos. Chem. Phys., 7(15), 4135-4147, 2007.

Cocker III, D. R., Flagan, R. C. and Seinfeld, J. H.: State-of-the-art chamber facility for studying atmospheric aerosol chemistry, Environ. Sci. Technol., 35(12), 2594-2601, 2001a.

Cusack, M., Pérez, N., Pey, J., Wiedensohler, A., Alastuey, A. and Querol, X.: Variability of sub-micrometer particle number size distributions and concentrations in the Western Mediterranean regional background, Tellus B, 65, 19243, 2013.

Dusanter, S., Vimal, D., Stevens, P., Volkamer, R., Molina, L.T., Baker, A., Meinardi, S., Blake, D., Sheehy, P. and Merten, A.: Measurements of OH and HO_2 concentrations during the MCMA-2006 field campaign–Part 2: Model comparison and radical budget, Atmos. Chem. Phys., 9(18), 6655-6675, 2009.

Emanuelsson, E., Hallquist, M., Kristensen, K., Glasius, M., Bohn, B., Fuchs, H., Kammer, B., Kiendler-Scharr, A., Nehr, S. and Rubach, F.: Formation of anthropogenic secondary organic aerosol (SOA) and its influence on biogenic SOA properties, Atmos. Chem. Phys., 13(5), 2837-2855, 2013.

Emmerson, K., Carslaw, N., Carpenter, L., Heard, D., Lee, J. and Pilling, M.: Urban atmospheric chemistry during the PUMA campaign 1: Comparison of modelled OH and HO_2 concentrations with measurements, J. Atmos. Chem., 52(2), 143-164, 2005.

Emmerson, K. M., Carslaw, N., Carslaw, D., Lee, J. D., McFiggans, G., Bloss, W. J., Gravestock, T., Heard, D. E., Hopkins, J. and Ingham, T.: Free radical modelling studies during the UK TORCH Campaign in Summer, Atmos. Chem. Phys., 7(1), 167-181, 2007.

Forstner, H. J. L., Flagan, R. C. and Seinfeld, J. H.: Secondary organic aerosol from the photooxidation of aromatic hydrocarbons: Molecular composition, Environ. Sci. Technol., 31(5), 1345-1358, 1997.

Guicherit, R.: Photochemical smog formation in the Netherlands (in Dutch). Report No. G 646, TNO Research Institute for Environmental Hygiene, 104, 1975.

Hallquist, M., Wenger, J., Baltensperger, U., Rudich, Y., Simpson, D., Claeys, M., Dommen, J., Donahue, N., George, C. and Goldstein, A.: The formation, properties and impact of secondary organic aerosol: current and emerging issues, Atmos. Chem. Phys., 9(14), 5155-5236, 2009.

Handisides, G. M., Plaß-Dülmer, C., Gilge, S., Bingemer, H. and Berresheim, H.: Hohenpeissenberg Photochemical Experiment (HOPE 2000): Measurements and photostationary state calculations of OH and peroxy radicals, Atmos. Chem. Phys., 3(5), 1565-1588, 2003.

Healy, R. M., Temime, B., Kuprovskyte, K. and Wenger, J. C.: Effect of relative humidity on gas/particle partitioning and aerosol mass yield in the photooxidation of p-xylene, Environ. Sci. Technol., 43(6), 1884-1889, 2009.

Henze, D. K., Seinfeld, J. H., Ng, N. L., Kroll, J. H., Fu, T. M., Jacob, D. J. and Heald, C. L.: Global modeling of secondary organic aerosol formation from aromatic hydrocarbons: high-vs. low-yield pathways, Atmos. Chem. Phys., 8(9), 2405-2421, 2008.

Hurley, M. D., Sokolov, O., Wallington, T. J., Takekawa, H., Karasawa, M., Klotz, B. Ö., Barnes, I. and Becker, K. H.: Organic aerosol formation during the atmospheric degradation of toluene. Environ. Sci. Technol., 35(7), 1358-1366, 2001.

Izumi, K., and Fukuyama, T.: Photochemical aerosol formation from aromatic hydrocarbons in the presence of NO_x, Atmos. Environ. A-Gen., 24(6), 1433-1441, 1990.

Jenkin, M., Saunders, S., Wagner, V. and Pilling, M.: Protocol for the development of the Master Chemical Mechanism, MCM v3 (Part B): tropospheric degradation of aromatic volatile organic compounds, Atmos. Chem. Phys., 3(1), 181-193, 2003.

Jiang, W.: Instantaneous secondary organic aerosol yields and their comparison with overall aerosol yields for aromatic and biogenic hydrocarbons, Atmos. Environ., 37(38), 5439-5444, 2003.

Johnson, D., Jenkin, M.E., Wirtz, K. and Martin-Reviejo, M.: Simulating the formation of secondary organic aerosol from the photooxidation of aromatic hydrocarbons, Environ. Chem., 2(1), 35-48, 2005.

Kamens, R.M., Zhang, H., Chen, E. H., Zhou, Y., Parikh, H. M., Wilson, R.L., Galloway, K.E., Rosen, E. P.: Secondary organic aerosol formation from toluene in an atmospheric hydrocarbon mixture: water and particle seed effects, Atmos. Environ., 45(13), 2324-2334, 2011.

Kanakidou, M., Seinfeld, J., Pandis, S., Barnes, I., Dentener, F., Facchini, M., Van Dingenen, R., Ervens, B., Nenes, A., Nielsen, C.: Organic aerosol and global climate modelling: a review, Atmos. Chem. Phys., 5(4), 1053-1123, 2005.

Kanaya, Y., Hofzumahaus, A., Dorn, H.-P., Brauers, T., Fuchs, H., Holland, F., Rohrer, F., Bohn, B., Tillmann, R., Wegener, R.: Comparisons of observed and modeled OH and HO_2 concentrations during the ambient measurement period of the HO_x Comp field campaign, Atmos. Chem. Phys., 12(5), 2567-2585, 2012.

Kautzman, K. E., Surratt, J. D., Chan, M. N., Chan, A. W. H., Hersey, S. P., Chhabra, P. S., Dalleska, N. F., Wennberg, P. O., Flagan, R. C., Seinfeld, J. H.: Chemical composition of gas-and aerosol-phase products from the photooxidation of naphthalene, J. Phys. Chem. A, 114(2), 913-934, 2009.

Koch, R., Knispel, R., Elend, M., Siese, M. and Zetzsch, C.: Consecutive reactions of aromatic-OH adducts with NO, NO_2 and O_2: benzene, naphthalene, toluene, *m*- and *p*-xylene, hexamethylbenzene, phenol, m-cresol and aniline, Atmos. Chem. Phys., 7(8), 2057-2071, 2007.

Kroll, J. H. and Seinfeld, J. H.: Representation of secondary organic aerosol laboratory chamber data for the interpretation of mechanisms of particle growth, Environ. Sci. Technol., 39(11), 4159-4165, 2005.

Kroll, J. H. and Seinfeld, J. H.: Chemistry of secondary organic aerosol: Formation and evolution of low-volatility organics in the atmosphere, Atmos. Environ., 42(16), 3593-3624, 2008.

Kroll, J. H., Ng, N. L., Murphy, S. M., Varutbangkul, V., Flagan, R. C. and Seinfeld, J. H.: Chamber studies of secondary organic aerosol growth by reactive uptake of simple carbonyl compounds, J. Geophys. Res. Atmos. (1984–2012), 110(D23), 2005.

Kroll, J. H., Ng, N. L., Murphy, S. M., Flagan, R. C. and Seinfeld, J. H.: Secondary organic aerosol formation from isoprene photooxidation, Environ. Sci. Technol., 40(6), 1869-1877, 2006.

Kroll, J. H., Chan, A.W. H., Ng, N. L., Flagan, R. C. and Seinfeld, J. H.: Reactions of semivolatile organics and their effects on secondary organic aerosol formation. Environ. Sci. Technol., 41(10), 3545-3550, 2007.

Kuwata, M., Zorn, S.R. and Martin, S.T. 2011. Using elemental ratios to predict the density of organic material composed of carbon, hydrogen, and oxygen, Environ. Sci. Technol., 46(2), 787-794.

Lee, J. D., Lewis, A. C., Monks, P. S., Jacob, M., Hamilton, J. F., Hopkins, J. R., Watson, N. M., Saxton, J. E., Ennis, C. and Carpenter, L. J.: Ozone photochemistry and elevated isoprene during the UK heatwave of August 2003, Atmos. Environ., 40(39), 7598-7613, 2006.

Malloy, Q. G., Nakao, S., Qi, L., Austin, R., Stothers, C., Hagino, H. and Cocker III, D. R.: Real-Time Aerosol Density Determination Utilizing a Modified Scanning Mobility Particle Sizer—Aerosol Particle Mass Analyzer System, Aerosol. Sci. Tech., 43(7), 673-678, 2009.

Martín-Reviejo, M. and Wirtz, K.: Is benzene a precursor for secondary organic aerosol? Environ. Sci. Technol., 39(4), 1045-1054, 2005.

Na, K., Sawant, A. A., Song, C. and Cocker III, D. R.: Primary and secondary carbonaceous species in the atmosphere of Western Riverside County, California. Atmos. Environ., 38(9), 1345-1355, 2004.

Nakao, S., Clark, C., Tang, P., Sato, K. and Cocker III, D.: Secondary organic aerosol formation from phenolic compounds in the absence of NO_x, Atmos. Chem. Phys, 11, 10649-10660, 2011a.

Nakao, S., Liu, Y., Tang, P., Chen, C., Zhang, J. and Cocker III, D.: Role of glyoxal in SOA formation from aromatic hydrocarbons: gas-phase reaction trumps reactive uptake, Atmos. Chem. Phys. Discuss, 11, 30599-30625, 2011b.

Nehr, S., Bohn, B. and Wahner, A.: Prompt HO_2 formation following the reaction of OH with aromatic compounds under atmospheric conditions, J. Phys. Chem. A, 116(24), 6015-6026, 2012.

Ng, N. L., Kroll, J. H., Chan, A. W. H., Chhabra, P. S., Flagan, R. C. and Seinfeld, J. H.: Secondary organic aerosol formation from *m*-xylene, toluene, and benzene, Atmos. Chem. Phys., 7(14), 3909-3922, 2007.

Ng, N. L., Kroll, J. H., Keywood, M.D., Bahreini, R., Varutbangkul, V., Flagan, R.C., Seinfeld, J.H., Lee, A. and Goldstein, A. H.: Contribution of first-versus second-generation products to secondary organic aerosols formed in the oxidation of biogenic hydrocarbons, Environ. Sci. Technol., 40(7), 2283-2297, 2006.

Nishino, N., Arey, J. and Atkinson, R.: Formation yields of glyoxal and methylglyoxal from the gas-phase OH radical-initiated reactions of toluene, xylenes, and

trimethylbenzenes as a function of NO_2 concentration, J. Phys. Chem. A, 114(37), 10140-10147, 2010.

Odum, J. R., Hoffmann, T., Bowman, F., Collins, D., Flagan, R. C. and Seinfeld, J. H.: Gas/particle partitioning and secondary organic aerosol yields, Environ. Sci. Technol., 30(8), 2580-2585, 1996.

Presto, A. A., Huff Hartz, K. E. and Donahue, N. M.: Secondary organic aerosol production from terpene ozonolysis. 2. Effect of NOx concentration, Environ. Sci. Technol., 39(18): 7046-7054, 2005.

Qi, L., Nakao, S., Tang, P. and Cocker III, D. R.: Temperature effect on physical and chemical properties of secondary organic aerosol from *m*-xylene photooxidation, Atmos. Chem. Phys., 10(8), 3847-3854, 2010.

Parikh, H.M., Carlton, A.G., Vizuete, W. and Kamens, R.M.: Modeling secondary organic aerosol using a dynamic partitioning approach incorporating particle aqueous-phase chemistry. Atmos. Environ., 45(5), 1126-1137, 2011.

Rattigan, O.V., Dirk Felton, H., Bae, M.-S., Schwab, J.J. and Demerjian, K.L: Multi-year hourly PM2.5 carbon measurements in New York: Diurnal, day of week and seasonal patterns, Atmos. Environ., 44(16), 2043-2053, 2010.

Ren, X., Harder, H., Martinez, M., Lesher, R.L., Oliger, A., Shirley, T., Adams, J., Simpas, J.B. and Brune, W.H.: HO_x concentrations and OH reactivity observations in New York City during PMTACS-NY2001, Atmos. Environ., 37(26), 3627-3637, 2003.

Seinfeld, J. and Pandis, S.: Atmospheric chemistry and physics: from air pollution to climate change. John Wiley & Sons Publications, Hoboken, New Jersey, US, 2006.

Sillman, S.: The relation between ozone, NO_x and hydrocarbons in urban and polluted rural environments, Atmos. Environ., 33(12), 1821-1846, 1999.

Song, C., Na, K. and Cocker III, D. R.: Impact of the hydrocarbon to NO_x ratio on secondary organic aerosol formation, Environ. Sci. Technol., 39(9), 3143-3149, 2005.

Song, C., Na, K., Warren, B., Malloy, Q., Cocker III, D.R.: Impact of propene on secondary organic aerosol formation from *m*-xylene, Environ. Sci. Technol., 41(20), 6990-6995, 2007a.

Song, C., Na, K., Warren, B., Malloy, Q. and Cocker III, D. R.: Secondary organic aerosol formation from m-xylene in the absence of NOx. Environ. Sci. Technol., 41(21), 7409-7416, 2007b.

Song, C., Na, K., Warren, B., Malloy, Q. and Cocker III, D. R.: Secondary organic aerosol formation from the photooxidation of *p*-and *o*-xylene. Environ. Sci. Technol., 41(21), 7403-7408, 2007c.

Talukdar, R., Zhu, L., Feierabend, K. and Burkholder, J.: Rate coefficients for the reaction of methylglyoxal (CH3COCHO) with OH and NO_3 and glyoxal $(HCO)_2$ with NO_3. Atmos. Chem. Phys., 11, 10837-10851, 2011.

Volkamer, R., San Martini, F., Molina, L. T., Salcedo, D., Jimenez, J. L. and Molina, M. J.: A missing sink for gas-phase glyoxal in Mexico City: Formation of secondary organic aerosol. Geophys. Res. Lett., 34(19), 2007.

Warren, B., Song, C. and Cocker III, D. R.: Light intensity and light source influence on secondary organic aerosol formation for the m-xylene/NOx photooxidation system, Environ. Sci. Technol., 42(15), 5461-5466, 2008.

White, S. J., Jamie, I. M., and Angove, D. E.: Chemical characterisation of semi-volatile and aerosol compounds from the photooxidation of toluene and NOx, Atmos. Environ., 83, 237-244, 2014.

Williams, M.L., Broughton, G., Bower, J., Drury, V., Lilley, K., Powell, K., Rogers, F. andStevenson, K.: Ambient NO_x concentrations in the UK 1976–1984—a summary, Atmos. Environ., 22(12), 2819-2840, 1988.

Zhao, J., Zhang, R., Misawa, K. and Shibuya, K.: Experimental product study of the OH-initiated oxidation of *m*-xylene, J. Photoch. Photobio. A., 176(1), 199-207, 2005.

Zhou, Y., Zhang, H., Parikh, H.M., Chen, E.H., Rattanavaraha, W., Rosen, E.P., Wang, W. and Kamens, R.M.: Secondary organic aerosol formation from xylenes and mixtures of toluene and xylenes in an atmospheric urban hydrocarbon mixture: water and particle seed effects (II), Atmos. Environ., 45(23), 3882-3890, 2011.

Ziemann, P.J.: Evidence for low-volatility diacyl peroxides as a nucleating agent and major component of aerosol formed from reactions of O_3 with cyclohexene and homologous compounds, J. Phys.Chem. A, 106(17), 4390-4402, 2002.

Ziemann, P. J. and Atkinson, R.: Kinetics, products, and mechanisms of secondary organic aerosol formation, Chem. Soc. Rev., 41(19), 6582-6605, 2012.

2.7 Tables and Figures

Table 2.1 Experimental Conditions of Five Reaction Scenarios under Black Lights (k_1=0.40 min^{-1})

			Initial Injection ppb			Continuous Injection	
RS	Run ID	HC	NO	NO_2	H_2O_2	Compound	Amount
1	1748A	112	62.18	7.81	N/A	N/A	N/A
1	1749B	98.0	59.27	7.64	N/A	N/A	N/A
1	1774A	98.1	27.33	0.65	N/A	N/A	N/A
1	1841A	79.6	36.83	2.49	N/A	N/A	N/A
1	1843A	69.2	42.29	0	N/A	N/A	N/A
1	1843B	70.1	42.67	0	N/A	N/A	N/A
1	1872B	72.8	22.22	0	N/A	N/A	N/A
2	1749A	99.0	58.37	8.32	1000	N/A	N/A
2	1795B	71.4	17.73	1.24	1000	N/A	N/A
2	1849B	82.4	17.97	0	1000	N/A	N/A
2	1858B	125	19.96	0.52	1000	N/A	N/A
2	1859B	111	51.84	2.05	1000	N/A	N/A
2	1863B	71.5	50.74	0.1	1000	N/A	N/A
2	1867B	78.0	22.84	28.6	1000	N/A	N/A
3	1748B	112	62.44	7.74	N/A	HONO	750ul/hr[a]
3	1774B	94.4	27.1	1.22	N/A	HONO	250ul/hr[b]
4	1777A[d]	83.0	19.17	2.30	1000	NO	~5ppb/hr
4	1778A[c,d]	67.5	20	1.42	1000	NO	~15ppb/hr
4	1795A	68.3	19.41	0.90	1000	NO	~5ppb/hr
4	1858A	128	19.89	0.53	1000	NO	~5ppb/hr
4	1863A	72.1	20.35	0	1000	NO	~5ppb/hr
4	1867A	80.7	21.75	1.65	1000	NO	5ppb/hr*
4	1868A	70.5	18.91	0.56	1000	NO	7.5ppb/hr*
4	1885A	82.3	23.97	0	1000	NO	10ppb/hr*
5	1801A	127	20.66	1.27	1000	NO_2	~5ppb/hr
5	1849A	79.5	17.76	0	1000	NO_2	~5ppb/hr
5	1859A	113	18.92	1.38	1000	NO_2	~5ppb/hr
5	1872A	72.1	21.48	0.02	1000	NO_2	~5ppb/hr
5	1885B	83.2	23.86	0.13	1000	NO_2	~10ppb/hr

Note: 1- Classic Scenario; 2- H_2O_2 Scenario; 3- Continuous HONO Scenario; 4-Stepwise/Continous* NO Scenario; 5-Stepwise NO_2 Scenario; a) Injection by droplets, assuming one drop is 150 ul; b) Injection by syringe; c) ~30ppb NO is injected at the third hour; d) m-xylene data are measured by a different GC column compared with other experiment

Table 2.2 Correlation between Overall Yields, Instant Yield and Average Radical Concentration of Four Reaction Scenarios

	·OH	HO_2·	RO_2·	HO_2·*RO_2·	HO_2·/RO_2·	·OH/HO_2·	NO/HO_2·
OAY	0.506	0.548	0.529	0.528	0.517	-0.549	-0.419
p-value	0.008	0.004	0.005	0.006	0.007	0.001	0.033
IAY	0.543	0.537	0.304	0.386	0.618	-0.552	-0.386
p-value	0.004	0.005	0.131	0.051	0.001	0.003	0.051

Note: OAY: overall aerosol yield; IAY: instant yield. p-value determines the appropriateness of rejecting the null hypothesis in a hypothesis test. P-values range from 0 to 1, 0-reject null hypothesis and 1 accept null hypothesis. Alpha (α) level used is 0.05. If the p-value of a test statistic is less than alpha, the null hypothesis is rejected .Run 1778A are not included due to extreme high NO injection rate and low [RO_2·].

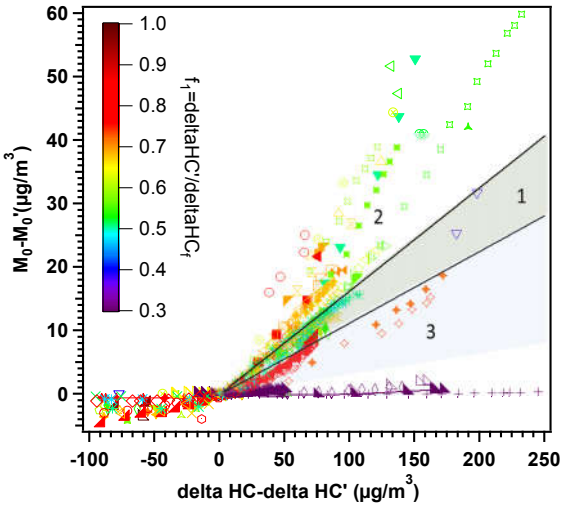

Figure 2.1 Modified (X&Y offset) SOA growth curves of 56 classic *m*-xylene photooxidation experiments under black lights (k_1=0.13 min^{-1})

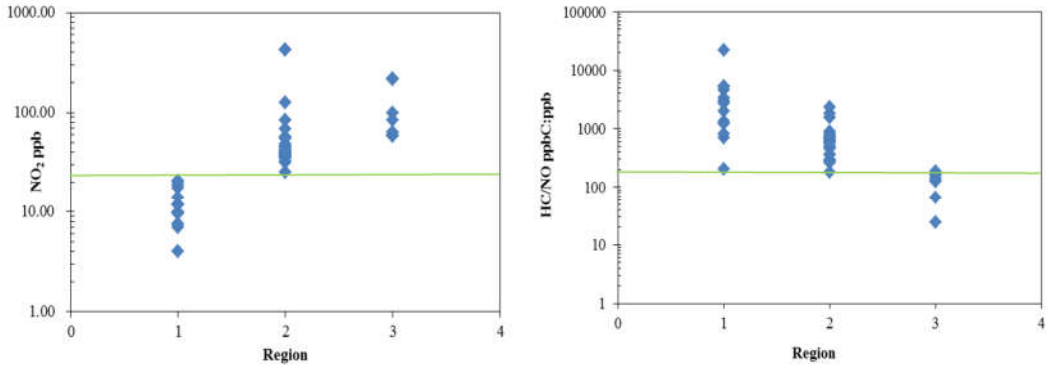

Figure 2.2 Relationship between the SOA growth rate and NO_2 concentration (a) and HC/NO ratio (b)

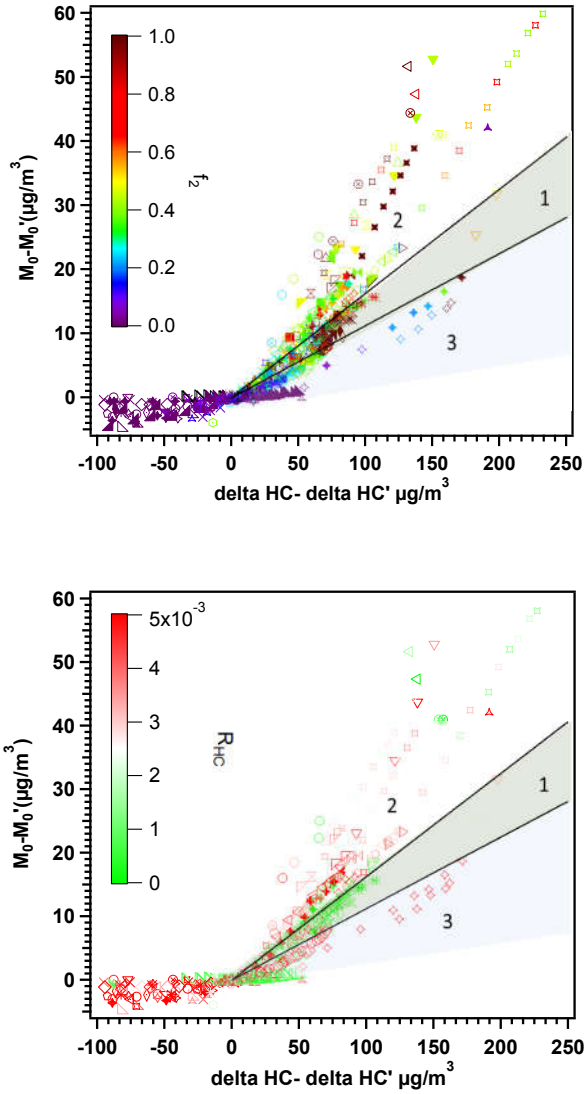

Figure 2.3 a) Modified SOA growth curves of 52 classic *m*-xylene photooxidation experiments colored with f_2 (fraction of $RO_2\cdot$ reacts with $HO_2\cdot$); b) Modified SOA growth curves of 52 classic *m*-xylene photooxidation experiments colored by hydrocarbon reaction rated (R_{HC})

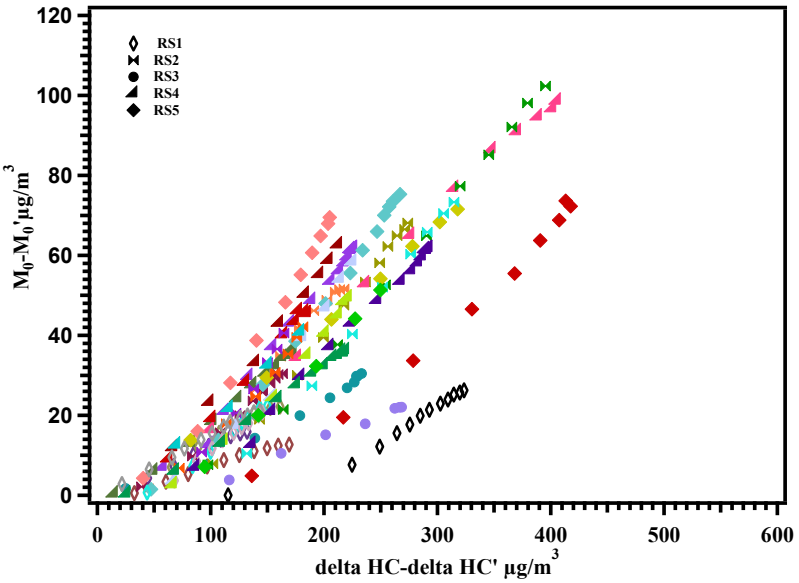

Figure 2.4 Modified SOA growth curve of five reaction scenarios

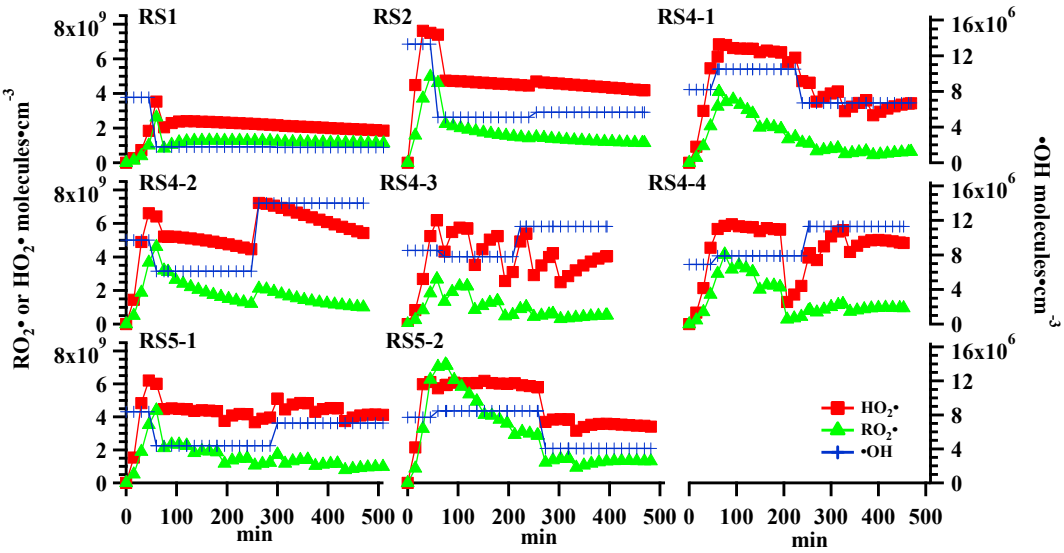

Figure 2.5 Times series ·OH, HO_2· and RO_2· change of RS1:1774A; RS2:1795B; RS4: 1) 1795A, 2) 1867A, 3) 1778A, 4) 1777A); RS5: 1) 1849A, 2) 1801A

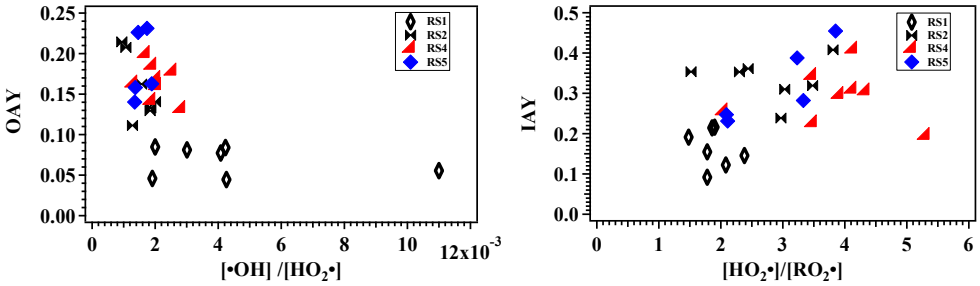

Figure 2.6 Relationship between yield and radical ratio: a) Overall aerosol yield (OAY) and $\cdot OH/HO_2\cdot$; b) Instantaneous aerosol yield (IAY) and $HO_2\cdot/RO_2\cdot$

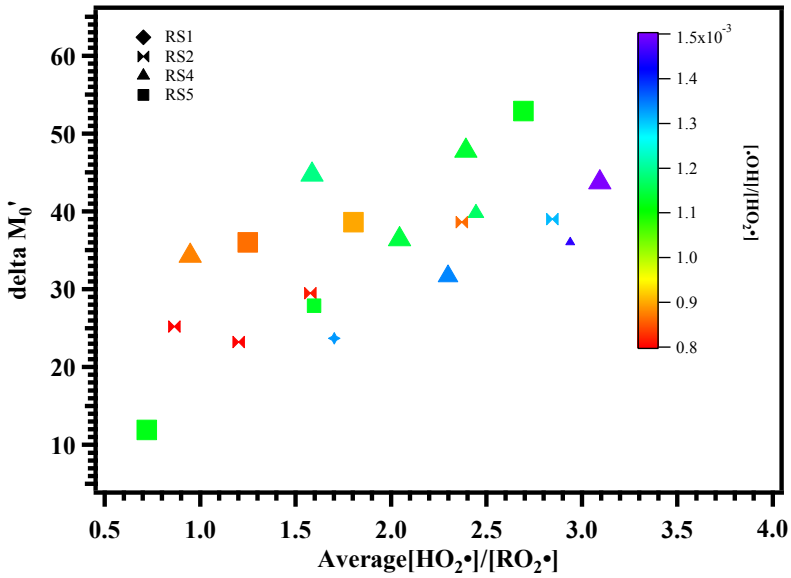

Figure 2.7 Relationship between ΔM_0' and $[HO_2\cdot]/[RO_2\cdot]$ during ΔHC-$\Delta HC'$= [0,175] $\mu g/m^3$ colored with injected$[\cdot OH]/[HO_2\cdot]$ and sized with NO_x injection rate (Bigger size resembles smaller NO_x injection rate)

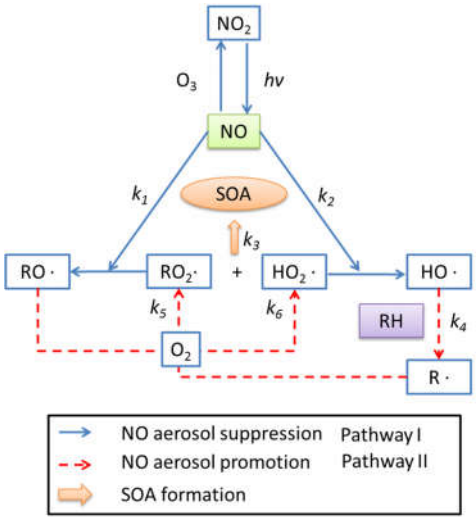

a)

k_1 = 9.23 $e^{-12}cm^3 \cdot moldecule^{-1} \cdot s^{-1}$(Carter, 2010); k_2= 8.50 $e^{-12}cm^3 \cdot moldecule^{-1} \cdot s^{-1}$ (Bohn & Zetzsch, 1997); k_3= 7.63$e^{-12}cm^3 \cdot moldecule^{-1} \cdot s^{-1}$(Carter, 2010); k_4= 2.31$e^{-12}cm^3 \cdot moldecule^{-1} \cdot s^{-1}$(Calvert, et al., 2002); k_5= 1.80 $e^{-15}cm^3 \cdot moldecule^{-1} \cdot s^{-1}$ (Koch, et al., 2007); k_6= 8.00 $e^{-14}cm^3 \cdot moldecule^{-1} \cdot s^{-1}$(Calvert, et al., 2002); k_7 =4.00 $e^{-11}cm^3 \cdot moldecule^{-1} \cdot s^{-1}$(Calvert, et al., 2002), the reaction rate of RO· with NO_2, not showed

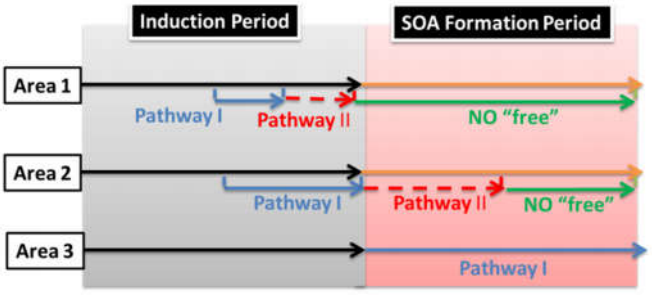

b)

Figure 2.8 a) Relationship between NO and SOA formation from HO_2· and RO_2·; b) Progressive dominate reaction pathways and phases during classic *m*-xylene photooxidation

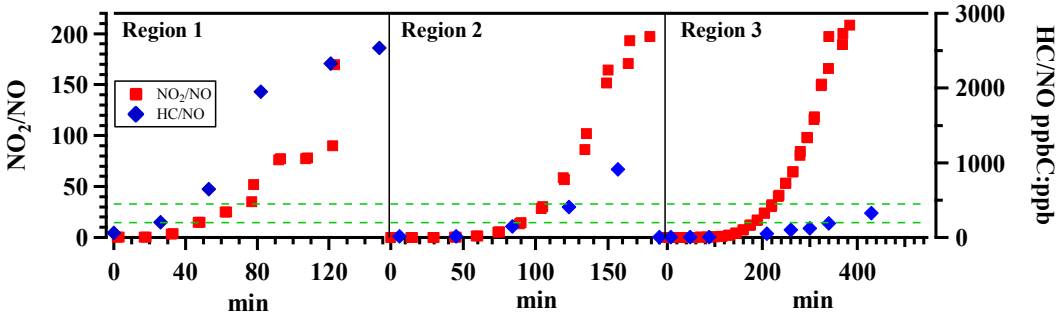

Figure 2.9 Typical instant NO_2/NO and HC/NO change trend in three regions (Region 1: 219A; Region 2: 566A; Region 3: 249A； green dash line promotion HC/NO range)

3. Role of methyl group number on SOA formation from aromatic hydrocarbons photooxidation under low NO_x conditions

3.1 Introduction

Aromatic hydrocarbons are major anthropogenic SOA precursors (Kanakidou, et al., 2005; Henze, et al., 2008). Monocyclic aromatic hydrocarbons with less than four methyl groups are ubiquitous in the atmosphere (Singh et al., 1985; Singh et al., 1992; Fraser, et al., 1998; Pilling and Bartle, 1999; Holzinger, et al., 2001; Buczynska, et al., 2009; Hu et al., 2015). Monocyclic aromatic hydrocarbons with more than 4 methyl groups are barely investigated in previous ambient studies, possibly due to a vapor pressure decrease with carbon number (Pankow and Asher, 2008; Table S3.1). However, a recent study observed that compounds with low vapor pressure are available to evaporate into the atmosphere (Vŏ and Morris, 2014). Monocyclic aromatic hydrocarbons with more than three methyl groups contributes to a large portion of components in products such as gasoline and crude oil (Diehl and Sanzo, 2005; Darouich, et al., 2006). Moreover, hydrocarbon reactivity and OH reaction rate constant (k_{OH}) increase with methyl group number (k_{OH} Table S3.1; Glasson and Tuesday, 1970; Calvert, et al, 2002; Atkinson and Arey, 2003; Aschmann, et al, 2013). OH-initiated reactions, particularly OH addition to the aromatic ring, dominate aromatic photooxidation (Calvert, et al., 2002). Hence, photooxidation occurs rapidly once these low vapor pressure aromatic hydrocarbons evaporate into atmosphere. In addition, an increase in carbon number is associated with a decrease in vapor pressure (Pankow and Asher, 2008). Higher carbon number products with a similar

amount of functional groups have a higher tendency to participate in the particle phase. However, aging of organic aerosol is a combination of functionalization, fragmentation and oligomerization (Jimenez, et al., 2009; Kroll, et al., 2009). Therefore, rapid aging does not necessarily lead to the highly oxidized compounds, which serve as an important source of SOA.

Recent studies have found that SOA yields from OH initiated alkane and alkene reactions increase with carbon chain length and decrease with the increase of branched structure (Lim, and Ziemann, 2009; Matsunaga, et al., 2009; Tkacik, et al., 2012). However, SOA yield from monocyclic aromatics are found to decrease with carbon number by adding methyl groups to the aromatic ring (Odum, et al., 1997a; Cocker, et al., 2001b; Sato, et al., 2012). This indicates that the role of methyl groups on the aromatic ring is different than for alkane and alkene hydrocarbons. Previous studies show that the relative methyl group position determines the alkoxyl radical (RO·) fragmentation ratio in alkane and alkene hydrocarbon oxidation (Atkinson, 2007; Ziemann, 2011). Therefore, it is necessary to explore the impact of methyl groups on SOA formation during monocyclic aromatic hydrocarbon oxidation.

Previous studies on SOA formation from monocyclic aromatic hydrocarbon in the presence of NO_x have been conducted at high NO_x levels (e.g., Odum, et al., 1997b; Cocker, et al., 2001b; Sato, et al., 2012). Ng, et al (2007) observed that SOA yield decreases with increasing carbon number under high NO_x conditions and no trends were observed for no NO_x conditions. Reaction mechanisms vary for different NO_x conditions

(e.g., Song, et al., 2005; Kroll and Seinfeld, 2008) and thus impact SOA chemical composition. Therefore, it is necessary to investigate methyl group impact on urban SOA formation from monocyclic aromatic hydrocarbon under more atmospherically relevant low NO_x conditions.

SOA budget underestimation of the urban environment is associated with mechanism uncertainty in aromatic hydrocarbon photooxidation and possibly missing aromatic hydrocarbon precursors (Henze, et al., 2008; Hallquist, et al., 2009). Previous chamber studies seldom investigate SOA formation from monocyclic aromatic with more than 3 methyl groups (e.g. pentamethylbenzene and hexamethylbenzene). This study investigates SOA formation from the photooxidation of seven monocyclic aromatic hydrocarbon (ranging from benzene to hexamethylbenzene) under the low NO_x (HC/NO>10 ppbC:ppb) condition. The impact of methyl group number on SOA yield, chemical composition and other physical properties are demonstrated. Possible methyl group impact on aromatic ring oxidation, decomposition and subsequent oligomerization are discussed.

3.2 Method

3.2.1 Environmental chamber

All experiments were conducted in the UC Riverside/CE-CERT indoor dual 90 m^3 environmental chambers, which are described in detail elsewhere (Carter et al., 2005). All experiments were conducted at dry conditions (RH<0.1%), in the absence of inorganic

seed aerosol and with temperature controlled to 27±1°C. Two movable top frames were slowly lowered during each experiment to maintain a slight positive differential pressure (~0.02 inches of water) between the reactors and enclosure to minimize dilution and/or contamination of the reactors. 272 115 W Sylvania 350BL blacklights are used as light sources for photooxidation.

A known volume of high purity liquid hydrocarbon precursors (benzene Sigma-Aldrich, 99%; toluene Sigma-Aldrich, 99.5%; *m*-xylene Sigma-Aldrich, 99%; 1, 2, 4-trimethylbenzene Sigma-Aldrich, 98%) were injected through a heated glass injection manifold system and flushed into the chamber with pure N_2. A glass manifold packed with glass wool inside a temperature controlled oven (50-80 °C) is used to inject solid hydrocarbon precursors (1, 2, 4, 5-tetramethylbenzene Sigma-Aldrich, 98%; pentamethylbenzene Sigma-Aldrich, 98%; hexamethylbenzene Sigma-Aldrich, 99%). NO was introduced by flushing pure N_2 through a calibrated glass bulb filled to a predetermined partial pressure of pure NO. All hydrocarbons and NO are injected and well mixed before the lights were turned on to commence the reaction.

3.2.2 Particle and Gas Measurement

Particle size distribution between 27 nm and 686 nm was monitored by dual custom built Scanning Mobility Particle Sizers (SMPS) (Cocker et al., 2001a). Particle effective density was measured with a Kanomax Aerosol Particle Mass Analyzer (APM-SMPS) system (Malloy et al., 2009). Particle volatility was measured by a Volatility Tandem Differential Mobility Analyzer (VTDMA) (Rader and McMurry, 1986) with a Dekati®

Thermodenuder controlled to 100°C and a 17 s heating zone residence time (Qi, et al., 2010b). Volume fraction remaining (VFR) is calculated as $(D_{p,\text{ after TD}}/D_{p,\text{ before TD}})^3$.

Evolution of particle-phase chemical composition was measured by a High Resolution Time of Flight Aerosol Mass Spectrometer (HR-ToF-AMS; Aerodyne Research Inc.) (Canagaratna et al., 2007; DeCarlo et al., 2006). The sample was vaporized by a 600 °C oven followed by a 70 eV electron impact ionization. f_x in this study is calculated as the fraction of the organic signal at *m/z*=x. For example, f_{44} and f_{43} are the ratios of the organic signal at *m/z* 44 and 43 to the total organic signal, respectively (Chhabra et al., 2011; Duplissy et al., 2011). Elemental ratios for total organic mass, oxygen to carbon (O/C), and hydrogen to carbon (H/C) were determined using the elemental analysis (EA) technique (Aiken et al., 2007, 2008). Data was analyzed with ToF-AMS analysis toolkit Pika 1.15D with 1.56D Squirrel.

The Agilent 6890 Gas Chromatograph – Flame Ionization Detector was used to measure aromatic hydrocarbon concentrations. A Thermal Environmental Instruments Model 42C chemiluminescence NO analyzer was used to monitor NO, NO_y-NO and NO_y. The gas-phase reaction model SAPRC-11 developed by Carter and Heo (2012) was utilized to predict radical concentrations (·OH, HO_2·, RO_2· and NO_3·).

3.3 Results

3.3.1 SOA yield relationship with methyl group number

SOA yields from the photooxidation of seven monocyclic aromatic hydrocarbons are calculated as the mass based ratio of aerosol formed to hydrocarbon reacted (Odum, et al., 1996). The HC/NO ratio ranged from 12.6-110 ppbC:ppb for all experiments used in this study. Experiment conditions and SOA yield are listed from the current work (Table 3.1) along with additional *m*-xylene experiment conditions from previous studies (Table S3.2) (Song, et al, 2005) in the UCR CE-CERT chambers. SOA yield as a function of particle mass concentration (M_0) for all seven monocyclic aromatic precursors (Fig. 3.1) includes experiments listed in both Table 3.1 and Table S3.2. Each individual experiment is marked and colored by the number of methyl groups on each precursor aromatic ring. It is observed that SOA yield decreases as the number of methyl groups increases (Fig. 3.1). A similar yield trend is also observed in previous studies on SOA formation from monocyclic aromatic hydrocarbons, however, different absolute yield values are found, presumably due to higher NO_x levels (Odum, et al., 1997b; Kleindienst et al., 1999; Cocker et al., 2001b; Takekawa et al., 2003; Ng, et al., 2007; Sato, et al., 2012). SOA yields of benzene under comparable low NO_x conditions are higher than that in Sato, et al (2012), Borrás and Tortajada-Genaro (2012) and Martín-Reviejo and Wirtz (2005).

The two product semi-empirical model described by Odum, et al. (1996) is used to fit SOA yield as a function of M_0. Briefly, the two product model assumes that aerosol forming products can be lumped into lower and higher volatility groups whose mass

fraction is defined by α_i and a partitioning parameter $K_{om,\,i}$ ($m^3 \cdot \mu g^{-1}$) described extensively in Odum, et al. (1996). Each monocyclic aromatic hydrocarbon is fitted individually except for those with methyl group number greater than or equal to 4, which are grouped as C_{10+}. The experimental fitting parameters (α_1, $K_{om,\,1}$, α_2 and $K_{om,\,2}$ in Table 3.2) in the two product model were determined by minimizing the sum of the squared of the residuals. The higher-volatility partitioning parameter parameter ($K_{om,2}$) in all yield curve fitting are assigned to a fixed value by assuming similar high volatile compounds are formed during all monocyclic aromatic hydrocarbon photooxidation experiments. Benzene has much higher mass-based stoichiometric coefficients (α_2) than the other monocyclic aromatic compounds indicating that the pathway leading to higher volatility products formation is favored. The lower volatility partitioning parameters ($K_{om,\,1}$) vary widely for each monocyclic aromatic yield fitting curve. Benzene has the lowest $K_{om,\,1}$, toluene has the highest $K_{om,\,1}$, and the rest of monocyclic aromatics have similar mid-range $K_{om,\,1}$ values. The extremely low $K_{om,\,1}$ of benzene indicates that pathways associated with significant volatility decrease occur far less during benzene photooxidation than for monocyclic aromatic compounds with methyl groups. Further, $K_{om,\,1}$ is much lower in multi-methyl group monocyclic aromatic hydrocarbons (with the exception of toluene) while α_1 decreases with methyl group number. This suggests that increasing methyl group number on the aromatic ring suppresses formation of lower volatility products therefore lowering the mass based aerosol yield. This suggests that monocyclic aromatics with more methyl groups are less oxidized per mass since the methyl group carbon is not well oxidized compared with the ring carbon.

The aromatic SOA growth curves (particle concentration M_0 vs. hydrocarbon consumption ΔHC) under similar HC/NO_x are shown in Fig. S3.1. The slope of the growth curve is negatively correlated with the parent aromatics reaction rate (k_{OH}). This observation contrasts with a previous study that observed positive correlation between SOA formation rate and hydrocarbon reaction rate for systems where initial semivolatile products dominate gas-particle phase partitioning (Chan, et al., 2007). The reverse relationship observation in this study indicates that the effect of methyl group number on SOA yield is greater than that of the increasing k_{OH} on SOA yield. There are two possibilities for the methyl group number effect: 1) the methyl group facilitates initial semivolatile products to react into more volatile compounds; 2) the methyl group prevents further generation semivolatile products formation by stereo-hindrance. Therefore, the methyl group increases hydrocarbon mass consumption more than particle mass formation.

The relationship between radical levels and SOA yield was also analyzed. Table S3.3 lists modeled individual average radical concentrations throughout photooxidation while Table S3.4 lists the correlation between SOA yields and individual average radical concentrations. None of the radical parameters (e.g. $\cdot OH/HO_2\cdot$, $HO_2\cdot/ RO_2\cdot$ etc.) is strongly correlated with SOA yield. Average OH radical concentration is the only parameter investigated with a statistically significant correlation ($p<0.05$), as k_{OH} varies with aromatic species and lower average OH concentrations are present with higher k_{OH}. Fig. S3.2 shows the time evolution of $[\cdot OH]$, $[RO_2\cdot]$ and $[HO_2\cdot]$ for different aromatic precursors under similar initial aromatic and NO_x loadings. Higher $[\cdot OH]$ is observed for

aromatic precursors with lower k_{OH} while peroxide radicals ([$RO_2\cdot$] and [$HO_2\cdot$]), which depend on both k_{OH} and [$\cdot OH$], are similar for all precursors. This suggests that SOA mass yield is determined by precursor structure rather than gas-phase oxidation state since radical conditions for each aromatic hydrocarbon are comparable and [$RO_2\cdot$] and [$HO_2\cdot$] reactions are expected to determine SOA formation (Kroll and Seinfeld, 2008)

3.3.2 SOA chemical composition relationship with methyl group number

3.3.2.1 f_{44} vs f_{43}

Organic peaks at *m/z* 43 and *m/z* 44 are key fragments from AMS measurement toward characterization of oxygenated compounds in organic aerosol (Ng, et al., 2010; Ng, et al., 2011). A higher f_{44} and a lower f_{43} indicates a higher degree of oxidation (Ng et al., 2010, 2011).The f_{44} and f_{43} evolution during SOA formation from different monocyclic aromatic hydrocarbon photooxidation is shown for low NO_x conditions (Fig. 3.2). Each marker type represents an individual monocyclic aromatic hydrocarbon with the marker colored by photooxidation time (light to dark). The f_{44} and f_{43} range are comparable to previous chamber studies with slight shift due to differences in initial conditions (e.g. NO_x etc.) (Ng, et al., 2010; Chhabra, et al., 2011; Loza, et al., 2012; Sato, et al., 2012). SOA compositions from monocyclic aromatic hydrocarbon photooxidation under low NO_x are in the low-volatility OOA (LV-OOA) and semi-volatile OOA (SVOOA) range of the f_{44} vs f_{43} triangle (Ng, et al., 2010) with those from benzene on the left side, toluene inside and other monocyclic aromatics on the right side of the triangle confirming that laboratory SOA f_{44} vs f_{43} is precursor dependent (Chhabra, et al., 2011). Evolution of

SOA composition (Heald, et al., 2010; Jimenez, et al., 2009) refers to SOA chemical composition changes with time and f_{44} and f_{43} evolution refers to the change of f_{44} and f_{43} with time. Significant f_{44} and f_{43} evolution is observed for benzene and slightly for toluene, *m*-xylene and tetramethylbenzene.

In this work, average f_{44} and f_{43} are examined to demonstrate the methyl group impact on SOA chemical composition from monocyclic aromatic hydrocarbons. Average f_{44} vs f_{43} is marked with the aromatic compound name in Fig. 3.2. Generally decreasing f_{44} and increasing f_{43} are observed with increasing number of methyl groups on the aromatic ring. Similar trends are also observed in previous studies (Ng, et al., 2010; Chhabra et al., 2011; Sato, et al., 2012). The f_{44} vs f_{43} trend is quantified by linear curve fitting (f_{44}= -0.58 f_{43} + 0.19, R_2 = 0.94). f_{28} is assumed to be equal to f_{44} in the AMS frag Table of Unit Resolution Analysis, which describes the mathematical formulation of the apportionment at each unit resolution sticks to aerosol species, based on ambient studies (Zhang, et al., 2005; Takegawa et al., 2007) and CO^+/CO_2^+ ratio for SOA from aromatic oxidation is found around ~1 (0.9-1.3) (Chhabra et al., 2011). The slope of ~0.5 indicates that $2\Delta f_{44}=-\Delta f_{43}$ or $\Delta(f_{28}+f_{44}) =-\Delta f_{43}$ in SOA formed from monocyclic aromatic hydrocarbons with different numbers of methyl groups. The CO_2^+ fragment ion at *m/z* 44 and $C_2H_3O^+$ fragment ion at *m/z* 43 are two major AMS fragmentation ions from aromatic secondary organic aerosol. No significant $C_3H_7^+$ is observed at *m/z* 43. CO_2^+ represents oxidized aerosol and is associated with carboxylic acids (Alfarra, et al., 2004, Aiken, et al., 2007, Takegawa, et al., 2007; Canagaratna, et al., 2015) while $C_2H_3O^+$ is associated with carbonyls (McLafferty and Turecek, 1993; Ng, et al., 2011). The CO^+ fragment ion at *m/z*

28 can originate from carboxylic acid or alcohol (Canagaratna, et al., 2015). The $\Delta(f_{28}+f_{44}) = -\Delta f_{43}$ relationship observed in this study imply that adding the methyl group to the aromatic ring changes SOA from CO_2^+ to $C_2H_3O^+$ implying a less oxidized SOA chemical composition in AMS mass fragments. While bicyclic hydrogen peroxides are considered to be the predominant species in aerosol phase from monocyclic aromatic photooxidation (Johnson, et al., 2004, 2005; Wyche, et al., 2009; Birdsall et al., 2010; Birdsall and Elrod, 2011; Nakao, et al., 2011), they are less likely to contribute to the CO_2^+ ion fragment. Possible mechanisms to produce SOA products that form the CO_2^+ fragments as well as produce $C_2H_3O^+$ fragments by adding methyl group are described in detail in Section 3.4.

3.3.2.2 H/C vs O/C

Elemental analysis (Aiken, et al., 2007, 2008) is used to elucidate SOA chemical composition and SOA formation mechanisms (Heald, et al., 2010; Chhabra, et al., 2011). Fig. 3.3a shows the H/C and O/C time evolution of average SOA formed from hydrocarbon photooxidation of various monocyclic aromatics under low NO_x conditions (marked and colored similarly to Fig. 3.2). The H/C and O/C ranges are comparable to previous chamber studies with slight shift due to difference in initial conditions (e.g. NO_x etc.) (Chhabra, et al., 2011; Loza, et al., 2012; Sato, et al., 2012). All data points are located in between slope=-1 and slope=-2 (Fig. 3.3a, lower left corner, zoom out panel). This suggests that SOA components from monocyclic aromatic photooxidation contain both carbonyl (ketone or aldehyde) and acid (carbonyl acid and hydroxycarbonyl)

functional groups. These elemental ratios also confirm that SOA formed from monocyclic aromatic hydrocarbon photooxidation under low NO_x are among the LV-OOA and SV-OOA regions (Ng, et al., 2011). The change of elemental ratio (H/C and O/C) with time is referred as elemental ratio evolution. The elemental ratio evolution agrees with the f_{44} vs f_{43} evolution (significant evolution in benzene and slightly for toluene, *m*-xylene and 1,2,4,5-tetramethylbenzene). This study concentrates on average H/C and O/C in order to demonstrate the methyl group impact on SOA chemical composition from monocyclic aromatic hydrocarbons.

Average H/C and O/C location is marked (Fig. 3.3a) for each aromatic compound by name. It is observed that H/C and O/C from SOA formed from *m*-xylene, 1, 2, 4-trimethylbenzene and monocyclic aromatics with more than three methyl groups are similarly distributed in H/C vs O/C. A general decrease in O/C and an increase in H/C are noted as the number of methyl groups on the aromatic ring increase, which is consistent with other studies (Chhabra, et al., 2011; Sato, et al., 2012). The trend indicates that monocyclic aromatics are less oxidized per carbon as the number of methyl groups increases, which can be attributed to less oxidation of the methyl groups compared to the aromatic ring carbons. The elemental ratio trends (O/C decreases and H/C increases as the number of methyl groups increases) are also consistent with the decreasing yield trends with increasing the number of methyl groups (Section 3.3.1), suggesting that SOA yield is dependent on SOA chemical composition. It should also be noticed that the higher O/C and lower H/C observed in SOA formed from 1,2,4-trimethylbenzne (three-methyl-substitute aromatic hydrocarbon) than that from *m*-xylene (two-methyl-substitute

aromatic hydrocarbon) is due to the isomer impact on SOA chemical composition, which is discussed in Chapter 4. Further, the yield and O/C ratio agrees with recent findings that O/C ratio is well correlated to aerosol volatility (Section 3.3.3.2) (Cappa and Wilson, 2012, Yu, et al., 2014) thereby affecting the extent of gas to particle partitioning. The H/C vs O/C trend linear curve (H/C= -1.34 O/C + 2.00, R^2 = 0.95) shows an approximately -1 slope with a y-axis (H/C) intercept of 2. The H/C vs O/C trend slope observed in this work is similar to the toluene and *m*-xylene elemental ratio slope observed under high NO_x and H_2O_2 only conditions observed in Chhabra et al (2011).

The Van Krevelen diagram can also be used to analyze the oxidation pathway from initial SOA precursor to final SOA chemical composition by comparing the initial H/C and O/C ratios from the precursor hydrocarbon to the final SOA H/C and O/C ratios. Fig. 3.3b shows the aromatic precursor location on the left (texted with aromatic hydrocarbon name and colored by methyl group number) and average SOA chemical composition on the right. The SOA H/C increase in the final SOA chemical composition follows the initial aromatic precursor elemental ratio trend. A large O/C increase with a slight H/C increase is observed moving from precursor to SOA composition. SOA formation from hydroperoxide bicyclic compounds contributes to O/C increases without loss of H. The slight H/C increase might result from hydrolysis of ring opened product oligomerization (Jang and Kamens, 2001; Jang et al., 2002; Kalberer, et al., 2004; Sato, et al., 2012). A slight H/C decrease rather than increase is observed in the hexamethylbenzene data suggesting that the six methyl groups sterically inhibits certain reaction mechanism (eg. hydrolysis) to obtain H.

3.3.2.3 OS_c and its prediction

O/C alone may not capture oxidative changes as a result of breaking and forming of bonds (Kroll, et al., 2009). Oxidation state of carbon ($OS_c \approx 2O/C-H/C$) was introduced into aerosol phase component analysis by Kroll et al. (2011). It is considered to be a more accurate metric for describing oxidation in atmospheric organic aerosol (Ng et al., 2011; Canagaratna, et al., 2015; Lambe, et al., 2015) and therefore better correlated with gas-particle partitioning (Aumont, et al., 2012). Average SOA OS_c in this study ranges from -0.9 to 0.3 for monocyclic aromatic photooxidation under low NO_x conditions (Fig. 3.4b) and is comparable to previous studies (Kroll, et al., 2011 (toluene, *m*-xylene and trimethylbenzene); Sato, et al., 2012 (benzene and 1,3,5-trimethylbenzene)). OS_c observed is consistent with OS_c observed in field studies (Kroll, et al., 2011) especially in urban sites (e.g. -1.6～0.1, Mexico City) and supports the major role of monocyclic aromatic precursors in producing anthropogenic aerosol. Average SOA OS_c values are consistent with the LV-OOA and SV-OOA regions (Ng, et al., 2011; Kroll, et al., 2011). OS_c only increases with oxidation time for benzene photooxidation (0.2～0.4).

The methyl group substitute ($-CH_3$) affects O/C and H/C ratios by increasing both carbon and hydrogen number as they relate to SOA OS_c. It is hypothesized here that the methyl group impacts remain similar in SOA elemental ratios as they do in the aromatic precursor ($-CH_3$ dilution effect). This would imply that the methyl group effect on SOA elemental ratio and OS_c from monocyclic aromatic hydrocarbons is predictable from benzene oxidation. Eq-1 and Eq-2 show the prediction formula for O/C and H/C,

respectively, where *i* represents the methyl group number on the monocyclic aromatic precursor, $O/C_{benzene\_SOA}$ and $H/C_{benzene\_SOA}$ are the measured O/C and H/C in SOA from benzene photooxidation experiments.

$$O/C_{pre,i\_SOA} = \frac{6}{i+6}(O/C_{benzene\_SOA}) \quad \text{Eq-1}$$

$$H/C_{pre,i\_SOA} = \frac{2i}{i+6} + \frac{6}{i+6}(H/C_{benzene\_SOA}) \quad \text{Eq-2}$$

Fig. 3.4a shows a comparison of measured (red) and predicted (green) H/C and O/C location marked with corresponding SOA precursor methyl groups. The difference between predicted and measured H/C and O/C ranges from -6.4～1.2% and -11.8～20.9%, respectively. However, the predicted H/C vs O/C line (Eq-1 & Eq-2) is H/C= -1.38O/C +2.00. This is comparable to a measured data fitting line (Section 3.3.2.2 H/C= -1.34 O/C + 2.00, R_2 = 0.95). Predicted OS_c is then calculated based on the predicted H/C and O/C. Fig. 3.4b compares measured (red) and predicted (green) OS_c. The largest O/C and OS_c overestimation is observed in *m*-xylene (marked as 2 in Fig. 4a, bar 2 in Fig. 3.4b). This could be explained by the isomer selected for the two-methyl-group monocyclic aromatic hydrocarbon (*m*-xylene). A detailed analysis on isomer structure impact on SOA chemical composition is found in Chapter 4. The largest O/C and OS_c underestimation is observed in hexamethylbenzene (marked as 6 in Fig. 3.4a, bar 6 in Fig. 3.4b). This suggests that the methyl groups attached to every aromatic carbon exert a steric inhibition effect on certain aromatic oxidation pathways, thus leading to increased importance of aerosol formation from other reaction pathways (possibly fragmentation

Kroll, et al., 2011, see Section 3.4) to form SOA. It is also noticed that O/C and OS_c is slightly overestimated in SOA formed from pentamethylbenzene. This indicates that the methyl group hindrance impact on aromatic hydrocarbon oxidation should be explained by multiple pathways which have different impact on SOA formation.

The correlation between organic mass loading and chemical composition is also analyzed. Organic mass loading is well correlated (Pearson correlation) with chemical composition parameters including f_{44} (0.907), f_{43} (-0.910), H/C (-0.890) and O/C (0.923) (Fig. S3.3). However, previous studies show that O/C and f_{44} decrease as organic mass loading increases (Shilling et al., 2009; Ng, et al., 2010; Pfaffenberger, et al., 2013). The findings of this study indicate that molecular species drive SOA chemical composition rather than organic mass. The positive trend between f_{44} and organic mass loading is driven by benzene and toluene experiments (Fig. S3.3) where the high mass loading results are concurrent with high f_{44} results. However, the f_{44} change with mass loading increase during benzene and toluene photooxidation is less significant compared with the f_{44} difference caused by number of methyl groups on aromatic ring. Moreover, no significant correlation was found between mass loading and f_{44} or O/C when compared under similar mass loadings (including f_{44} at low mass loading time point of toluene and benzene photoxidation). Organic nitrate accounts for less than 10% organic in SOA components in all monocyclic aromatic hydrocarbon photooxidation experiments in this work according to AMS measurement and will not be discussed.

3.3.3 Physical property relationship with methyl group number

3.3.3.1 SOA Density

SOA mass density is a fundamental parameter in understanding aerosol morphology, dynamics, phase and oxidation (De Carol, et al., 2004; Katrib, et al., 2005; Dinar, et al., 2006; Cross, et al., 2007). SOA density ranged from 1.24-1.44 g/cm^3 for all aromatic-NO_x photooxidation experiments in this study. The range is comparable to previous studies under similar conditions (Ng, et al; 2007; Sato, et al., 2010; Esther B Borrás and Tortajada-Genaro, 2012). A general decreasing density trend is found with increasing methyl group number on precursor aromatic rings (see Fig. 3.5a). Correlation between SOA density and chemical composition was statistically analyzed (Table S3.5). Besides the strong correlation with methyl group number (-0.943, Fig. 3.5a), SOA density was also well correlated with O/C ratio (0.873, Fig. 3.5b) and other measures of bulk chemical composition (Table S3.5). Bahreini et al (2005) reported a density increase trend with f_{44} in other compounds while Pang, et al. (2006) found that SOA density increases with O/C ratio. Kuwata, et al., 2011(Eq-3) and Nakao, et al., 2013 suggested a quantified relationship between SOA density and SOA elemental ratio. Eq-3 developed by

$$\rho = \frac{12+H/C+16\times O/C}{7+5\times H/C+4.15\times O/C} \qquad \text{Eq-3}$$

Kuwata, et al. (2011) is used in this work to predict density based on elemental ratio in order to explore the methyl group impact on SOA formation. Fig. 3.5c shows a good

agreement between predicted and measured SOA densities (-6.58% ~ 10.42%). However, SOA density difference between prediction and measurement change from positive (0 or1 methyl group) to negative (2, 3, 4 or 5 methyl groups) with increasing methyl group number (except hexamethylbenzene) implying that the increase of methyl groups promotes mechanism(s) leading to changes in the ratio of several key organic fragments (e.g., *m/z* 28: *m/z* 44) thereby challenging the applicability of the default fragment table for elemental ratio analysis. It is possible that $CO^+/CO_2^+$and H_2O^+/CO_2^+ ratios are different in SOA formed from different aromatic precursors. Nakao, et al (2013) shows that H_2O^+/CO_2^+ increases with methyl group number due to the constant H_2O^+ fraction and a decrease in CO_2^+ fraction. Canagaratna, et al (2015) demonstrated that $CO^+/CO_2^+$and H_2O^+/CO_2^+ are underestimated in certain compounds (especially alcohols). Assuming that the major impact of methyl group on SOA composition is to change –COOH to -$COCH_3$ (or other cyclic isomers), f_{CO2+} will decrease but H_2O^+ and CO^+ fraction might not change linearly. The alcohol contribution to $CO^+/CO_2^+$and H_2O^+/CO_2^+ gradually grows as the methyl group prevents acid formation. Therefore, AMS measurements might underestimate O/C. This is consistent with the density prediction from elemental ratios where a change of error from positive to negative is seen as the number of methyl groups changes from less than two to two or more than two, with the exception of hexamethylbenzene. This might relate to the difference in SOA formation pathways due to steric hindrance of the six methyl groups during hexamethylbenzene oxidation.

3.3.3.2 SOA Volatility

SOA volatility is a function of oxidation, fragmentation, oligomerization and SOA mass (Kalberer, et al., 2004; Salo, et al., 2011; Tritscher, et al., 2011; Yu, et al., 2014). Bulk SOA volatility can be described by the VFR after heating SOA to a fixed temperature in a thermodenuder. VFRs for SOA formed early in the experiment are around 0.2 for all monocyclic aromatic precursors and then increase as the experiment progresses. Increasing VFR indicates the gas to particle partitioning of more oxidized products, which may include oligomerization products formed during aromatic photooxidation. The VFR trends and ranges are comparable to previous studies (Kalberer et al., 2004; Qi et al., 2010a; Qi et al., 2010b; Nakao et al., 2012). Fig. 3.6a shows the relationship between SOA precursor methyl group number and SOA VFR at the end of the experiment (VFR_{end}). VFR shows a significant decreasing trend with increasing methyl group number from benzene to 1, 2, 4, 5-tetramethylbenzene. This implies that volatility of SOA-forming products increases as the number of methyl groups on the aromatic ring increases. There is also a slight increase in VFR from 1, 2, 4, 5-tetramethylbenzene to hexamethylbenzene; however, VFR in SOA formed from all C_{10+} group aromatics is lower than that of 1, 2, 4-trimethylbenzene. The changing VFR trend suggests that chemical components contributing to SOA formation become different when more than four methyl groups are attached to a single aromatic ring. A positive correlation (0.755, $p=0.05$) found between mass loading and VFR_{end} implies that the lower the volatility in the products formed from aromatic hydrocarbons, the higher the SOA mass concentration. An opposite correlation between mass loading and VFR is found in

previous studies due to the partitioning of more volatile compounds to the particle phase at high mass loading (Tritscher, et al., 2011;Salo, et al., 2011). Therefore, mass loading does not directly lead to the VFR trend in the current study, rather it is the methyl group number in the SOA precursor that affects the composition of SOA and therefore the monocyclic aromatic hydrocarbon yield (section 3.3.1) and volatility. The correlation between SOA volatility (VFR) and chemical composition is statistically analyzed (Table S3.5). O/C (0.937, $p = 0.002$) and OS_c (0.932, $p = 0.02$) have the highest correlation with VFR_{end}. Previous studies also observed that lower aerosol volatility is correlated to higher O/C ratio (Cappa and Wilson, 2012, Yu, et al., 2014) and OS_c (Aumont, et al., 2012; Hildebrandt Ruiz, et al., 2014). Fig. 3.6b and Fig. 3.6c illustrate the VFR_{end} and O/C or OS_c relationship among all the monocyclic aromatic precursors investigated in this study. Benzene and toluene are located on the right upper corner in both graphs suggesting that significantly more oxidized and less volatile components are formed from monocyclic aromatic precursors with less than two methyl groups. The VFR_{end} and chemical components relationship becomes less significant when only monocyclic aromatic precursors with more than two methyl groups are considered.

3.4 Discussion

3.4.1 SOA formation pathway from aromatic hydrocarbon

Bicyclic peroxide compounds are considered to be important SOA forming products from monocyclic aromatic photooxidation (Johnson, et al., 2004, 2005; Song, et al., 2005; Wyche, et al., 2009; Birdsall et al., 2010; Birdsall and Elrod, 2011; Nakao, et al., 2011).

However, the significant CO_2^+ fragment (f_{44}) observed for SOA by the AMS indicates a contribution of an additional pathway to SOA formation from monocyclic aromatic hydrocarbon photooxidation since it is unlikely that bicyclic peroxides could produce a CO_2^+ in the AMS. Hydrogen abstraction from the methyl group is not further discussed here as it accounts for less than 10% monocyclic aromatic oxidation pathway (Calvert, et al., 2002). However, it is important to consider the further reaction of bicyclic peroxide ring scission products, especially in the presence of NO_x (Jang and Kamens, 2001; Atkinson and Arey, 2003; Song, et al., 2005; Hu, et al., 2007; Birdsall and Elrod, 2011; Carter and Heo, 2013). First generation ring scission products include 1, 2-dicarbonyls (glyoxal and methylglyoxal) and unsaturated 1, 4-dicarbonyls (Forstner, et al., 1997; Jang and Kamens, 2001; Birdsall and Elrod, 2011). These dicarbonyls are small volatile molecules that are unlikely to directly partition into the particle phase. However, these small molecules can potentially grow into low volatility compounds through oligomerization. Previous studies suggest that oligomerization can be an important pathway for SOA formation from monocyclic aromatic precursors (Edney, et al., 2001; Baltensperger, et al., 2005; Hu, et al., 2007; Sato, et al., 2012). While Kalberer, et al (2004) proposed an oligomerization pathway of 1, 2-dicarbonyls, Arey, et al (2008) found that unsaturated 1, 4-dicarbonyls have a higher molar yield than 1, 2-dicarbonyls in OH radical-initiated reaction of monocyclic aromatic hydrocarbons. Further, OH radical reaction and photolysis rates are observed to be lower in 1, 2-dicarbonyls photolysis (Plum, et al., 1983; Chen, et al., 2000; Salter, et al., 2013; Lockhart, et al; 2013) than unsaturated 1, 4-dicarbonyls (Bierbach, et al., 1994; Xiang, et al; 2007). This suggests

that secondary reaction of unsaturated 1, 4-dicarbonyls is more important than that of 1, 2-dicarbonyls. Previous studies have found that unsaturated 1, 4-dicarbonyls react to form small cyclic furanone compounds (Jang and Kamens, 2001; Bloss, et al., 2005; Aschmann, et al., 2011). Oligomerization is possible for these small cyclic compounds based on their similar molecular structure with glyoxal and methylglyoxal (Fig. 3.7 c-2-1 & c-2-2 pathway, Fig. S3.4). Products from further oligomerization of ring opening compounds can also partition into the aerosol phase and contribute to SOA formation. Hydrolysis is necessary in both oligomerization pathways (Fig. S3.4 and Kalberer, et al., 2004), which is consistent with the slight H/C increase observed for most monocyclic aromatic hydrocarbon photooxidation results in this study. However, Nakao et al. (2012) showed that the glyoxal impact on SOA formation is majorly due to OH radical enhancement with glyoxal instead of oligomerization, especially under dry conditions. This indicates that oligomerization from small cyclic furanone is more likely to contribute more to SOA formation than 1, 2- dicarbonyl in this work. Other pathways reported in previous studies are also possible to contribute to SOA formation here (Edney, et al., 2001 (polyketone); Jang and Kamens, 2001 (aromatic ring retaining products; six and five member non-aromatic ring products; ring opening products); Bloss, et al., 2005 (benzoquinone, epoxide, phenol); Carter and Heo, 2013 (bicyclic hydroperoxide)). Our work only addresses differences in the oligomerization pathway contribution to form SOA from monocyclic aromatic hydrocarbons.

A simplified monocyclic aromatic oxidation mechanism for low NO_x conditions is shown (Fig. 3.7 & Fig. 3.8; the figures only illustrate monocyclic aromatic oxidation related to

particle formation). Fig. 3.7 illustrates the oxidation, fragmentation and oligomerization after initial OH addition to aromatic ring, Fig. 3.8 shows the kinetic scheme for SOA formation from monocyclic aromatic hydrocarbons. S_1, S_2 and S_3 represent bicyclic hydroperoxide compounds, ring opening compounds and oligomerization products, respectively. Table S3.6 summarizes the predicted vapor pressures of the benzene photooxidation products using SIMPOL (Pankow and Asher, 2008). The bicyclic hydroperoxide (S_1, Fig. 3.8) is more volatile than the oligomers (S_3 in Fig. 3.8). The volatilities of the bicyclic hydroperoxides are sufficiently high to allow additional oxidation (e.g. add one more hydroperoxide functional group to form $C_6H_6O_8$). The further oxidized bicyclic hydroperoxide vapor pressure is predicted to be similar to oligomerization products from reaction of c-2-1 (Fig. S3.4) with glyoxal. The higher vapor pressure of oligomer products from glyoxal as compared to oligomers from other products indicates that bicyclic hydroperoxides (S_1) contribute more to SOA formation in benzene than oligomerization products (S_3), especially at higher particle mass loadings, as compared with monocyclic aromatic hydrocarbons containing methyl groups according to the two product model fitting (Fig. 1 and Table. 3.2).

3.4.2 Methyl group number impact on SOA formation pathway from aromatic hydrocarbon

It is observed that as the number of methyl groups on the monocyclic aromatic precursor increases, mass yield (Section 3.3.1), overall oxidation per carbon (Section 3.3.2), and SOA density all decrease and SOA volatility increases. The observed yield trend is

attributed to the increasing methyl group number enhancing aromatic fragmentation and inhibiting oligomerization. First, the methyl group stabilizes the ring opening radical (Atkinson, 2007; Ziemann, 2011), thus favoring the ring opening pathway. Second, the methyl group hinders cyclic compound formation and oligomerization (Fig. 3.7). Oligomerization is unlikely to occur directly from non-cyclic dicarbonyls (Kalberer, et al, 2004) or indirectly from cyclic compounds formed by unsaturated dicarbonyls (Fig. S3.5) with increasing methyl group number. Methyl groups both inhibit oligomerization (Fig.3.7 (c-1-3)) and prevent the formation of cyclic compounds from unsaturated dicarbonyls (Fig.3.7 (c-2-3)) when methyl groups are attached to both ends of an unsaturated dicarbonyl. Oligomerization is possible for these ketones through reactions such as aldol condensation and hemiacetal formation (Jang et al., 2002) under acidic conditions. However, this is less favored for the current study in the absence of acidic seeds. Hence, less cyclic compounds are available for subsequent oligomerization, leading to more volatile products and a decrease in SOA formation. Moreover, the SOA composition trend is well explained by a $-CH_3$ dilution effect. Previous studies on the different gas phase (Forstner, et al., 1997; Yu, et al., 1997) and particle phase (Hamilton, et al., 2005; Sato, et al., 2007; Sato, et al., 2012) products supports this methyl group dilution theory. A typical example is that more 3-methyl-2,5-furandione is observed in *m*-xylene than toluene and vice versa for 2,5-furandione. Sato et al. (2010) suggests that more low-reactive ketones are produced rather than aldehydes with increasing number of substituents. However, most ketones or aldehydes detected are so volatile that they mostly exist in the gas phase (Forstner, et al., 1997; Yu, et al., 1997; Cocker, et al.,

2001b; Jang and Kamens, 2001). Taken collectively, this implies the importance of oligomerization and methyl substitutes on SOA formation.

The observation of a slight H/C decrease from hexamethylbenzene to its SOA components in contrast with the increasing trend for monocyclic aromatic photooxidation for zero to five methyl group substitutes (Section 3.3.2.2) suggests that hydrolysis followed by oligomerization might not be significant when all aromatic ring carbons have attached methyl groups. Besides, the higher O/C and lower H/C (or the higher OS_c) than predicted in Section 3.3.2.3 indicates that SOA components from hexamethylbenzene photooxidation are more oxidized per carbon due to oxidation of the methyl groups, which is possibly related to the steric hindrance of the six methyl groups. Moreover, there is a slightly increasing trend in VFR from 1, 2, 4, 5-tetramethylbenzene to hexamethylbenzene (Section 3.3.3.2). Further studies (e.g. photooxidation using isotope labeled methyl group hexamethylbenzene) are required to probe the unique SOA aspects from hexamethylbenzene photooxidation.

3.5 Conclusion

The impact of the number of methyl group substituents on SOA formation has been comprehensively studied in this work by integrating SOA yield with SOA chemical composition and SOA physical properties. A generally decreasing trend is found in the SOA mass yield and the carbon number averaged oxidation level with increasing number of methyl groups. SOA physical properties agree with yield and oxidation results. Therefore, this study demonstrates that the addition of methyl group substitutes to

monocyclic aromatic precursors decreases the oxidation of aromatic hydrocarbon to less volatile compounds. Offsetting the amount of CO_2^+ and $C_2H_3O^+$ suggests a methyl group dilution effect on SOA formation from monocyclic aromatic hydrocarbons. The proposed methyl group dilution effect is then applied successfully to the predict SOA elemental ratio. Overall, this study clearly demonstrates the methyl group impact on SOA formation from monocyclic aromatic hydrocarbons.

Benzene and toluene are evaluated as the most important monocyclic aromatic precursors to SOA formation among the six compounds studied due to their high SOA yields and highly oxidized components. Hexamethylbenzene is found to be significantly more oxidized than predicted based on other monocyclic aromatic hydrocarbons studied here. This implies uniqueness in the methyl group behavior (no –H on aromatic ring) in hexamethylbenzene. Oligomerization is proposed to be an important pathway for SOA formation from monocyclic aromatic hydrocarbons. It is likely that oligomerization is even more valuable to SOA formation from monocyclic aromatic hydrocarbons under polluted areas (catalyzed effect, Jang, et al., 2002; Iinuma, et al., 2004; Noziere, et al., 2008) and ambient humidity (Liggio, et al., 2015a, b; Hastings, et al., 2005).

3.6 Reference

Aiken, A. C., DeCarlo, P. F. and Jimenez, J. L.: Elemental analysis of organic species with electron ionization high-resolution mass spectrometry, Anal. Chem., 79(21), 8350-8358, 2007.

Aiken, A. C., DeCarlo, P. F., Kroll, J. H., Worsnop, D. R., Huffman, J. A., Docherty, K. S., Ulbrich, I. M., Mohr, C., Kimmel, J. R., Sueper, D., Sun, Y., Zhang, Q., Trimborn, A., Northway, M., Ziemann, P. J., Canagaratna, M. R., Onasch, T. B., Alfarra, M. R., Prevot, A. S. H., Dommen, J., Duplissy, J., Metzger, A., Baltensperger, U. and Jimenez, J. H.: O/C and OM/OC ratios of primary, secondary, and ambient organic aerosols with high-resolution time-of-flight aerosol mass spectrometry, Environ. Sci. Technol., 42(12), 4478-4485, 2008.

Alfarra, M. R., Coe, H., Allan, J. D., Bower, K. N., Boudries, H., Canagaratna, M. R., Jimenez, J. L., Jayne, J. T., Garforth, A. A., Li, S-M. and Worsnop, D. R.: Characterization of urban and rural organic particulate in the lower Fraser valley using two aerodyne aerosol mass spectrometers, Atmos. Environ., 38(34), 5745-5758, 2004.

Arey, J., Obermeyer, G., Aschmann, S. M., Chattopadhyay, S., Cusick, R. D. and Atkinson, R.: Dicarbonyl products of the OH radical-initiated reaction of a series of aromatic hydrocarbons, Environ. Sci. Technol., 43(3), 683-689, 2008.

Aschmann, S. M., Arey, J. and Atkinson, R.: Rate constants for the reactions of OH radicals with 1, 2, 4, 5-tetramethylbenzene, pentamethylbenzene, 2, 4, 5-trimethylbenzaldehyde, 2, 4, 5-trimethylphenol, and 3-methyl-3-hexene-2, 5-dione and products of OH+ 1, 2, 4, 5-tetramethylbenzene, J. Phys. Chem. A., 117(12), 2556-2568, 2013.

Aschmann, S. M., Nishino, N., Arey, J. and Atkinson, R.: Kinetics of the Reactions of OH Radicals with 2-and 3-Methylfuran, 2, 3-and 2, 5-Dimethylfuran, and E-and Z-3-Hexene-2, 5-dione, and Products of OH+ 2, 5-Dimethylfuran, Environ. Sci. Technol., 45(5), 1859-1865, 2011.

Atkinson, R.: Rate constants for the atmospheric reactions of alkoxy radicals: An updated estimation method, Atmos. Environ., 41(38), 8468-8485, 2007.

Atkinson, R. and Arey, J.: Atmospheric degradation of volatile organic compounds, Chem. Rev., 103(12), 4605-4638, 2003.

Aumont, B., Valorso, R., Mouchel-Vallon, C., Camredon, M., Lee-Taylor, J. and Madronich, S.: Modeling SOA formation from the oxidation of intermediate volatility n-alkanes, Atmos. Chem. Phys., 12(16), 7577-7589, 2012.

Bahreini, R., Keywood, M. D., Ng, N. L., Varutbangkul, V., Gao, S., Flagan, R. C., Seinfeld, J. H., Worsnop, D. R. and Jimenez, J. L.: Measurements of secondary organic aerosol from oxidation of cycloalkenes, terpenes, and *m*-xylene using an Aerodyne aerosol mass spectrometer, Environ. Sci. Technol., 39(15), 5674-5688, 2005.

Baltensperger, U., Kalberer, M., Dommen, J., Paulsen, D., Alfarra, M. R., Coe, H., Fisseha, R., Gascho, A., Gysel, M., Nyeki, S., Sax, M., Steinbacher, M., Prevot, A. S. H., Sjögren, S., Weingartnera, E. and Zenobib, R.: Secondary organic aerosols from anthropogenic and biogenic precursors, Faraday. Discuss., 130, 265-278, 2005.

Bierbach, A., Barnes, I., Becker, K. H. and Wiesen, E.: Atmospheric chemistry of unsaturated carbonyls: Butenedial, 4-oxo-2-pentenal, 3-hexene-2, 5-dione, maleic anhydride, 3H-furan-2-one, and 5-methyl-3H-furan-2-one, Environ. Sci. Technol., 28(4), 715-729, 1994.

Birdsall, A. W., Andreoni, J. F. and Elrod, M. J.: Investigation of the role of bicyclic peroxy radicals in the oxidation mechanism of toluene, J. Phys. Chem. A., 114(39), 10655-10663, 2010.

Birdsall, A. W. and Elrod, M. J.: Comprehensive NO-dependent study of the products of the oxidation of atmospherically relevant aromatic compounds, J. Phys. Chem. A., 115(21), 5397-5407, 2011.

Bloss, C., Wagner, V., Jenkin, M. E., Volkamer, R., Bloss, W. J., Lee, J. D., Heard, D. E., Wirtz, K., Martin-Reviejo, M., Rea, G, Wenger, J. C., and Pilling M. J.: Development of a detailed chemical mechanism (MCMv3. 1) for the atmospheric oxidation of aromatic hydrocarbons, Atmos. Chem. Phys., 5(3), 641-664, 2005.

Borrás, E. and Tortajada-Genaro, L. A.: Secondary organic aerosol formation from the photo-oxidation of benzene, Atmos. Environ., 47, 154-163, 2012.

Buczynska, A. J., Krata, A., Stranger, M., Godoi, A. F. L., Kontozova-Deutsch, V., Bencs, L., Naveau, I., Roekens, E. and Van Grieken, R.: Atmospheric BTEX-concentrations in an area with intensive street traffic, Atmos. Environ., 43(2), 311-318, 2009.

Calvert, J. G., Atkinson, R., Becker, K. H., Kamens, R. M., Seinfeld, J. H., Wallington, T. J. and Yarwood, G.: The mechanisms of atmospheric oxidation of aromatic hydrocarbons, Oxford University Press New York, 2002.

Canagaratna, M. R., Jayne, J. T., Jimenez, J. L., Allan, J. D., Alfarra, M. R., Zhang, Q., Onasch, T. B., Drewnick, F., Coe, H., Middlebrook, A., Delia, A., Williams, L. R., Trimborn, A. M., Northway, M. J., DeCarlo, P. F., Kolb, C. E., Davidovits, P. and

Worsnop D. R.: Chemical and microphysical characterization of ambient aerosols with the aerodyne aerosol mass spectrometer, Mass. Spectrom. Rev., 26(2), 185-222, 2007.

Canagaratna, M. R., Jimenez, J. L., Kroll, J. H., Chen, Q., Kessler, S. H., Massoli, P., Hildebrandt Ruiz, L., Fortner, E., Williams, L. R., Wilson, K. R., Surratt, J. D., Donahue, N. M., Jayne, J. T. and Worsnop, D. R.: Elemental ratio measurements of organic compounds using aerosol mass spectrometry: characterization, improved calibration, and implications, Atmos. Chem. Phys., 15(1), 253-272, 2015.

Cappa, C. D. and Wilson, K. R.: Multi-generation gas-phase oxidation, equilibrium partitioning, and the formation and evolution of secondary organic aerosol, Atmos. Chem. Phys., 12(20), 9505-9528, 2012.

Carter, W. P. L. and Heo, G.: Development of revised SAPRC aromatics mechanisms, Atmos. Environ., 77, 404-414, 2013.

Carter, W. P. L., Cocker III, D. R., Fitz, D. R., Malkina, I.L., Bumiller, K., Sauer, C.G., Pisano, J.T., Bufalino, C., Song, C.: A new environmental chamber for evaluation of gas-phase chemical mechanisms and secondary aerosol formation, Atmos. Environ., 39(40), 7768-7788, 2005.

Carter, W. P. L. and Heo, G.: Development of Revised SAPRC Aromatics Mechanisms, California Air Resources Board, Sacramento, CA, USA, 2012.Chan, A. W. H., Kroll, J. H., Ng, N. L. and Seinfeld, J. H.: Kinetic modeling of secondary organic aerosol formation: effects of particle-and gas-phase reactions of semivolatile products, Atmos. Chem. Phys., 7(15), 4135-4147, 2007.

Chen, Y., Wang, W. and Zhu, L.: Wavelength-dependent photolysis of methylglyoxal in the 290-440 nm region, J. Phys. Chem. A., 104(47), 11126-11131, 2000.

Chhabra, P. S., Ng, N. L., Canagaratna, M. R., Corrigan, A. L., Russell, L. M., Worsnop, D. R., Flagan, R. C. and Seinfeld, J. H.: Elemental composition and oxidation of chamber organic aerosol, Atmos. Chem. Phys., 11(17), 8827-8845, 2011.

Cocker III, D. R.., Flagan, R. C. and Seinfeld, J. H.: State-of-the-art chamber facility for studying atmospheric aerosol chemistry, Environ. Sci. Technol., 35(12), 2594-2601, 2001a.

Cocker III, D. R., Mader, B. T., Kalberer, M., Flagan, R.C. and Seinfeld, J. H.: The effect of water on gas–particle partitioning of secondary organic aerosol: II. *m*-xylene and 1, 3, 5-trimethylbenzene photooxidation systems, Atmos. Environ., 35(35), 6073-6085, 2001b.

Cross, E. S., Slowik, J. G., Davidovits, P., Allan, J. D., Worsnop, D. R., Jayne, J. T., Lewis, D. K., Canagaratna, M. and Onasch, T. B.: Laboratory and ambient particle

density determinations using light scattering in conjunction with aerosol mass spectrometry, Aerosol Sci. Tech., 41(4), 343-359., 2007.

Darouich, T. AI., Behar, F. and Largeau., C.: Thermal cracking of the light aromatic fraction of Safaniya crude oil–experimental study and compositional modelling of molecular classes. Org. Geochem., 37(9), 1130-1154, 2006.

DeCarlo, P. F., Kimmel, J. R., Trimborn, A., Northway, M. J., Jayne, J. T., Aiken, A. C., Gonin, M., Fuhrer, K., Horvath, T., Docherty, K. S., Worsnop, D. R. and Jimenez, J. L.: Field-deployable, high-resolution, time-of-flight aerosol mass spectrometer. Anal. Chem., 78(24), 8281-8289, 2006.

DeCarlo, P. F., Slowik, J. G., Worsnop, D. R., Davidovits, P. and Jimenez, J. L.: Particle morphology and density characterization by combined mobility and aerodynamic diameter measurements. Part 1: Theory, Aerosol Sci. Tech., 38(12), 1185-1205, 2004.

Diehl, J. W. and Sanzo, F. P. Di.: Determination of aromatic hydrocarbons in gasolines by flow modulated comprehensive two-dimensional gas chromatography, J. Chromatogr. A., 1080(2): 157-165, 2005.

Dinar, E., Mentel, T. and Rudich, Y.: The density of humic acids and humic like substances (HULIS) from fresh and aged wood burning and pollution aerosol particles, Atmos. Chem. Phys., 6(12), 5213-5224, 2006.

Duplissy, J., DeCarlo, P. F., Dommen, J., Alfarra, M. R., Metzger, A., Barmpadimos, I., Prevot, A. S., Weingartner, E., Tritscher, T. and Gysel, M.: Relating hygroscopicity and composition of organic aerosol particulate matter, Atmos. Chem. Phys., 11(3), 1155-1165, 2011.

Edney, E., Driscoll, D., Weathers, W., Kleindienst, T., Conver, T., McIver, C. and Li, W.: Formation of polyketones in irradiated toluene/propylene/NO_x/air mixtures, Aerosol Science & Technology, 35(6), 998-1008, 2001.

Forstner, H. J. L., Flagan, R. C. and Seinfeld, J. H.: Secondary organic aerosol from the photooxidation of aromatic hydrocarbons: Molecular composition, Environ. Sci. Technol., 31(5), 1345-1358, 1997.

Fraser, M. P., Cass, G. R., Simoneit, B. R. and Rasmussen, R.: Air quality model evaluation data for organics. 5. C_6-C_{22} nonpolar and semipolar aromatic compounds, Environ. Sci. Technol., 32(12), 1760-1770, 1998.

Glasson, W. A. and Tuesday, C. S.: Hydrocarbon reactivities in the atmospheric photooxidation of nitric oxide, Environ. Sci. Technol., 4(11), 916-924., 1970.

Hallquist, M., Wenger, J. C., Baltensperger, U., Rudich, Y., Simpson, D., Claeys, M., Dommen, J., Donahue, N. M., George, C., Goldstein, A. H., Hamilton, J. F., Herrmann, H., Hoffmann, T., Iinuma, Y., Jang, M., Jenkin, M. E., Jimenez, J. L., Kiendler-Scharr, A., Maenhaut, W., McFiggans, G., Mentel, Th. F., Monod, A., Prévôt, A. S. H., Seinfeld, J. H., Surratt, J. D., Szmigielski, R. and Wildt, J.: The formation, properties and impact of secondary organic aerosol: current and emerging issues, Atmos. Chem. Phys., 9(14), 5155-5236, 2009.

Hamilton, J. F., Webb, P. J., Lewis, A. C. and Reviejo, M. M.: Quantifying small molecules in secondary organic aerosol formed during the photo-oxidation of toluene with hydroxyl radicals, Atmos. Environ., 39(38), 7263-7275, 2005.

Hastings, W. P., Koehler, C. A., Bailey, E. L. and De Haan, D. O.: Secondary organic aerosol formation by glyoxal hydration and oligomer formation: Humidity effects and equilibrium shifts during analysis, Environ. Sci. Technol., 39(22), 8728-8735, 2005.

Heald, C. L., Kroll, J. H., Jimenez, J. L., Docherty, K. S., DeCarlo, P. F., Aiken, A. C., Chen, Q., Martin, S. T., Farmer, D. K. and Artaxo, P.: A simplified description of the evolution of organic aerosol composition in the atmosphere, Geophys. Res. Lett, 37(8), L08803, 2010.

Henze, D. K., Seinfeld, J. H., Ng, N. L., Kroll, J. H., Fu, T-M., Jacob, D. J., Heald, C. L.: Global modeling of secondary organic aerosol formation from aromatic hydrocarbons: high-vs. low-yield pathways, Atmos. Chem. Phys., 8(9), 2405-2421, 2008.

Hildebrandt Ruiz, L., Paciga, A., Cerully, K., Nenes, A., Donahue, N. M. and Pandis, S. N.: Aging of secondary organic aerosol from small aromatic VOCs: changes in chemical composition, mass yield, volatility and hygroscopicity, Atmos. Chem. Phys. Disc., 14(22), 31441-31481, 2014.

Holzinger, R., Kleiss, B., Donoso, L. and Sanhueza, E.: Aromatic hydrocarbons at urban, sub-urban, rural (8° 52′ N; 67° 19′ W) and remote sites in Venezuela, Atmos. Environ., 35(29), 4917-4927, 2001.

Hu, D., Tolocka, M., Li, Q. and Kamens, R. M.: A kinetic mechanism for predicting secondary organic aerosol formation from toluene oxidation in the presence of NOx and natural sunlight, Atmos. Environ., 41(31), 6478-6496, 2007.

Hu, L., Millet, D. B., Baasandorj, M., Griffis, T. J., Travis, K. R., Tessum, C. W., Marshall, J. D., Reinhart, W. F., Mikoviny, T., Müller, M., Wisthaler, A., Graus, M., Warneke, C., and de Gouw, J.:Emissions of C_6–C_8 aromatic compounds in the United States: Constraints from tall tower and aircraft measurements, J. Geophys. Res.-Atmos., 120(2), 826-842, 2015.

Iinuma, Y., Böge, O., Gnauk, T. and Herrmann, H.: Aerosol-chamber study of the α-pinene/O_3 reaction: influence of particle acidity on aerosol yields and products, Atmos. Environ., 38(5), 761-773, 2004.

Jang, M., Czoschke, N. M., Lee, S., and Kamens, R. M.: Heterogeneous atmospheric aerosol production by acid-catalyzed particle-phase reactions, Science, 298(5594), 814-817, 2002.

Jang, M. and Kamens, R.M.: Characterization of secondary aerosol from the photooxidation of toluene in the presence of NO_x and 1-propene, Environ. Sci. Technol., 35(18), 3626-3639, 2001.

Jimenez, J. L., Canagaratna, M. R., Donahue, N. M., Prevot, A. S. H., Zhang, Q., Kroll, J. H., DeCarlo, P. F., Allan, J. D., Coe, H., Ng, N. L., Aiken, A. C., Docherty, K. S., Ulbrich, I. M., Grieshop, A. P., Robinson, A. L., Duplissy, J., Smith, J. D., Wilson, K. R., Lanz, V. A., Hueglin, C., Sun, Y. L., Tian, J., Laaksonen, A., Raatikainen, T., Rautiainen, J., Vaattovaara, P., Ehn, M., Kulmala, M., Tomlinson, J. M., Collins, D. R., Cubison, M. J., Dunlea1, E., J., Huffman, J. A., Onasch, T. B., Alfarra, M. R., Williams, P. I., Bower, K., Kondo, Y., Schneider, J., Drewnick, F., Borrmann, S., Weimer, S.,, Demerjian, K., Salcedo, D., Cottrell, L., Griffin, R., Takami, A., Miyoshi, T., Hatakeyama, S., Shimono, A., Sun, J. Y., Zhang, Y. M., Dzepina, K., Kimmel, J. R., Sueper, D., J. Jayne, T., Herndon, S. C., Trimborn, A. M., Williams, L. R., Wood, E. C., Middlebrook, A. M., Kolb C. E., Baltensperger, U. and Worsnop D. R.: Evolution of organic aerosols in the atmosphere, Science, 326(5959), 1525-1529, 2009.

Johnson, D., Jenkin, M. E., Wirtz, K., Martin-Reviejo, M.: Simulating the formation of secondary organic aerosol from the photooxidation of aromatic hydrocarbons, Environ. Chem., 2(1), 35-48, 2005.

Johnson, D., Jenkin, M. E., Wirtz, K., Martin-Reviejo, M.: Simulating the formation of secondary organic aerosol from the photooxidation of toluene, Environ. Chem., 1(3), 150-165, 2004.

Kalberer, M., Paulsen, D., Sax, M., Steinbacher, M., Dommen, J., Prevot, A. S. H., Fisseha, R., Weingartner, E., Frankevich, V. and Zenobi, R.: Identification of polymers as major components of atmospheric organic aerosols, Science, 303(5664), 1659-1662, 2004.

Kanakidou, M., Seinfeld, J. H., Pandis, S. N., Barnes, I., Dentener, F. J, Facchini, M. C., Van Dingenen, R., Ervens, B., Nenes, A., Nielsen, C. J., Swietlicki, E., Putaud, J. P., Balkanski, Y., Fuzzi, S., Horth, J., Moortgat, G. K., Winterhalter, R., Myhre, C. E. L., Tsigaridis, K., Vignati, E., Stephanou, E. G., and Wilson, J.: Organic aerosol and global climate modelling: a review, Atmos. Chem. Phys., 5(4), 1053-1123, 2005.

Katrib, Y., Martin, S. T., Rudich, Y., Davidovits, P., Jayne, J. T. and Worsnop, D. R.: Density changes of aerosol particles as a result of chemical reaction, Atmos. Chem. Phys., 5(1), 275-291, 2005.

Kleindienst, T. E., Smith, D. F., Li, W., Edney, E. O., Driscoll, D. J., Speer, R. E. and Weathers, W. S.: Secondary organic aerosol formation from the oxidation of aromatic hydrocarbons in the presence of dry submicron ammonium sulfate aerosol, Atmos. Environ., 33(22), 3669-3681, 1999.

Kroll, J. H., Donahue, N. M., Jimenez, J. L., Kessler, S. H., Canagaratna, M. R., Wilson, K. R., Altieri, K .E., Mazzoleni, L. R., Wozniak, A. S., Bluhm, H., Mysak, E. R., Smith, J. D., Kolb, C. E. and Worsnop D. R.: Carbon oxidation state as a metric for describing the chemistry of atmospheric organic aerosol, Nature Chemistry, 3(2), 133-139, 2011.

Kroll, J. H. and Seinfeld, J. H.: Chemistry of secondary organic aerosol: Formation and evolution of low-volatility organics in the atmosphere, Atmos. Environ., 42(16), 3593-3624, 2008.

Kroll, J. H., Smith, J. D., Che, D. L., Kessler, S. H., Worsnop, D. R. and Wilson, K.R.: Measurement of fragmentation and functionalization pathways in the heterogeneous oxidation of oxidized organic aerosol, Phys. Chem. Chem. Phys., 11(36), 8005-8014, 2009.

Kuwata, M., Zorn, S. R. and Martin, S. T.: Using elemental ratios to predict the density of organic material composed of carbon, hydrogen, and oxygen, Environ. Sci. Technol., 46(2), 787-794, 2011.

Lambe, A. T., Chhabra, P. S., Onasch, T. B., Brune, W. H., Hunter, J. F., Kroll, J. H., Cummings, M. J., Brogan, J. F., Parmar, Y., Worsnop, D. R., Kolb, C. E., and Davidovits, P.: Effect of oxidant concentration, exposure time, and seed particles on secondary organic aerosol chemical composition and yield, Atmos. Chem. Phys., 15(6), 3063-3075, 2015.

Liggio, J., Li, S.-M., McLaren, R.: Heterogeneous reactions of glyoxal on particulate matter: Identification of acetals and sulfate esters, Environ. Sci. Technol., 39(6), 1532-1541, 2015a.

Liggio, J., Li, S.-M., McLaren, R.: Reactive uptake of glyoxal by particulate matter. J. Geophys. Res.-Atmos., 110, D10304, 2015b.

Lim, Y. B. and Ziemann, P. J.: Effects of molecular structure on aerosol yields from OH radical-initiated reactions of linear, branched, and cyclic alkanes in the presence of NO_x, Environ. Sci. Technol., 43(7), 2328-2334, 2009a.

Lockhart, J., Blitz, M., Heard, D., Seakins, P. and Shannon, R.: Kinetic study of the OH+ glyoxal reaction: experimental evidence and quantification of direct OH recycling, J. Phys. Chem. A., 117(43), 11027-11037, 2013.

Loza, C. L., Chhabra, P. S., Yee, L. D., Craven, J. S., Flagan, R. C. and Seinfeld, J. H.: Chemical aging of *m*-xylene secondary organic aerosol: laboratory chamber study, Atmos. Chem. Phys., 12(1), 151-167, 2012.

Malloy, Q. G., Nakao, S., Qi, L., Austin, R., Stothers, C., Hagino, H. and Cocker III, D. R.: Real-Time Aerosol Density Determination Utilizing a Modified Scanning Mobility Particle Sizer—Aerosol Particle Mass Analyzer System, Aerosol Sci. Tech., 43(7), 673-678, 2009.

Martín-Reviejo, M. and Wirtz, K.: Is benzene a precursor for secondary organic aerosol? Environ. Sci. Technol., 39(4), 1045-1054, 2005.

McLafferty, F.W. and Tureček, F.: Interpretation of mass spectra. Univ Science Books, Sausalito, CA, USA, 1993.

Nakao, S., Clark, C., Tang, P., Sato, K. and Cocker III, D. R.: Secondary organic aerosol formation from phenolic compounds in the absence of NO_x, Atmos. Chem. Phys, 11, 10649-10660, 2011.

Nakao, S., Liu, Y., Tang, P., Chen, C.-L., Zhang, J. and Cocker III, D. R.: Chamber studies of SOA formation from aromatic hydrocarbons: observation of limited glyoxal uptake, Atmos. Chem. Phys., 12(9), 3927-3937, 2012.

Nakao, S., Tang, P., Tang, X., Clark, C. H., Qi, L., Seo, E., Asa-Awuku, A. and Cocker III, D. R.: Density and elemental ratios of secondary organic aerosol: Application of a density prediction method, Atmos. Environ., 68, 273-277, 2013.

Ng, N. L., Canagaratna, M. R., Jimenez, J. L., Chhabra, P. S., Seinfeld, J. H. and Worsnop, D. R.: Changes in organic aerosol composition with aging inferred from aerosol mass spectra, Atmos. Chem. Phys, 11(13), 6465-6474, 2011.

Ng, N. L., Canagaratna, M. R., Zhang, Q., Jimenez, J. L., Tian, J., Ulbrich, I. M., Kroll, J. H., Docherty, K. S., Chhabra, P. S., Bahreini, R., Murphy, S. M., Seinfeld, J. H., Hildebrandt, L., Donahue, N. M., DeCarlo, P. F., Lanz, V. A., Prévôt, A. S. H., Dinar E., Rudich Y. and Worsnop D. R.: Organic aerosol components observed in Northern Hemispheric datasets from Aerosol Mass Spectrometry, Atmos. Chem. Phys., 10(10), 4625-4641, 2010.

Ng, N. L., Kroll, J. H., Chan, A. W. H., Chhabra, P. S., Flagan, R. C. and Seinfeld, J. H.: Secondary organic aerosol formation from *m*-xylene, toluene, and benzene, Atmos. Chem. Phys., 7(14), 3909-3922, 2007.

Noziere, B., Dziedzic, P. and Córdova, A.: Products and kinetics of the liquid-phase reaction of glyoxal catalyzed by ammonium ions (NH_4^+), J. Phys. Chem. A., 113(1), 231-237, 2008.

Odum, J. R., Hoffmann, T., Bowman, F., Collins, D., Flagan, R. C. and Seinfeld, J. H.: Gas/particle partitioning and secondary organic aerosol yields, Environ. Sci. Technol., 30(8), 2580-2585, 1996.

Odum, J. R., Jungkamp, T., Griffin, R., Flagan, R. C. and Seinfeld, J. H.: The atmospheric aerosol-forming potential of whole gasoline vapor, Science, 276(5309), 96-99, 1997a.

Odum, J. R., Jungkamp, T., Griffin, R. J., Forstner, H., Flagan, R. C. and Seinfeld, J.H.: Aromatics, reformulated gasoline, and atmospheric organic aerosol formation, Environ. Sci. Technol., 31(7), 1890-1897, 1997b.

Pang, Y., Turpin, B. and Gundel, L.: On the importance of organic oxygen for understanding organic aerosol particles, Aerosol Sci. Tech., 40(2), 128-133, 2006.

Pankow, J. F. and Asher, W. E.: SIMPOL. 1: a simple group contribution method for predicting vapor pressures and enthalpies of vaporization of multifunctional organic compounds, Atmos. Chem. Phys., 8(10), 2773-2796, 2008.

Pfaffenberger, L., Barmet, P., Slowik, J. G., Praplan, A. P., Dommen, J., Prévôt, A. S. H. and Baltensperger, U. : The link between organic aerosol mass loading and degree of oxygenation: an α-pinene photooxidation study, Atmos. Chem. Phys., 13(13), 6493-6506, 2013.

Pilling, M. J. and Bartle, K. D.: A catalogue of urban hydrocarbons for the city of Leeds: atmospheric monitoring of volatile organic compounds by thermal desorption-gas chromatography, J. Environ. Monitor., 1(5), 453-458, 1999.

Plum, C. N., Sanhueza, E., Atkinson, R., Carter, W. P. and Pitts, J. N.: Hydroxyl radical rate constants and photolysis rates of alpha-dicarbonyls, Environ. Sci. Technol., 17(8), 479-484, 1983.

Qi, L., Nakao, S., Malloy, Q., Warren, B. and Cocker, D. R.: Can secondary organic aerosol formed in an atmospheric simulation chamber continuously age? Atmos. Environ., 44(25), 2990-2996, 2010a.

Qi, L., Nakao, S., Tang, P. and Cocker III, D. R.: Temperature effect on physical and chemical properties of secondary organic aerosol from *m*-xylene photooxidation, Atmos. Chem. Phys., 10(8), 3847-3854, 2010b.

Rader, D. J. and McMurry, P. H.: Application of the tandem differential mobility analyzer to studies of droplet growth or evaporation, J. Aerosol. Sci., 17(5), 771-787, 1986.

Salo, K., Hallquist, M., Jonsson, Å.M., Saathoff, H., Naumann, K.-H., Spindler, C., Tillmann, R., Fuchs, H., Bohn, B., Rubach, F., Mentel, T. F., Müller, L., Reinnig, M., Hoffmann, T., and Donahue, N. M.: Volatility of secondary organic aerosol during OH radical induced ageing, Atmos. Chem. Phys., 11(21), 11055-11067, 2011.

Salter, R. J., Blitz, M. A., Heard, D. E., Kovács, T., Pilling, M. J., Rickard, A. R. and Seakins, P.W.: Quantum yields for the photolysis of glyoxal below 350 nm and parameterisations for its photolysis rate in the troposphere, Phys. Chem. Chem. Phys., 15(14), 4984-4994, 2013.

Sato, K., Hatakeyama, S. and Imamura, T.: Secondary organic aerosol formation during the photooxidation of toluene: NO_x dependence of chemical composition, J. Phys. Chem. A., 111(39), 9796-9808, 2007.

Sato, K., Takami, A., Isozaki, T., Hikida, T., Shimono, A. and Imamura, T.: 2010. Mass spectrometric study of secondary organic aerosol formed from the photo-oxidation of aromatic hydrocarbons, Atmos. Environ., 44(8), 1080-1087, 2010.

Sato, K., Takami, A., Kato, Y., Seta, T., Fujitani, Y., Hikida, T., Shimono, A. and Imamura, T. 2012. AMS and LC/MS analyses of SOA from the photooxidation of benzene and 1, 3, 5-trimethylbenzene in the presence of NO_x: effects of chemical structure on SOA aging, Atmos. Chem. Phys, 12, 4667-4682, 2012.

Shilling, J. E., Chen, Q., King, S. M., Rosenoern, T., Kroll, J. H., Worsnop, D. R., DeCarlo, P. F., Aiken, A. C., Sueper, D., Jimenez, J. L. and Martin, S. T.: Loading-dependent elemental composition of α-pinene SOA particles, Atmos. Chem. Phys., 9(3), 2009.

Singh, H.B., Salas, L., Viezee, W., Sitton, B. and Ferek, R.: 1992. Measurement of volatile organic chemicals at selected sites in California, Atmos. Environ. A-Gen., 26(16), 2929-2946, 1992.

Singh, H. B., Salas, L. J., Cantrell, B. K. and Redmond, R. M.: Distribution of aromatic hydrocarbons in the ambient air, Atmos. Environ. (1967), 19(11), 1911-1919, 1985.

Song, C., Na, K. and Cocker III, D. R.: Impact of the hydrocarbon to NO_x ratio on secondary organic aerosol formation, Environ. Sci. Technol., 39(9), 3143-3149, 2005.

Takegawa, N., Miyakawa, T., Kawamura, K. and Kondo, Y.: Contribution of selected dicarboxylic and ω-oxocarboxylic acids in ambient aerosol to the m/z 44 signal of an Aerodyne aerosol mass spectrometer, Aerosol Sci. Tech., 41(4), 418-437, 2007.

Takekawa, H., Minoura, H. and Yamazaki, S.: Temperature dependence of secondary organic aerosol formation by photo-oxidation of hydrocarbons, Atmos. Environ., 37(24), 3413-3424, 2003.

Tkacik, D. S., Presto, A. A., Donahue, N. M. and Robinson, A. L.: Secondary organic aerosol formation from intermediate-volatility organic compounds: cyclic, linear, and branched alkanes, Environ. Sci. Technol., 46(16), 8773-8781, 2012.

Tritscher, T., Dommen, J., DeCarlo, P. F., Gysel, M., Barmet, P. B., Praplan, A. P., Weingartner, E., Prévôt, A. S. H., Riipinen, I., Donahue, N. M. and Baltensperger, U.: Volatility and hygroscopicity of aging secondary organic aerosol in a smog chamber, Atmos. Chem. Phys., 11(22), 11477-11496, 2011.

Võ, U.-U.T. and Morris, M.P.: Nonvolatile, semivolatile, or volatile: Redefining volatile for volatile organic compounds. Journal of the Air & Waste Management Association, 64(6), 661-669, 2014.

Wyche, K. P., Monks, P. S., Ellis, A. M., Cordell, R. L., Parker, A. E., Whyte, C., Metzger, A., Dommen, J., Duplissy, J., Prevot, A. S. H., Baltensperger, U., Rickard, A. R., and Wulfert, F.: Gas phase precursors to anthropogenic secondary organic aerosol: detailed observations of 1, 3, 5-trimethylbenzene photooxidation, Atmos. Chem. Phys., 9(2), 635-665, 2009.

Xiang, B., Zhu, L. and Tang, Y.: Photolysis of 4-Oxo-2-pentenal in the 190-460 nm Region, J. Phys. Chem. A., 111(37), 9025-9033, 2007.

Yu, J., Jeffries, H. E. and Sexton, K. G. 1997. Atmospheric photooxidation of alkylbenzenes—I. Carbonyl product analyses, Atmos. Environ., 31(15), 2261-2280, 1997.

Yu, L., Smith, J., Laskin, A., Anastasio, C., Laskin, J., Zhang, Q.: Chemical characterization of SOA formed from aqueous-phase reactions of phenols with the triplet excited state of carbonyl and hydroxyl radical, Atmos. Chem. Phys., 14(24), 13801-13816, 2014.

Zhang, Q., Alfarra, M. R., Worsnop, D. R., Allan, J. D., Coe, H., Canagaratna, M. R. and Jimenez, J. L.: Deconvolution and quantification of hydrocarbon-like and oxygenated

organic aerosols based on aerosol mass spectrometry, Environ. Sci. Technol., 39(13), 4938-4952, 2005.

Ziemann, P.: Effects of molecular structure on the chemistry of aerosol formation from the OH-radical-initiated oxidation of alkanes and alkenes, International Reviews in Physical Chemistry, 30(2), 161-195, 2011.

3.7 Tables and Figures

Table 3.1 Experiment conditions*

Precursor	ID	HC/NO[a]	NO[b]	HC[b]	ΔHC[c]	M_0[c]	Yield
Benzene	1223A	98.1	59.5	972	398	139	0.35
	1223B	49.3	119	979	453	105	0.23
	1236A	104	53.6	928	407	106	0.26
	1236B	36.4	154	938	450	34.9	0.08
	1237A	62.7	41.6	435	266	45.9	0.17
	1237B	129	21.1	453	253	51.4	0.20
	1618A	102	35.4	603	354	46.3	0.13
Toluene	1101A	29.0	19.2	79.7	206	30.1	0.15
	1101B	58.8	9.40	78.8	176	25.1	0.14
	1102A	12.2	43.3	75.7	223	21.8	0.10
	1102B	17.5	33.0	82.5	238	22.2	0.09
	1106A	13.2	20.1	38.0	126	9.80	0.08
	1106B	24.4	10.6	36.9	111	12.4	0.11
	1468A	26.1	64.1	239	667	130	0.20
	1468B	26.5	63.0	238	671	127	0.19
m-Xylene	1191A	12.6	52.2	82.1	298	15.2	0.05
	1191B	14.6	45.7	83.6	340	14.6	0.04
	1193A	15.5	36.8	71.1	239	13.6	0.06
	1193B	15.2	36.5	69.5	236	11.2	0.05
	1516A	27.8	26.7	92.9	357	48.7	0.14
	1950A	14.1	45.5	80.0	327	26.3	0.08
	1950B	14.6	45.9	83.6	345	28.7	0.08
1,2,4-Trimethylbenzene	1117A	69.8	10.3	80.0	335	16.8	0.05
	1117B	34.8	20.7	80.0	368	18.2	0.05
	1119A	14.1	49.8	78.0	385	19.6	0.05
	1119B	17.1	41.6	79.0	390	25.5	0.07
	1123A	71.0	10.1	80.0	300	11.2	0.04
	1123B	32.6	22.1	80.0	345	15.4	0.05
	1126A	69.3	10.1	77.5	286	12.6	0.04
	1126B	28.1	24.3	75.9	333	15.4	0.05
	1129B	24.2	15.6	42.0	201	5.60	0.03
1,2,4,5-Tetramethylbenzene	1531A	72.0	25.0	180	752	17.9	0.02
	1603A	109	11.2	122	469	3.12	0.01
	1603B	110	11.1	123	464	2.54	0.01
	2085A	60.6	33.4	202	862	29.2	0.03
	2085B	136	12.9	175	502	8.20	0.02
Pentamethylbenzene	1521A	68.8	23.5	147	893	32.7	0.04
	1627A	77.9	20.0	142	769	20.6	0.03

	1627B	26.6	50.0	121	719	24.8	0.03
Hexamethylbenzene	1557A	72.0	28.0	168	999	23.4	0.02
	2083A	78.4	11.6	76.0	442	15.2	0.03
	2083B	41.3	22.0	76.0	483	14.0	0.03

Note: a) Unit of HC/NO are ppbC:ppb; b)Unit of NO and HC are ppb; c)Unit of Δ HC and M_0 are $\mu g \cdot m^{-3}$, M_0 is a wall loss and density corrected particle mass concentration; * Only newly added data are listed here and published data are listed in Table S3.2.

Table 3.2 Two product yield curve fitting parameters

Yield Curve	α_1	$K_{om,1}$ ($m^3 \cdot \mu g^{-1}$)	α_2	$K_{om,2}$ ($m^3 \cdot \mu g^{-1}$)
Benzene	0.082	0.017	0.617	0.005
Toluene	0.185	0.080	0.074	0.005
m-Xylene	0.148	0.047	0.079	0.005
1,2,4-Trimethylbenzene	0.099	0.047	0.079	0.005
C_{10+}	0.048	0.047	0.065	0.005

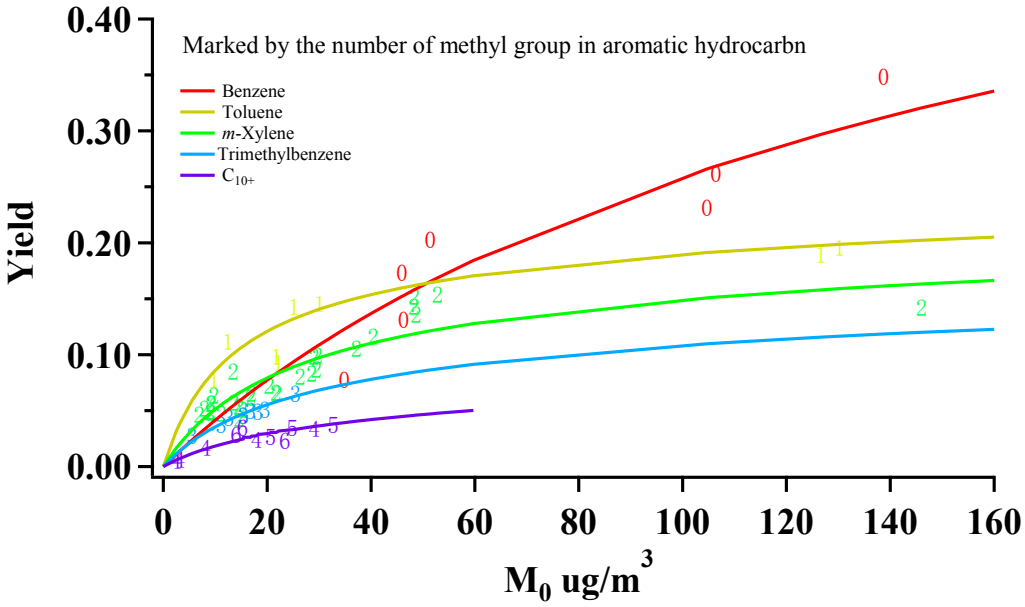

Figure 3.1 Aromatic SOA yields as a function of M_0

*Note: Song, et al. (2005) *m*-xylene data are also included

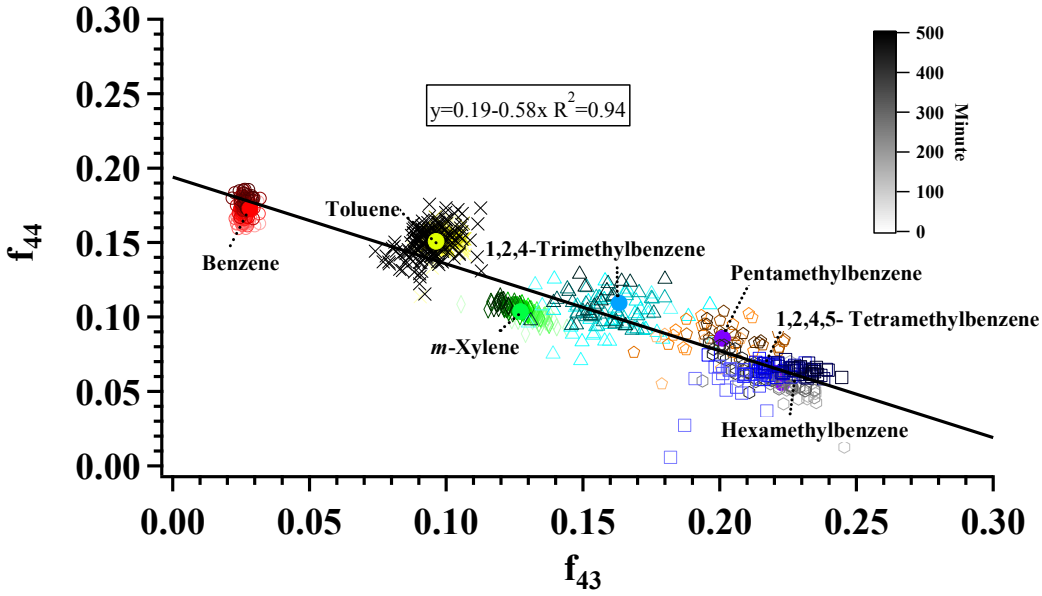

Figure 3.2 f_{44} and f_{43} evolution in SOA formed from photooxidation of different monocyclic aromatic hydrocarbons under low NO_x

(Benzene 1223A; Toluene 1468A; *m*-Xylene 1950A; 1,2,4-Trimethylbenzene 1119A; 1,2,4,5-Tetramethylbenzene 2085A; Pentamethylbenzene 1627A; Hexamethylbenzene 2083A; colored solid circle markers represent the location of average f_{44} and f_{43} value during photooxidation)

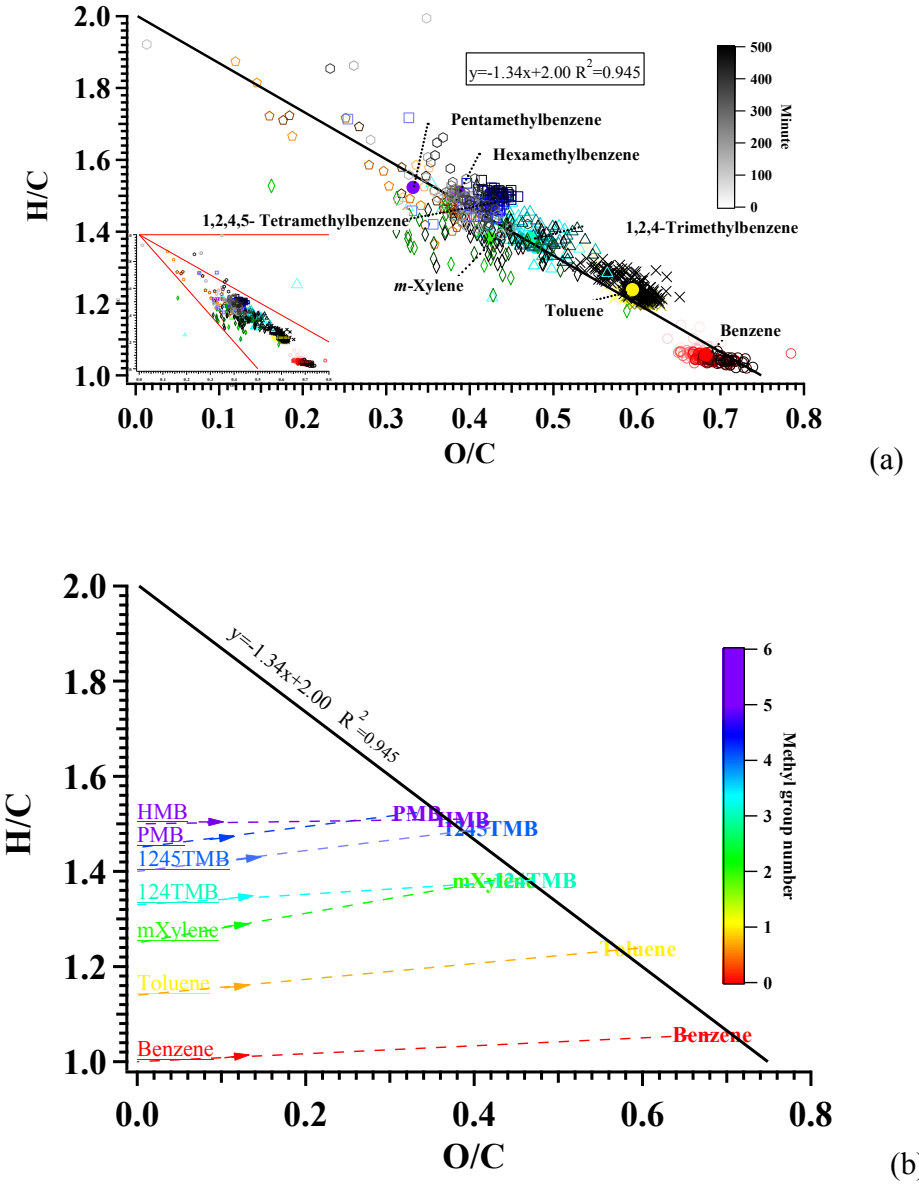

Figure 3.3 a) H/C and O/C evolution; the inset graph shows the measured values relative to the classic triangle plot (Ng et al., 2010). b) Average H/C and O/C in SOA formed from monocyclic aromatic hydrocarbon photooxidation under low NO_x (Benzene 1223A; Toluene 1468A; *m*-Xylene 1191A; 1, 2, 4-Trimethylbenzene 1119A; 1, 2, 4, 5-Tetramethylbenzene 2085A; Pentamethylbenzene 1627A; Hexamethylbenzene 2083A).

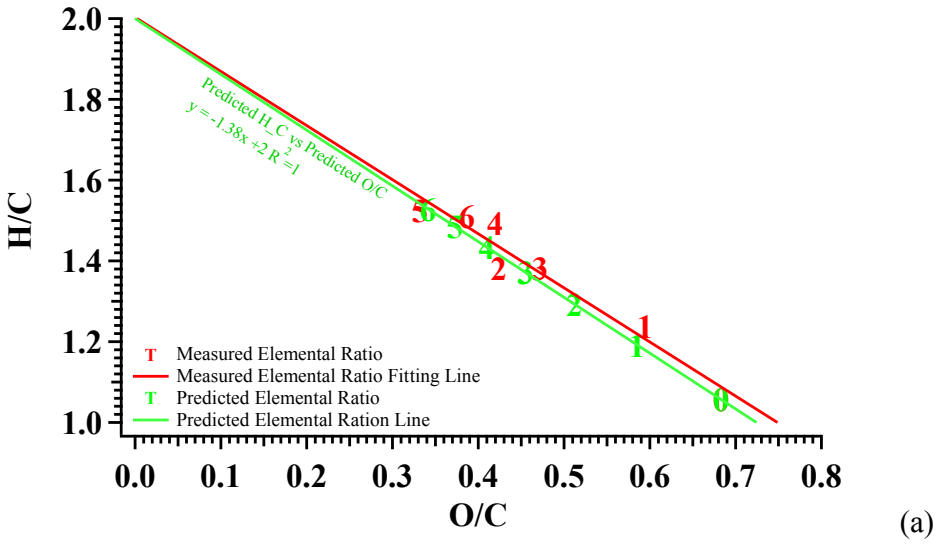

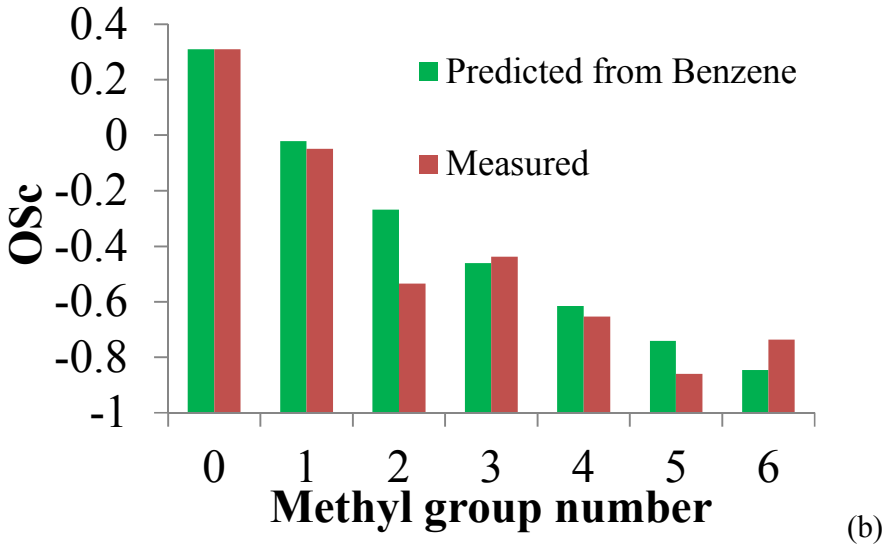

Figure 3.4 Comparison of predicted and measured O/C (a), H/C (a) and oxidation state (OSc) (b) in SOA formation from monocyclic aromatic hydrocarbon photooxidation under low NO_x (Benzene 1223A; Toluene 1468A; m-Xylene 1191A; 1, 2, 4-Trimethylbenzene 1119A; 1,2,4,5-Tetramethylbenzene 1306A; Pentamethylbenzene 1627A; Hexamethylbenzene 1557A).

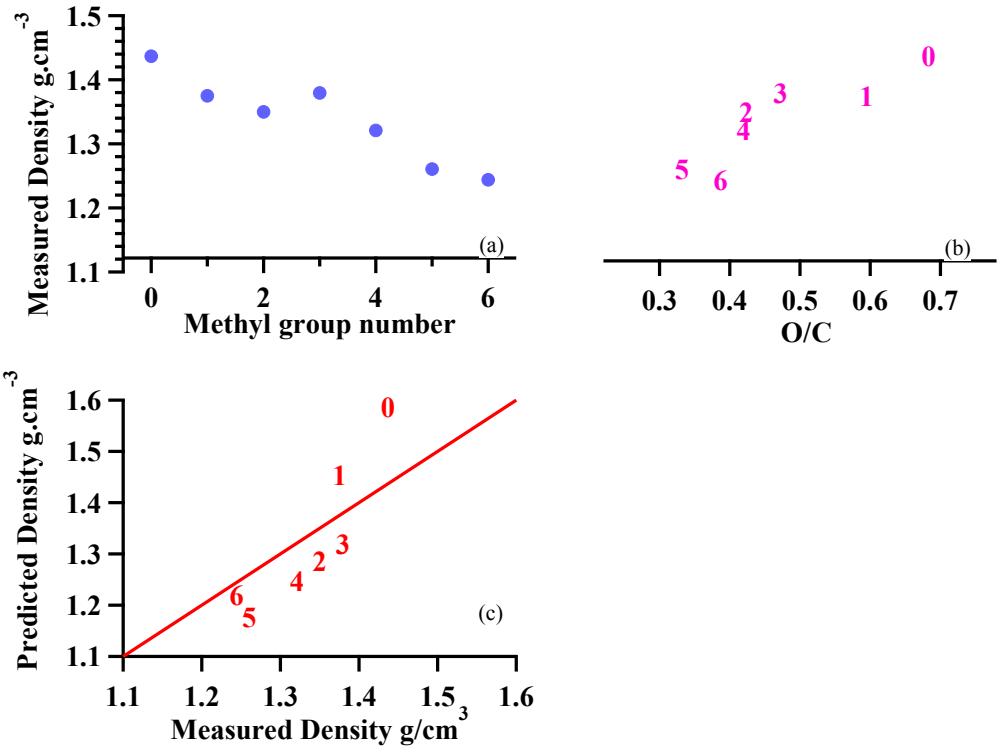

Figure 3.5 Relationship between (a) SOA density and methyl group number; (b) SOA density and O/C; (c) predicted and measured density from monocyclic aromatic hydrocarbon photooxidation under low NO_x (number mark represents number of methyl groups on aromatic hydrocarbon ring).

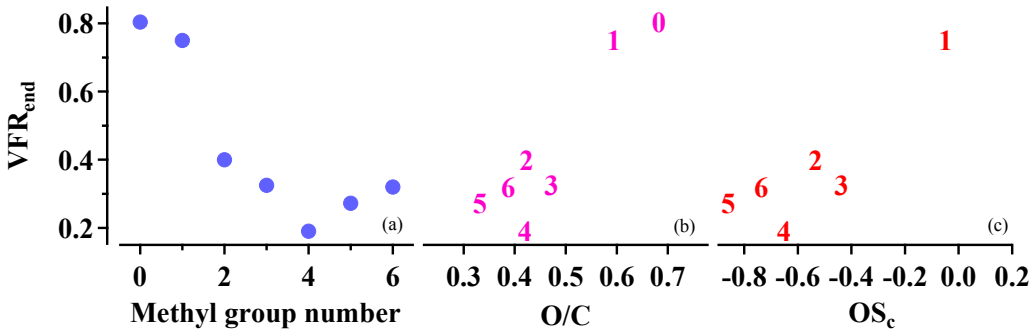

Figure 3.6 Relationship between a) SOA volatility and methyl group number; b) SOA volatility and O/C; c) SOA volatility and oxidation state (OS_c) from monocyclic aromatic hydrocarbon photooxidation under low NO_x (number mark represents number of methyl groups on aromatic hydrocarbon ring).

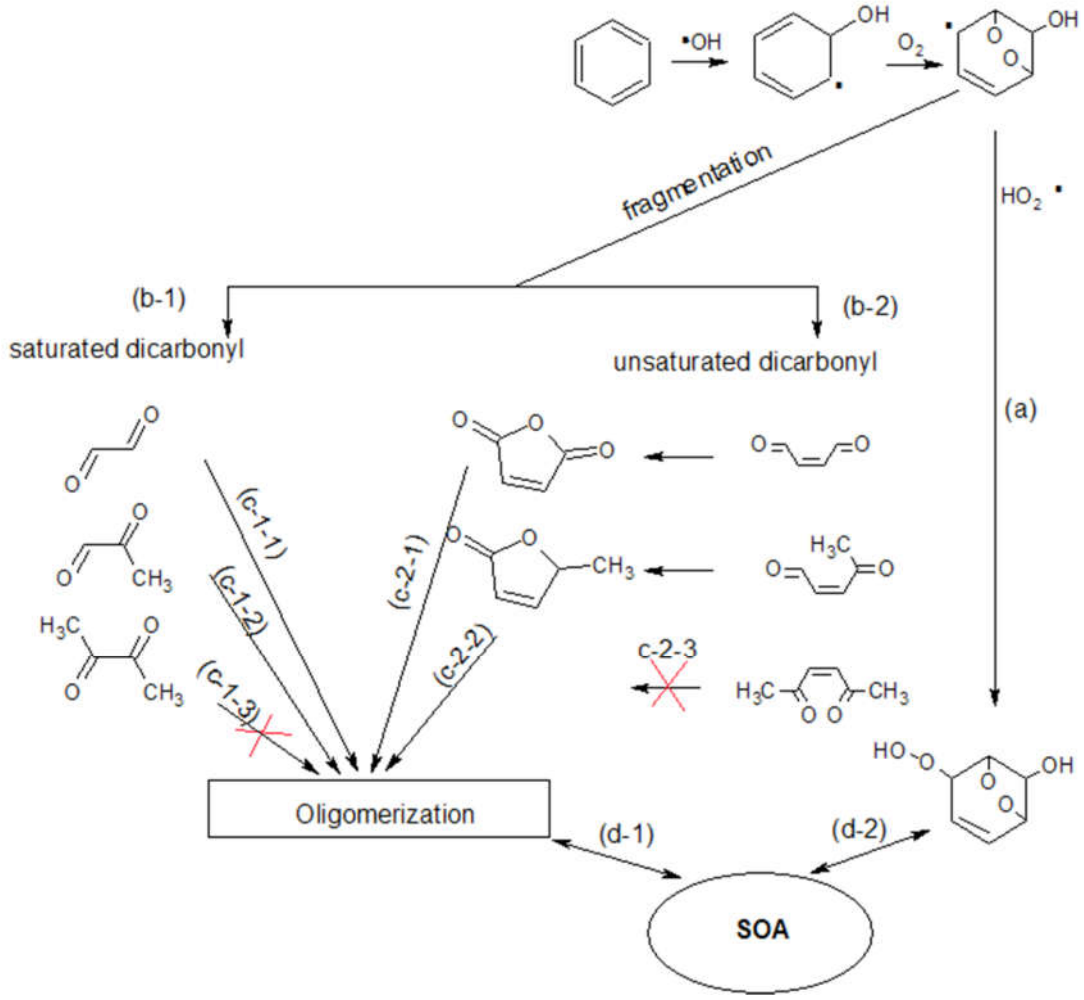

Figure 3.7 Monocyclic aromatic hydrocarbon oxidation pathways related to SOA formation (methyl substitute on aromatic ring not shown).

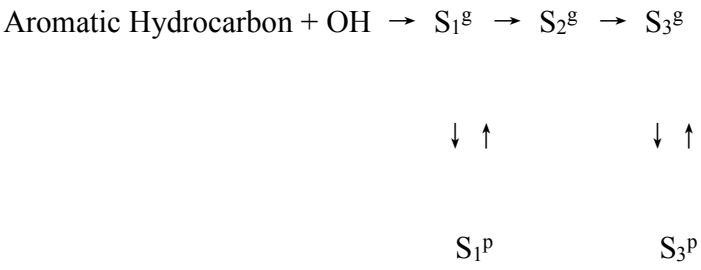

Figure 3.8 Kinetic scheme for SOA formation from monocyclic aromatic hydrocarbon.

4. Impact of molecular structure on secondary organic aerosol formation from aromatic hydrocarbon photooxidation under low NO_x conditions

4.1 Introduction

Organic aerosols are critical to human health (Dockery, et al., 1993; Krewski, et al., 2003; Davidson et al., 2005), climate change (IPCC, 2007) and visibility (Pöschl 2005; Seinfeld and Pandis, et al., 2006). Global anthropogenic secondary organic aerosol (SOA) sources are underestimated by current models (Henze, et al., 2008; Matsui, et al., 2009; Hallquist, et al., 2009; Farina, et al., 2010) and are more likely to increase due to the increase of known anthropogenic emissions (Heald, et al., 2008). Therefore, it is crucial to explore SOA formation mechanism from anthropogenic precursors.

Aromatic hydrocarbons are major anthropogenic SOA precursors (Kanakidou, et al., 2005; Henze, et al., 2008; Derwent, et al., 2010). C_8 (ethylbenzene, xylenes) and C_9 (ethyltoluenes and trimethylbenzenes) aromatics are important aromatic hydrocarbons in the atmosphere besides toluene and benzene (Monod, et al., 2001; Millet, et al., 2005; Heald, et al., 2008; Kansal, et al., 2009; Hu, et al., 2015). The major sources of C_8 and C_9 aromatic hydrocarbons are fuel evaporation (Kaiser, et al., 1992; Rubin, et al., 2006; Miracolo, et al., 2012), tailpipe exhaust (Singh, et al, 1985; Monod, et al., 2001; Lough, et al., 2005; Na, et al., 2005; Correa and Arbilla, et al., 2006) and solvent use (Zhang, et al., 2013). C_8 aromatic hydrocarbons (ethylbenzene and xylenes (ortho, meta and para) are categorized as hazardous air pollutants (HAPs) under the US Clean Air Act Amendments of 1990 (http://www.epa.gov/ttnatw01/orig189.html)). Toluene and C_8

aromatics dominate the anthropogenic SOA precursors and SOA yield from all C_9 aromatics is currently predicted to be equal to that of toluene (Bahreini, et al., 2009). The chemical composition of aromatic SOA remains poorly understood with less than 50% of aromatic hydrocarbon photooxidation products identified (Forstner, et al., 1997; Fisseha, et al., 2004; Hamilton et al., 2005; Sato et al., 2007). Aromatic hydrocarbon photooxidation mechanisms remain uncertain except for the initial step (~90% OH-addition reaction) (Calvert, et al., 2002). Hence, understanding the atmospheric reaction mechanisms of C_8 and C_9 aromatic hydrocarbons and properly quantifying their SOA formation potential presents unique challenges due to the variety in their molecular structure and the electron density of the aromatic ring.

Volatile organic compound (VOC) structure impacts the gas phase reaction mechanism (Ziemman and Atkinson, 2012) and kinetic reaction rate (eg. k_{OH} Atkinson, 1987) thereby influencing the resulting SOA properties and mass yield. Molecular structure impacts on SOA formation from alkanes have been previously studied (Lim and Ziemann, 2009; Ziemann, 2011; Lambe, et al., 2012; Tkacik, et al., 2012; Yee, et al., 2013; Loza, et al., 2014). It is generally observed that SOA yield decreases from cyclic alkanes to linear alkanes and to branched alkanes. The relative location of the methyl group on the carbon chain also affects SOA yield (Tkacik, et al., 2012). It is further found that the SOA yield and structure relationship is influenced by C=C groups (Ziemann, 2011). Understanding the SOA yield and structure relationship of aromatic compounds in a similar way is necessary due to the atmospheric importance of aromatic hydrocarbons.

Previously, aromatic studies categorized SOA yield solely based on substitute number (Odum, 1997a, b). However, those chamber experiments were conducted at high NO_x conditions, which are well above levels present in the atmosphere. Song, et al (2005, 2007) found that initial HC/NO_x ratios significantly impact SOA yields during aromatic photooxidation with yields increasing as NO_x levels decreased. Ng et al. (2007) shows there is no significant yield difference between one substitute (toluene) and two substitute (*m*-xylene) aromatics in the absence of NO_x. The current work focuses on molecular structure impact on SOA formation at more atmospherically relevant NO_x and aerosol loadings. Li et al (2016) demonstrated the methyl group number impact on SOA formation under low NO_x conditions. Also, aromatic compounds with para position alkyl groups have been observed to form less SOA under various NO_x conditions than their isomers in previous studies. Izumi and Fukuyama (1990) found that *p*-xylene, *p*-ethyltoluene and 1, 2, 4-trimethylbenzene have low SOA formation potential under high NO_x conditions. Song, et al (2007) observed that *p*-xylene has the smallest SOA yield among all xylenes in the presence of NO_x. The relative methyl position to -OH in dimethyl phenols also impacts SOA yield in the absence of NO_x (Nakao, et al., 2011), while Song et al.(2007) observed no significant SOA yield difference between *o*-xylene and *p*-xylene under NO_x free conditions. Moreover, previous studies mainly focused on the carbon number effect on SOA formation (Lim and Ziemann, 2009; Chapter 3) and seldom addressed the substitute carbon length impact on VOC oxidation and hence SOA formation. Different percentages of similar compounds are found when the substitute carbon length on the aromatic ring changes (Forstner, et al., 1997; Huang, et al., 2007;

Huang, et al., 2011). For example, a lower percentage of 3-methyl-2, 5-furanone is observed in toluene than that of 3-ethyl-2, 5-furanone in ethylbenzene (Forstner, et al., 1997). Further, the branching structure on the aromatic substitute might impact the reaction pathway. It is possible that fragmentation is more favored on branched substitute alkoxy radicals than n-alkane substituents similar to alkanes (Atkinson, et al., 2003).

Few studies comprehensively consider the overall alkyl effect on SOA formation from aromatic hydrocarbons, including the substitute number, position, carbon chain length and branching structure, especially under low NO_x conditions. It is valuable to understand the relationship between aromatic hydrocarbon molecular structures and SOA physical and chemical characteristics. The effects of OH exposure (Lambe, et al., 2011 (alkane), 2015), mass loading (Shilling, et al., 2009 (α-pinene); Pfaffenberger, et al., 2013(α-pinene)) and NO condition (Ng, et al., 2007; Eddingsaas, et al., 2012(α-pinene)) on SOA physical and chemical characteristics are previously discussed. However, few studies address the molecular structure effect of the precursor on SOA chemical composition, especially under atmospherically relevant conditions. Sato et al (2012) shows the chemical composition difference between ethylbenzene, *m*-xylene, *o*-xylene, 1, 2, 4-trimethylbenzene and 1, 3, 5-trimethylbenzene under high absolute NO_x conditions and hypothesizes that ketones prevent further oxidation during aromatic photooxidation compared with aldehydes. The SOA products detected in Sato's study are mainly small volatile compounds which are less likely to partition into the particle phase (Chhabra, et al., 2011). Therefore, the study of Sato, et al. (2012) indicates that further oxidation or oligmerization might contribute to SOA formation during aromatic photooxidation. Less

SOA characterization data on propylbenzene and ethyltoluene compared with trimethylbenzene is available. However, Bahreini, et al. (2009) suggests that the sum of the propylbenzene and ethyltoluene is on average a factor of 4–10 more abundant than trimethylbenzene.

This work examines twelve aromatic hydrocarbons, all of which are isomers with eight or nine carbons, to investigate the impact of molecular structure on SOA formation from aromatic hydrocarbon photooxidation under low NO_x (10-138 ppb). Here, we investigate the substitute number, substitute position, alkyl carbon chain length and alkyl branching impacts on aromatic hydrocarbon oxidation. The effects of molecular structure impact on SOA yield, chemical composition (H/C, O/C, OS_c, f_{44}, f_{43}, f_{57} and f_{71}) and physical properties (density and VFR) are demonstrated. Alkyl substitute dilution conjecture is further developed from methyl dilution theory (Chapter 3).

4.2 Method

4.2.1 Environmental chamber

The UC Riverside/CE-CERT indoor dual 90 m^3 environmental chambers were used in this study and are described in detail elsewhere (Carter et al., 2005). Experiments were all conducted at dry conditions (RH<0.1%), in the absence of inorganic seed aerosol and with temperature controlled to 27±1°C. Seeded experiments to minimize wall effects have also been conducted in our chamber experiment with no measurable difference observed between the seeded and non-seeded experiment. Two movable top frames were

slowly lowered during each experiment to maintain a slight positive differential pressure (~0.02" H_2O) between the reactors and enclosure to minimize dilution and/or contamination of the reactors. 272 115 W Sylvania 350BL blacklights are used as light sources for photooxidation.

A known volume of high purity liquid hydrocarbon precursors (ethylbenzene Sigma-Aldrich, 99.8%; n-propylbenzene Sigma-Aldrich, 99.8%; isopropylbenzene Sigma-Aldrich, analytical standard; *m*-xylene Sigma-Aldrich, 99%; *o*-xylene Sigma-Aldrich, 99%; *p*-xylene Sigma-Aldrich, 99%; *m*-ethyltoluene Sigma-Aldrich, 99%; *o*-ethyltoluene Sigma-Aldrich, 99%; *p*-ethyltoluene Sigma-Aldrich, ⩾95%; 1, 2, 3-trimethylbenzene Sigma-Aldrich, OEKANAL analytical standard; 1, 2, 4-trimethylbenzene Sigma-Aldrich, 98%; 1, 3, 5-trimethylbenzene Sigma-Aldrich, analytical standard) was injected through a heated glass injection manifold system and flushed into the chamber with pure N_2. NO was introduced by flushing pure N_2 through a calibrated glass bulb filled to a predetermined partial pressure of pure NO. All hydrocarbons and NO are injected and well mixed before lights are turned on to start the experiment.

4.2.2 Particle and Gas Measurement

Particle size distribution between 27 nm and 686 nm was monitored by dual custom built Scanning Mobility Particle Sizers (SMPS) (Cocker et al., 2001). Particle effective density was measured with an Aerosol Particle Mass Analyzer (APM-SMPS) system (Malloy et al., 2009). Particle volatility was measured by a Dekati® Thermodenuder Volatility Tandem Differential Mobility Analyzer (VTDMA) (Rader and McMurry, 1986) with a

17 s heating zone residence time (Qi, et al., 2010a). The heating zone was controlled to 100 °C in this study with Volume Fraction Remaining (VFR) calculated as $(D_{p,\ after\ TD}/D_{p,\ before\ TD})^3$.

Particle-phase chemical composition evolution was measured by a High Resolution Time of Flight Aerosol Mass Spectrometer (HR-ToF-AMS; Aerodyne Research Inc.) (Canagaratna et al., 2007; DeCarlo et al., 2006). The sample was vaporized by a 600 °C oven under vacuum followed by a 70 eV electron impact ionization. f_x in this study is calculated as the mass fraction of the organic signal at *m/z*=x. For example, f_{44}, f_{43}, f_{57} and f_{71} are the ratios of the organic signal at *m/z* 44, 43, 57 and 71 to the total organic signal, respectively (Chhabra et al., 2011; Duplissy et al., 2011). Elemental ratios for total organic mass, oxygen to carbon (O/C), and hydrogen to carbon (H/C) were determined using the elemental analysis (EA) technique (Aiken et al., 2007, 2008). Data was analyzed with ToF-AMS analysis toolkit Squirrel 1.56D /Pika 1.15D version. Evolution of SOA composition (Heald, et al., 2010; Jimenez, et al., 2009) refers to SOA chemical composition changes with time. f_{44} and $f_{43+57+71}$ evolution and H/C and O/C evolution refer to the change of f_{44} and $f_{43+57+71}$ with time and the change of H/C and O/C with time, respectively.

The Agilent 6890 Gas Chromatograph – Flame Ionization Detector was used to measure aromatic hydrocarbon concentrations. A Thermal Environmental Instruments Model 42C chemiluminescence NO analyzer was used to monitor NO, NO_y-NO and NO_y. The gas-

phase reaction model SAPRC-11 developed by Carter and Heo (2013) was utilized to predict radical concentrations ($\cdot OH$, $HO_2\cdot$, $RO_2\cdot$ and $NO_3\cdot$).

4.3 Result

4.3.1 SOA yield

Photooxidation of twelve C_8 and C_9 aromatic hydrocarbons were studied for low NO_x conditions (HC/NO ratio 11.1-171 ppbC: ppb). SOA yields for all aromatic hydrocarbons were calculated according to Odum, et al. (1996) as the mass ratio of aerosol formed to parent hydrocarbon reacted. Experimental conditions and SOA yields are listed (Table 4.1) along with additional *m*-xylene, *o*-xylene, *p*-xylene and 1, 2, 4-trimethylbenzene experimental conditions from previous studies (Song, et al, 2005; Song, et al, 2007; Chapter 3) (Table S4.2). The uncertainty associated with 10 replicate *m*-xylene and NO experiments SOA yield is <6.65%. SOA yield as a function of particle mass concentration (M_o), shown in Fig. 4.1, includes experiments listed in both Table 4.1 and Table S4.2. It is observed that both alkyl substitute number and position affect SOA yield. The SOA yield of two-substitute C_8 and C_9 aromatic hydrocarbons depends more on the substitute location than substitute length. This means that the yield trend of *o*-xylene is analogous to that of *o*-ethyltoluene. Similarly, the yield trends for meta and para position substituted C_8 and C_9 aromatic hydrocarbons will be analogous to each other. Ortho isomers (*o*-xylene and *o*-ethyltoluene, marked as solid and hollow green circles, respectively) have the highest SOA yield for similar aerosol concentrations while para isomers (*p*-xylene and *p*-ethyltoluene, marked as solid and hallow blue diamonds,

respectively) have the lowest SOA yield level. Lower SOA yield for para isomers are consistent with previous observation by Izumi and Fukuyama (1990). Izumi and Fukuyama (1990) also suggest that 1, 2, 4-trimethylbenzene yields are lower than for other aromatic hydrocarbons. The current study does not show a significant SOA yield difference between 1, 2, 4-trimethylbenzene and 1, 3, 5-trimethylbenzene. It is difficult to compare 1, 2, 3-trimethylbenzene yields with the former two trimethylbenzenes since 1, 2, 3-trimethylbenzene mass loading is much higher than the former two.

Aromatic hydrocarbons having only one substitute (ethylbenzene, n-propylbenzene and isopropylbenzene) or three substitutes (1, 2, 3-trimethylbenzene, 1, 2, 4-trimethylbenzene and 1, 3, 5-trimethylbenzene) tend to have yields similar to the meta position two alkyl aromatics. Odum, et al (1997b) categorized SOA yield formation potential solely based on substitute number and stated that aromatics with less than two methyl or ethyl substitutes form more particulate matter than those with two or more methyl or ethyl substitutes on the aromatic ring. However, Odum's work was conducted for high NO_x conditions and had insufficient data to compare isomer yield differences (e.g., only two low mass loadings for *o*-xylene data). The strong low yield (two or more substitutes) and high yield (less than two methyl or ethyl substitutes) trends for high NO_x conditions (Odum, et al., 1997) are not observed for low NO_x aromatic experiments in this study. Rather, high yield is observed only for benzene (Chapter 3) while low yield is seen for substituted aromatic hydrocarbons. Similar SOA yield trends from different C_8 and C_9 aromatic isomers are further confirmed by comparing yields at similar radical conditions (Table S4.4, Fig. S4.2). It is also found that molecular structure exerts a greater impact on

SOA yield than reaction kinetics (supplemental material, Table S4.5). A two product model described by Odum, et al. (1996) is used to fit SOA yield curves as a function of M_o. The twelve aromatics are categorized into five groups to demonstrate the alkyl group number and position effect on SOA formation. The five groups include one substitute group (1S), ortho position two alkyl group (ortho), meta position two alkyl group (meta), para position two alkyl group (para) and three substitute group (3S). Fitting parameters (α_1, $K_{om,1}$, α_2 and $K_{om,2}$; Table 4.2) in the two product model are determined by minimizing the sum of the squared residuals. The lower volatility partitioning parameter ($K_{om,2}$) is the same for all yield curve fits by assuming similar high volatile compounds are formed during all aromatic hydrocarbon photooxidation experiments. The ortho group is associated with a much higher $K_{om,1}$ compared with other aromatic groups, indicating aromatic hydrocarbon oxidation with an ortho position substitute forms much lower volatility products than other isomers. $K_{om,1}$ are also slightly higher in the meta group and one substitute groups than in the three substitute and para substitute groups.

A slight SOA yield difference remains within each group (Fig. S4.1&Table S4.3), indicating the influence of factors other than alkyl group position. Generally, lower yields are found in aromatics with higher carbon number substitute alkyl groups, such as when comparing propylbenzene (i- and n-) with ethylbenzene or toluene (Chapter 3), *m*-ethyltoluene with *m*-xylene and *p*-ethyltoluene with *p*-xylene, respectively. These differences are explained by the proposed alkyl group dilution effect (Section 4.4). However, the differences between xylenes and their corresponding ethyltoluenes are not statistically significant.

4.3.2 Chemical composition

4.3.2.1 f_{44} vs $f_{43+57+71}$

The ratio of alkyl substitute carbon number (H:C >1) to the aromatic ring carbon number impacts SOA composition since the H:C ratio on the alkyl substitute is larger than 1 and the H:C ratio on aromatic ring itself is no more than 1. *m/z* 43 ($C_2H_3O^+$ and $C_3H_7^+$) combined with *m/z* 44 (CO_2^+) are critical to characterize oxygenated compounds in organic aerosol (Ng, et al., 2010; Ng, et al., 2011). $C_2H_3O^+$ is the major contributor to *m/z* 43 in SOA formed from aromatic hydrocarbons having only methyl substitute (Chapter 3) while $C_3H_7^+$ fragments are observed in this work for SOA from propylbenzene and isopropylbenzene (Fig. S4.4, Table S4.6). The $C_nH_{2n-1}O^+$ (n=carbon number of the alkyl substitute) fragment in SOA corresponds to a C_nH_{2n+1}- alkyl substitute to the aromatic ring. $C_3H_5O^+$ (*m/z* 57) and $C_4H_7O^+$ (*m/z* 71) are important when investigating SOA from ethyl or propyl substitute aromatic precursors. While m/z 57 ($C_4H_9^+$) and m/z 71 ($C_5H_{11}^+$) are often considered as markers for hydrocarbon-like organic aerosol in ambient studies (Zhang et al., 2015; Ng et al., 2010), oxygenated organic aerosol $C_3H_5O^+$and $C_4H_7O^+$ are the major fragments at m/z 57 and m/z 71, respectively, (Fig. S4.4, Table S4.6) in current chamber SOA studies, especially during the photooxidation of ethyl and propyl substituted aromatics. Therefore, m/z 57 and m/z 71 are also considered beside $C_2H_3O^+$ at m/z 43 in SOA chamber studies as OOA to compare the oxidation of different aromatic hydrocarbons. Fig. S4.4 lists all fragments found at *m/z* 43, 44, 57 and 71 and Fig. S4.5 shows the fraction of each *m/z* in SOA formed from all aromatic hydrocarbons studied.

The *m/z* 43+*m/z* 44+*m/z* 57+*m/z* 71 accounts for 21.2%~29.5% of the total mass fragments from all C_8 and C_9 aromatics studied, suggesting similar oxidation pathways. Only a small fraction (<~0.7%) of *m/z* 71 ($C_4H_7O^+$) or *m/z* 57 ($C_3H_5O^+$) was observed in ethyltoluenes and trimethylbenzenes, respectively.

This work extends the traditional f_{44} vs f_{43} ($C_2H_3O^+$) chemical composition analysis by including oxidized fragments ($C_3H_5O^+$ m/z 57 and $C_4H_7O^+$ m/z 71) of the longer (non-methyl) alkyl substitutes. Therefore, f_{44} vs $f_{43}+f_{57}+f_{71}$ is plotted instead of f_{44} vs f_{43}. Fig S4.3 shows the evolution of f_{44} and $f_{43+57+71}$ in SOA formed from the photooxidation of different aromatic hydrocarbons at low NO_x conditions. f_{44} and $f_{43+57+71}$ ranges are comparable to previous chamber studies (Ng, et al., 2010; Chhabra, et al., 2011; Loza, et al., 2012; Sato, et al., 2012). Only slight f_{44} and $f_{43+57+71}$ evolution during chamber photooxidation is observed for the C_8 and C_9 isomers hence only the average f_{44} and $f_{43+57+71}$ will be analyzed in this work .

A modification is applied to the mass based *m/z* fraction in order to compare the mole relationship between *m/z* 44 and *m/z* 43+*m/z* 57+m/z 71(Eq-1).

$$f'_{43+57+71} = \frac{44}{43}f_{43} + \frac{44}{57}f_{57} + \frac{44}{71}f_{71} \qquad \text{Eq-1}$$

The average f_{44} vs $f'_{43+57+71}$for all C_8 and C_9 isomers (Fig. 4.2) are located around the trend line for methyl group substituted aromatic hydrocarbons (Chapter 3), implying a similarity in the SOA components formed from alkyl substituted aromatic hydrocarbons. A decreasing trend in oxidation from upper left to lower right is included in Fig 4.2,

similar to what Ng, et al (2011) found in the f_{44} vs f_{43} graph, especially while comparing similar structure compounds. The methyl group location on the aromatic ring impacts f_{44}: $f'_{43+57+71}$. Decreasing f_{44} and increasing $f'_{43+57+71}$ trends are observed from *p*-xylene to *o*-xylene to *m*-xylene and from 1, 2, 4-trimethylbenzene to 1, 2, 3-trimethylbenzene to 1, 3, 5-trimethylbenezene. The $f'_{43+57+71}$ may partially depend on the relative position between the alkyl substitute and the peroxide oxygen of the bicyclic peroxide. For instance, allylically stabilized five-membered bicyclic radicals are the most stable bicyclic radical formed from aromatic hydrocarbon photooxidation (Andino, et al., 1996). Two meta position substitutes connected to the aromatic ring carbon with -C-O- yield higher fractions of $C_nH_{2n-1}O^+$ fragments than the para and ortho position, which have at most one substitute connected with -C-O- (Fig. S4.6). CO_2^+ are generally formed during MS electrical ionization from carbonates, cyclic anhydrides and lactones (McLafferty and Turecek, 1993) indicating that the CO_2^+ is associated with -O-C-O- structure. Within the AMS, the CO_{2+} is also associated with decarboxylation of organic acids during heating followed by electrical ionization of the CO_2. We hypothesize that CO_2^+ formation from bicyclic peroxides is insignificant since CO_2 loss is not expected come from -C-O-O- structure during thermal decomposition. Therefore, it is the reaction products of bicyclic peroxides that lead to the formation of CO_2^+ and the difference in f_{44}. This indicates that the alkyl groups are more likely to contribute to SOA formation at the meta position than the ortho and para position. Bicyclic peroxides formed from the OH-addition reaction pathway and their dissociation reaction products are both used to explain the substitute location impact on f_{44} and $f'_{43+57+71}$ relationship. However, the existence of longer alkyl

substitutes diminishes the alkyl substitute location impact. SOA f_{44} and $f'_{43+57+71}$ in ethyltoluenes are all analogous to *m*-xylene. One substitute C_8 and C_9 aromatic hydrocarbons have similar f_{44} and $f'_{43+57+71}$ with slightly lower f_{44} and $f'_{43+57+71}$ compared to toluene (Chapter 3). Longer alkyl substitutes may not lower the average oxidation per mass as further oxidation of the longer chain alkyls may render other oxidized components not included in Fig. 4.2. Their lower total $f_{44}+f'_{43+57+71}$ (Fig. S4.5) further supports the possibility of oxidation of the longer alkyl substitutes. It is also possible that oligomerization from highly oxidized carbonyls contribute more to the SOA formation from aromatics with long chain alkyl substitute. Elemental ratio (Section 4.3.2.2) and oxidation state (Section 4.3.2.3) are further used to evaluate the impact of increasing alkyl group size on SOA formation.

4.3.2.2 H/C vs O/C

Elemental analysis (Aiken, et al., 2007, 2008) serves as a valuable tool to elucidate SOA chemical composition and SOA formation mechanisms (Heald, et al., 2010; Chhabra, et al., 2011). Fig. S4.7 shows H/C and O/C evolution in SOA formed from the photooxidation of different aromatic hydrocarbons under low NO_x (marked and colored similarly to Fig. S4.3). H/C and O/C ranges are comparable to previous chamber studies (Chhabra, et al., 2011 (*m*-xylene and toluene); Loza, et al., 2012 (*m*-xylene); Sato, et al., 2012 (benzene and 1, 3, 5-trimethylbenzene)). The SOA elemental ratio for C_8 and C_9 aromatic isomers are located near the alkyl number trend line found in Chapter 3 for methyl substituents, indicating a similarity between SOA from various alkyl substituted

hydrocarbons. SOA formed is among the low volatility oxygenated organic aerosol (LV-OOA) and semi-volatile oxygenated organic aerosol (SV-OOA) regions (Ng, et al., 2011). The evolution trend agrees with Fig. S4.3 (Section 4.3.2.1), which means no significant H/C and O/C evolution is observed in the current study. Therefore, average H/C and O/C with standard deviation provided is used to explore the impact of molecular structure on SOA chemical composition. The current study concentrates on experimentally averaged H/C and O/C to explore the impact of molecular structure on SOA chemical composition.

Average H/C and O/C locations are marked with aromatic compound names in Fig. 4.3. All H/C and O/C are located around the predicted values for C_8 and C_9 SOA (dark solid circle) based on the elemental ratio of benzene SOA (Chapter 3). This confirms the presence of a carbon dilution effect in all isomers. Ortho position aromatic hydrocarbons (*o*-xylene or *o*-ethyltoluene) lead to a more oxidized SOA (higher O/C and lower H/C) than that of meta (*m*-xylene or *m*-ethyltoluene) and para (*p*-xylene or *p*-ethyltoluene) aromatics. SOA formed from 1, 2, 4-trimethylbenzene and 1, 2, 3-trimethylbenzene is more oxidized than that from 1, 3, 5-trimethylbenzene. It is noticed that 1, 2, 4-trimethylbenzene and 1, 2, 3-trimethylbenzene both contain an ortho position moiety on the aromatic ring. This indicates that the ortho position aromatic hydrocarbon is readily oxidized and this ortho position impact on oxidation extends to triple substituted aromatic hydrocarbons. Substitute length also plays an important role in aromatic hydrocarbon oxidation. Overall, SOA from a one-substitute aromatic with more carbon in the substitute is located at a more oxidized area of the O/C vs. H/C chart (lower right in Fig.

4.3.) than those multiple substitute aromatic isomers with the same total number of carbon as the single substituted aromatic. SOA from isopropylbenzene is located in a lower position of the chart and to the right of propylbenzene indicating that branch carbon structure on the alkyl substitute of aromatic hydrocarbons leads to a more oxidized SOA. Lines in Fig. S4.8 connect the O/C and H/C of resulting SOA to that of the aromatic precursor. Most SOA components show a slight H/C increase and a dramatic O/C increase from the precursor, which is consistent with results observed for methyl substituted aromatics (Chapter 3). However, H/C barely increases (1.33 to 1.34) from the propylbenzene precursor to its resulting SOA and there is even a decreasing trend from isopropylbenzene to its SOA. This indicates that a high H/C component loss reaction such as alkyl part dissociation during photooxidation is an important reaction to SOA formation from longer carbon chain containing aromatic hydrocarbons. The carbon chain length of propylbenzene increases the possibility of alkyl fragmentation. The branching structure of isopropylbenzene facilitates fragmentation through the stability of tertiary alkyl radicals. Elemental ratio differences between xylenes and ethyltoluenes can be attributed to the alkyl dilution effect, similar to the methyl dilution theory in Chapter 3. Prediction of elemental ratios from toluene and xylenes are discussed later (Section 4.4) to further quantify the carbon length and branching effect on SOA formation from aromatic hydrocarbons.

4.3.2.3 OS_c

Oxidation state ($OS_c \approx 2O/C-H/C$) was introduced into aerosol phase component analysis by Kroll et al. (2011). It is considered to be a more accurate metric for describing oxidation in atmospheric organic aerosol than H/C and O/C (Ng et al., 2009; Canagaratna, et al., 2015; Lambe, et al., 2015) and therefore well correlated with gas-particle partitioning (Aumont, et al., 2012;). Average OS_c of SOA formed from C_8 and C_9 aromatic isomers ranges from -0.54 to -0.17 and -0.82 to -0.22, respectively (Fig. 4.4), implying that the precursor molecular structure impacts the OS_c of the resulting SOA. An OS_c decrease with alkyl substitute length is observed in one-substitute aromatic hydrocarbons from toluene (toluene OS_c=-0.049; Chapter 3) to propylbenzene. However, OS_c provides the average oxidation value per carbon not considering whether these carbons start from an aromatic ring carbon or an alkyl carbon. Alkyl carbons are associated with more hydrogen than aromatic ring carbons, thus leading to a lower precursor OS_c and therefore lower SOA OS_c. Dilution conjecture in Section 4.4 will be used to further explore the carbon chain length effect on aromatic hydrocarbon oxidation by considering the precursor H:C ratio. Single substitute aromatic hydrocarbons generally show higher OS_c than multiple substitute ones, consistent with the yield trend of Odum, et al (1997b). However, it is also found that ortho position moiety containing two or three substitute aromatic hydrocarbons have analogous or even higher OS_c to single substitute aromatic hydrocarbons (*o*-xylene -0.03±0.098 to ethylbenzene -0.173±0.033; 1,2,4-trimethylbenzene -0.425±0.072 and *o*-ethyltoluene -0.481±0.030 to propylbenzene -0.421±0.111). This suggests that both substitute number and position are critical to

aromatic hydrocarbon oxidation and therefore SOA formation. OS_c trends also support that the meta position suppresses oxidation while the ortho position promotes oxidation when the OS_c of xylenes (*o*-xylene>*p*-xylene>(insignificant) *m*-xylene), ethyltoluenes (*o*-ethyltoluene>*p*-ethyltoluene>(insignificant) *m*-ethyltoluene) and especially, trimethylbenzenes (1, 2, 4-trimethylbenzene (ortho moiety containing)> (insignificant)1, 2, 3-trimethylbenzene (ortho moiety containing)>1, 3, 5-trimethylbenzene (meta moiety containing)) are compared separately. Further, SOA formed from isopropylbenzene shows the highest OS_c among all C_9 isomers, nearly equivalent to that of ethylbenzene. This demonstrates that the branching structure of the alkyl substitute can enhance further oxidation of aromatic hydrocarbons.

4.3.3 Physical property

4.3.3.1 SOA Density

SOA density is a fundamental parameter in understanding aerosol morphology, dynamics, phase and oxidation (De Carol, et al., 2004; Katrib, et al., 2005; Dinar, et al., 2006; Cross, et al., 2007). SOA density ranges from 1.29-1.38 g/cm^3 from aromatic photooxidation under low NO_x conditions in this study (Fig. 4.5). The range is comparable to previous studies under similar conditions (Borrás and Tortajada-Genaro 2012; Ng, et al; 2007; Sato, et al., 2010). There is no significant difference in the density of SOA formed from C_8 and C_9 aromatic hydrocarbon isomers and molecular structure is not observed to be a critical parameter to determine SOA density. The standard deviation results from differences in initial conditions (e.g., initial HC/NO) that also determine the

oxidation of aromatic hydrocarbons (Chapter 2) and thus further affect density. SOA density is correlated with the O/C ratio and OS_c (0.551 and 0.540, Table 4.3), consistent with the observation of Pang, et al. (2006) that SOA density increases with increasing O/C ratio. The density prediction method developed by Kuwata, et al. (2011) based on O/C and H/C is evaluated as

$$\rho = \frac{12+H/C+16\times O/C}{7+5\times H/C+4.15\times O/C} \quad \text{Eq-2}$$

The black lines (Fig. 4.5) are predicted (Eq-2) densities and show a good agreement between predicted and measured SOA densities (-6.01% ~ 7.62%). A comparatively large negative error is found in meta containing aromatic hydrocarbons including *m*-xylene, *m*-ethyltoluene and *1,3,5*-trimethylbenzene. It is noted that there should be more alkyl substitutes in SOA formed from meta position aromatics than other aromatics since meta position alkyl substitutes are more likely to participate into SOA products than other aromatics (Section 4.3.2.1 and Section 4.3.2.2). Previous work suggests that the increase of methyl groups could lead to a change in several key organic fragments (e.g., CO^+, CO_2^+ and H_2O^+) thereby altering the default fragment table for elemental ratio analysis. This agrees with the density underestimation in SOA formed from meta position aromatics and supports the preference of meta position alkyl substitute to SOA products.

4.3.3.2 SOA Volatility

SOA volatility is associated with reactions such as oxidation, fragmentation, oligomerization and mass loading (Kalberer, et al., 2004; Salo, et al., 2011; Tritscher, et

al., 2011; Yu, et al., 2014). SOA volatility in this study is measured as VFR. Initial (<30 minutes after new particle formation) SOA VFRs are around 0.2 for all the aromatic precursors studied and increase up to 0.58 during photooxidation. This suggests that aromatic hydrocarbon oxidation undergoes an evolution from volatile compounds to semivolatile compounds. The VFR trends and ranges are comparable to previous studies (Kalberer et al., 2004; Qi et al., 2010a; Qi et al., 2010b; Nakao et al., 2012). Fig. 4.6 shows the VFR at the end of aromatic hydrocarbon photooxidation (VFR_{end}). A decreasing VFR_{end} trend is found as the number of substitutes increase and for meta position (e.g. *m*-xylene) or meta position containing (e.g. 1, 3, 5-trimethylbenzene) aromatic precursors. Correlations among VFR_{end} and chemical composition are observed in the aromatic hydrocarbons studied here (Table 4.3). This is consistent with recent findings that O:C ratio is correlated to aerosol volatility (Section 4.3.3.2) (Cappa, et al., 2012, Yu, et al., 2014), thereby affecting the gas-particle partitioning, which in turn relates to SOA yield. It is also observed that VFR_{end} is strongly correlated (-0.937) with reaction rate constant (k_{OH}). Higher k_{OH} is associated with faster reaction rates of initial aromatic precursors and is therefore expected to lead to further oxidation for a given reaction time. However, the inverse correlation between k_{OH} and VFR_{end} indicates that k_{OH} value represents more than just the kinetic aspects. k_{OH} increases with increasing number of substitutes on the aromatic ring. Additionally, aromatic hydrocarbons with meta position substitutes have higher k_{OH} than those with para and ortha (Table S4.1) position substitutes. This suggests that the precursor molecular structures for aromatics

associated with k_{OH} values determine the extent of oxidation of the hydrocarbons and therefore impact SOA volatility more than simply the precursor oxidation rate.

4.4 Alkyl Dilution Conjecture on SOA formation from aromatic hydrocarbons

The dependence of SOA formation on molecular structure can be partially represented by the alkyl carbon number. Carbon dilution theory proposed by Li et al (2016) successfully explain that methyl group impacts remain similar in SOA elemental ratios as in the aromatic precursor. The chemical composition of SOA formation from alkyl substituted aromatics is predicted by simply adding the alkyl substitute into the chemical composition of SOA formed from pure aromatic ring precursor (benzene). Methyl dilution theory (Chapter 3) is extended to alkyl substitute dilution conjecture in order to investigate the influence of longer alkyl substitutes compared with methyl group substitutes. A robust prediction of SOA H/C and O/C trends for longer (C2+) alkyl substituted aromatics based on the methyl substituted aromatics will suggest a similarity in the role of methyl and longer alkyl to SOA formation; an underestimation or overestimation will indicate different oxidation pathways for aromatics with differing alkyl substitute length. Fig. 4.7a and Fig. 4.7b shows the predicted elemental ratio and OS_c for SOA formed from longer alkyl substitutes ($-C_nH_{2n+1}$, $n>1$) based on methyl only substitute. The elemental ratio of SOA formed from single substitute aromatic hydrocarbons including ethylbenzene, propylbenzene and isopropylbenzene are predicted by toluene and those of ethyltoluenes are predicted by corresponding xylenes with similar alkyl substitute location. H/C and O/C are generally well predicted by alkyl dilution

effect, expect for *o*-ethyltoluene and iso-propylbenzene. O/C (15%), H/C (1%) and OS_c (13%) of *o*-ethyltoluene are slightly overestimated by alkyl dilution effect. This indicates that *o*-ethyltoluene is less oxidized than *o*-xylene possibly due to the hindrance effect of the longer alkyl substitute.

OS_c is underestimated in SOA formed from single substitute aromatic hydrocarbons, especially for isopropylbenzene (-49%) and ethylbenzene (-25%). This implies that longer alkyl substitutes are more oxidized than the methyl group on toluene. A direct ·OH reaction with the alkyl part of the aromatic is more favored on longer alkyl chains since tertiary and secondary alkyl radicals are more stable than primary alkyl radicals (Forstner, et al., 1997). It is also possible that oligomerization from highly oxidized carbonyl component might be more favored for long chain single alkyl substituted aromatics. The less significant OS_c underestimation from xylenes to ethyltoluenes (meta and para) is due to the presence of an "inert" methyl group which lowers the average OS_c. Fragmentation on alkyl substitute of isopropylbenzene can lead to a higher OS_c (-0.22±0.04) than propylbenzene (-0.42±0.11), which possibly occurs while forming 2, 5-furandione or 3-*H*-furan-2-one due to the increased stability of the isopropyl radical compared to the n-propyl radical. It is also possible that longer carbon chain substitutes might have higher probability to form other cyclic or low vapor pressure products by additional reaction due to their increased length. The similarity in f_{44} and $f'_{43+57+71}$ but discrepancy (insignificant) in elemental ratio among all single substitute C_8 and C_9 aromatics supports that additional reactions leading to further oxidization of alkyl substitutes can occur.

4.5 Conclusion

This study elucidates molecular structure impact on a major anthropogenic SOA source, photooxidation of aromatic hydrocarbons, under atmospherically relevant NO_x conditions by analyzing SOA yield, chemical composition and physical properties. These observations, when taken together, indicate the roles of alkyl substitute number, location, carbon chain length and branching structure in aromatic hydrocarbon photooxidation. SOA yield of all C_8 and C_9 aromatic hydrocarbon isomers are comprehensively provided in this study with a focus on the impact of molecular structure. It is demonstrated that aromatic hydrocarbon oxidation and SOA formation should not be simply explained by substitute number. The promoting of SOA formation by the ortho position is found along with confirmation of the suppression effect by the para position during oxidation of aromatic hydrocarbons. It is possible due to the alkyl substitute location impact on the further oxidation of five-membered bicyclic radicals. Different carbonyl compounds can form as the ring opening products from the dissociation of five-membered bicyclic radical. It is assumed that oligomerization of these carbonyl compounds can contribute to SOA (Chapter 3). Aromatic hydrocarbons with para position alkyl substitute tend to form more ketone like dicarbonyl compounds than other aromatics. Ketone might contribute less to oligomerization formation compared with aldehyde as suggested in Chapter 3. Meta position alkyl substitutes on aromatic ring lead to a lower extent of aromatic hydrocarbon oxidation. It might be due to a higher percentage of carbonyl with alkyl substitute formed during the oxidation of meta containing aromatics (e.g. methylgloxal, 2-methyl-4-oxopent-2-enal), which contributes to oligomerization and thereby SOA

formation. Evidence is provided to demonstrate aromatic oxidation increase with alkyl substitute chain length and branching structure. Further, carbon dilution theory developed by Li., et al (2016) is extended to this study. Carbon dilution theory not only serves as a tool to explain the difference in SOA components due to the difference in substitute alkyl carbon number but also acts as a standard to determine the oxidation mechanism based on alkyl substitute structure. Moreover, the five subcategories of aromatics and their two product modeling curve fitting parameters in this work at more realistic NO_x loadings provide a more precise prediction of SOA formation form aromatic hydrocarbons under atmospheric conditions. Previous studies found that the humidity insignificantly impacts SOA yield from aromatic hydrocarbons (Cocker, et al., 2001) or maintains the SOA yield relationship between isomers (Zhou, et al., 2001). Therefore, it is predicted that the observation found under dry conditions in this study, especially the molecular structure impact on SOA formation from different aromatic isomers could be extended to atmospherically relevant humidity conditions. However, recent studies observe that the hydration of carbonyls and epoxides could lead to further heterogeneous reaction and oligomerization (Jang, et al., 2002; Liggio, et al., 2005; Minerath and Elrod, et al., 2009; Lal, et al., 2012). It is possible that aerosol compositions and the hygroscopic properties could be altered after the heterogeneous reactions, especially under humid conditions. The impact of molecular structure impact on SOA formation under humidity condition needs to be further studied to extend the findings in current the work. This study improves the understanding of SOA formation from aromatic hydrocarbons and contributes to more accurate SOA prediction from aromatic precursors. Further study is

warranted to reveal the detailed oxidation pathway of aromatic hydrocarbons with longer (carbon number >1) alkyl substitutes.

4.6 Reference

Aiken, A. C., DeCarlo, P. F., and Jimenez, J. L.: Elemental analysis of organic species with electron ionization high-resolution mass spectrometry, Anal. Chem., 79(21), 8350-8358, 2007.

Aiken, A. C., DeCarlo, P. F., Kroll, J. H., Worsnop, D. R., Huffman, J. A., Docherty, K. S., Ulbrich, I. M., Mohr, C., Kimmel, J. R., Sueper, D., Sun, Y., Zhang, Q., Trimborn, A., Northway, M., Ziemann, P. J., Canagaratna, M. R., Onasch, T. B., Alfarra, M. R., Prevot, A. S. H., Dommen, J., Duplissy, J., Metzger, A., Baltensperger, U., and Jimenez, J. H.: O/C and OM/OC ratios of primary, secondary, and ambient organic aerosols with high-resolution time-of-flight aerosol mass spectrometry, Environ. Sci. Technol., 42(12), 4478-4485, 2008.

Andino, J. M., Smith, J. N., Flagan, R. C., Goddard, W. A., and Seinfeld, J.H.: Mechanism of atmospheric photooxidation of aromatics: A theoretical study, J. Phys. Chem-US., 100(26), 10967-10980, 1996.

Atkinson, R.: A structure‐activity relationship for the estimation of rate constants for the gas‐phase reactions of OH radicals with organic compounds, Int. J. Chem. Kinet., 19(9), 799-828, 1987.

Atkinson, R., and Arey, J.: Atmospheric degradation of volatile organic compounds, Chem. Rev., 103(12), 4605-4638, 2003.

Aumont, B., Valorso, R., Mouchel-Vallon, C., Camredon, M., Lee-Taylor, J., and Madronich, S.: Modeling SOA formation from the oxidation of intermediate volatility n-alkanes, Atmos. Chem. Phys., 12(16), 7577-7589, 2012.

Bahreini, R., Ervens, B., Middlebrook, A., Warneke, C., De Gouw, J., DeCarlo, P., Jimenez, J., Brock, C., Neuman, J., Ryerson, T., Stark, H., Atlas, E., Brioude, J., Fried, A., Holloway, J. S., Peischl, J., Richter, D., Walega, J., Weibring, P., Wollny, A. G., and Fehsenfeld, F. C.: Organic aerosol formation in urban and industrial plumes near Houston and Dallas, Texas, J. Geophys. Res.-Atmos., 114(D7), 2009.

Borrás, E., and Tortajada-Genaro, L. A.: Secondary organic aerosol formation from the photo-oxidation of benzene, Atmos. Environ., 47, 154-163, 2012.

Calvert, J. G., Atkinson, R., Becker, K. H., Kamens, R. M., Seinfeld, J. H., Wallington, T. J., and Yarwood, G.: The mechanisms of atmospheric oxidation of aromatic hydrocarbons, Oxford University Press New York, 2002.

Canagaratna, M. R., Jayne, J. T., Jimenez, J. L., Allan, J. D., Alfarra, M. R., Zhang, Q., Onasch, T. B., Drewnick, F., Coe, H., Middlebrook, A., Delia, A., Williams, L. R., Trimborn, A. M., Northway, M. J., DeCarlo, P. F., Kolb, C. E., Davidovits, P., and Worsnop D. R.: Chemical and microphysical characterization of ambient aerosols with the aerodyne aerosol mass spectrometer, Mass. Spectrom. Rev., 26(2), 185-222, 2007.

Canagaratna, M. R., Jimenez, J. L., Kroll, J. H., Chen, Q., Kessler, S. H., Massoli, P., Hildebrandt Ruiz, L., Fortner, E., Williams, L. R., Wilson, K. R., Surratt, J. D., Donahue, N. M., Jayne, J. T., and Worsnop, D. R.: Elemental ratio measurements of organic compounds using aerosol mass spectrometry: characterization, improved calibration, and implications, Atmos. Chem. Phys., 15(1), 253-272, 2015.

Cappa, C. D., and Wilson, K. R.: Multi-generation gas-phase oxidation, equilibrium partitioning, and the formation and evolution of secondary organic aerosol, Atmos. Chem. Phys., 12(20), 9505-9528, 2012.

Carter, W. P. L., Cocker III, D. R., Fitz, D. R., Malkina, I.L., Bumiller, K., Sauer, C.G., Pisano, J.T., Bufalino, C., Song, C.: A new environmental chamber for evaluation of gas-phase chemical mechanisms and secondary aerosol formation, Atmos. Environ., 39(40), 7768-7788, 2005.

Carter, W. P. L., and Heo, G.: Development of Revised SAPRC Aromatics Mechanisms, Atmos. Environ., 77, 404-414, 2013.

Chhabra, P. S., Ng, N. L., Canagaratna, M. R., Corrigan, A. L., Russell, L. M., Worsnop, D. R., Flagan, R. C., and Seinfeld, J. H.: Elemental composition and oxidation of chamber organic aerosol, Atmos. Chem. Phys., 11(17), 8827-8845, 2011.

Cocker III, D. R., Flagan, R. C., and Seinfeld, J. H.: State-of-the-art chamber facility for studying atmospheric aerosol chemistry, Environ. Sci. Technol., 35(12), 2594-2601, 2001.

Correa, S. M., and Arbilla, G.: Aromatic hydrocarbons emissions in diesel and biodiesel exhaust. Atmos. Environ., 40(35), 6821-6826, 2006

Cross, E. S., Slowik, J. G., Davidovits, P., Allan, J. D., Worsnop, D. R., Jayne, J. T., Lewis, D. K., Canagaratna, M., and Onasch, T. B.: Laboratory and ambient particle density determinations using light scattering in conjunction with aerosol mass spectrometry, Aerosol Sci. Tech., 41(4), 343-359., 2007.

Davidson, C. I., Phalen, R. F., and Solomon, P. A.: Airborne particulate matter and human health: A review, Aerosol Sci. Tech., 39(8), 737-749, 2005.

DeCarlo, P. F., Kimmel, J. R., Trimborn, A., Northway, M. J., Jayne, J. T., Aiken, A. C., Gonin, M., Fuhrer, K., Horvath, T., Docherty, K. S., Worsnop, D. R., and Jimenez, J. L.: Field-deployable, high-resolution, time-of-flight aerosol mass spectrometer. Anal. Chem., 78(24), 8281-8289, 2006.

DeCarlo, P. F., Slowik, J. G., Worsnop, D. R., Davidovits, P., and Jimenez, J. L.: Particle morphology and density characterization by combined mobility and aerodynamic diameter measurements. Part 1: Theory, Aerosol Sci. Tech., 38(12), 1185-1205, 2004.

Derwent, R. G., Jenkin, M. E., Utembe, S. R., Shallcross, D. E., Murrells, T. P., and Passant, N. R.: Secondary organic aerosol formation from a large number of reactive man-made organic compounds. Sci. Total. Environ., 408(16), 3374-3381, 2010.

Dinar, E., Mentel, T., and Rudich, Y.: The density of humic acids and humic like substances (HULIS) from fresh and aged wood burning and pollution aerosol particles, Atmos. Chem. Phys., 6(12), 5213-5224, 2006.

Dockery, D. W., Pope, C. A., Xu, X., Spengler, J. D., Ware, J. H., Fay, M. E., Ferris Jr, B. G., and Speizer, F. E.: An association between air pollution and mortality in six US cities, New. Engl. J. Med., 329(24), 1753-1759, 1993.

Duplissy, J., DeCarlo, P. F., Dommen, J., Alfarra, M. R., Metzger, A., Barmpadimos, I., Prevot, A. S., Weingartner, E., Tritscher, T., and Gysel, M.: Relating hygroscopicity and composition of organic aerosol particulate matter, Atmos. Chem. Phys., 11(3), 1155-1165, 2011.

Eddingsaas, N. C., Loza, C. L., Yee, L. D., Chan, M., Schilling, K. A., Chhabra, P. S., Seinfeld, J. H., and Wennberg, P. O.: α-pinene photooxidation under controlled chemical conditions–Part 2: SOA yield and composition in low-and high-NO_x environments, Atmos. Chem. Phys, 12(16), 7413-7427, 2012.

Farina, S. C., Adams, P. J., and Pandis, S. N.: Modeling global secondary organic aerosol formation and processing with the volatility basis set: Implications for anthropogenic secondary organic aerosol. J. Geophys. Res.-Atmos., 115(D9), 2010.

Fisseha, R., Dommen, J., Sax, M., Paulsen, D., Kalberer, M., Maurer, R., Höfler, F., Weingartner, E., and Baltensperger, U.: Identification of organic acids in secondary organic aerosol and the corresponding gas phase from chamber experiments, Anal. Chem., 76(22), 6535-6540, 2004.

Forstner, H. J. L., Flagan, R. C., and Seinfeld, J. H.: Secondary organic aerosol from the photooxidation of aromatic hydrocarbons: Molecular composition, Environ. Sci. Technol., 31(5), 1345-1358, 1997.

Hallquist, M., Wenger, J. C., Baltensperger, U., Rudich, Y., Simpson, D., Claeys, M., Dommen, J., Donahue, N. M., George, C., Goldstein, A. H., Hamilton, J. F., Herrmann, H., Hoffmann, T., Iinuma, Y., Jang, M., Jenkin, M. E., Jimenez, J. L., Kiendler-Scharr, A., Maenhaut, W., McFiggans, G., Mentel, Th. F., Monod, A., Prévôt, A. S. H., Seinfeld, J. H., Surratt, J. D., Szmigielski, R., and Wildt, J.: The formation, properties and impact of secondary organic aerosol: current and emerging issues, Atmos. Chem. Phys., 9(14), 5155-5236, 2009.

Hamilton, J. F., Webb, P. J., Lewis, A. C., and Reviejo, M. M.: Quantifying small molecules in secondary organic aerosol formed during the photo-oxidation of toluene with hydroxyl radicals, Atmos. Environ., 39(38), 7263-7275, 2005.

Heald, C. L., Goldstein, A. H., Allan, J. D., Aiken, A. C., Apel, E., Atlas, E. L., Baker, A. K., Bates, T. S., Beyersdorf, A. J., Blake, D. R., A., Campos, T., Coe, H., Crounse, J. D., DeCarlo, P. F., de Gouw, J. A., Dunlea, E. J., Flocke, F. M., Fried, Goldan, P., Griffin R. J., Herndon, S. C., Holloway, J. S., Holzinger, R., Jimenez J. L., Junkermann, W., Kuster, W. C., Lewis, A. C., Meinardi, S., Millet, D. B., Onasch, T., Polidori, A., Quinn, P. K., Riemer, D. D., Roberts, J. M., Salcedo, D., Sive, B., Swanson, A. L., Talbot, R., Warneke, C., Weber, R. J., Weibring, P., Wennberg, P. O., Worsnop, D. R., Wittig, A. E., Zhang, R., Zheng, J., and Zheng, W.: Total observed organic carbon (TOOC) in the atmosphere: a synthesis of North American observations, Atmos. Chem. Phys., 8(7), 2007-2025, 2008.

Heald, C. L., Kroll, J. H., Jimenez, J. L., Docherty, K. S., DeCarlo, P. F., Aiken, A. C., Chen, Q., Martin, S. T., Farmer, D. K., and Artaxo, P.: A simplified description of the evolution of organic aerosol composition in the atmosphere, Geophys. Res. Lett, 37(8), 2010.

Henze, D. K., Seinfeld, J. H., Ng, N. L., Kroll, J. H., Fu, T-M., Jacob, D. J., and Heald, C. L.: Global modeling of secondary organic aerosol formation from aromatic hydrocarbons: high-vs. low-yield pathways, Atmos. Chem. Phys., 8(9), 2405-2421, 2008.

Hu, L., Millet, D. B., Baasandorj, M., Griffis, T. J., Travis, K. R., Tessum, C. W., Marshall, J. D., Reinhart, W. F., Mikoviny, T., Müller, M., Wisthaler, A., Graus, M., Warneke, C., and de Gouw, J.:Emissions of C_6–C_8 aromatic compounds in the United States: Constraints from tall tower and aircraft measurements, J. Geophys. Res.-Atmos., 120(2), 826-842, 2015.

Huang, M., Wang, Z., Hao, L., and Zhang, W.: Theoretical investigation on the mechanism and kinetics of OH radical with ethylbenzene: Int. J. Quantum. Chem., 111(12), 3125-3134, 2011

Huang, M., Zhang, W., Hao, L., Wang, Z., Zhao, W., Gu, X., Guo, X., Liu, X., Long, B., and Fang, L.: Laser desorption/ionization mass spectrometric study of secondary organic

aerosol formed from the photooxidation of aromatics, J. Atmos. Chem., 58(3), 237-252, d 2007.

IPCC.: Intergovernmental Panel on Climate Change: Climate Change 2007: The Physical Science Basis, Cambridge University Press, UK, 6, 07, 2007.

Izumi, K., and Fukuyama, T. : Photochemical aerosol formation from aromatic hydrocarbons in the presence of NO_x, Atmos. Environ. A-Gen., 24(6), 1433-1441, 1990.

Jang, M., Czoschke, N. M., Lee, S., and Kamens, R. M.: Heterogeneous atmospheric aerosol production by acid-catalyzed particle-phase reactions, Science, 298(5594), 814-817, 2002.

Jimenez, J. L., Canagaratna, M. R., Donahue, N. M., Prevot, A. S. H., Zhang, Q., Kroll, J. H., DeCarlo, P. F., Allan, J. D., Coe, H., Ng, N. L., Aiken, A. C., Docherty, K. S., Ulbrich, I. M., Grieshop, A. P., Robinson, A. L., Duplissy, J., Smith, J. D., Wilson, K. R., Lanz, V. A., Hueglin, C., Sun, Y. L., Tian, J., Laaksonen, A., Raatikainen, T., Rautiainen, J., Vaattovaara, P., Ehn, M., Kulmala, M., Tomlinson, J. M., Collins, D. R., Cubison, M. J., Dunlea1, E., J., Huffman, J. A., Onasch, T. B., Alfarra, M. R., Williams, P. I., Bower, K., Kondo, Y., Schneider, J., Drewnick, F., Borrmann, S., Weimer, S.,, Demerjian, K., Salcedo, D., Cottrell, L., Griffin, R., Takami, A., Miyoshi, T., Hatakeyama, S., Shimono, A., Sun, J. Y., Zhang, Y. M., Dzepina, K., Kimmel, J. R., Sueper, D., J. Jayne, T., Herndon, S. C., Trimborn, A. M., Williams, L. R., Wood, E. C., Middlebrook, A. M., Kolb C. E., Baltensperger, U. and Worsnop D. R.: Evolution of organic aerosols in the atmosphere, Science, 326(5959), 1525-1529, 2009.

Kaiser, E. W., Siegl, W. O., Cotton, D. F., and Anderson, R.W.: Effect of fuel structure on emissions from a spark-ignited engine. 2. Naphthene and aromatic fuels, Environ. Sci. Technol., 26(8), 1581-1586, 1992.

Kalberer, M., Paulsen, D., Sax, M., Steinbacher, M., Dommen, J., Prevot, A. S. H., Fisseha, R., Weingartner, E., Frankevich, V., and Zenobi, R.: Identification of polymers as major components of atmospheric organic aerosols, Science, 303(5664), 1659-1662, 2004.

Kanakidou, M., Seinfeld, J. H., Pandis, S. N., Barnes, I., Dentener, F. J, Facchini, M. C., Van Dingenen, R., Ervens, B., Nenes, A., Nielsen, C. J., Swietlicki, E., Putaud, J. P., Balkanski, Y., Fuzzi, S., Horth, J., Moortgat, G. K., Winterhalter, R., Myhre, C. E. L., Tsigaridis, K., Vignati, E., Stephanou, E. G., and Wilson, J.: Organic aerosol and global climate modelling: a review, Atmos. Chem. Phys., 5(4), 1053-1123, 2005.

Kansal, A.: Sources and reactivity of NMHCs and VOCs in the atmosphere: a review, J. Hazard. Mater, 166(1), 17-26, 2009.

Katrib, Y., Martin, S. T., Rudich, Y., Davidovits, P., Jayne, J. T., and Worsnop, D. R.: Density changes of aerosol particles as a result of chemical reaction, Atmos. Chem. Phys., 5(1), 275-291, 2005.

Krewski, D., Burnett, R., Goldberg, M., Hoover, B.K., Siemiatycki, J., Jerrett, M., Abrahamowicz, M., and White, W. : Overview of the reanalysis of the Harvard six cities study and American Cancer Society study of particulate air pollution and mortality, Toxicol. Env. Heal. A., 66(16-19), 1507-1552, 2003.

Kuwata, M., Zorn, S. R., and Martin, S. T.: Using elemental ratios to predict the density of organic material composed of carbon, hydrogen, and oxygen, Environ. Sci. Technol., 46(2), 787-794, 2011.

Lal, V., Khalizov, A. F., Lin, Y., Galvan, M. D., Connell, B. T., and Zhang, R.: Heterogeneous reactions of epoxides in acidic media. J. Phys. Chem. A., 116(24), 6078-6090, 2012.

Lambe, A. T., Onasch, T. B., Croasdale, D. R., Wright, J. P., Martin, A. T., Franklin, J. P., Massoli, P., Kroll, J. H., Canagaratna, M. R., Brune, W. H., Worsnop D. R., and Davidovits P.: Transitions from functionalization to fragmentation reactions of laboratory secondary organic aerosol (SOA) generated from the OH oxidation of alkane precursors, Environ. Sci. Technol., 46(10), 5430-5437, 2012.

Lambe, A. T., Chhabra, P. S., Onasch, T. B., Brune, W. H., Hunter, J. F., Kroll, J. H., Cummings, M. J., Brogan, J. F., Parmar, Y., Worsnop, D. R., Kolb, C. E., and Davidovits, P.: Effect of oxidant concentration, exposure time, and seed particles on secondary organic aerosol chemical composition and yield, Atmos. Chem. Phys., 15(6), 3063-3075, 2015.

Liggio, J., Li, S.-M., and McLaren R.: Heterogeneous reactions of glyoxal on particulate matter: Identification of acetals and sulfate esters, Environ. Sci. Technol., 39(6): 1532-1541, 2005.

Lim, Y. B., and Ziemann, P. J.: Effects of molecular structure on aerosol yields from OH radical-initiated reactions of linear, branched, and cyclic alkanes in the presence of NO_x, Environ. Sci. Technol., 43(7), 2328-2334, 2009.

Lough, G. C., Schauer, J. J., Lonneman, W. A., and Allen, M. K.: Summer and winter nonmethane hydrocarbon emissions from on-road motor vehicles in the Midwestern United States, J. Air. Waste. Manage., 55(5), 629-646, 2005.

Loza, C. L., Chhabra, P. S., Yee, L. D., Craven, J. S., Flagan, R. C. and Seinfeld, J. H.: Chemical aging of *m*-xylene secondary organic aerosol: laboratory chamber study, Atmos. Chem. Phys., 12(1), 151-167, 2012.

Loza, C. L., Craven, J. D., Yee, L. D., Coggon, M. M., Schwantes, R. H., Shiraiwa, M., Zhang, X., Schilling, K. A, Ng, N. L., Canagaratna, M. R., Ziemann, P. J., Flagan, R. C., and Seinfeld, J. H.: Secondary organic aerosol yields of 12-carbon alkanes. Atmos. Chem. Phys., 14(3), 1423-1439, 2014.

Malloy, Q. G., Nakao, S., Qi, L., Austin, R., Stothers, C., Hagino, H., and Cocker III, D. R.: Real-Time Aerosol Density Determination Utilizing a Modified Scanning Mobility Particle Sizer—Aerosol Particle Mass Analyzer System, Aerosol. Sci. Tech., 43(7), 673-678, 2009.

Matsui, H., Koike, M., Takegawa, N., Kondo, Y., Griffin, R., Miyazaki, Y., Yokouchi, Y., and Ohara, T.: Secondary organic aerosol formation in urban air: Temporal variations and possible contributions from unidentified hydrocarbons, J. Geophys. Res.-Atmos, 114(D4), D04201, 2009.

McLafferty, F. W., and Turecek, F.: Interpretation of mass spectra. University Science Books, Mill Valley, California, 1993.

Millet, D. B., Donahue, N. M., Pandis, S. N., Polidori, A., Stanier, C. O., Turpin, B. J., and Goldstein, A. H.: Atmospheric volatile organic compound measurements during the Pittsburgh Air Quality Study: Results, interpretation, and quantification of primary and secondary contributions, J. Geophys. Res.-Atmos, 110(D7), D07S07, 2005.

Minerath, E. C. and Elrod, M. J.: Assessing the potential for diol and hydroxy sulfate ester formation from the reaction of epoxides in tropospheric aerosols. Environ. Sci. Technol., 43(5), 1386–1392, 2009.

Miracolo, M. A., Drozd, G. T., Jathar, S. H., Presto, A. A., Lipsky, E. M., Corporan, E., and Robinson, A.L.: Fuel composition and secondary organic aerosol formation: Gas-turbine exhaust and alternative aviation fuels. Environ. Sci. Technol., 46(15), 8493-8501, 2012.

Monod, A., Sive, B. C., Avino, P., Chen, T., Blake, D. R., and Rowland, F. S.: Monoaromatic compounds in ambient air of various cities: a focus on correlations between the xylenes and ethylbenzene, Atmos. Environ., 35(1), 135-149, 2001.

Na, K., Moon, K.-C., and Kim, Y. P.: Source contribution to aromatic VOC concentration and ozone formation potential in the atmosphere of Seoul. Atmos. Environ., 39(30), 5517-5524, 2005.

Nakao, S., Clark, C., Tang, P., Sato, K., and Cocker III, D.: Secondary organic aerosol formation from phenolic compounds in the absence of NO_x, Atmos. Chem. Phys., 11, 10649-10660, 2011.

Nakao, S., Liu, Y., Tang, P., Chen, C.-L., Zhang, J., and Cocker III, D. R.: Chamber studies of SOA formation from aromatic hydrocarbons: observation of limited glyoxal uptake, Atmos. Chem. Phys., 12(9), 3927-3937, 2012.

Ng, N. L., Canagaratna, M. R., Jimenez, J. L., Chhabra, P. S., Seinfeld, J. H., and Worsnop, D. R.: Changes in organic aerosol composition with aging inferred from aerosol mass spectra, Atmos. Chem. Phys., 11(13), 6465-6474, 2011.

Ng, N. L., Canagaratna, M. R., Zhang, Q., Jimenez, J. L., Tian, J., Ulbrich, I. M., Kroll, J. H., Docherty, K. S., Chhabra, P. S., Bahreini, R., Murphy, S. M., Seinfeld, J. H., Hildebrandt, L., Donahue, N. M., DeCarlo, P. F., Lanz, V. A., Prévôt, A. S. H., Dinar E., Rudich Y., and Worsnop D. R.: Organic aerosol components observed in Northern Hemispheric datasets from Aerosol Mass Spectrometry, Atmos. Chem. Phys., 10(10), 4625-4641, 2010.

Ng, N. L., Kroll, J. H., Chan, A. W. H., Chhabra, P. S., Flagan, R. C., and Seinfeld, J. H.: Secondary organic aerosol formation from *m*-xylene, toluene, and benzene, Atmos. Chem. Phys., 7(14), 3909-3922, 2007.

Odum, J. R., Hoffmann, T., Bowman, F., Collins, D., Flagan, R. C., and Seinfeld, J. H.: Gas/particle partitioning and secondary organic aerosol yields, Environ. Sci. Technol., 30(8), 2580-2585, 1996.

Odum, J. R., Jungkamp, T., Griffin, R., Flagan, R. C., and Seinfeld, J. H.: The atmospheric aerosol-forming potential of whole gasoline vapor, Science, 276(5309), 96-99, 1997a.

Odum, J. R., Jungkamp, T., Griffin, R. J., Forstner, H., Flagan, R. C., and Seinfeld, J.H.: Aromatics, reformulated gasoline, and atmospheric organic aerosol formation, Environ. Sci. Technol., 31(7), 1890-1897, 1997b.

Pöschl, U.: Atmospheric aerosols: Composition, transformation, climate and health effects, Angew. Chem. Int. Edit., 44(46), 7520-7540, 2005.

Pang, Y., Turpin, B., and Gundel, L.: On the importance of organic oxygen for understanding organic aerosol particles, Aerosol. Sci. Tech., 40(2), 128-133, 2006.

Pfaffenberger, L., Barmet, P., Slowik, J. G., Praplan, A. P., Dommen, J., Prévôt, A. S. H., and Baltensperger, U. : The link between organic aerosol mass loading and degree of oxygenation: an α-pinene photooxidation study, Atmos. Chem. Phys., 13(13), 6493-6506, 2013.

Qi, L., Nakao, S., Malloy, Q., Warren, B., and Cocker III, D. R.: Can secondary organic aerosol formed in an atmospheric simulation chamber continuously age? Atmos. Environ., 44(25), 2990-2996, 2010a.

Qi, L., Nakao, S., Tang, P., and Cocker III, D. R.: Temperature effect on physical and chemical properties of secondary organic aerosol from *m*-xylene photooxidation, Atmos. Chem. Phys., 10(8), 3847-3854, 2010b.

Rader, D. J. and McMurry, P. H.: Application of the tandem differential mobility analyzer to studies of droplet growth or evaporation, J. Aerosol. Sci., 17(5), 771-787, 1986.

Rubin, J. I., Kean, A. J., Harley, R. A., Millet, D. B., and Goldstein, A. H.: Temperature dependence of volatile organic compound evaporative emissions from motor vehicles. J. Geophys. Res.-Atmos, 111(D3), 2006.

Salo, K., Hallquist, M., Jonsson, Å.M., Saathoff, H., Naumann, K.-H., Spindler, C., Tillmann, R., Fuchs, H., Bohn, B., Rubach, F., Mentel, T. F., Müller, L., Reinnig, M., Hoffmann, T., and Donahue, N. M.: Volatility of secondary organic aerosol during OH radical induced ageing, Atmos. Chem. Phys., 11(21), 11055-11067, 2011.

Sato, K., Hatakeyama, S., and Imamura, T.: Secondary organic aerosol formation during the photooxidation of toluene: NO_x dependence of chemical composition, J. Phys. Chem. A., 111(39), 9796-9808, 2007.

Sato, K., Takami, A., Isozaki, T., Hikida, T., Shimono, A., and Imamura, T.: 2010. Mass spectrometric study of secondary organic aerosol formed from the photo-oxidation of aromatic hydrocarbons, Atmos. Environ., 44(8), 1080-1087, 2010.

Sato, K., Takami, A., Kato, Y., Seta, T., Fujitani, Y., Hikida, T., Shimono, A., and Imamura, T. 2012. AMS and LC/MS analyses of SOA from the photooxidation of benzene and 1, 3, 5-trimethylbenzene in the presence of NO_x: effects of chemical structure on SOA aging, Atmos. Chem. Phys, 12, 4667-4682, 2012.

Seinfeld, J. and Pandis, S.: Atmospheric chemistry and physics: from air pollution to climate change. John Wiley & Sons Publications, Hoboken, New Jersey, US, 2006.

Shilling, J. E., Chen, Q., King, S. M., Rosenoern, T., Kroll, J. H., Worsnop, D. R., DeCarlo, P. F., Aiken, A. C., Sueper, D., Jimenez, J. L., and Martin, S. T.: Loading-dependent elemental composition of α-pinene SOA particles, Atmos. Chem. Phys., 9(3), 771-782, 2009.

Singh, H. B., Salas, L. J., Cantrell, B. K., and Redmond, R. M.: Distribution of aromatic hydrocarbons in the ambient air, Atmos. Environ., (1967), 19(11), 1911-1919, 1985.

Song, C., Na, K., and Cocker III, D. R.: Impact of the hydrocarbon to NO_x ratio on secondary organic aerosol formation, Environ. Sci. Technol., 39(9), 3143-3149, 2005.

Song, C., Na, K., Warren, B., Malloy, Q., Cocker III, D. R.: Secondary organic aerosol formation from the photooxidation of *p*-and *o*-xylene. Environ. Sci. Technol., 41(21), 7403-7408, 2007.

Tkacik, D. S., Presto, A. A., Donahue, N. M., and Robinson, A. L.: Secondary organic aerosol formation from intermediate-volatility organic compounds: cyclic, linear, and branched alkanes, Environ. Sci. Technol., 46(16), 8773-8781, 2012.

Tritscher, T., Dommen, J., DeCarlo, P. F., Gysel, M., Barmet, P. B., Praplan, A. P., Weingartner, E., Prévôt, A. S. H., Riipinen, I., Donahue, N. M., and Baltensperger, U.: Volatility and hygroscopicity of aging secondary organic aerosol in a smog chamber, Atmos. Chem. Phys., 11(22), 11477-11496, 2011.

Yee, L. D., Kautzman, K. E., Loza, C. L., Schilling, K. A., Coggon, M. M., Chhabra, P. S., Chan, M. N., Chan, A. W. H, Hersey, S., Crounse, J. Wennberg, P. O., Flagan, R. C., and Seinfeld, J. H.: Secondary organic aerosol formation from biomass burning intermediates: phenol and methoxyphenols. Atmos. Chem. Phys., 13(16), 8019-8043, 2013.

Yu, L., Smith, J., Laskin, A., Anastasio, C., Laskin, J., and Zhang, Q.: Chemical characterization of SOA formed from aqueous-phase reactions of phenols with the triplet excited state of carbonyl and hydroxyl radical, Atmos. Chem. Phys., 14(24), 13801-13816, 2014.

Zhang, Q., Alfarra, M. R., Worsnop, D. R., Allan, J. D., Coe, H., Canagaratna, M. R., and Jimenez, J. L.: Deconvolution and quantification of hydrocarbon-like and oxygenated organic aerosols based on aerosol mass spectrometry, Environ. Sci. Technol., 39(13), 4938-4952, 2005.

Zhang, Y., Wang, X., Barletta, B., Simpson, I.J., Blake, D.R., Fu, X., Zhang, Z., He, Q., Liu, T., Zhao, X., and Ding, X.: Source attributions of hazardous aromatic hydrocarbons in urban, suburban and rural areas in the Pearl River Delta (PRD) region. J. Hazard. Mater., 250, 403-411, 2013.

Ziemann, P.: Effects of molecular structure on the chemistry of aerosol formation from the OH-radical-initiated oxidation of alkanes and alkenes, International Reviews in Physical Chemistry, 30(2), 161-195, 2011.

Ziemann, P.J., and Atkinson, R.: Kinetics, products, and mechanisms of secondary organic aerosol formation. Chem. Soc. Rev., 41(19), 6582-6605, 2012.

4.7 Tables and Figures

Table 4.1 Experiment conditions

Precursor	ID	HC/NO ppbC:ppb	NO ppb	HC ppb	ΔHC $\mu g \cdot m^{-3}$	M_o[a] $\mu g \cdot m^{-3}$	Yield
Ethylbenzene	1142A	17.0	47.4	101	331	22.0	0.066
	1142B	12.0	66.6	99.9	341	4.40	0.013
	1146A	35.6	22.2	99.0	257	36.0	0.140
	1146B	23.0	34.8	100	331	23.6	0.071
	1147B	74.9	36.5	342	626	88.1	0.141
	2084A	81.1	23.9	242	374	54.0	0.145
	2084B	93.8	20.3	238	266	44.3	0.167
Propylbenzene	1245A	41.0	22.1	101	231	11.8	0.051
	1246A	26.8	68.5	204	421	22.9	0.054
Isopropylbenzene	1247A	40.3	22.4	100	301	33.2	0.110
	1247B	18.6	48.1	99.3	300	16.6	0.055
	1253A	31.9	56.4	200.	538	53.1	0.099
	1253B*	17.6	100	196	526	16.5	0.031
o-Xylene	1315A	13.2	49.8	82.2	324	26.3	0.081
	1315B	28.8	22.2	80.0	27	25.4	0.091
	1320A	12.8	50.0	80.0	335	18.4	0.055
	1321A	31.0	20.5	79.2	263	16.2	0.061
	1321B	61.3	10.4	80.0	226	9.80	0.044
p-Xylene	1308A	15.5	55.6	78.4	279	6.80	0.024
	1308B	171	22.9	78.8	274	11.3	0.041
m-Ethyltoluene	1151A	17.9	62.5	84.8	409	8.30	0.020
	1151B	31.0	32.3	86.4	415	28.7	0.069
	1199A	8.8	45.4	100.2	447	72.0	0.161
	1222B	41.7	69.4	100.0	484	70.9	0.146
	1226B	11.3	137.6	201.1	895	138	0.154
	1232A	27.5	122.0	200.0	901	150	0.167
	1232B	33.1	67.5	194.8	751	117	0.155
	1421A	41.0	22.1	97.9	409	46.2	0.112
	1421B	18.0	44.9	98.7	477	54.6	0.114
o-Ethyltoluene	1179A	16.3	52.9	91.7	399	86.5	0.216
	1179B	15.8	52.9	93.0	415	75.3	0.181
	1202A	18.5	60.3	99.7	422	69.9	0.166
	1215A	29.2	107.9	180.3	637	151	0.237
	1413A	12.2	21.3	100.4	371	64.5	0.174
	1413B	24.1	45.8	98.4	455	64.4	0.141
p-Ethyltoluene	1194A	19.9	90.7	196	741	90.4	0.122
	1194B	13.0	88.4	200	761	73.0	0.096

	1197A	13.1	56.4	192	653	66.4	0.102
	1197B	14.8	98.5	192	710	58.4	0.082
	1214B	26.0	53.4	102	418	29.1	0.069
	1601A	39.9	31.2	109	452	17.6	0.039
1, 2, 3-Trimethylbenzene	1158A	19.8	10.3	79.9	296	22.2	0.075
	1158B	15.6	22.4	79.9	379	32.3	0.085
	1162A	15.8	33.4	80.1	391	46.5	0.119
	1162B	14.9	40.0	80.4	399	46.6	0.117
1, 3, 5-Trimethylbenzene	1153A	65.2	11.0	79.5	309	12.4	0.040
	1153B	35.3	20.4	80	381	19.6	0.051
	1156A	22.3	32.3	80.2	379	24.8	0.065
	1156B	15.5	46.1	79.6	390	19.0	0.049
	1329B	11.1	64.8	80.0	296	3.00	0.007

Note: a) M_o is a wall loss and density corrected particle mass concentration; * Not used in curve fitting

Table 4.2 Two product yield curve fitting parameters for one, two (ortha, meta and para) and three alkyl substitutes

Yield Curve	α_1	$K_{om,1}$ ($m^3 \cdot \mu g^{-1}$)	α_2	$K_{om,2}$ ($m^3 \cdot \mu g^{-1}$)	MSRE[a]
One Substitutes	0.144	0.039	0.137	0.005	5.38
Two Substitutes-ortho	0.158	0.249	0.024	0.005	2.03
Two Substitutes-meta	0.156	0.040	0.080	0.005	2.51
Two Substitutes-para	0.154	0.025	0.036	0.005	1.21
Three Substitutes	0.180	0.025	0.052	0.005	0.84

Note: a) Mean squared error (MSRE) = [(Fitted Yield - Measured Yield)/ Measured Yield]^2/(Number of Data Points)

Table 4.3 Correlation among SOA density, volatility (VFR) and SOA chemical composition

	f_{44}	f_{57}	f_{71}	O/C	H/C	OS_c	k_{OH}
Density	0.324	-0.056	-0.38	0.551	-0.301	0.540	-0.249
p-value[b]	0.304	0.862	0.223	0.063	0.341	0.070	0.435
VFR_{end}[a]	0.537	0.56	0.399	0.471	-0.586	0.593	-0.937
p-value[b]	0.089	0.073	0.224	0.144	0.058	0.055	0.000

Note: a) VFR_{end} volume fraction remaining at the end of photooxidation; b) p-Values range from 0 to 1, 0-reject null hypothesis and 1 accept null hypothesis. Alpha (α) level used is 0.05. If the p-value of a test statistic is less than alpha, the null hypothesis is rejected

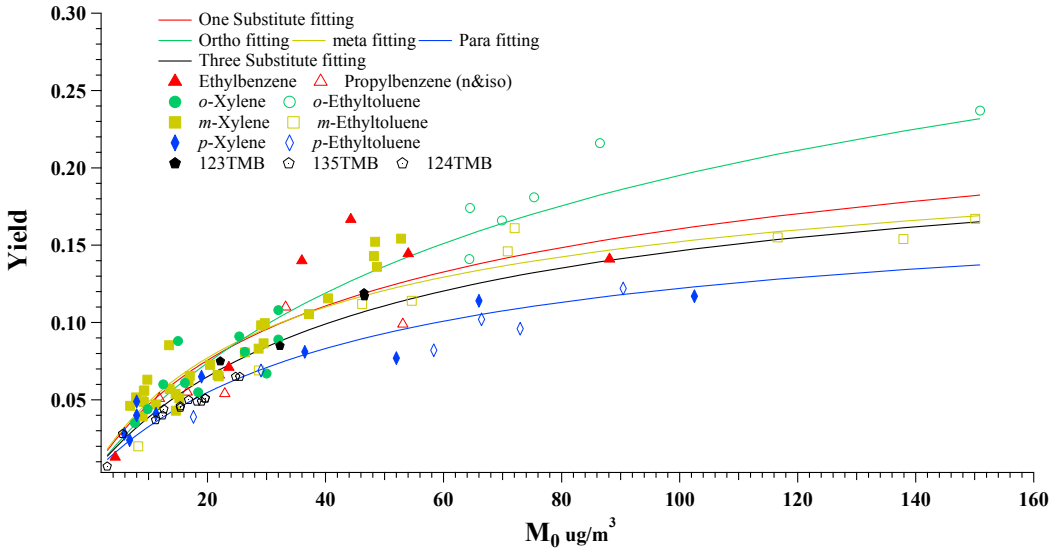

Note: Song, et al, 2005; Song, et al, 2007; Chapter 3data are also included; 123TMB- 1, 2, 3-Trimethylbenzene; 135TMB- 1, 3, 5-Trimethylbenzene; 124TMB- 1, 2, 4-Trimethylbenzene.

Figure 4.1 Aromatic SOA yields as a function of M_o

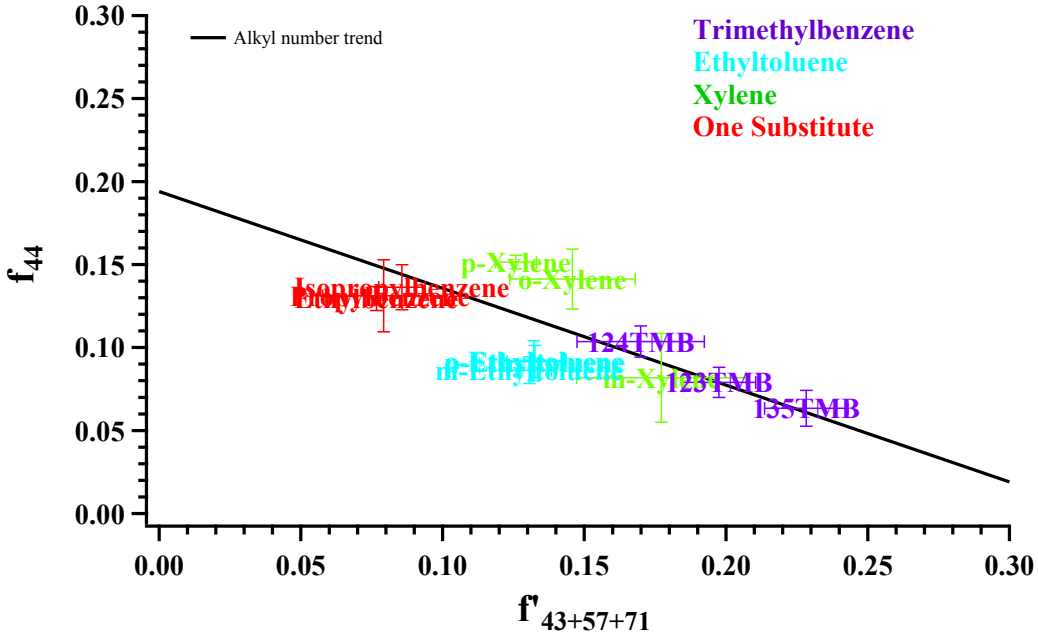

Figure 4.2 f_{44+} vs. $f'_{43+57+71}$ in SOA formed from different aromatic hydrocarbon photooxidation under low NO_x colored by aromatic isomer type and marked with individual aromatic hydrocarbon species:

Ethylbenzene 2084A; Propylbenzene 1245A; Isopropylbenzene 1247A; *m*-Xylene 1191A; *m*-Ethyltoluene 1199A; *o*-Xylene 1320A; *o*-Ethyltoluene 1179A; *p*-Xylene 1308A; *p*-Ethyltoluene 1194A; 1, 2, 3-Trimethylbenzene (123TMB) 1162A;1, 2, 4-Trimethylbenzene (124TMB) 1119A; 1, 3, 5-Trimethylbenzene (135TMB) 1156A. Alkyl number trend is the linear fitting in (Li., et al., 2015a) *Error bar stands for f_{44+} and $f'_{43+57+71}$ standard deviation when significant particles are formed (>5μg/m^3).

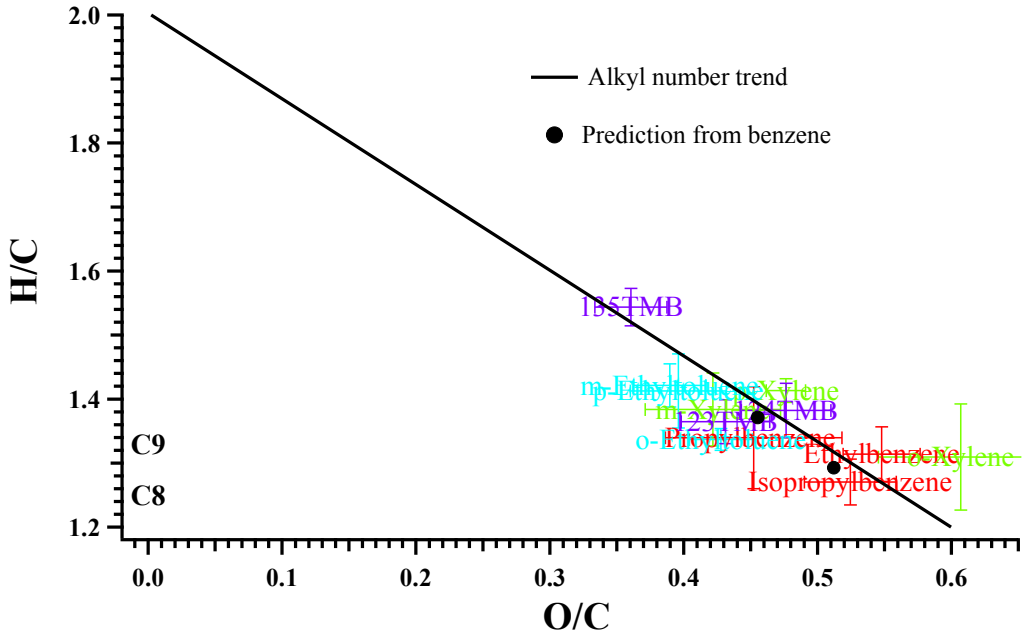

Figure 4.3 H/C vs. O/C in SOA formed from different aromatic hydrocarbon photooxidation under low NO_x colored by aromatic isomer type and marked with individual aromatic hydrocarbon species (C8 and C9 on the lower left indicate the location of initial aromatic hydrocarbon precursor):

Ethylbenzene 2084A; Propylbenzene 1245A; Isopropylbenzene 1247A; *m*-Xylene 1191A; *m*-Ethyltoluene 1199A; *o*-Xylene 1320A; *o*-Ethyltoluene 1179A; *p*-Xylene 1308A; *p*-Ethyltoluene 1194A; 1, 2, 3-Trimethylbenzene (123TMB) 1162A; 1, 2, 4-Trimethylbenzene (124TMB) 1119A; 1, 3, 5-Trimethylbenzene (135TMB) 1156A. Alkyl number trend is the linear fitting in (Li., et al., 2015a). Solid black cycles are SOA elemental ratio from C_8 and C_9 aromatic hydrocarbon predicted by SOA elemental ratio formed from benzene. *Error bar stands for H/C and O/C standard deviation when significant particles are formed (>5μg/m^3).

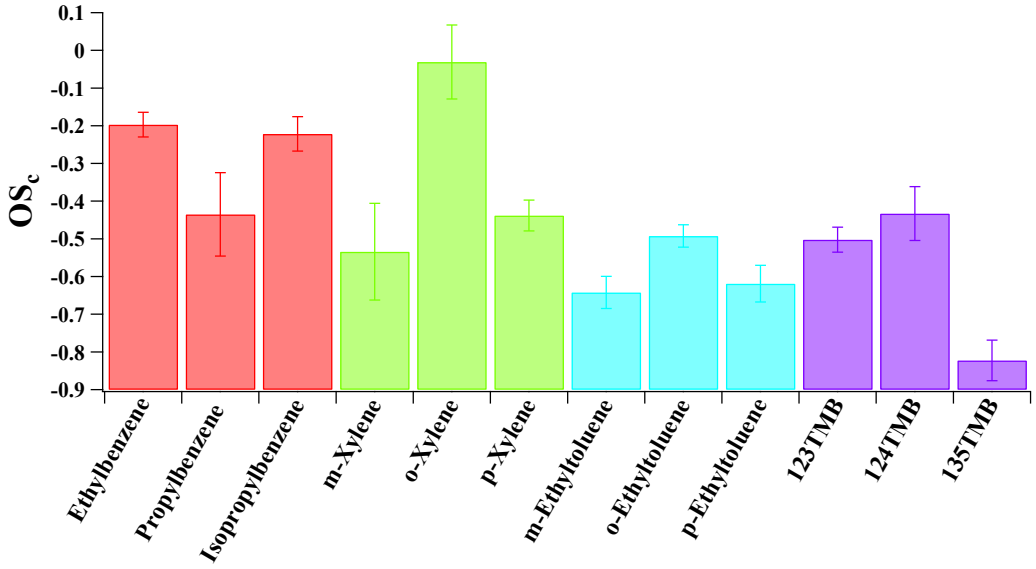

Figure 4.4 Oxidation state (OS_c) of SOA formed from different aromatic hydrocarbon photooxidation under low NO_x:

Ethylbenzene 2084A; Propylbenzene 1245A; Isopropylbenzene 1247A; *m*-Xylene 1191A; *m*-Ethyltoluene 1199A; *o*-Xylene 1320A; *o*-Ethyltoluene 1179A; *p*-Xylene 1308A; *p*-Ethyltoluene 1194A; 1, 2, 3-Trimethylbenzene (123TMB) 1162A; 1, 2, 4-Trimethylbenzene (124TMB) 1119A; 1, 3, 5-Trimethylbenzene(135TMB) 1156A.

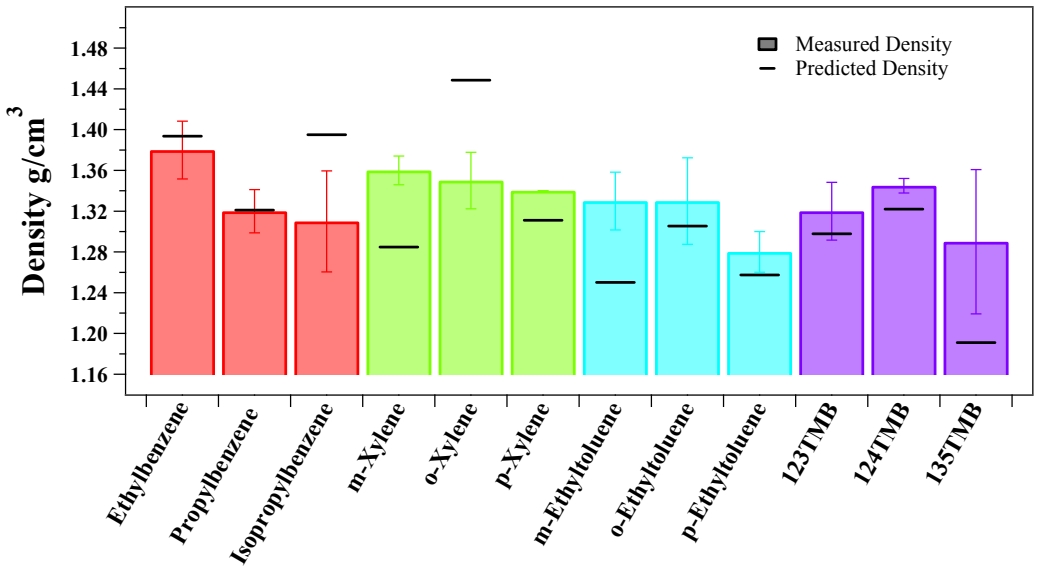

Figure 4.5 Measured and predicted SOA density from different aromatic hydrocarbon photooxidation under low NO_x

(Colored with substitute number and length, one substitute-red, xylenes-green, ethyltoluenes-blue and trimethylbenzene-purple; black line is predicted density according to Kuwata, et al., 2011); 123TMB- 1, 2, 3-Trimethylbenzene; 135TMB- 1, 3, 5-Trimethylbenzene; 124TMB- 1, 2, 4-Trimethylbenzene.

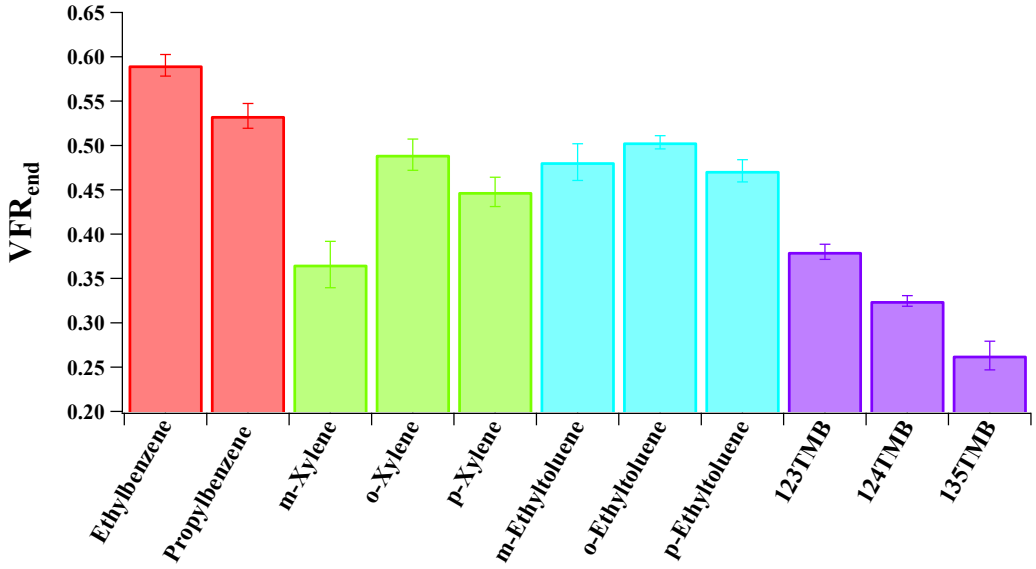

Figure 4.6 SOA Volume fraction remaining (VFR_{end}) at the end of aromatic hydrocarbon photooxidation under low NO_x

(Colored with substitute number and length, one substitute-red, xylenes-green, ethyltoluenes-blue and trimethylbenzene-purple); 123TMB- 1, 2, 3-Trimethylbenzene; 135TMB- 1, 3, 5-Trimethylbenzene; 124TMB- 1, 2, 4-Trimethylbenzene.

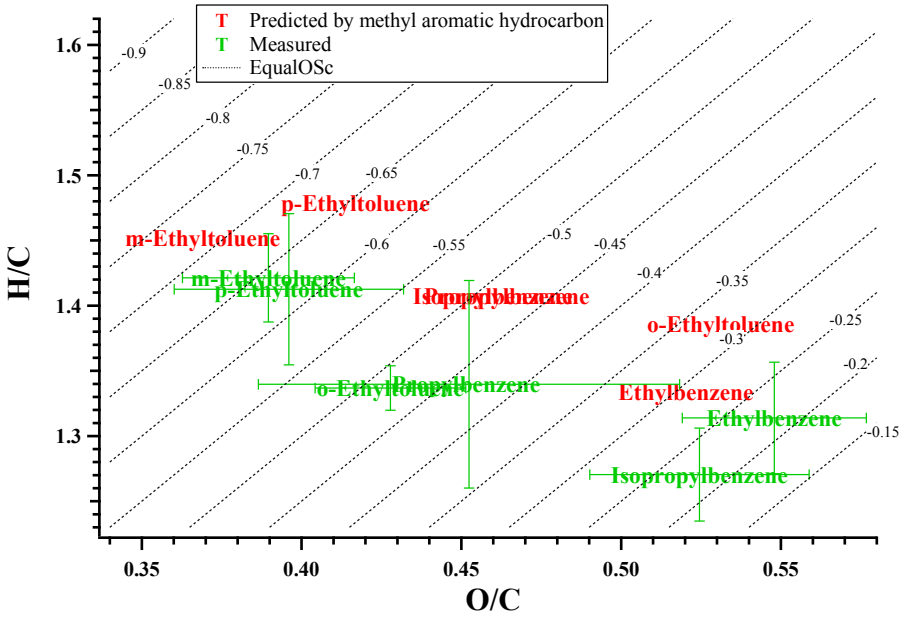

(a)

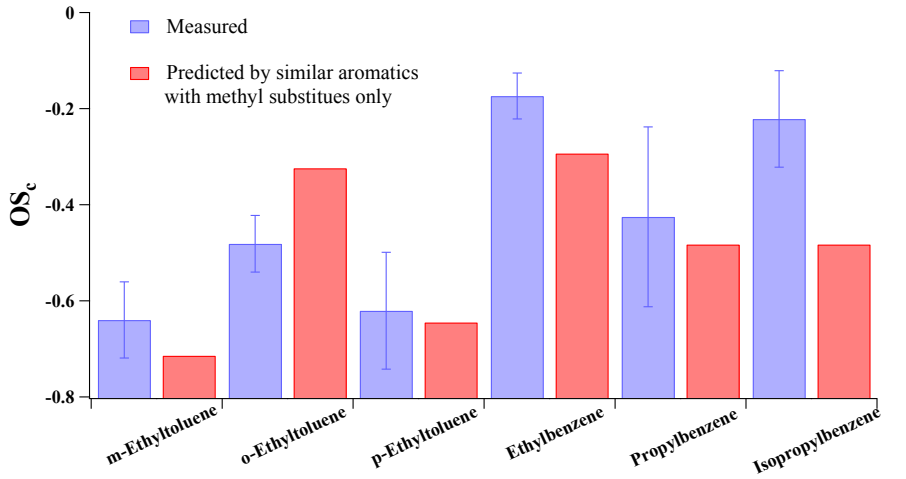

(b)

Figure 4.7 Comparison of measured and predicted elemental ratio (a) and oxidation state (b) of SOA formed from longer alkyl substitute ($-C_2H_{2n+1}$, n>1). Ethyltoluenes are predicted by corresponding xylenes and one substitute aromatic hydrocarbons are predicted by toluene.

*Predicted elemental ratio of isopropylbenzene is same as propylbenzene (not showed in Fig. a)

5. Novel Approach for Evaluating Secondary Organic Aerosol from Aromatic Hydrocarbons: Unified Method for Predicting Aerosol Composition and Formation

5.1 Introduction

Challenges remain in predicting anthropogenic secondary organic aerosol (SOA) with anthropogenic SOA sources underestimated in current models by a factor of upto 10 (Volkamer, et al., 2006; Gaydos, et al., 2007; Henze, et al., 2008; Matsui, et al., 2009; Hallquist, et al., 2009; Farina, et al., 2010; Tsimpidi, et al., 2010; Hayes, et al., 2015;) Woody, et al., 2016). It is imperative to develop SOA predictive frameworks in order to help models predict SOA formation from a wide variety of aerosol precursors given limited experimental resources. Aromatic hydrocarbons are an example of a major class of anthropogenic SOA precursors (Kanakidou, et al., 2005; Derwent, et al., 2010; Freney, et al., 2014; Farina, et al., 2010) that can benefit from such a predictive framework as their SOA formation is explored for increasingly relevant atmospheric conditions.

Importing reasonable SOA formation parameters into models is essential for accurate estimates of global and regional SOA budgets. SOA yield is a function of the extent of gas-to-particle conversion, which depends on the vapor pressure of the absorbing species (Odum, et al., 1996). Recent studies also demonstrate the importance of aqueous chemistry (Lim, et al., 2010) and heterogonous reaction (Jang, et al., 2002). However, collecting reliable SOA parameters for every aerosol precursor requires significant effort and time. Therefore, a general rule to predict SOA yield and chemical composition by precursor

category is valuable for SOA prediction. Traditionally, two-product models simulate SOA yield by categorizing all oxidation products into two lumped semi-volatile products according to their gas-particle phase partitioning coefficient (Pankow, et al., 1994; Odum, et al., 1996). The volatility basis set (VBS) stems from the two-product model by assigning VOC oxidation products to volatility "bins", which spans across multiple ambient organic effective saturation mass concentrations (C∗) (Donahue, et al., 2006). Several models have also been established based on the two product and/or VBS model by adding tunable parameters that estimate chemical polarity, polymerization, fragmentation, functionalization and elemental ratio (Pankow, et al., 2009; Barsanti, et al., 2011; Cappa and Wilson, 2012; Donahue, et al., 2012). More complicated models are also developed considering explicit gas and particle phase reaction mechanisms (Aumont, et al., 2005; Valorso, et al., 2011; Zhang, et al., 2013) and phase state impact (Gaydos, et al., 2007; Zuend, et al., 2010; Shiraiwa, et al., 2012). Newly developed models are calibrated and tuned with alkanes (Cappa and Wilson, 2012; Zhang and Seinfeld, 2013) and biogenic SOA precursors (Barsanti, et al., 2011; Donahue, et al., 2012). Ensuring the accuracy of SOA prediction form aromatic hydrocarbon photooxidation under ambient conditions improves the SOA prediction in current models (Jathar, et al., 2015). Due to the limited understanding of aromatic oxidation chemistry, the applicability of these models to a variety of aromatic hydrocarbons requires further work.

Earlier two-product model fittings to aromatic hydrocarbon oxidation are not applicable to ambient atmospheric conditions (Odum, et al., 1997; Cocker, et al., 2001a) as they were conducted at NO_x concentrations that are not atmospherically relevant

(>100ppb~1000ppb). Recent studies on the photooxidation of aromatic hydrocarbons at lower NO_x levels only focus on a few selected aromatic precursors (Song, et al., 2005; Song, et al., 2007; Ng, et al., 2007). Therefore, a new systematic study on SOA formation as a function of aromatic molecular structure is required at more relevant atmospheric conditions to elucidate how these compounds are truly behaving in the atmosphere. Odum's (1997) work summarizes the SOA yields formed from the oxidation of aromatics into two groups (low yield and high yield group). This work improves upon this earlier work by providing SOA yields at more realistic conditions (e.g., NO_x concentration simulating urban regions) with tighter controls on the environmental conditions (e.g., temperature and light intensity). Our earlier work (Chapter 3 found traditional mass based SOA yields for aromatic hydrocarbons are associated with the number of alkyl substitutes in aromatic precursor. Further studies are still needed to explore the underlying mechanisms leading to the relationship in between SOA formation and aromatic hydrocarbon molecular structure.

Elemental analysis (Aiken, et al., 2007, 2008) can help elucidate SOA chemical composition and formation mechanisms (Heald, et al., 2010; Chhabra, et al., 2011). Previous SOA product studies observed a decrease in O/C and an increase in H/C with the addition of alkyl substitutes attached to the precursor aromatic ring (Chhabra, et al., 2011; Loza, et al., 2012; Sato, et al., 2012), resulting in a lower measured oxidation state of carbon (OSc) (Kroll, et al., 2011) with increasing number of alkyl substitutes. However, the low H/C ratio or high degree of unsaturation (Double Bond Equivalent=4) of the aromatic ring makes the H/C of aromatic hydrocarbons more dependent on the number of

substituted alkyl carbons than more saturated precursors. This dependence of H/C on alkyl carbon substitutes is likely retained in aromatic SOA products. Further, the carbon on the aromatic ring may behave differently than the alkyl substitute carbon with respect to overall O/C. Therefore, evaluating the extent of aromatic hydrocarbon oxidation solely relying on average SOA H/C and O/C without distinguishing between alkyl substitute and aromatic ring carbons may conceal the compositional similarity among SOA from different aromatics. Refinement of the SOA elemental ratio interpretation is required to clarify the contribution of different functional groups to the SOA formation from aromatic hydrocarbons.

The motivation of this study is to improve the understanding of aromatic hydrocarbon SOA formation using innovative methods developed within this study. SOA yield and chemical composition are reanalyzed on the basis of the aromatic ring using fifteen years of UC Riverside/CE-CERT chamber data on 17 aromatic hydrocarbons with HC:NO ratio ranging from 11.1 ppbC:ppb to 171 ppbC:ppb. Specific and general alkyl substitute or molecular structure impacts to SOA formation from single ring aromatic hydrocarbons are explored.

5.2 Method

All experiments (Table S 5.1) were conducted in the UC Riverside/CE-CERT indoor dual 90 m^3 environmental chambers (Carter, et al., 2005). Experiments were conducted at dry conditions (RH<0.1%), in the absence of inorganic seed aerosol and with temperature controlled to 27±1°C. Particle size distribution between 27 nm and 686 nm was monitored

by dual custom built Scanning Mobility Particle Sizers (SMPS) (Cocker, et al., 2001b). Particle effective density was measured with a Kanomax Aerosol Particle Mass Analyzer (APM-SMPS) system (Malloy, et al., 2009). Evolution of particle-phase chemical composition was measured by a High Resolution Time of Flight Aerosol Mass Spectrometer (HR-ToF-AMS; Aerodyne Research Inc.) (DeCarlo, et al., 2006; Canagaratna, et al., 2007). The Agilent 6890 Gas Chromatograph – Flame Ionization Detector was used to measure aromatic hydrocarbon concentrations. A Thermal Environmental Instruments Model 42C chemiluminescence NO analyzer was used to monitor NO, NO_y-NO and NO_y.

A suite of 17 aromatic hydrocarbon (zero to six alkyl substitutes ranging in carbon number from one to three) SOA precursors was studied. Detailed environmental conditions for 17 aromatic precursors are described previously (Chapter 3 and Chapter 4). The reaction activities (e.g. k_{OH}*[OH], $[HO_2]$*$[RO_2]$) are comparable for all aromatic precursors studies (Chapter 3 and 4). Seeded experiments to minimize wall effects have also been conducted in our chamber experiment with no measurable difference observed between the seeded and non-seeded experiment. This indicates that the gas-phase wall loss might not actually be significant in our chamber for aromatic SOA experiments.

This study defines a ring normalized SOA yield (Yield′) by adjusting yield from per aromatic precursor mass consumption to per aromatic ring mass assumption to elucidate the SOA formation potential per aromatic ring or per mole instead of the traditional per total mass method. Ring normalized SOA yield (Yield′) is calculated as

$$\text{Yield}' = \frac{M_0}{(\Delta HC_i/MW_i)\times MW_{AR}} = \frac{M_0}{\Delta HC_i} \times \frac{MW_i}{MW_{AR}} = \text{Yield}_i \times \frac{MW_i}{MW_{AR}} \quad \text{Eq-1}$$

where MW_i (g·mol^{-1}) is the molecular weight of a specific aromatic hydrocarbon i (g·mol^{-1}), MW_{AR} is the molecular weight of an aromatic ring (78 g·mol^{-1} assuming C_6H_6). $Yield_i$ is the traditional SOA mass yield of each aromatic hydrocarbon (*i*) precursor defined by Odum et al.(1996) as

$$\text{Yield}_i = \frac{M_0}{\Delta HC_i} \quad \text{Eq-2}$$

where M_0 (μg·m^{-3}) is the particle phase organic mass concentration produced from the amount of aromatic hydrocarbon (*i*) precursor reacted, ΔHC_i (μg·m^{-3}).

Elemental ratios (Aiken, et al., 2007, 2008) have been reported using AMS data in many studies (Chhabra, et al., 2011; Loza, et al., 2012; Sato, et al., 2012). Recent work by Li et al (2016a) demonstrates that the addition of methyl groups to the aromatic ring reduces the average oxidation extent of carbon in SOA formed from aromatic hydrocarbons. The current work redefines elemental ratio on an aromatic ring basis (Eq-3& Eq-4) to examine the oxygen and hydrogen content in SOA on a per aromatic ring basis. Therefore, we define O/R and H/R as the oxygen and hydrogen content per aromatic ring, calculated as follows:

$$O/_R = C/_{R_i} \times O/_C \quad \text{Eq-3}$$

$$H/_R = C/_{R_i} \times H/_C \quad \text{Eq-4}$$

where C/R_i represents carbon number on aromatic hydrocarbon *i* and *H/C* and *O/C* are the traditional mole based elemental ratios (Aiken, et al., 2007, 2008).

5.3 Results

5.3.1 Ring Normalized SOA Yield (Yield′)

The physical meaning of ring normalized SOA yield (Yield′) is SOA formation per mass of aromatic ring consumed. Yield′ technically compares SOA yield from aromatic hydrocarbons on a mole basis since the mass of aromatic ring consumed is proportional to the mole of aromatic hydrocarbon consumed. It is reported that SOA yields from aromatic hydrocarbons decrease with an increase of the number of methyl groups (Chapter 3). The ring normalized SOA yield (Yield′) scales up the low SOA yield by using the ratio of the molecular weight of aromatic precursor and benzene, which is larger than 1, and improves the SOA yield similarity among all aromatic precursors. Ring normalized SOA Yield (Yield′) as well as traditional mass based SOA yield are listed in Table S5.2. Yield′ and M_0 relationships are plotted (Fig 5.1) similarly to the traditional SOA yield curve in Odum′s work (1996). The benzene yield fitting curve in Fig.1 (pink curve) is the same as Fig. S5.1 and is provided as a reference Yield curve. Yield′ from all aromatic hydrocarbons cluster around the fitted curve of benzene (pink curve, Fig 5.1) instead of scattering to lower yield curves, traditionally used to describe aromatic SOA formation (Fig S5.1) (Chapter 3 and 4). The improvement from scattering to gathering in SOA yield suggests that a similar amount of SOA is formed during the photooxidaiton of each aromatic hydrocarbon when similar amount of aromatic ring involved in the reaction. Similarity of the ring normalized SOA yield among all aromatic hydrocarbons reveals that the aromatic ring contributes more to SOA formation than the alkyl substitute. A semi-empirical two product model fit

approach similar to Odum et al (1996) is used to fit the Yield′ versus M_0 data in this work to further demonstrate the similarity among all SOA yield′ for aromatic hydrocarbons. The overall two product model fitting parameters (α_1', $K_{om,1}'$, α_2' *and* $K_{om,2}'$, Table 5.1) were determined by minimizing the sum of the square of the residuals.

The 17 aromatic hydrocarbons studied (consisting of 129 data points) are fit with a single curve with a mean squared relative error (MSRE) of 13.7×10^{-2} (Table S5.3), nearly half of the MSRE (24.6×10^{-2}) of the single curve fit performed using traditional yield and M_0. The difference (Fig. 5.1) between the benzene fitted curve (Pink) and the overall yield′ fitted curve (Dark) indicates a lower yield in benzene at lower mass loading (<50 μg/m^3) and a higher yield at higher mass loading (>100 μg/m^3) than the ring normalized SOA yield (Yield′). Overall, the application of ring normalized SOA yield reveal that SOA formation from aromatic hydrocarbons are dependent on the mole of aromatic ring reacted rather than the mass of whole aromatic molecular mass consumed during the photooxidation.

5.3.2 Aromatic Ring Based SOA Elemental Ratio

O/R and H/R calculate SOA chemical composition on a precursor aromatic ring basis. They are derived from O/C and H/C and advances O/C and H/C by integrating the impact of the precursor molecular structure on SOA formation into the bulk chemical composition analysis. An average O/R=4.08±0.26 (standard deviation equally weights O/R for each group of aromatic hydrocarbons with similar total number of carbon) is observed for SOA originating from the 17 aromatic hydrocarbons studied in this work (Fig. 5.2). The similarity of O/R from single aromatic ring hydrocarbons with different number of total

carbons (6 to 12) indicates that each aromatic precursor gains four oxygen when oxidized to SOA regardless of alkyl substitution. Observed H/R increases in SOA composition along with increasing H/R of the aromatic precursor, which can be seen by the approximately flat dotted lines connecting the H/R of the aromatic precursors to the average H/R of resulting SOA in Fig 5.2.

The bulk SOA composition during aromatic photooxidation can be predicted according to alkyl carbon number (*n*) as

$$\mathrm{C}:\mathrm{H}:\mathrm{O} = (6+\mathrm{n}):(6+2\mathrm{n}):4 \qquad \text{Eq-5}$$

where n is the number of alkyl carbons.

Current work provides a simple and reliable method to explain and further predict SOA composition from aromatic precursors for implementation into SOA models. Eq-5 further implies that the average double bond equivalents of aromatic SOA is 4.

5.3.3 Influence of Isomers on SOA Yield′

While a single Yield′ curve fitting provides a reasonable estimation of Yield′ for all aromatic compounds, the estimation for individual aromatics can be further improved by accounting for structural isomer effects. Previous work on isomer trends using mass based yield (e.g., Li et al., 2016b) directly applies to Yield′ as isomers have identical molecular weights. Therefore, the overall yield fit can be further refined by using separate curves for ortho-, meta-, and para- isomers (Fig 5.3). Slightly higher SOA yields observed during aromatic hydrocarbon photooxidation for ortho position isomers and lower SOA yields

from para position isomers (Li et al., 2016b) are persistent in ring normalized SOA yields. Benzene has a somewhat unique trend likely due to enhanced bicyclic hydroperoxide formation (Li et al., 2016a) and is therefore given a fourth curve in this refined analysis. Ring normalized yields between aromatics with similar structure (ortho, meta, para) but differing carbon numbers are observed to collapse onto single curves defined by their structure. Mono substituted aromatics and trimethylbenzene isomers most closely associate with the meta- isomer curve and are therefore lumped into the same meta-isomer curve. Aromatics with 4 or more substituents (C_{10+}) tend to have lower Yield′ falling closest to the para curve. This agrees with the suppression impact of para isomers and C_{10+} aromatic hydrocarbons is proposed in earlier work (Song, et al., 2005; Malloy, et al., 2009). Therefore, only C_{10+} and two substitute aromatics including para and ortho structure have a small either promotion or suppression effect on SOA formation. AMT1 represents the major SOA formation trend for aromatic hydrocarbons.

The four refined curves (all ortho aromatics, AO; all meta aromatics, mono- substituted aromatics, and trimethylbenzenes, AMT1; all para aromatics and C_{10+} aromatics, AP10; and benzene) are then fit with a modified (Yield′ instead of Y) two product model (α_1', α_2', $K_{om,1}'$, $K_{om,2}'$; Table 5.1). A constant $K_{om,2}'$ (more volatile lumped species parameter) is assumed for all curve fits to focus on the yield difference caused by the less volatile ($K_{om,1}'$) products. MSRE for the AMT1 curve decrease from 17.9×10^{-2} to 14.8×10^{-2} when SOA yield is normalized on a ring basis. Similar MSRE decreases are also observed (Table S5.3) for the AP10 and AO while applying ring normalized SOA yield instead of traditional mass based yield. The benzene curve (α_1= 0.082, $K_{om,1}$=0.017, α_2=0,617 and $K_{om,2}$=0.005)

(Chapter 3) is seen to behave most similarly to the lowest yield group (AP10) at atmospherically relevant mass loadings (<50 $\mu g \cdot m^{-3}$), most similar to the median yield group (AMT1) at median mass loadings (50-110 $\mu g \cdot m^{-3}$) and closest to highest yield group (AO) at the highest mass loadings (>110 $\mu g \cdot m^{-3}$). Using a single curve (Section 5.3.1) to describe all experiments increases the MSRE to 24.64×10^{-2}.

5.3.4 Influence of Isomers on SOA elemental ratio

While a general O/R and H/R is observed for the 17 aromatic precursors studied, some minor variations are observed between isomers (Fig. 5.4; Fig. S5.2). SOA formed from *m*-xylene and 1, 3, 5-trimethylbenzene show slightly higher H/R and lower O/R compared with their aromatic isomers, which indicates a slightly lower overall oxidation of the meta isomers compared to the ortho and para isomers. However, there is no significant H/R and O/R difference among meta, para and ortho ethyltoluenes due to the effect of a longer chain alkyl substitute attached to aromatic ring (Chapter 4). Propylbenzene and isopropylbenzene photooxidation have somewhat lower H/R and higher O/R than the other C_9 isomer suggesting that the longer alkyl substitutes may themselves partially oxidize.

5.4 Discussion

There are ongoing initiatives to identify and account for all possible processes related to SOA formation from hydrocarbon precursors. Advanced models are being developed as more mechanisms are clarified while the gap between model prediction and measured data continues to suggest that further work is needed. However, there remains a need to simplify these processes in order to reasonably estimate aerosol formation in atmospheric models

while using a practical number of environmental chamber experiments and computing modules. The two-product model is extensively used in current atmospheric models (Binkowski, et al., 2003; Jenkin, et al., 2003; Tsigaridis, and Kanakidou, 2003; Kanakidou, et al., 2005) and extends to various models (Donahue, et al. ,2006; Pankow and Barsanti, 2009; Barsanti, et al., 2011; Donahue, et al., 2012; Cappa and Wilson, 2012) as a result of its simplicity. A modified two-product model has been developed in this work to upgrade the model predictions without increasing fitting parameters.

While precursor carbon number is expected to influence SOA formation, increasing one alkyl carbon number only decreases the vapor pressure 0.3 times (Pankow and Asher, 2008) -- a comparatively small change compared with reactions such as functionalization. SOA yield increases with carbon number agree with the precursor vapor pressure decrease trend for n-alkanes (Lim and Ziemann, et al., 2005). However, studies on aromatic precursors observe decreases in SOA yield with increasing precursor carbon number (Shiraiwa, et al., 2012; Odum, et al., 1997; Cocker, et al., 2001a; Chapter 3; Sato, et al., 2012). This indicates mechanisms more than functionalization contribute to the photooxidation of aromatic hydrocarbons since lower vapor pressure aromatic precursor produces less low volatility products on a mass basis. The matter of fact is that VOC oxidation is a combination of functionalization, fragmentation and oligomerization (Jimenez, et al., 2009; Kroll, et al., 2009). The ring normalized SOA yield analyzes SOA yield data on a mole basis or functional group (aromatic ring) basis of SOA precursors, instead of mass basis. This adjustment provides further insights into SOA formation mechanism by directly using SOA yield. The current study demonstrates that ring normalized SOA yields (Yield′) are

similar among all aromatic hydrocarbons. It indicates that the aromatic ring structure is a driving force for SOA formation during aromatic hydrocarbon photooxidation. Alkyl substitute impacts on aromatic hydrocarbon reaction rate and reaction mechanism are less prominent compared with aromatic ring structure. The valuable contribution of the ring normalized yield to SOA model prediction is that SOA yield for aromatic hydrocarbon can be simply represented by a single set of parameters (α and K_{om}) instead of relying on various sets of parameters specifically for individual precursors.

Previous studies identified similar aromatic oxidation products from various aromatic precursors (Forstner, et al., 1997; Kleindienst, et al., 1999). It is likely that most aromatics have similar reaction pathways with branching ratios determined by oxidation conditions and molecular structure. Earlier work demonstrated that the reaction activities (k_{OH}*[OH]) are comparable during the photooxidation of all 17 aromatic precursors studied (Chapter 3&4). The current work found a similar amount of oxygen added per aromatic precursor ring for all 17 aromatic hydrocarbons studied. The O/R standard deviation is only 6.4% of its average value while the O/C standard deviation is 27.1% of O/C average (0.48±0.13). Similar O/R values and their trend are expected to observe among all the aromatic hydrocarbons under ambient conditions since a measurable evolution of H/C and O/C is not observed for aromatic precursors (Chapter 3&4) as oxidation levels are changed through the course of the experiment. Additionally, the hydrogen per aromatic ring in resulting SOA is determined by the number of hydrogens in the aromatic precursor. These findings address the SOA chemical composition similarity found in aromatic hydrocarbon oxidation, which is consistent with the similar ring normalized adjusted yield (Yield′). The similarities can only be observed

when SOA yield and chemical composition are analyzed on an aromatic ring basis developed in this work. These aromatic hydrocarbons are different in alkyl substitute number and structure with only the aromatic ring as the common structure for all the aromatic hydrocarbons. This work demonstrates that the aromatic ring, not the alkyl substitutes, is the key contributor to the SOA formation from aromatic hydrocarbons. SOA formation from bicyclic hydroperoxides pathway (Carter and Heo, 2013) and oligomerization (Chapter 3) maintains the alkyl substitutes in the oxidation products and relies on the aromatic ring to the form the oxidized products. Therefore, bicyclic hydroperoxides pathway and oligomerization are suggested as two potential mechanisms leading to the similarity in SOA formation from different aromatics observed in this work. The success of applying a ring based chemical composition analysis in aromatic hydrocarbon studies indicates the importance of a molecular structure (aromatic ring) based chemical composition analysis, which could possibly extended to other groups of SOA precursors.

SOA yield and composition trends discussed in this work are all based on aromatic photooxidation under NO_x conditions simulating urban area. This work provides more realistic SOA yield of aromatics under ambient conditions than earlier works (e.g. Odum, et al., 1996). More important, this work provides a single curve prediction method for SOA yield of aromatics, which is even simpler than the two yield groups suggested by Odum et al (1996). The current work demonstrates that the oxidation of the aromatic hydrocarbon ring and not of the alkyl substituents is the driving force for SOA formation and composition from single ring aromatic hydrocarbons. This ring normalized SOA yield

method is initially applied to an existing aromatic hydrocarbon photooxidation dataset; however, its use need not be necessarily restricted to aromatics and should be evaluated on other classes of SOA precursors. The core of the concept is to compare SOA formation from a group of similar precursors on a basis of the critical functional group. Application of this method in future studies may facilitate understanding of SOA formation mechanism.

5.5 Reference

Aiken, A. C., DeCarlo, P. F., and Jimenez, J. L.: Elemental analysis of organic species with electron ionization high-resolution mass spectrometry, Anal. Chem., 79(21), 8350-8358, 2007.

Aiken, A. C., DeCarlo, P. F., Kroll, J. H., Worsnop, D. R., Huffman, J. A., Docherty, K. S., Ulbrich, I. M., Mohr, C., Kimmel, J. R., Sueper, D., Sun, Y., Zhang, Q., Trimborn, A., Northway, M., Ziemann, P. J., Canagaratna, M. R., Onasch, T. B., Alfarra, M. R., Prevot, A. S. H., Dommen, J., Duplissy, J., Metzger, A., Baltensperger, U., and Jimenez, J. H.: O/C and OM/OC ratios of primary, secondary, and ambient organic aerosols with high-resolution time-of-flight aerosol mass spectrometry, Environ. Sci. Technol., 42(12), 4478-4485, 2008.

Aumont, B.; Szopa, S., and Madronich, S.: Modelling the evolution of organic carbon during its gas-phase tropospheric oxidation: development of an explicit model based on a self generating approach, Atmos. Chem. Phys., 5, (9), 2497-2517, 2005.

Barsanti, K. C.; Smith, J. N., and Pankow, J. F.: Application of the np+mP modeling approach for simulating secondary organic particulate matter formation from α-pinene oxidation, Atmos. Environ., 45, (37), 6812-6819, 2011.

Binkowski, F. S., and Roselle, S. J.: Models‐3 Community Multiscale Air Quality (CMAQ) model aerosol component 1. Model description: J. Geophys. Res.: Atmos. 108, (D6), 4183, 2003.

Canagaratna, M. R., Jayne, J. T., Jimenez, J. L., Allan, J. D., Alfarra, M. R., Zhang, Q., Onasch, T. B., Drewnick, F., Coe, H., Middlebrook, A., Delia, A., Williams, L. R., Trimborn, A. M., Northway, M. J., DeCarlo, P. F., Kolb, C. E., Davidovits, P. and Worsnop D. R.: Chemical and microphysical characterization of ambient aerosols with the aerodyne aerosol mass spectrometer, Mass. Spectrom. Rev., 26(2), 185-222, 2007.

Cappa, C. D. and Wilson, K. R.: Multi-generation gas-phase oxidation, equilibrium partitioning, and the formation and evolution of secondary organic aerosol, Atmos. Chem. Phys., 12(20), 9505-9528, 2012.

Carter, W.P., Cocker III, D.R., Fitz, D.R., Malkina, I.L., Bumiller, K., Sauer, C.G., Pisano, J.T., Bufalino, C., Song, C. 2005. A new environmental chamber for evaluation of gas-phase chemical mechanisms and secondary aerosol formation, Atmos. Environ., 39(40), 7768-7788.

Carter, W.P., Heo, G. 2013. Development of revised SAPRC aromatics mechanisms, Atmos. Environ., 77, 404-414.

Chhabra, P. S., Ng, N. L., Canagaratna, M. R., Corrigan, A. L., Russell, L. M., Worsnop, D. R., Flagan, R. C. and Seinfeld, J. H.: Elemental composition and oxidation of chamber organic aerosol, Atmos. Chem. Phys., 11(17), 8827-8845, 2011

Cocker III, D.R., Flagan, R.C., Seinfeld, J.H. 2001a. State-of-the-art chamber facility for studying atmospheric aerosol chemistry, Environ. Sci. Technol., 35(12), 2594-2601.

Cocker III, D.R., Mader, B.T., Kalberer, M., Flagan, R.C., Seinfeld, J.H. 2001b. The effect of water on gas–particle partitioning of secondary organic aerosol: II. *m*-xylene and 1,3,5-trimethylbenzene photooxidation systems, Atmos. Environ., 35(35), 6073-6085.

DeCarlo, P. F., Kimmel, J. R., Trimborn, A., Northway, M. J., Jayne, J. T., Aiken, A. C., Gonin, M., Fuhrer, K., Horvath, T., Docherty, K. S., Worsnop, D. R. and Jimenez, J. L.: Field-deployable, high-resolution, time-of-flight aerosol mass spectrometer, Anal. Chem., 78(24), 8281-8289, 2006.

Derwent, R. G., Jenkin, M. E., Utembe, S. R., Shallcross, D. E., Murrells, T. P., and Passant, N. R.: Secondary organic aerosol formation from a large number of reactive man-made organic compounds, Sci. Total. Environ., 408(16), 3374-3381, 2010.

Donahue, N. M.; Robinson, A. L.; Stanier, C. O., and Pandis, S. N.: Coupled partitioning, dilution, and chemical aging of semivolatile organics, Environ. Sci. Technol., 40, (8), 2635-2643, 2006.

Donahue, N. M.; Kroll, J.; Pandis, S. N., and Robinson, A. L. A two-dimensional volatility basis set–Part 2: Diagnostics of organic-aerosol evolution. Atmos. Chem. Phys., 12, (2), 615-634, 2012.

Farina, S. C., Adams, P. J., and Pandis, S. N.: Modeling global secondary organic aerosol formation and processing with the volatility basis set: Implications for anthropogenic secondary organic aerosol, J. Geophys. Res.-Atmos., 115(D9), 2010.

Forstner, H. J. L., Flagan, R. C. and Seinfeld, J. H.: Secondary organic aerosol from the photooxidation of aromatic hydrocarbons: Molecular composition, Environ. Sci. Technol., 31(5), 1345-1358, 1997.

Freney, E. J.; Sellegri, K.; Canonaco, F.; Colomb, A.; Borbon, A.; Michoud, V.; Doussin, J.-F.; Crumeyrolle, S.; Amarouche, N.; Pichon, J.-M. Bourianne, T.; Gomes, L.; Prevot, A. S. H.; Beekmann, M. and Schwarzenböeck, A.: Characterizing the impact of urban emissions on regional aerosol particles: airborne measurements during the MEGAPOLI experiment, Atmos. Chem. Phys., 14, (3), 1397-1412, 2014.

Gaydos, T. M.; Pinder, R.; Koo, B.; Fahey, K. M.; Yarwood, G. and Pandis, S. N.: Development and application of a three-dimensional aerosol chemical transport model, PMCAMx, Atmos. Environ., 41, (12), 2594-2611, 2007.

Hallquist, M., Wenger, J. C., Baltensperger, U., Rudich, Y., Simpson, D., Claeys, M., Dommen, J., Donahue, N. M., George, C., Goldstein, A. H., Hamilton, J. F., Herrmann, H., Hoffmann, T., Iinuma, Y., Jang, M., Jenkin, M. E., Jimenez, J. L., Kiendler-Scharr, A., Maenhaut, W., McFiggans, G., Mentel, Th. F., Monod, A., Prévôt, A. S. H., Seinfeld, J. H., Surratt, J. D., Szmigielski, R., and Wildt, J.: The formation, properties and impact of secondary organic aerosol: current and emerging issues, Atmos. Chem. Phys., 9(14), 5155-5236, 2009.

Hayes, P. L., Carlton, A. G., Baker, K. R., Ahmadov, R., Washenfelder, R. A., Alvarez, S., Rappenglück, B., Gilman, J. B., Kuster, W. C., de Gouw, J. A., Zotter, P., Prévôt, A. S. H., Szidat, S., Kleindienst, T. E., Offenberg, J. H., Ma, P. K., and Jimenez, J. L.: Modeling the formation and aging of secondary organic aerosols in Los Angeles during CalNex 2010. Atmos. Chem. Phys., 15(10): 5773-5801, 2015.

Heald, C. L., Kroll, J. H., Jimenez, J. L., Docherty, K. S., DeCarlo, P. F., Aiken, A. C., Chen, Q., Martin, S. T., Farmer, D. K., and Artaxo, P.: A simplified description of the evolution of organic aerosol composition in the atmosphere, Geophys. Res. Lett, 37(8), 2010

Henze, D. K., Seinfeld, J. H., Ng, N. L., Kroll, J. H., Fu, T-M., Jacob, D. J., and Heald, C. L.: Global modeling of secondary organic aerosol formation from aromatic hydrocarbons: high-vs. low-yield pathways, Atmos. Chem. Phys., 8(9), 2405-2421, 2008.

Jang, M., Czoschke, N. M., Lee, S., and Kamens, R. M.: Heterogeneous atmospheric aerosol production by acid-catalyzed particle-phase reactions, Science, 298(5594), 814-817, 2002.

Jenkin, M., Saunders, S., Wagner, V. and Pilling, M.: Protocol for the development of the Master Chemical Mechanism, MCM v3 (Part B): tropospheric degradation of aromatic volatile organic compounds, Atmos. Chem. Phys., 3(1), 181-193, 2003.

Jimenez, J. L., Canagaratna, M. R., Donahue, N. M., Prevot, A. S. H., Zhang, Q., Kroll, J. H., DeCarlo, P. F., Allan, J. D., Coe, H., Ng, N. L., Aiken, A. C., Docherty, K. S., Ulbrich, I. M., Grieshop, A. P., Robinson, A. L., Duplissy, J., Smith, J. D., Wilson, K. R., Lanz, V. A., Hueglin, C., Sun, Y. L., Tian, J., Laaksonen, A., Raatikainen, T., Rautiainen, J., Vaattovaara, P., Ehn, M., Kulmala, M., Tomlinson, J. M., Collins, D. R., Cubison, M. J., Dunlea1, E., J., Huffman, J. A., Onasch, T. B., Alfarra, M. R., Williams, P. I., Bower, K., Kondo, Y., Schneider, J., Drewnick, F., Borrmann, S., Weimer, S.,, Demerjian, K., Salcedo, D., Cottrell, L., Griffin, R., Takami, A., Miyoshi, T., Hatakeyama, S., Shimono, A., Sun, J. Y., Zhang, Y. M., Dzepina, K., Kimmel, J. R., Sueper, D., J. Jayne, T.,

Herndon, S. C., Trimborn, A. M., Williams, L. R., Wood, E. C., Middlebrook, A. M., Kolb C. E., Baltensperger, U. and Worsnop D. R.: Evolution of organic aerosols in the atmosphere, Science, 326(5959), 1525-1529, 2009.

Kanakidou, M., Seinfeld, J., Pandis, S., Barnes, I., Dentener, F., Facchini, M., Van Dingenen, R., Ervens, B., Nenes, A. and Nielsen, C.: Organic aerosol and global climate modelling: a review, Atmos. Chem. Phys., 5(4), 1053-1123, 2005.

Kleindienst, T. E., Smith, D. F., Li, W., Edney, E. O., Driscoll, D. J., Speer, R. E. and Weathers, W. S.: Secondary organic aerosol formation from the oxidation of aromatic hydrocarbons in the presence of dry submicron ammonium sulfate aerosol, Atmos. Environ., 33(22), 3669-3681, 1999.

Kroll, J. H., Donahue, N. M., Jimenez, J. L., Kessler, S. H., Canagaratna, M. R., Wilson, K. R., Altieri, K .E., Mazzoleni, L. R., Wozniak, A. S., Bluhm, H., Mysak, E. R., Smith, J. D., Kolb, C. E. and Worsnop D. R.: Carbon oxidation state as a metric for describing the chemistry of atmospheric organic aerosol, Nature Chemistry, 3(2), 133-139, 2011.

Kroll, J. H., Smith, J. D., Che, D. L., Kessler, S. H., Worsnop, D. R. and Wilson, K.R.: Measurement of fragmentation and functionalization pathways in the heterogeneous oxidation of oxidized organic aerosol, Phys. Chem. Chem. Phys., 11(36), 8005-8014, 2009.

Lim, Y. B., Tan, Y., Perri, M. J., Seitzinger, S. P., and Turpin, B. J.: Aqueous chemistry and its role in secondary organic aerosol (SOA) formation, Atmos. Chem. Phys., 10, 10521–10539, 2010.

Lim, Y. B. and Ziemann, P. J.: Products and mechanism of secondary organic aerosol formation from reactions of n-alkanes with OH radicals in the presence of NO_x, Environ. Sci. Technol., 39, (23), 9229-9236, 2005.

Loza, C. L., Chhabra, P. S., Yee, L. D., Craven, J. S., Flagan, R. C. and Seinfeld, J. H.: Chemical aging of *m*-xylene secondary organic aerosol: laboratory chamber study, Atmos. Chem. Phys., 12(1), 151-167, 2012.

Malloy, Q. G., Nakao, S., Qi, L., Austin, R., Stothers, C., Hagino, H., and Cocker III, D. R.: Real-Time Aerosol Density Determination Utilizing a Modified Scanning Mobility Particle Sizer—Aerosol Particle Mass Analyzer System, Aerosol. Sci. Tech., 43(7), 673-678, 2009.

Matsui, H., Koike, M., Takegawa, N., Kondo, Y., Griffin, R., Miyazaki, Y., Yokouchi, Y., and Ohara, T.: Secondary organic aerosol formation in urban air: Temporal variations and possible contributions from unidentified hydrocarbons, J. Geophys. Res.-Atmos, 114(D4), D04201, 2009.

Ng, N. L., Kroll, J. H., Chan, A. W. H., Chhabra, P. S., Flagan, R. C. and Seinfeld, J. H.: Secondary organic aerosol formation from *m*-xylene, toluene, and benzene, Atmos. Chem. Phys., 7(14), 3909-3922, 2007.

Odum, J. R., Hoffmann, T., Bowman, F., Collins, D., Flagan, R. C., and Seinfeld, J. H.: Gas/particle partitioning and secondary organic aerosol yields, Environ. Sci. Technol., 30(8), 2580-2585, 1996.

Odum, J. R., Jungkamp, T., Griffin, R. J., Forstner, H., Flagan, R. C., and Seinfeld, J.H.: Aromatics, reformulated gasoline, and atmospheric organic aerosol formation, Environ. Sci. Technol., 31(7), 1890-1897, 1997.

Pankow, J. F.: An absorption model of gas/particle partitioning of organic compounds in the atmosphere, Atmos. Environ., 28, (2), 185-188, 1994.

Pankow, J. F. and Asher, W. E.: SIMPOL. 1: a simple group contribution method for predicting vapor pressures and enthalpies of vaporization of multifunctional organic compounds, Atmos. Chem. Phys., 8(10), 2773-2796, 2008.

Pankow, J. F., and Barsanti, K. C.: The carbon number-polarity grid: A means to manage the complexity of the mix of organic compounds when modeling atmospheric organic particulate matter, Atmos. Environ., 43, (17), 2829-2835, 2009.

Sato, K., Takami, A., Kato, Y., Seta, T., Fujitani, Y., Hikida, T., Shimono, A. and Imamura, T. 2012. AMS and LC/MS analyses of SOA from the photooxidation of benzene and 1, 3, 5-trimethylbenzene in the presence of NO_x: effects of chemical structure on SOA aging, Atmos. Chem. Phys, 12, 4667-4682, 2012.

Shiraiwa, M., Pfrang, C., Koop, T. and Pöschl, U.: Kinetic multi-layer model of gas-particle interactions in aerosols and clouds (KM-GAP): linking condensation, evaporation and chemical reactions of organics, oxidants and water, Atmos. Chem. Phys., 12, (5), 2777-2794, 2012.

Song, C., Na, K. and Cocker III, D. R.: Impact of the hydrocarbon to NO_x ratio on secondary organic aerosol formation, Environ. Sci. Technol., 39(9), 3143-3149, 2005.

Song, C., Na, K., Warren, B., Malloy, Q. and Cocker III, D. R.: Secondary organic aerosol formation from the photooxidation of *p*-and *o*-xylene. Environ. Sci. Technol., 41(21), 7403-7408, 2007.

Tsigaridis, K. and Kanakidou, M.: Global modelling of secondary organic aerosol in the troposphere: a sensitivity analysis, Atmos. Chem. Phys., 3, (5), 1849-1869, 2003.

Tsimpidi, A. P., Karydis, V. A., Zavala, M., Lei, W., Molina, L., Ulbrich, I. M., Jimenez, J. L. and Pandis, S. N.: Evaluation of the volatility basis-set approach for the simulation of organic aerosol formation in the Mexico City metropolitan area, Atmos. Chem. Phys., 10(2): 525-546, 2010.

Volkamer, R., Jimenez, J. L., San Martini, F., Dzepina, K., Zhang, Q., Salcedo, D., Molina, L. T., Worsnop, D. R., and Molina, M. J.: Secondary organic aerosol formation from anthropogenic air pollution: Rapid and higher than expected, Geophys. Res. Lett., 33, (17), L17811, 2006.

Woody, M. C., K. R. Baker, P. L. Hayes, J. L. Jimenez, B. Koo and H. O. Pye.: Understanding sources of organic aerosol during CalNex-2010 using the CMAQ-VBS, Atmos. Chem. Phys., 16(6): 4081-4100.10, 2016.

Zhang, X. and Seinfeld, J. H.: A functional group oxidation model (FGOM) for SOA formation and aging, Atmos. Chem. Phys., 13, (12), 5907-5926, 2013,.

Zuend, A., Marcolli, C., Peter, T. and Seinfeld, J. H.: Computation of liquid-liquid equilibria and phase stabilities: implications for RH-dependent gas/particle partitioning of organic-inorganic aerosols., Atmos. Chem. Phys., 10, (16), 7795-7820, 2010.

5.6 Tables and Figures

Table 5.1Two product yield curve fitting parameters for ring normalized SOA yield (Yield′) vs M_0 ($\mu g \cdot m^{-3}$) in All ortho (AO), All_meta_TMB_1S (AMT1), All para_C_{10+} (AP10) and Benzene

Yield′ Curve	α_1'	$K_{om,1}'$ ($m^3 \cdot \mu g^{-1}$)	α_2'	$K_{om,2}'$ ($m^3 \cdot \mu g^{-1}$)
All	**0.310**	**0.021**	**0.086**	**0.005**
AO	0.120	0.022	0.685	0.005
AMT1	0.300	0.021	0.077	0.005
AP10	0.280	0.017	0.030	0.005
Benzene*	0.082	0.017	0.617	0.005

*Note: $\alpha_1=\alpha_1' = 0.082$, $K_{om,1}= K_{om,1}'=0.017$, $\alpha_2=\alpha_2'=0{,}617$ and $K_{om,2}= K_{om,2}'= 0.005$ (Chapter 3).

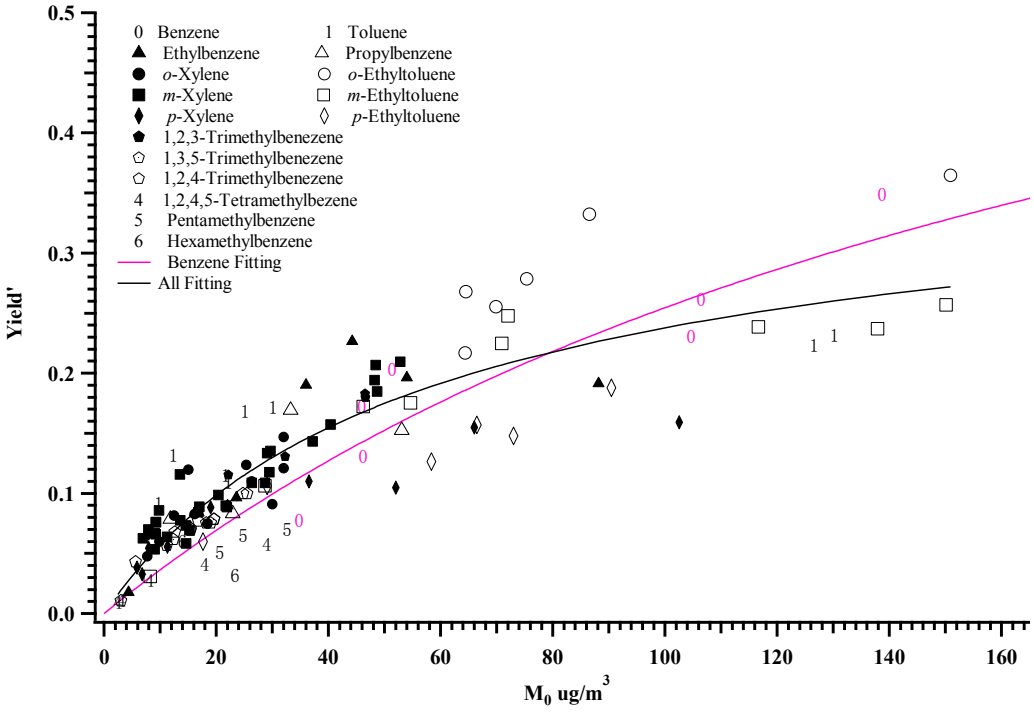

Figure 5.1 Molecular weight adjusted SOA Yield (Yield′) as a function of mass loading (M_0 μg/m^3)

(Each marker or number stands for one or two (hollow triangle stands for n-Propylbenzene and Isopropylbenzene) aromatic hydrocarbons as listed in the graph legend. Numbers stand for aromatic hydrocarbon without isomers studied. 0: Benzene; 1：Toluene; 4：1, 2, 4, 5-Tetramethylbenzene; 5: Pentamethylbenzene; 6: Hexamethylbenzene. Pink curve: Two product model benzene curve fitting; Black curve: Molecular weight adjusted SOA Yield Two product model curve fitting for 17 aromatic hydrocarbons.

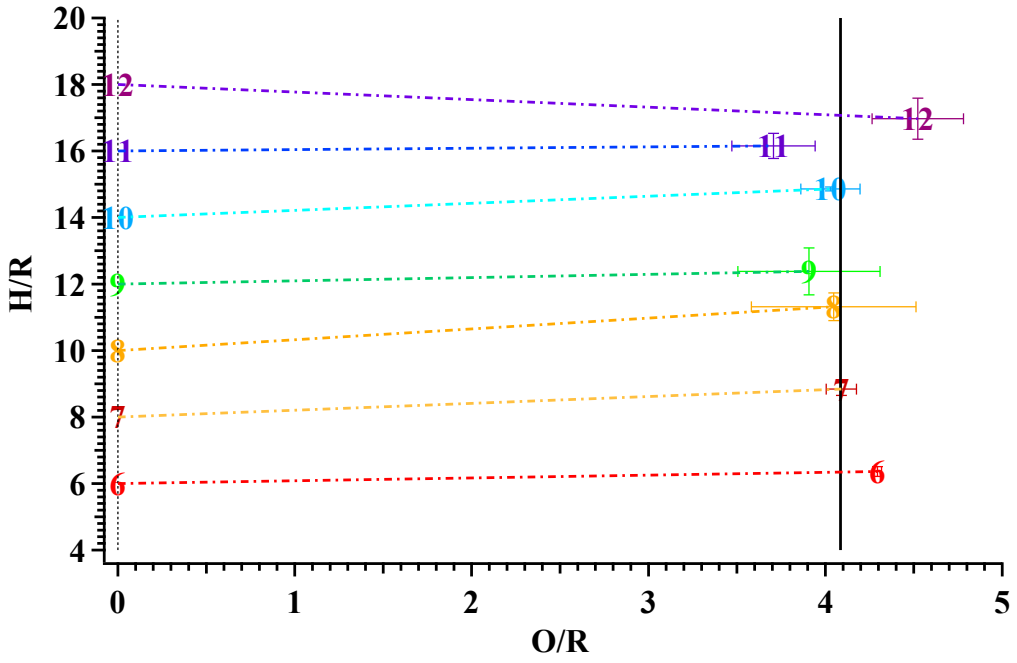

Figure 5.2 Aromatic ring based elemental ratios (H/R vs O/R) from the photooxidation of 17 aromatic hydrocarbons

(Left hand number group represents location of aromatic precursors and dashed line O/R=0; right hand represents average location of SOA chemical composition from corresponding aromatic hydrocarbon(s) with same carbon number and solid line represents the location of average O/R=4.08 ; 6: Benzene; 7:Toluene; 8: Ethylbenzene and Xylenes (meta, para and ortho); 9: Propylbenzene (n- and iso) and Trimethylbenzenes (1,2,4-Trimethylbenzene, 1,2,3-Trimethylbenzene and 1,3,5-Trimethylbenzene); 10: 1,2,4,5-Tetramethylbenzene; 11: Pentamethylbenzene; 12: Hexamethylbenzene.

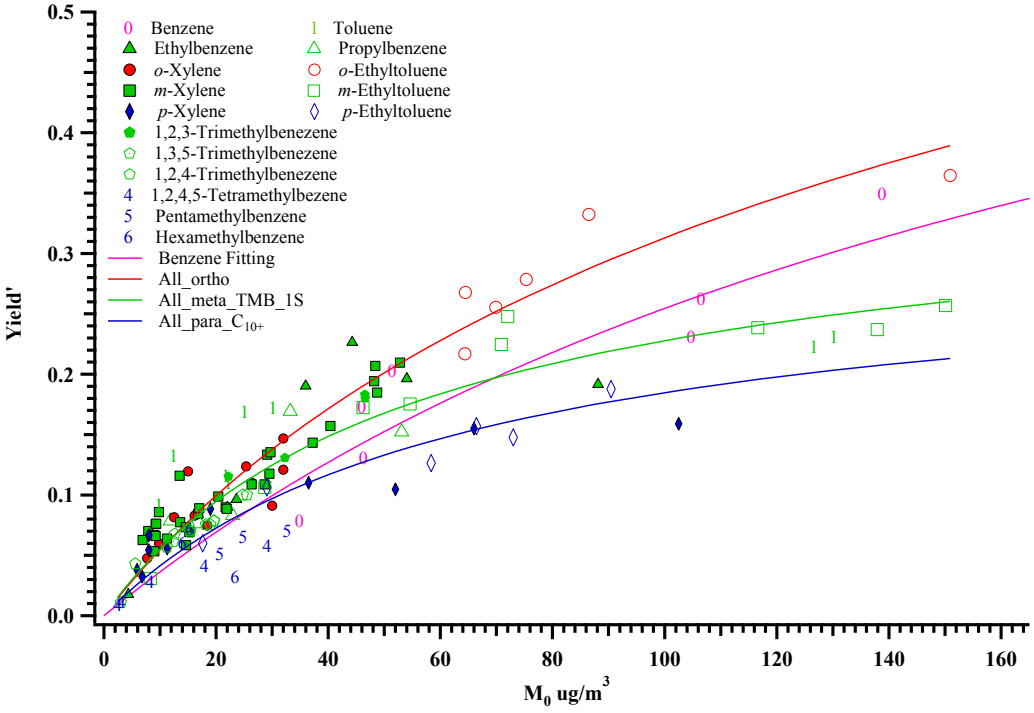

Figure 5.3 Molecular weight adjusted SOA Yield (Yield′) as a function of mass loading (M_0 μg·m^{-3})

(Each marker or number stands for one or two (hollow green triangle stands for n-Propylbenzene and Isopropylbenzene) aromatic hydrocarbon as listed in graph. Number stands for aromatic hydrocarbon without isomers studied. 0: Benzene; 1： Toluene; 4： 1, 2, 4, 5-Tetramethylbenzene; 5: Pentamethylbenzene; 6: Hexamethylbenzene. Curves are fitted two-product model curves of each isomer group. Pink: Benzene; Red: ortho (AO); Green: meta, one substitute and Trimethylbenzenes (AMT1); Blue: para and those with 4 more alkyl substitutes (AP10). Marker and number colors are same as their fitting curves)

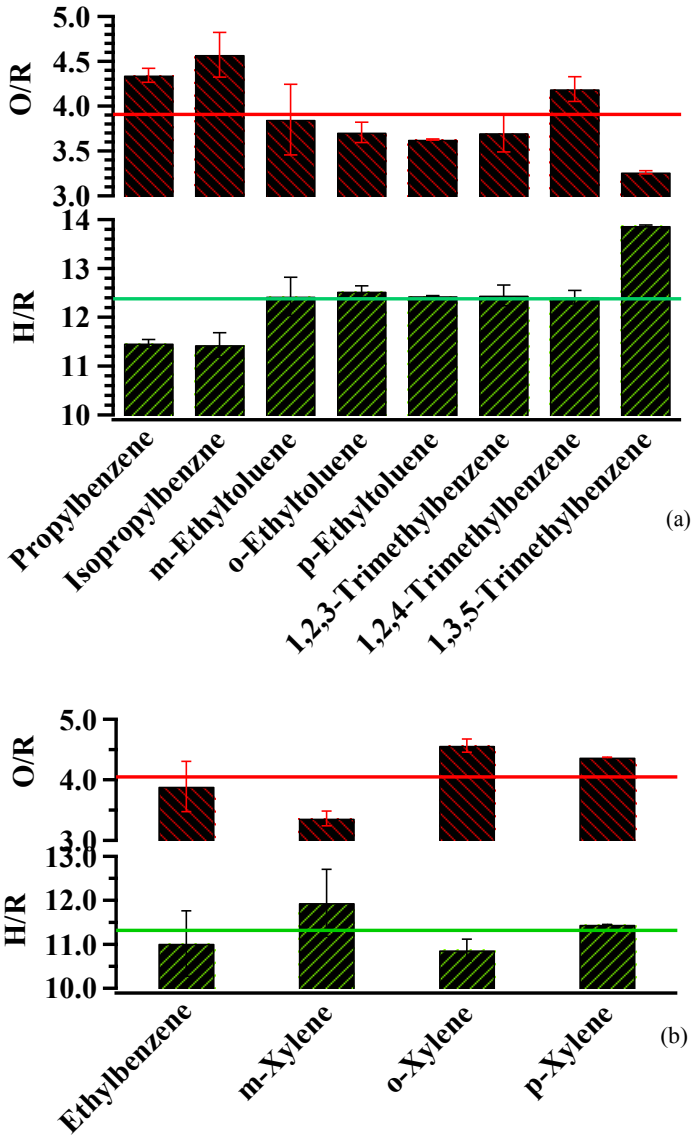

Figure 5.4 Aromatic ring based elemental ratios from photooxidation of C_9 (a) and C_8 (b) aromatic hydrocarbons

(Error bars are H/R and O/R standard deviation of all experiments in the photooxidation of each aromatic hydrocarbon; red lines are average O/R values for C_8 and C_9 isomers; green dashed lines are average H/R values for C_8 and C_9 isomers).

6. Contribution of methyl group to SOA formation during the photooxidation of xylenes under low NO_x conditions

6.1 Introduction

Aromatic hydrocarbons are major anthropogenic SOA precursors (Kanakidou, et al., 2005; Henze, et al., 2008). It is considered that OH-initiated reaction results in ~10% H-abstraction from one methyl group to form a methylbenzyl radical and ~90% OH addition to the aromatic ring to form hydroxycyclohexadienyl radical (Calvert, et al., 2002). However, the mechanism of SOA formation from aromatic hydrocarbons remains uncertain (Hallquist, et al., 2009). Identified aromatic photooxidation products include benzaldehyde, nitrophenol, benzoquinone, phthalic acid, unsaturated anhydride, epoxide, carbonyl and carboxylic acid (Forstner, et al., 1997; Yu, et al., 1997; Smith, et al., 1999; Sato, et al., 2007; Borrás and Tortajada-Genaro, 2012; McDonald et al., 2012; Lund et al., 2013). However, summation of identified compounds account for less than 50% of the reacted carbon (Forstner, et al., 1997; White, et al., 2014). The identified products are mostly formed under non-atmosphere relevant high-NO_x conditions (Yu, et al., 1997; Forstner, et al., 1997; Smith, et al., 1999; Kleindienst, et al., 1999; Cocker, et al., 2001; Jang and Kamens, 2001; Fisseha, et al., 2004; Sato, et al., 2007; Müller, et al., 2012; Praplan, et al., 2014) , based on offline filter sample analysis (Hamilton, et al., 2005; Borrás and Tortajada-Genaro, 2012) or only focused on gas phase products (Wyche, et al, 2009). It is noticed that recent studies also suggest that oligomerization attributes to a large portion of SOA components during the photooxidation aromatics photooxidation

(Kalberer, et al., 2004; Gross, et al., 2006; Chapter 3). The combination of isotope labeled SOA precursors with state-of-art instruments enhances the analysis of SOA formation pathways. White, et al. (2014) used toluene with all H labeled (Toluene-d_8) or all carbon labeled with ^{13}C (Toluene-$^{13}C_7$) to interpret products measured by GC-MS (Gas Chromatography–Mass Spectrometry) and to exclude pretreatment interference in offline filter analysis.

Molecular structure exerts a significant impact on SOA formation mechanism and therefore determine SOA yield. Aromatic isomer study indicates that aromatic with alkyl substitutes in *para*- position suppress SOA formation compared with those in *meta* or *ortho* position (Izumi and Fukuyama, 1990; Song, et al., 2007; Chapter 4). Exploring the differences in the photooxidation products among different aromatic isomers facilitates the understanding of alkyl substitute location impact on SOA formation from aromatics, which is essential to elucidate SOA formation mechanisms from aromatic hydrocarbons.

Xylenes (m-, p-, and o-xylene) are the second most important ambient aromatic hydrocarbons after toluene (Zhou, et al., 2011). Xylenes compose fundamental position structures that could be extended to more complicated aromatic structures. SOA formation results from a combination of functionalization, fragmentation and oligomerization (Jimenez, et al., 2009; Kroll, et al., 2009). It is important to distinguish the role of different functional groups, such as aromatic ring and methyl substitute, during photooxidation. In this study, SOA formation from *m*-xylene and *p*-xylene with methyl group labeled with ^{13}C is investigated to demonstrate the methyl group

contribution to SOA formation from aromatics in low NO_x condition. Also, the nitric oxide (NO) contribution to organic nitrate and SOA formation is studied by using isotope labeled ^{15}NO. Real time gas phase and particle phase mass spectrometers (SIFT-MS, PTR-MS and HR-TOF-AMS) are applied to illustrate the distribution of methyl-carbon during xylene photooxidation. This study aims to shed lights on the mechanism of SOA formation from aromatic hydrocarbons.

6.2 Methods

6.2.1 Environmental chamber

The UC Riverside/CE-CERT indoor dual 90 m^3 environmental chambers were used in this study and are described in detail elsewhere (Carter et al., 2005). Experiments were all conducted at dry conditions (RH<0.1%), in the absence of inorganic seed aerosol and with temperature controlled to 27±1°C. Two movable top frames were slowly lowered during each experiment to maintain a slight positive differential pressure (~0.02" H_2O) between the reactors and enclosure to minimize dilution and/or contamination of the reactors. 276 pieces of 115 W Sylvania 350BL blacklights are used as light sources for photooxidation. A known volume of high purity liquid hydrocarbon precursor ($^{13}C_2$) *m*-xylene: Sigma-Aldrich, 99% atom ^{13}C, ($^{12}C_2$) *m*-xylene: Sigma-Aldrich, ⩾99.5%, ($^{13}C_2$), *p*-xylene: Sigma-Aldrich, 99% atom ^{13}C, ($^{12}C_2$) *p*-xylene: Sigma-Aldrich, ⩾99%) was injected through a heated glass injection manifold system and flushed into the chamber with pure N_2. NO or ^{15}NO (SigmaAldrich, 98 atom % ^{15}N) was introduced by flushing

pure N_2 through a calibrated glass bulb filled to a predetermined partial pressure of pure NO. All initial experimental conditions are listed in Table. 6.1.

6.2.2 Particle and Gas Measurement

Particle size distribution between 27 nm and 686 nm was monitored by a custom built Scanning Mobility Particle Sizer (SMPS) (Cocker et al., 2001). Particle effective density was measured with an Aerosol Particle Mass Analyzer (APM-SMPS) system (Malloy et al., 2009). Particle phase chemical composition evolution was obtained with a High Resolution Time of Flight Aerosol Mass Spectrometer (HR-ToF-AMS; Aerodyne Research Inc.) (Canagaratna et al., 2007; DeCarlo et al., 2006). The sample is vaporized by a 600 °C oven followed by 70 eV electron impact ionization. The AMS was switched between a high resolution "W-mode" and a high sensitivity "V-mode". The high resolution "W-mode" allowed for identification of different elemental compositions from each unit mass using the PIKA toolbox (DeCarlo et al., 2006). Isotopic specie concentrations are analyzed by using peak fitting without the constraint of corresponding parent species. f_X in this study is calculated as the fraction of the organic signal at certain fragments. For example, f_{CO2+} and f_{C2H3O+} are the ratios of the organic signal at CO_2^+ and $C_2H_3O^+$, respectively, to the total organic signal.

The Agilent 6890 Gas Chromatograph – Flame Ionization Detector equipped with a DB-5 column was used to measure concentrations of reactants. Gas phase composition was determined with a Proton Transfer Reaction Mass Spectrometer (PTR-MS, standard PTR-QMS series, Ionicon Analytik, Austria) (Lindinger et al., 1998) or Selected Ion

Flow Tube-Mass Spectrometer (SIFT-MS; Syft Technologies) (Prince et al., 2010). NO_X was monitored by a Thermo Environmental Instruments model 42C chemiluminescence NO_X analyzer.

6.3 Result

6.3.1 Contribution of methyl group to significant organic fragments in particle phase products

The m/z 43 (C_2H_3O) and m/z 44 (CO_2) are prominent fragment peaks observed by the AMS during the photooxidation of none-isotopic xylene precursors, including *m*-xylene (Table S6.1, 931A f_{C2H3O+} =14.95% and f_{CO2+}=9.63%) and *p*-xylene (2087A f_{C2H3O+} =12.03% and f_{CO2+}=6.72%). A significant increase of organic fragment percentage at m/z 44 (f_{44}), with a corresponding decrease in organic fragment percentage at m/z 43 (f_{43}), are observed in SOA formed from the photooxidation of ^{13}C labeled xylenes (929A *m*-xylene and 2088A *p*-xylene) when comparing those from none-isotopic xylenes (Table 6.1, Fig. 6.1). The increase of m/z 44 results from the presence of an additional $^{13}CCH_3O^+$ peaks while the concentration of $C_2H_3O^+$ decreases at m/z 43 (Fig. S6.1 &Fig. S6.2). The contribution of methyl carbon to each fragment is quantified as

$$P_{^{13}CC_{x-1}H_yO_z} = \frac{[^{13}CC_{x-1}H_yO_z]}{[C_xH_yO_z]+[^{13}CC_{x-1}H_yO_z]+[^{13}C_2C_{x-2}H_yO_z]} \quad \text{Eq-1}$$

$$P_{^{13}C_2C_{x-2}H_yO_z} = \frac{[^{13}CC_{x-1}H_yO_z]}{[C_xH_yO_z]+[^{13}CC_{x-1}H_yO_z]+[^{13}C_2C_{x-2}H_yO_z]} \quad \text{Eq-2}$$

where $P_{^{13}CC_{x-1}H_yO_z}$ and $P_{^{13}C_2C_{x-2}H_yO_z}$ are the percentage of isotope containing fragments in the sum of their parent and associated isotope containing fragments; $^{13}CC_{x-1}H_yO_z$ and $^{13}C_2C_{x-2}H_yO_z$ are fragments containing one and two isotope labeled carbons, correspondingly; $[C_xH_yO_z]$, $[^{13}CC_{x-1}H_yO_z]$ and $[^{13}C_2C_{x-2}H_yO_z]$ are fragment intensities of the parent fragment and the isotope fragments containing one or two isotope carbons, respectively. Large $P_{^{13}CCH_3O}$ are found during the photooxidation of isotope labeled xylene at m/z 44 (Table 6.2 *m*-xylene, $P_{^{13}CCH_3O_2}$ = 71.9%; *p*-xylene, $P_{^{13}CCH_3O_2}$ = 77.6%). The high $P_{^{13}CCH_3O_2}$ indicates a large contribution of methyl carbon to non-acid oxygenates fragments (Ng, et al., 2011). The importance of methyl group to $C_2H_3O^+$ fragments in SOA agrees with previously observed increase in f_{C2H3O+} with increasing number of methyl groups attached to aromatic ring precursor as well as the smaller $f_{C_2H_3O^+}$ (~0.03) in SOA formed from the photooxidation of benzene compared with other methyl substituted aromatic hydrocarbons (Chapter 3). $C_2H_3O^+$ usually composes a carbonyl functional group (-C (O)-) and a methyl group ($-CH_3$). It is less likely from the oxygenated methyl with an aromatic ring carbon which has high double bond equivalent (DBE=2). Therefore, the high fraction of $^{13}C_2H_3O^+$ suggests that methyl groups of xylene are not well oxidized during the photooxidation, especially under the low NO_x conditions studied.

The fractions of isotope labeled fragments in highly oxidized components (e.g. CO_2^+) are further investigated to study the potential of the oxidation in methyl groups. $P_{^{13}CO_2}$ (Eq-1) is calculated by using an isotopic xylene experiment. A slight amount (Table 6.2,

$P_{^{13}CO_2}$ =11.5%) of $^{13}CO_2$ is observed during the photooxidation of *m*-xyleneand no observable $^{13}CO_2$ is detected during the photooxidation of *p*-xylene. A slight increase at m/z 45 due to $^{13}CO_2^+$ increase in the photooxidation of isotopic xylenes may not be observed in the comparison of average $f_{m/z}$ with non-isotopic experiment (Fig. 6.1), since m/z 45 includes other fragments (e.g. CHO_2^+, $C_2H_5O^+$) which might be slightly variant in different experiments.The low $P_{^{13}CO_2}$ and low f_{CO2+} indicate that the oxidation of methyl substitute is of minor importance to SOA bulk composition during the oxidation xylenes. Therefore, insignificant (within the O/C standard deviation reported) differences are observed in O/C and H/C in SOA formed from *m*-xylene and *p*-xylene (Chapter 4). The higher $P_{^{13}CO_2}$ in SOA formed from *m*-xylene than *p*-xylene suggests that methyl substitute in *m*-xylene is more oxidized compared with that in *p*-xylene during photooxidation. The oxidation of methyl substitute may lead to aromatic ring containing products such as m-toluic acid and thereby contributes to the higher $P_{^{13}CO_2}$ in *m*-xylene than *p*-xyelen. The higher oxidation of methyl group in *m*-xylenemay lead to the formation of less volatile products compared with *p*-xylene and therefore has higher SOA yield. It is noted that the hinderanc effect of methyl group on further oxidation of ring opeinging products also contributes the difference in SOA yield between *m*-xyelen and *p*-xylene. The oxidation of methyl substitute is estimated to contribute to 6.2% (ΔHC=300 μg/m^3, $M_{o,p\text{-xylene}}$=9 μg/m^3, $M_{o,m\text{-xylene}}$=27.8 μg/m^3,) of SOA mass increase in *m*-xyelene compared with by assuming the contribution of methyl substitute to CO_2^+ is similar as that to the SOA mass concentration. Therefore, the oxidaiotn of methyl substitute is not a major contributor to the difference in SOA yield. . Different fractions of methyl substitute

may remain in particle phase during the photooxidation of different isomers since aging is a combination of functionalization, fragmentation and oligermerization. Further discussion in Section 6.3.2 and 6.4.

CO^+ (m/z 28), which represents carbonyl fraction, is also an important organic fragment in addition to CO_2^+ and $C_2H_3O^+$. It is difficult to separate CO^+ peak from N_2 peak. However, $^{13}CO^+$ (m/z 29) is potentially available to be separated from other peaks (especially, CHO^+; ^{15}NN= 0.0070874*N_2) since $^{13}CO_2^+$ are capable to be separated from CHO_2^+. Nevertheless, no significant $P_{^{13}CO}$ (assuming [^{12}CO] = [$^{12}CO_2$]) is observed. This suggests methyl carbon in xylenes are barely oxidized into carbonyl carbon. The difference in $P_{^{13}CO}$ and $P_{^{13}CO_2}$ trend (Table 6.2), especially during the photooxidation of *m*-xylene, further suggests that the m/z 28=m/z 44 assumption, traditionally used in AMS data analysis, need to be adjusted according to SOA precursors in chamber studies to better understand the oxidation of different precursors.

The contributions of methyl carbon to organic fragments other than CO_2^+, $C_2H_3O^+$ and CO^+ are also calculated (Table S 6.2). Fragments with high percentage of isotope mostly relate to a high H:C ratio suggesting that methyl substitutes are not well oxidized compared with ring carbon.

The m/z 46 (NO_2^+) and m/z 30 (NO^+) peaks, observed in SOA formed during the non-isotope containing experiment, are largely shift to m/z 47 ($^{15}NO_2^+$) and m/z 31 ($^{15}NO^+$), respectively, during the photooxidation of *m*-xylene with ^{15}NO. No other shift is observed in during the photooxidation of *m*-xylene with ^{15}NO. This confirms that all organic

nitrates formed during the oxidation of *m*-xylene appears at m/z 46 (NO_2^+) and m/z 30 (NO^+). The less than 10% organic nitrate observed under low NO_x conditions in this study properly estimate the contribution of organic nitrate to SOA formation in urban atmosphere .

6.3.2 Evolution of bulk SOA $^{13}C/^{12}C$ during the photooxidation of ^{13}C containing xylenes

The evolution of $^{13}C/^{12}C$ in SOA during the photooxiation of $^{13}CH_3$- containing xylenes indicates the extent of methyl carbon participation in SOA formation during the photooxidation of xylenes and further suggests aromatic hydrocarbon reaction pathways. A mole ratio of $^{13}C/^{12}C$ in particle phase is calculated by using high resolution fragments in HR-TOF-AMS with all significant (Diff > 0.05 Hz/ns) peaks included (Fig. 6.2). It is assumed that $^{12}CO=^{12}CO_2$.$^{13}C/^{12}C$ is nearely constant during photooxidation after initial nucleation (happened around 120 min to 150 min) in all xylenes and conditions studied. The major reaction that impacts $^{13}C/^{12}C$ should be fragmentation (aromatic ring opening), which is largely influenced by NO concentration (Jang, et al., 2001; Song, et al., 2005). The influence of NO on aromatic ring decomposition mostly occurs before nucleation when NO concentration is sufficiently high to dominate $NO+RO_2$ reaction (Ng, et al., 2007; Chapter 25). Therefore, it is reasonable to observe a steady $^{13}C/^{12}C$ after particle formed.

$^{13}C/^{12}C$ for the higher NO_x condition (929A) is larger than that in lower NO_x (928A) condition. It is possible that the higher NO concentration might serve as an impetus for

certain methyl-rich ring opening products (e.g., 3,5-dimethyl-2(5H)-furanone ($^{13}C/^{12}C$=0.4) instead of 5-methyl-2(5H)-furanone ($^{13}C/^{12}C$=0.25)). *p*-Xylene has a higher average $^{13}C/^{12}C$ compared with *m*-xylene assuming NO_x impact on *m*-xylene can be extended to *p*-xylene. It is possible that methyl-rich ring retaining products (e.g. bicyclic hydroperoxide with two methyl, $^{13}C/^{12}C$=0.33) contribute more to SOA formation from *p*-xylene than that from *m*-xylene and ring opening products from *p*-xylene photooxidaton are less likely to further react into low volatility products than that from *m*-xylene (Section 6.4.1).

6.3.3 Contribution of methyl group to gas phase products

A series of gas phase products are identified during the photooxidation of xylenes under low NO_x conditions (Table 6.3). Gas phase mass spectrum shifts during the photooxidation of ^{13}C labeled xylenes compared with that of none-isotope xylenes demonstrate the contribution of methyl group carbon to corresponding gas phase products. The difference between the mass spectrum from ^{13}C labeled xylenes and that from non-isotope labeled xylenes represents the number of methyl carbon in each gas phase product. The carbon composition (number of ^{13}C and ^{12}C) and sources (methyl carbon or aromatic ring carbon) in gas phase products are identified according to the agreement in the intensities of those gas phase products between the isotopic runs and non-isotopic runs (Fig. S6.3 and Fig. S6.4). Isotope carbons mostly remain as methyl group carbon in gas phase products. However, the identification of two isotope carbon containing products at MW=120 (MW=122 in isotope experiment) indicating the

formation 4-methylbenzaldehyde, in which one methyl carbon is oxidized into carbonyl carbon. It is also found that carbon in formaldehyde can formboth isotope and none-isotope sources. The contribution of methyl carbon to gas phase products are calculated as

$$P_{^{13}C,j} = \frac{[j_{^{13}C}]}{[(j-n)_{^{13}C}]} \qquad \text{Eq-3}$$

where $P_{^{13}C,j}$ is the percentage of isotope containing products in the identified products; $[j_{^{13}C}]$ is the signal intensity in PTR-MS or SIFT-MS at m/z= j in the isotope containing experiment; $[(j-n)_{^{13}C}]$ is the signal intensity in PTR-MS or SIFT-MS at m/z=j-n in a parallel non-isotope containing experiment and n=1 or 2 depending on the number of isotope carbon at j. ^{13}C contributes to 42.28% and 46.02% of formaldehyde formation during the photooxidation of *m*-xylene and *p*-xylene under the low NO_x condition studied according to Eq-3. This indicates that methyl carbon can be partially oxidized in gas phase. Most identified products observed in this study are consistent with previous studies and agree with the mechanisms proposed (Yu, et al., 1997a; Yu, et al., 1997b; Smith, et al., 1999; Jang and Kames, 2001; Jenkin, et al, 2003; Bloss, et al 2005; Borrás, and Tortajada-Genaro, 2012; Müller, et al, 2012). The current study also verifies that the formation of several gas phase products depends on methyl group location on aromatic ring including 2,4-dimethylfuran (meta only), maleic anhydride (meta only), 3,5-Dimethyl-2(5H)-furanone (meta only) and 4-methylbenzaldehyde (para only).

6.4 Discussion

6.4.1 The extent of oxidation in methyl carbon and aromatic ring carbon

Methyl carbon accounts for less than 12% mass percentage of CO_2^+, which is an important marker for SOA aging (Ng, et al., 2011), in the photooxidation of xylene under low NO_x conditions. The contribution of methyl carbon and ring carbon to overall oxygen content is quantified as

$$\mathrm{O}:{}^{12}C = \sum_i [(1-P_i)\alpha_i(\mathrm{O}:{}^{12}C)_{i,1} + P_i\alpha_i(\mathrm{O}:{}^{12}C)_{i,2}] \quad \text{Eq-4}$$

$$\mathrm{O}:{}^{13}C = \sum_i P_i\alpha_i(\mathrm{O}:{}^{13}C)_i \quad \text{Eq-5}$$

where $O:{}^{12}C$ and $O:{}^{13}C$ are the adjusted *O:C* associated with non-isotope carbon and isotope carbon, respectively; *i* is a specific organic fragment; P_i is the percentage of isotope containing fragments at *i* and is already defined in Eq-1 and Eq-2; α_i is the mass to mole adjusting coefficient, which is calculated as reciprocal of molecular weight of *i*; $(O:{}^{12}C)_{i,2}$ and $(O:{}^{12}C)_{i,1}$ are mole ratios of *O:C* assigned to ^{12}C at identified fragments *i* containing ^{13}C or not, respectively; and $(O:{}^{13}C)_i$ is the mole ratio of *O:C* assigned to ^{13}C at identified fragments *i*. The ratio of $O:{}^{12}C$ and $O:{}^{13}C$ ($R_{O,12/13}$) suggests the relative importance of aromatic ring carbon and methyl carbon to overall oxidation. Three major oxygenated fragments ($C_2H_3O^+$, CO_2^+ and CO^+) are included in the oxygen contribution calculation and corresponding P_i and $(O:C)_i$ are listed in Table 6.2 and Table S6.1. It is found that $R_{O,12/13}$ is ~21 and ~54 in the photooxidation of methyl carbon labeled *m*-xylene and *p*-xylene, respectively. This suggests that oxidized ring carbon contributes to

at least 20 times more to overall oxygen than methyl carbon in SOA during the photooxidation of xylene under low NO_x condition despite only being three times higher in the parent xylene. Therefore, the potential of oxygen gaining of each ring carbon is 7 and 18 times higher than methyl carbon for m-xylene and p-xylene, repectively. Our recently published work observed that the aromatic ring obtains a near constant amount of oxygen (~4) during photooxidation under low NO_x conditions, regardless of the number or size of alkyl substitutes (Chapter 5). This work further confirms that the aromatic ring is a driving force to the photooxidation of aromatic hydrocarbon and therefore aromatic ring is much critical to SOA formation than alkyl substitute. ^{13}C labeled methyl carbons mostly coexistent with high H: C fragments in HR-TOF-AMS supporting its high contribution to overall H:C in SOA components and therefore consistent with a recent study demonstrating that alkyl substitute number determinates H/C ratio (Chapter 5).

6.4.2 Molecular structure impact on photooxidation pathways

A lower $^{13}C/^{12}C$ is observed in SOA formed from the photooxidaton of methyl labeled *m*-xylene than *p*-xylene. Meanwhile, isotopic fragment peaks (Section 6.3.1) suggest that methyl carbon is not well oxidized compared with the aromatic ring carbon. Hence, a lower $^{13}C/^{12}C$ indicates a lower content of less oxidized methyl substitutes. Previous studies found that SOA yield from *m*-xylene is higher than that from *p*-xylene (Song, et al., 2007; Chapter 4). This indicates that the lack of methyl groups, possibly by ring opening pathways, further enhances select reactions (e.g. oligomerization (Kalberer, et

al., 2004; Chapter 3)) to produce low volatility products. A possible explanation for the differences in $^{13}C/^{12}C$ and SOA yield between *m*-xylene and *p*-xylene is that oligomerization from ring opening products (e.g. maleic anhydride and 5-methyl-2(5H)-furanone, which lowers $^{13}C/^{12}C$ compared with bicyclic hydroperoxide), is favored in SOA formation from *m*-xylene while bicyclic hydroperoxide is favored in that from *p*-xylene.

6.5 Atmospheric Implication

The alkyl substitute on aromatic hydrocarbon may increase the complexity of SOA precuros and estimation of aromatic hydrocarbon photooxidation. However, this study confirms that aromatic ring is a driving force for the photooxidation of aromatic hydrocarbon and alkyl substitute is far less oxidized compared with aromatic ring carbon. The methyl carbon contributes less to the particle phase products than gas phase products according to the decrease in $^{13}C/^{12}C$ from SOA precursor formula to SOA composition and corresponding gas phase and particle phase mass spectrum. Therefore, the alkyl substitute exerts minimum impact on SOA formation. This study serves as a powerful proof for the recent finding that aromatic hydrocarbon obtains ~4 oxygen per aromatic ring regardless of alkyl substitute number (Chapter 5). Besides, the impact of molecular structure on the photooxidation of aromatic hydrocarbon is confirmed by isotope experiments. Oligomerization in addition to bicyclic hydroperoxide is proposed to explaindifferences in the SOA formation from m-xylene and p-xylene. In addition, the application of isotope SOA precursor in chamber studies is an innovative method to

explore the role of different functional group during atmospheric aging, which can be fapplied to future SOA formation studies.

6.6 Reference

Borrás, E. and Tortajada-Genaro, L. A.: Secondary organic aerosol formation from the photo-oxidation of benzene, Atmos. Environ., 47, 154-163, 2012.

Calvert, J. G., Atkinson, R., Becker, K. H., Kamens, R. M., Seinfeld, J. H., Wallington, T. J. and Yarwood, G.: The mechanisms of atmospheric oxidation of aromatic hydrocarbons, Oxford University Press New York, 2002.

Canagaratna, M. R., Jayne, J. T., Jimenez, J. L., Allan, J. D., Alfarra, M. R., Zhang, Q., Onasch, T. B., Drewnick, F., Coe, H., Middlebrook, A., Delia, A., Williams, L. R., Trimborn, A. M., Northway, M. J., DeCarlo, P. F., Kolb, C. E., Davidovits, P. and Worsnop D. R.: Chemical and microphysical characterization of ambient aerosols with the aerodyne aerosol mass spectrometer, Mass. Spectrom. Rev., 26(2), 185-222, 2007.

Carter, W. P. L., Cocker III, D. R., Fitz, D. R., Malkina, I.L., Bumiller, K., Sauer, C.G., Pisano, J.T., Bufalino, C., Song, C.: A new environmental chamber for evaluation of gas-phase chemical mechanisms and secondary aerosol formation, Atmos. Environ., 39(40), 7768-7788, 2005.

Cocker III, D. R.., Flagan, R. C. and Seinfeld, J. H.: State-of-the-art chamber facility for studying atmospheric aerosol chemistry, Environ. Sci. Technol., 35(12), 2594-2601, 2001a.

Cocker III, D. R., Mader, B. T., Kalberer, M., Flagan, R.C. and Seinfeld, J. H.: The effect of water on gas–particle partitioning of secondary organic aerosol: II. *m*-xylene and 1, 3, 5-trimethylbenzene photooxidation systems, Atmos. Environ., 35(35), 6073-6085, 2001b.

DeCarlo, P. F., Kimmel, J. R., Trimborn, A., Northway, M. J., Jayne, J. T., Aiken, A. C., Gonin, M., Fuhrer, K., Horvath, T., Docherty, K. S., Worsnop, D. R. and Jimenez, J. L.: Field-deployable, high-resolution, time-of-flight aerosol mass spectrometer. Anal. Chem., 78(24), 8281-8289, 2006.

Fisseha, R., Dommen, J., Sax, M., Paulsen, D., Kalberer, M., Maurer, R., Höfler, F., Weingartner, E., and Baltensperger, U.: Identification of organic acids in secondary organic aerosol and the corresponding gas phase from chamber experiments, Anal. Chem., 76(22), 6535-6540, 2004.

Forstner, H. J. L., Flagan, R. C., and Seinfeld, J. H.: Secondary organic aerosol from the photooxidation of aromatic hydrocarbons: Molecular composition, Environ. Sci. Technol., 31(5), 1345-1358, 1997.

Gross, D. S., Gälli, M. E., Kalberer, M., Prevot, A. S., Dommen, J., Alfarra, M. R., Duplissy, J., Gaeggeler, K., Gascho A., Metzger, A., Baltensperger U.: Real-time measurement of oligomeric species in secondary organic aerosol with the aerosol time-of-flight mass spectrometer, Anal. Chem., 78(7), 2130-2137, 2006.

Hallquist, M., Wenger, J. C., Baltensperger, U., Rudich, Y., Simpson, D., Claeys, M., Dommen, J., Donahue, N. M., George, C., Goldstein, A. H., Hamilton, J. F., Herrmann, H., Hoffmann, T., Iinuma, Y., Jang, M., Jenkin, M. E., Jimenez, J. L., Kiendler-Scharr, A., Maenhaut, W., McFiggans, G., Mentel, Th. F., Monod, A., Prévôt, A. S. H., Seinfeld, J. H., Surratt, J. D., Szmigielski, R. and Wildt, J.: The formation, properties and impact of secondary organic aerosol: current and emerging issues, Atmos. Chem. Phys., 9(14), 5155-5236, 2009.

Hamilton, J. F., Webb, P. J., Lewis, A. C. and Reviejo, M. M.: Quantifying small molecules in secondary organic aerosol formed during the photo-oxidation of toluene with hydroxyl radicals, Atmos. Environ., 39(38), 7263-7275, 2005.

Henze, D. K., Seinfeld, J. H., Ng, N. L., Kroll, J. H., Fu, T-M., Jacob, D. J., Heald, C. L.: Global modeling of secondary organic aerosol formation from aromatic hydrocarbons: high-vs. low-yield pathways, Atmos. Chem. Phys., 8(9), 2405-2421, 2008.

Izumi, K., and Fukuyama, T.: Photochemical aerosol formation from aromatic hydrocarbons in the presence of NO_x, Atmos. Environ. A-Gen., 24(6), 1433-1441, 1990.

Jang, M. and Kamens, R.M.: Characterization of secondary aerosol from the photooxidation of toluene in the presence of NO_x and 1-propene, Environ. Sci. Technol., 35(18), 3626-3639, 2001.

Jimenez, J. L., Canagaratna, M. R., Donahue, N. M., Prevot, A. S. H., Zhang, Q., Kroll, J. H., DeCarlo, P. F., Allan, J. D., Coe, H., Ng, N. L., Aiken, A. C., Docherty, K. S., Ulbrich, I. M., Grieshop, A. P., Robinson, A. L., Duplissy, J., Smith, J. D., Wilson, K. R., Lanz, V. A., Hueglin, C., Sun, Y. L., Tian, J., Laaksonen, A., Raatikainen, T., Rautiainen, J., Vaattovaara, P., Ehn, M., Kulmala, M., Tomlinson, J. M., Collins, D. R., Cubison, M. J., Dunlea1, E., J., Huffman, J. A., Onasch, T. B., Alfarra, M. R., Williams, P. I., Bower, K., Kondo, Y., Schneider, J., Drewnick, F., Borrmann, S., Weimer, S.,, Demerjian, K., Salcedo, D., Cottrell, L., Griffin, R., Takami, A., Miyoshi, T., Hatakeyama, S., Shimono, A., Sun, J. Y., Zhang, Y. M., Dzepina, K., Kimmel, J. R., Sueper, D., J. Jayne, T., Herndon, S. C., Trimborn, A. M., Williams, L. R., Wood, E. C., Middlebrook, A. M., Kolb C. E., Baltensperger, U. and Worsnop D. R.: Evolution of organic aerosols in the atmosphere, Science, 326(5959), 1525-1529, 2009.

Kalberer, M., Paulsen, D., Sax, M., Steinbacher, M., Dommen, J., Prevot, A. S. H., Fisseha, R., Weingartner, E., Frankevich, V. and Zenobi, R.: Identification of polymers as

major components of atmospheric organic aerosols, Science, 303(5664), 1659-1662, 2004.

Kanakidou, M., Seinfeld, J. H., Pandis, S. N., Barnes, I., Dentener, F. J, Facchini, M. C., Van Dingenen, R., Ervens, B., Nenes, A., Nielsen, C. J., Swietlicki, E., Putaud, J. P., Balkanski, Y., Fuzzi, S., Horth, J., Moortgat, G. K., Winterhalter, R., Myhre, C. E. L., Tsigaridis, K., Vignati, E., Stephanou, E. G., and Wilson, J.: Organic aerosol and global climate modelling: a review, Atmos. Chem. Phys., 5(4), 1053-1123, 2005.

Kleindienst, T. E., Smith, D. F., Li, W., Edney, E. O., Driscoll, D. J., Speer, R. E. and Weathers, W. S.: Secondary organic aerosol formation from the oxidation of aromatic hydrocarbons in the presence of dry submicron ammonium sulfate aerosol, Atmos. Environ., 33(22), 3669-3681, 1999.

Kroll, J. H., Smith, J. D., Che, D. L., Kessler, S. H., Worsnop, D. R. and Wilson, K.R.: Measurement of fragmentation and functionalization pathways in the heterogeneous oxidation of oxidized organic aerosol, Phys. Chem. Chem. Phys., 11(36), 8005-8014, 2009.

Lindinger, W., Hansel, A., and Jordan, A.: On-line monitoring of volatile organic compounds at pptv levels by means of proton-transfer-reaction mass spectrometry (PTR-MS) medical applications, food control and environmental research, Int. J. Mass. Spectrom., 173, 191-241, 1998.

Lund, A. K., Doyle-Eisele, M., Lin, Y.-H., Arashiro, M., Surratt, J. D., Holmes, T., Schilling, K. A., Seinfeld, J. H., Rohr, A. C., Knipping, E. M., and McDonald, D. J.: The effects of α-pinene versus toluene-derived secondary organic aerosol exposure on the expression of markers associated with vascular disease, Inhal. Toxicol., 25, 309-324, 2013.

Müller, M., Graus, M., Wisthaler, A., Hansel, A., Metzger, A., Dommen, J., and Baltensperger, U.: Analysis of high mass resolution PTR-TOF mass spectra from 1, 3, 5-trimethylbenzene (TMB) environmental chamber experiments, Atmos. Chem. Phys., 12, 829-843, 2012.

Malloy, Q. G., Nakao, S., Qi, L., Austin, R., Stothers, C., Hagino, H. and Cocker III, D. R.: Real-Time Aerosol Density Determination Utilizing a Modified Scanning Mobility Particle Sizer—Aerosol Particle Mass Analyzer System, Aerosol Sci. Tech., 43(7), 673-678, 2009.

McDonald, J. D., Doyle-Eisele, M., Kracko, D., Lund, A., Surratt, J. D., Hersey, S. P., Seinfeld, J. H., Rohr, A. C., and Knipping, E. M.: Cardiopulmonary response to inhalation of secondary organic aerosol derived from gas-phase oxidation of toluene, Inhal. Toxicol., 24, 689-697, 2012.

Ng, N. L., Kroll, J. H., Chan, A. W. H., Chhabra, P. S., Flagan, R. C. and Seinfeld, J. H.: Secondary organic aerosol formation from *m*-xylene, toluene, and benzene, Atmos. Chem. Phys., 7(14), 3909-3922, 2007.

Ng, N. L., Canagaratna, M. R., Jimenez, J. L., Chhabra, P. S., Seinfeld, J. H. and Worsnop, D. R.: Changes in organic aerosol composition with aging inferred from aerosol mass spectra, Atmos. Chem. Phys., 11(13), 6465-6474, 2011

Praplan, A., Hegyi-Gaeggeler, K., Barmet, P., Pfaffenberger, L., Dommen, J., and Baltensperger, U.: Online measurements of water-soluble organic acids in the gas and aerosol phase from the photooxidation of 1, 3, 5-trimethylbenzene, Atmos. Chem. Phys., 14, 8665-8677, 2014.

Prince, B. J., Milligan, D. B., and McEwan, M. J.: Application of selected ion flow tube mass spectrometry to real‐time atmospheric monitoring, Rapid. Communin. Mass. Sp., 24, 1763-1769, 2010.

Sato, K., Hatakeyama, S. and Imamura, T.: Secondary organic aerosol formation during the photooxidation of toluene: NO_x dependence of chemical composition, J. Phys. Chem. A., 111(39), 9796-9808, 2007.

Smith, D., Kleindienst, T., and McIver, C.: Primary product distributions from the reaction of OH with *m*-, *p*-xylene, 1, 2, 4-and 1, 3, 5-trimethylbenzene, J. Atmos. Chem., 34, 339-364, 1999.

Song, C., Na, K. and Cocker III, D. R.: Impact of the hydrocarbon to NO_x ratio on secondary organic aerosol formation, Environ. Sci. Technol., 39(9), 3143-3149, 2005.

Song, C., Na, K., Warren, B., Malloy, Q., Cocker III, D. R.: Secondary organic aerosol formation from the photooxidation of *p*-and *o*-xylene. Environ. Sci. Technol., 41(21), 7403-7408, 2007.

White, S. J., Jamie, I. M., and Angove, D. E.: Chemical characterisation of semi-volatile and aerosol compounds from the photooxidation of toluene and NOx, Atmos. Environ., 83, 237-244, 2014.

Wyche, K. P., Monks, P. S., Ellis, A. M., Cordell, R., Parker, A., Whyte, C., Metzger, A., Dommen, J., Duplissy, J., and Prevot, A.: Gas phase precursors to anthropogenic secondary organic aerosol: detailed observations of 1, 3, 5-trimethylbenzene photooxidation, Atmos. Chem. Phys., 9, 635-665, 2009.

Yu, J., and Jeffries, H. E.: Atmospheric photooxidation of alkylbenzenes—II. Evidence of formation of epoxide intermediates, Atmos. Environ., 31, 2281-2287, 1997.

Zhou, Y., Zhang, H., Parikh, H. M., Chen, E. H., Rattanavaraha, W., Rosen, E. P., Wang, W., and Kamens, R. M.: Secondary organic aerosol formation from xylenes and mixtures of toluene and xylenes in an atmospheric urban hydrocarbon mixture: water and particle seed effects (II), Atmos. Environ., 45, 3882-3890, 2011.

6.7 Tables and Figures

Table 6.1Experimental Conditions

Run ID	Compounds[a]	HC_i[b] ppb	$NO_{x,i}$[b] ppb
928A	($^{13}C_2$)*m*-xylene/NO	80.5	9.9
929A	($^{13}C_2$)*m*-xylene/NO	85.2	43.8
931A	*m*-xylene/NO	75.4	43.6
932A	*m*-xylene/^{15}NO	86.2	50.0*
2087A	*p*-xylene/NO	69.4	16.4
2088A	($^{13}C_2$)*p*-xylene/NO	66.1	18.7

Note: a) Compounds are none isotope containing unless they are labled; b) Initial concentration; *Target concentration

Table 6.2 Contribution of methyl substitute (^{13}C) to major particle phase products during aromatic hydrocarbon photooxidation

m/z	Fragments	Isotope fragments	Isotope m/z	Average P_{13C} [a]	
				m-xylene	*p*-xylene
43	C_2H_3O	$^{13}CCH_3O$	44	**71.9%**	**77.6%**
44	CO_2	$^{13}CO_2$	45	11.5%	4.70%[b]
28	CO	^{13}CO	29	0%[c]	0%[c]

Note: a) Average P_{13C} is calculate according to time series isotope containing fragment percentage value (Eq-1), starting from peak suspended particle concentration (HR-TOF-AMS Org > 2μg·m^{-3} for *m*-xylene and Org > 0.5μg·m^{-3}for *p*-xylene); b) Data is noisy and is difficult to find a trend; c) Assume $^{12}CO = ^{12}CO_2$, average $^{13}C / (^{12}C + ^{13}C) < 1e^{-15}$

Table 6.3 Contribution of methyl substitute (^{13}C) to significant gas phase products during xylene photooxidation

MW[a]	# ^{13}C[b]	*m*eta	*p*ara	Proposed Formula	Proposed product
30	0 or 1	✓	✓	CH_2O	formaldehyde
42	1	✓	✓	C_2H_3O+	$CH_3C(O)$-$(O)R$[1]
44	0	✓		C_2H_4O	ethenol[c]
	1	✓		C_2H_4O	acetaldehyde
45	0	✓		HNO_3	nitic acid[2] or nitrate fragments[3]
46	0	✓	✓	CH_2O_2	formic acid
58	0	✓		$C_2H_2O_2$	glyoxal
60	0	✓		$C_2H_4O_2$	Glycolaldehyde[4]
	1	✓	✓	$C_2H_4O_2$	acetic acid
72	1	✓	✓	$C_3H_4O_2$	methyl glyoxal
74	1		✓	$C_3H_6O_2$	Acetol[4]
86	0	✓		$C_3H_2O_3$	oxomalonaldehyde
	1		✓	$C_4H_6O_2$	2R,3S)-3-Methyl-2-oxiranecarbaldehyde[4]
	2	✓		$C_5H_{10}O$	Not sure
96	2	✓		C_6H_8O	2,4-Dimethylfuran
98	0	✓		$C_4H_2O_3$	maleic anhydride
98	1	✓	✓	$C_5H_6O_2$	a-angelic lactone; 3-methyl-2(5H)-furanone; 4-keto-2-pentenal
112	0	✓		$C_5H_4O_3$	Not sure
	1	✓	✓	$C_5H_4O_3$	citraconic anhydride
	2	✓		$C_6H_8O_2$	3,5-Dimethyl-2(5H)-furanone
120	2		✓	C_8H_8O	4-methylbenzaldehyde

Note: a) Molecular weight of gas phase prodcuts identified in non-isotopic experiment; b) Number of ^{13}C in a specific formula according to the shift in mass spectrum, 0-no shift, no ^{13}C, 1-1 g/mol shift, one ^{13}C, 2-2 g/mol shift, two ^{13}C; c) Not sure; 1) Spanel, et al 1997; 2) Grieshop, et al., 2009; 3) Müller, et al., 2012; 4) Yu, et al., 1997a

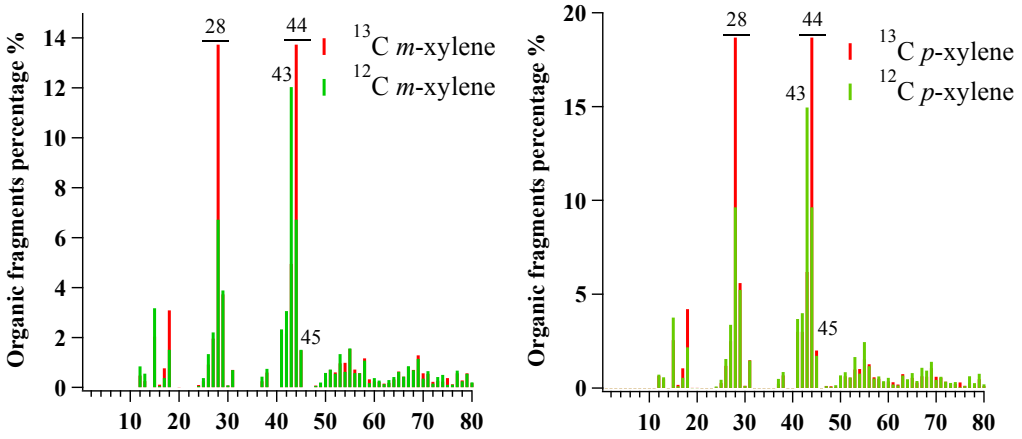

Figure 6.1 Comparison of organic mass spectrum in SOA formed from the photooxidation of xylenes:

a) ^{12}C (931A) and ^{13}C (929A) *m*-xylene; b) ^{12}C (2087A) and ^{13}C (2088A) *p*-xylene under low NO_X Conditions (Underline m/z number indicates abundant ^{13}C containing fragment)

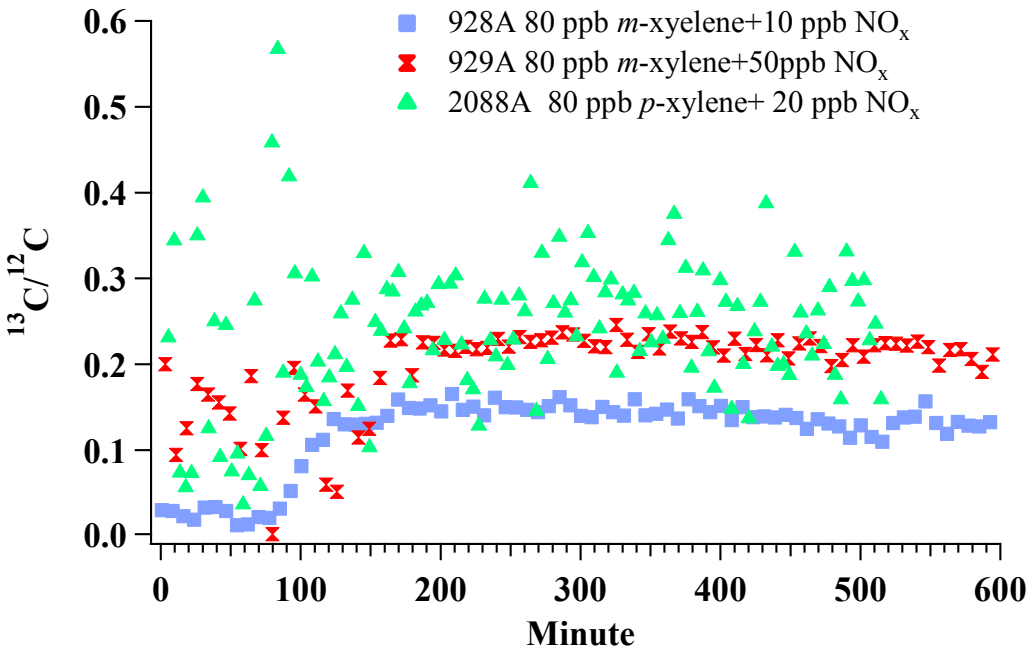

Figure 6.2 Evolution of bulk SOA $^{13}C/^{12}C$ during the photooxidation of ^{13}C *m*-xylene (928A and 929A) and ^{13}C *p*-xylene (2088A) under low NO_x Conditions

7. Missing Urban Aerosol Source: Critical Molecular Structure to Secondary Organic Aerosol Formation from Glycol Ethers

7.1 Introduction

Glycol ethers are compounds with formula of R−(OCH2CH2)$_n$−OR' (n=1,2,3) (EPA, 2000). They are widely used as solvents in consumer product industries including architecture coatings, cleaning products, adhesives, pesticides and pharmaceuticals (EPA, 2000; Singer, *et al.*, 2006; Fromme, *et al.,* 2013). Previous studies suggest that glycol ethers are sufficiently volatile to be atmospherically availabe (Cooper, *et al.*, 1995; Zhu, *et al* 2001; Singer, *et al*, 2006) and their presence in indoor air (Gibson, *et al* 1991; Nazaroff and Weschler 2004; Choi, *et al.*, 2010; Wieslander, and Norbäck, 2010a,b) even for those glycol ethers exempted by EPA, California Air Resources Board (CARB) and Ozone Transport Commission (OTC) in consumer product regulation as low vapor pressure-volatile organic compound (Võ and Morris, 2014). Emission of known glycol ethers in California are estimated to be 13.44 tons per day in 2020 a based on databases provided by the California Air Resources Board (CARB) and industrial sectors (Cocker, *et al* 2014). Therefore, it is important to understand the primary and secondary impact of glycol ethers on air quality and human health. The US Environmental Protection Agency classified glycol ethers as hazardous air pollutants (HAP) under the 1990 Clean Air Act Amendments.

The oxidization of intermediate and semi-volatile organic compound (IVOC and SVOC) is predicted to be a larger global source of net aerosol production than oxidation of traditional parent hydrocarbons (Pye and Seinfeld, 2010). A representative type of IVOC is long carbon chain alkane. Ethers are less volatile and more reactive in oxidation than

alkanes with the same amount of carbons (Pankow and Asher, 2008; Mellouki, et al 2003). Several glycol ethers (e.g. Diethylene glycol monoethyl ether and Diethylene glycol monobutyl ether) are recently identified as an important intermediate-volatile organic compound available to atmosphere (Võ and Morris, et al., 2014). However, SOA formation from glycol ethers is seldom investigated compared with other SVOCs such as terpenes, isoprene, aromatics and long chain alkanes. The secondary impact of glycol ether resulting from the oxidation of primary emissions requires further evaluation.

Gas phase oxidation of ethers and simple glycol ethers (n=1 in $R-(OCH_2CH_2)_n-OR'$, R'=H or alkyl group)) is well documented in previous studies (Tuazon, *et al* 1991; Wallington and Japar, 1991; Eberhard, *et al* 1993; Mellouki, *et al* 1995; Johnson, and Andino, 2001; Mellouki, *et al* 2003; Orlando, 2007; Tommaso, *et al* 2011). It is clear that the H-abstraction by ·OH, mostly at α-carbon H, forming alkoxy radical is the dominant initial step of ether atmospheric photooxidation (Aschmann, and Atkinson, 1998). Generally, major final products following alkoxy radical photooxidation of theses ethers are formates, ketones and aldehydes, which are formed mainly from fragmentation by carbon-carbon bond scission (Mellouki, *et al* 2003). Additionally, carbonates are also observed as important products in oxidation of other ethers (Wenger, *et al* 1999; Geiger and Becker, 1999; Platz, *et al* 1999). Further, hydroperoxides could be formed in absence of NO_x (Jenkin, *et al* 1993; Sehested, *et al* 1996) and NO_x could lead to nitrate formation including peroxynitrate and peroxyacyl nitrate (Aschmann and Atkinson 1999; Orlando, 2007; Malanca, *et al* 2009) and affect alkoxy radical decomposition (Collins, *et al* 2005; Orlando, 2007). Reaction with NO_3 radical may also contribute, to a small extent of the removal of some ethers

during night-time, while photolysis and reaction with O_3 are negligible (Chew, et al., 1998; Mellouki, *et al* 2003). This study focues on the daytime chemistry of ether with OH radical.

Early studies concentrated on gas phase oxidation and less focus on the potential of particle formation from glycol ethers. It is noted that a cyclic product is observed by Stemmler, *et al* (1996) from the oxidation of a simple glycol ether (2-Ethoxyethanol). Cyclization prevents fragmentation of ethers leading to higher molecular weight products, which are more likely to partition into the particle phase, especially for the oxidation of glycol ethers with higher initial molecular weight and low volatility. It is of necessity to study the oxidation of more complicated glycol ether and their contribution to SOA, especially those with higher molecular weight (e.g. n>1, in R - $(OCH_2CH_2)_n$−OR').

NO_x participates in ether oxidation by reaction with peroxide radical to form organic nitrate as mentioned above and may compete with the cyclization pathway (Stemmler, *et al* 1996). Further, Espada and Shepson (2005) discussed -OR' impact on ether organic nitrate product stability and yields. However, previous studies were mostly conducted with NO_x concentrations higher than hundreds ppb, which is less atmospherically relevant (Stemmler, *et al* 1996; Aschmann and Atkinson 1999; Orlando, 2007). It is important to study ether oxidation under atmospherically relevant NOx conditions in order to extend laboratory data to ambient prediction.

In this study, the potential of SOA formation from glycol ethers and the related ethers is investigated under H_2O_2 only and low NO_x condition. SOA yields and chemical compositions from different ethers are compared to explore the effect of glycol ether molecular structure on SOA formation. Further, the influence of NO and hydroxyl radical

(·OH) on SOA formation from ethers is discussed. Finally, the contribution of ethers to global SOA formation is evaluated.

7.2 Methods

7.2.1 Environmental chamber

The UC Riverside/CE-CERT indoor dual 90 m^3 environmental chambers were used in this study and are described in detail elsewhere (Carter et al., 2005). Experiments were all conducted at dry conditions (RH<0.1%), in the absence of inorganic seed aerosol, and with temperature controlled to 27±1°C. Two movable top frames were slowly lowered during each experiment to maintain a slight positive differential pressure (~0.02" H_2O) between the reactors and enclosure to minimize dilution and/or contamination of the reactors. 276 115 W Sylvania 350BL blacklights are used as light sources for photooxidation.

A known volume of high purity liquid ethers (boiling point >150 °C) were injected through a glass manifold inside a temperature controlled oven (oven temperature 80-120 °C adjusted according to ethers´ physical properties) and flushed into the chamber with pure N_2. More volatile ethers (boiling point <150 °C) were injected through a heated glass injection manifold system instead of a manifold inside the oven. A glass manifold packed with glass wool inside a temperature controlled oven is used to inject H_2O_2 (oven temperature 55-65 °C). NO was introduced by flushing pure N_2 through a calibrated glass bulb filled to a predetermined partial pressure of pure NO. All ethers and NO are injected and well mixed before the lights were turned on to commence the reaction.

7.2.2 Gas-phase analysis

Decay of *m*-xylene was measured by a pair of Agilent 6980 (Palo Alto, CA) gas chromatographs (GC) equipped with flame ionization detectors (FID) or Selected Ion Flow Tube-Mass Spectrometry (SIFT, Syft Technology, Voice 200®). A Thermal Environmental Instruments Model 42C chemiluminescence NO_x analyzer was used to monitor NO, NO_y-NO and NO_y. O_3 was monitored by a Dasibi Environmental Corp. Model 1003-AH O_3 analyzer.

7.2.3 Particle phase analysis

Aerosol growth was measured using an in-house built scanning mobility particle sizer (SMPS). The differential mobility analyzer is located inside the chamber enclosure to ensure that aerosol sizing was conducted at a temperature identical to the chamber temperature. Particle volume was corrected for particle wall loss assuming a first order wall loss decay as described in Cocker et al (2001a). Evolution of particle-phase chemical composition was measured by a High Resolution Time of Flight Aerosol Mass Spectrometer (HR-ToF-AMS; Aerodyne Research Inc.) (Canagaratna et al., 2007; DeCarlo et al., 2006). The sample was vaporized by a 600 °C oven followed by a 70 eV electron impact ionization. Elemental ratios for total organic mass, oxygen to carbon (O/C), and hydrogen to carbon (H/C) were determined using the elemental analysis (EA) technique (Aiken et al., 2007, 2008). Data were analyzed with the ToF-AMS analysis toolkit Pika 1.15D with 1.56D Squirrel.

7.2.4. Ethers Studied

A series of ethers (Fig. 7.1) are identified and used to investigate the impact of molecular structure on SOA formation from glycol ether (R −$(OCH_2CH_2)_n$−OR'). Diethylene glycol ethyl ether (Sigma-Aldrich, 99%, DEGEE) and diethylene glycol butyl ether (Sigma-Aldrich, ≥99%, DEGBE) are two basic ethers focused in current study due to their low volatility, wide application in consumer products and therefore higher potential to SOA formation. Diethylene glycol methyl ether (Sigma-Aldrich, ≥99%, DEGME) is selected to study the impact of carbon chain length in R- on SOA formation from glycol ether. Ethylene glycol diethyl ether (Sigma-Aldrich, 98%, EGDEE) is used to compare with DEGEE in order to demonstrate the importance of –OR' or -OH to SOA formation from glycol ether. Diethylene glycol dimethyl ether (Sigma-Aldrich, 99.5%, DEGDME) compared with DEGBE is used to distinguish between the role of − OH (R′=H) and alkoxy group (–OC_nH_{2n+1}, R′=Alkyl group) to SOA formation from glycol ether. Di(propylene glycol) butyl ether (eNovation Chemicals, >95%, DPGBE) and 1-(2-Methoxyethoxy)-2-methyl-2-propanol (Sigma-Aldrich, >98%, 12M2MP), comparing with corresponding glycol ethers (DEGBE and DEGME, respectively), are used to investigate the $–CH_3$ hindrance effect on –OH and its role to SOA formation. Further, 1, 3-diethoxy-2-propanol (Sigma-Aldrich, Aldrich^{CPR} 13D2P) and 3, 3-diethoxy-1-propanol (Sigma-Aldrich, 98%, 33D1P) are identified to evaluate the influence of –OH position on ether oxidation. 1, 2-Dimethoxyethane (Sigma-Aldrich, 99.5%) represents a simple glycol ether in this study to compare with earlier studies. Three experimental schemes used in this study are as followed: 1) with H_2O_2 only: ether+1ppm H_2O_2; 2) in presence of NO_x: ether+ ~20ppb NO; 3) NO_x

with sufficient OH: ether+1ppm H_2O_2+ ~20ppb NO (Table 7.1).

7.3 Results

7.3.1 SOA formation in absence of NO_X

The SOA formation potential of glycol ethers is investigated with H_2O_2 only. A substantial amount of SOA is formed during the photooxidation of two basic glycol ethers studied (DEGEE M_0=18.9-48.3 $\mu g \cdot m^{-3}$ and DEGBE M_0=154-177 $\mu g \cdot m^{-3}$). EGDEE with similar molecular structure to DEGEE but without –OR′ structure, forms less amount of SOA (4.4-10.3$\mu g \cdot m^{-3}$) than DEGEE. The reaction rate of EGDEE with ·OH is similar to that of DEGEE (Table S7.1) supporting that a similar amount of ethers are reacted under similar initial ·OH conditions. This suggests that the existence of –OH or –OR′ in glycol ether structure promotes the formation of less volatile products during the oxidation of glycol ether. An insignificant SOA formation from DEGDME, the isomer of DEGBE containing alkoxy group instead of −OH in the −OR. It indicates that the existence of –OH rather than alkoxy group in glycol ether structure activates the formation of less volatile products during the ether oxidation.

The relationship between -OH location in ether precursor and SOA formation is further studied. DPGBE, compared with DEGBE, has two more methyl groups attached to -$(OCH_2CH_2)_n$- carbon, at α and γ position of -OH respectively, and shows a lower amount (77.7-131 $\mu g \cdot m^{-3}$) of SOA formation when similar amount of ether (DPGBE vs DEGBE) are consumed (Table 7.1). Much less amount (~2 $\mu g \cdot m^{-3}$) of SOA is formed from 12M2MP, which has two more methyl groups at α position of –OH compared with DEGBE. This

suggests that adding methyl group to carbons in $-(OCH_2CH_2)_n-$ alter the preference of ether reaction pathways (e.g., isomerization, fragmentation and cyclization). It is possible that extra methyl group on carbon chain suppresses intermolecular cyclization associate with –OH, which is expected to form less volatile products from glycol ethers. It is noted that the adding of methyl groups next to –OH increases the overall reaction rate of ether (Porter, et al., 1997). The hindrance effect of methyl groups on the intermolecular cyclization related to –OH possibly results from the deactivation of H-abstraction at γ position carbon when more methyl groups are added next to −OH and therefore diminishes the cyclization reaction pathways associated with H-abstraction at γ position carbon.

The effect of –OH on ether reaction is further investigated by changing the location of -OH in the ether carbon bond. Sufficient amount of SOA is formed from 13D2P (M_0=29.2 $\mu g \cdot m^{-3}$) and 33D1P (M_0=38.9 $\mu g \cdot m^{-3}$). SOA formations from 13D2P and 33D1P are in between the amount of SOA formed from DEGEE and DEGBE when similar mole amount of ethers are reacted. It seems that the location of –OH in ethers exerts less impact on SOA formation according to SOA yield. Insignificant amount of SOA is formed during the photooxidation of 1, 2-dimethoxyethane consistent with these volatile products proposed in earlier study (Geiger and Becker, 1999).

SOA yield is calculated as a mass ratio of SOA formed to ether reacted during the photooxidation according to Odum's (1996) work. The relationship between SOA yield and mass loading during the photooxidation of ethers in absence of NO_x is showed as Fig.

7.1. A similar SOA yield is achieved by DEGEE (1991A) at lower mass loading compared with DEGBE (1999A). It is concluded that DEGEE has higher yields under low mass loading compared with DEGBE. This indicates that more low-volatility products are formed by the oxidation of DEGEE than DEGBE. DPGBE shows similar SOA yield at mass loading of 77.7μg·m^{-3} and 131 μg·m^{-3} suggesting a plateau of SOA yield at mass loading higher than 77.7μg·m^{-3}. It is predicted that DPGBE shows a lower SOA yield than DEGBE at higher mass loading (>150μg·m^{-3}). The earlier and lower plateau in the SOA yield curve of DPGBE compared with that of DEGBE indicates that a large amount of DPGBE oxidation products is substantially volatile to not participate into aerosol phase or less amount of semivolatile products (high-volatility products in two product Odum's model) are formed from the oxidation of DPGBE than that of DEGBE. It is possibly due to a larger fragmentation fraction caused by the increase of methyl group on carbons in $-(OCH_2CH_2)_n-$. EGDEE. 13D2P and 33D1P tend to have similar SOA yield to DEGEE, at least in the range of mass loading investigated in this work. No additional comparison among SOA yield is addressed in current work as other ethers forms insignificant (<5μg·m^{-3}) SOA. Following sections only focus on ethers that have significant SOA formation.

7.3.2 SOA chemical composition

7.3.2.1 Elemental ratio

Elemental ratio analysis (Aiken, et al., 2007, 2008) provides a mole based SOA chemical composition to probe into SOA formation mechanisms (Heald, et al., 2010; Chhabra, et al., 2011). Fig. 7.3a shows H/C and O/C evolution in SOA formed from the photooxidation of

different ethers under H_2O_2 only condition. Ether precursor location (Fig. 7.3) is marked by specie name in black text and the elemental ratio changing from precursor to SOA (average H/C and O/C) is presented (Fig .S7.1). The slope of H/C to O/C as the precursor is oxidized to SOA (Fig. S7.1, line marked with the slope of the line) is < -2 for all ethers studied. Oxidation of ethers is likely to include fragmentation of the −C−O− backbone (Geiger and Becker, 1999), cylization (Stemmler, et al., 1996), and oxidation of aliphatic carbons ($-CH_2-$) into carbonyl group (−C(=O)−) (Heald, et al., 2010). The slope of O/C vs. H/C during the oxidation for each oxidation pathway are -2 for carbonyl formation, <-2 for –O−C− fragmentation in addition to carbonyl formation, and -∞ for cylization. The observed slope decreases from -2.33 to -4.31 as carbon length of the R– group increases from methyl to butyl substituteconsistent with increasing cyclization (slope (-∞)) compared with fragmentation of the –C–O–. EGDEE and DPGBE have higher elemental ratio slope from precursor to SOA and lower SOA formation than that of DEGEE and DEGBE, respectively. This suggests greater fragmentation and less cyclization is during the oxidation of EGDEE and DPGBE than DEGEE and DEGBE, respectively, for ether with the same length of –R group.

Oxidation state of carbon ($OS_c \approx 2O/C - H/C$) was introduced into aerosol-phase component analysis by Kroll et al. (2011). Average ΔOS_c is calculated as the difference between the average SOA OS_c and the precursor OS_c. A decrease trend is found in OS_c and average ΔOS_c with an increase in carbon number (Fig. 7.3b). However, a lower ΔOS_c may not relate to the less oxidation of precursor as ether precursors with higher carbon numbers

are divided by a large number of carbon when similar number of oxygen is contained or added during a similar oxidation processes. Therefore, a carbon number normalized prcess is applied to better understand the extent of oxidation among ethers with different carbon number..

7.3.2.2 Precursor carbon number normalized elemental ratio

Precursor carbon number normalized elemental ratio parameters (*O/M, H/M and -Δ(H/M)*) derived from elemental ratio are introduced (Eq-1~3) to compare the extent of the oxidationfor SOA precursors with varying carbon number.

$$^{O}/_{M} = n_c \times {}^{O}/_{C} \quad \text{Eq-1}$$

$$^{H}/_{M} = n_c \times {}^{H}/_{C} \quad \text{Eq-2}$$

$$-\Delta\left(^{H}/_{M}\right) = \left(^{H}/_{M}\right)_{pre} - \left(^{H}/_{M}\right)_{SOA} \quad \text{Eq-3}$$

where *O/M* and *H/M* are precursor carbon number normalized elemental ratios; *O/C* and *H/C* are traditional mole based elemental ratios (Aiken, et al., 2007, 2008); n_c is the number of carbons in ether precursor; $(H/M)_{pre}$ and $(H/M)_{SOA}$ are *H/M* of the ether precursor and its SOA, respectively; -Δ*(H/M)* is the difference between ether precursor and its SOA in H/M.

O/M and -Δ*(H/M)* of SOA formed from all ethers studied are similar with an average value of 4.35±0.35 and 4.10±0.32, respectively. *O/M* represnts the average oxygen content of SOA and -Δ*(H/M)* represents the hydrogen loss of the precursor during oxidation assuming that oxidized products have the same number of carbons as their corresponding precursor.

That means SOA formation from ethers can be estimated by an oxidation process that adds oxygen until the SOA products contain an average~4 oxygen per precursor molecular by losing ~4 hydrogen from the precursor. It is noticed that most of the ethers that form SOA in this work start with 3 oxygen in precursor and double bond equivalent (DBE)=0, except for EGDEE (2 oxygen and DBE=0). Aliphatic carbon oxidized into carbonyl explains a loss of 2 hydrogens and a gain of 1 oxygen. Therefore, these ether precursors that contain 3 oxygen must have another step involved that lose 2 more hydrogen without oxygen addition to reach the final product. This addition step suggests the importance of cyclization pathway to SOA formation from ethers, which loses 2 hydrogen without increasing oxygen. Losing 4 hydrogen while gaining 2 oxygen during EGDEE can be readily explained by two aliphatic carbon oxidized into carbonyl conversion. It is noted all ethers except for EGDEE contain –OH functional groups associated with the cyclic mechanism. This suggests that importance of –OH to cyclization and therefore the overall SOA formation. These similar O/M values provide a general estimation for the required functionalization steps needed for an ether precursor to form SOA, especially for precursors containing 6-10 carbons. OS_c and carbon number (Fig. 7.3b) suggest that ether oxidation products are among SV-OOA and LV-OOA (Kroll, et al., 2011). The vapor pressure of products formed from the mechanism proposed above (aliphatic carbon to carbonyl coupled with cyclization) ranges from 10^{-3} to 10^{-6} atm based on SIMPOL prediction (Pankow and Asher, 2008) yielding saturation vapor pressure (C*) on the order of 10^5 $\mu g \cdot m^{-3}$ (Table S7.2). Therefore, cyclization products have too high of predicted C* to participate in SOA formation suggesting the importance of additional oligomerization reaction form SOA from ethers.

It is possible that oligomerization of fragmentation products also contributes to SOA formation from ethers. However, similar fragmentation products can be formed from other ethers observed to have insignificant SOA formation (eg. DEGDME vs DEGBE). Therefore, the oligomerization of common fragmentation products is unlikely to be a major contributor to SOA formation from ethers. Nevertheless, certain unique fragmentation products, especially those with a large number of carbon, may participate in gas-particle partitioning. Knowing the major similar reaction pathways for ether oxidation, the variation in *O/M* and -Δ*(H/M)* in Fig. 7.4a) and b) could be explained by the different ratios among fragmentation (with or without oxygen loss in –C–O–C–), cyclization and carbonyl formation for different ethers. It is noted that fragmentation is also associated with carbonyl formation on the terminal carbon. *O/M* and -Δ*(H/M)* are also used to demonstrate the difference in SOA formation from various ethers, in addition to the slope in H/C and O/C analysis from ether precursor to SOA (Section 7.3.2.1).

The influence of these reactions on *O/M* increase ranks from high to low as fragmentation without oxygen loss >carbonyl formation (+1) > fragmentation with one oxygen loss >cyclization (+0); the influence of these reactions on -Δ*(H/M)* increase ranks from high to low as cyclization =carbonyl formation(2)>fragmentation. A decrease in *O/M* and insignificantly in -Δ*(H/M)* from DEGME to DEGEE to DEGBE is possibly due to that cyclization and carbonyl formation in R-substitute is preferred when R–substitute carbon chain is longer compared with carbonyl formation with oxygen loss on R-substitute. This implication agrees with the observation in the elemental ratio slope (Section 7.3.2.1). It might be explained by a higher electron-donating of butyl, ethyl than that of methyl and

therefore makes the C–O less fragile when radical is formed by H-abstraction. The significantly higher *O/M* and -Δ*(H/M)* of 33D1P than the average indicate that 33D1P are more oxidized than other ethers, possibly by a larger fraction of multiple carbonyl formation. *O/M* and -Δ*(H/M)* of SOA formed from DPGBE are both slightly higher than those from DEGBE indicating that a higher fragmentation percentage in DPGBE than DEGBE. The lower *O/M* in EGDEE compared with other ether is due to the less amount of oxygen contained in initial ether precursor. Overall, this section confirms that SOA formation from ethers is a combination of fragmentation, carbonyl formation, cyclization and oligomerization.

7.3.2.3 f_{CO2}^{+}vs f_{C2H3O}^{+}

CO_2^+ (m/z=44) and $C_2H_3O^+$ (m/z=43) are two representative oxygenated fragments from oxygenated organic aerosol (OOA) (Ng, et al., 2011). Ng, et al demonstrate the relationship of OOA with a f_{44} vs f_{43} plot when fragments at m/z 44 and m/z 43 under ambient conditions are majorly CO_2^+ and $C_2H_3O^+$, respectively. The major m/z 44 fragments in the current include both $C_2H_4O^+$ and CO_2^+, due to the –(OCH_2CH_2)– structure in ether precursors. Also, the major fragments in current study at m/z 43 may refer to $C_3H_7^+$ and $C_2H_3O^+$ when R– in the ether precursor is a long alkyl substitute. Therefore, f_{CO2}^{+} vs f_{C2H3O}^{+} (Fig .7.5) is used to compare the oxidation of ethers instead of f_{44} vs f_{43}.

DEGME, DEGEE, and DEGBE (-$(OCH_2CH_2)_n$-OH) SOA formed from DEGME is observed to have higher CO_2^+ and lower $C_2H_3O^+$ compared to DEGEE. It is also found that the sum of SOA f_{CO2+} and f_{C2H3O+} from DEGEE and DEGME are approximately the same

(~0.2) implying CO_2^+ from DEGME is substituted for a portion (~50%) of $C_2H_3O^+$ from DEGEE since –O–CH_3 is oxidized to –O–CHO while –O–C_2H_5 is oxidized to –O–CH_2–CHO. This suggests that –O–C_2H_5 in DEGEE contributes approximately 50% of $C_2H_3O^+$ in SOA.SOA formed from DEGBE has lower CO_2^+ and $C_2H_3O^+$ than that of DEGEE and shows a significant oxidation evolution approaching the location of SOA formed from DEGEE. The smaller f_{CO2}^+ may result from the larger number of carbons in R– and the similar amount of oxygen in the ether precursors. It is found that f_{C2H3O}^+/f_{CO2}^+ is around 2 in SOA formed from DEGBE while it is about 1 from DEGEE. This is consistent with the larger number of carbons in R– and therefore a higher possibility to form $C_2H_3O^+$ from DEGBE than from DEGEE. f_{C2H3O}^+ in SOA from DEGBE tends to be similar to DEGEE after further oxidation. It is noted that the f_{CO2}^+ vs f_{C2H3O}^+ trending slope after 90 minutes of oxidation is apporximately 1 suggesting a similar increase in CO_2^+ and $C_2H_3O^+$. It is possible that fragmentation dominates DEGBE aging after initial oxidation increasing product volatility and therefore lowering SOA yield (Section 7.3.1).

Other Ethers EGDEE with no –OH groups in the precursor molecule has similar SOA f_{CO2}^+ and f_{C2H3O}^+ as that of DEGEE indicating that –OH is less likely contribute to acid functional group (CO_2^+) formation during ether oxidation. A larger f_{C2H3O}^+ and a similar f_{CO2}^+ is found in DPGBE compared with DEGEE suggesting that adding methyl group on α carbon has insignificant impact on f_{CO2}^+ but increases f_{C2H3O+}. This points out two implications: 1) CO_2^+ is majorly associated –CH_2–O– instead of HO–CH(R_1)- (R_1= –CH_3 or –H); 2) $C_2H_3O^+$ increases with the total number of carbons in alkyl substitutes. SOA formed from 13D2P and 33D1P shows much higher f_{CO2}^+ and f_{C2H3O}^+ than that of DEGEE

suggesting a higher oxidation tendency when –OH is in the middle of carbon chain instead of at the terminal position. It is observed that the activation of –OH can be at most extended to δ carbon (Porter, et al., 1997). Therefore, all the carbons in 13D2P and 33D1P are activated by –OH.

7.3.3 Representative products in particle and gas phase

7.3.3.1 Representative products in particle phase

Functional groups of ether oxidation products in particle phase is inferred from fragments generated from HR-TOF-AMS. General aldehyde, ketone, acid and ester fragments, such as CHO^+ (m/z 29), $C_2H_2O^+$ (m/z 42), $C_2H_3O^+$ (m/z 43), CHO_2^+ (m/z 45), C_2HO^+ (m/z 41) and $C_2H_4O_2^+$ (m/z 60) are observed in SOA as oxidation products for all ethers along with common fragments associated with ether structure (CH_3O^+ (m/z 31) and $C_2H_5O^+$ (m/z 45)) (Fig. S7.5).

DEGME, DEGEE, and DEGBE (-$(OCH_2CH_2)_n$-OH) The SOA mass spectrum from the oxidation of DEGME, DEGEE and DEGBE show additional major peaks at m/z 73 ($C_3H_5O_2^+$, all) and m/z 47 ($CH_3O_2^+$, DEGME), m/z 61 ($C_2H_5O_2^+$, DEGEE) and m/z 89 ($C_3H_7O_2^+$, DEGBE), which are the $C_nH_{2n+1}O_2^+$ (n=1, 2 and 4) analogues for DEGME, DEGEE and DEGBE, respectively (Table 7.2). The saturated oxygen atom of the ester group can act as a site to which a hydrogen atom can be transferred during electronic ionization (Mclaffery and Tureek, 1994). This suggests that $C_nH_{2n+1}O_2^+$ originating from the oxidation of the carbon (carbonyl formation) in R- adjacent to –O– is most likely to contribute to SOA formation instead of fragmenting into higher vapor pressure products. A

large amount of $C_3H_5O_2^+$ fragments is observed for ethers with $–(OCH_2CH_2)_2$ – OH structure. Similar ring structures are formed during the oxidation of ethers with $–(OCH_2CH_2)_2–$ OH structure, further suggesting that the cyclization pathway (Stemmler, et al, 1996) in ether oxidation relies on $–(OCH_2CH_2)_2–$OH structure. Less m/z 73 is observed in SOA formed from EGDEE, DPGBE, 13D2P and 33D1P than ethers with $–(OCH_2CH_2)_2–$OH.

Other Ethers EGDEE lacks the –OH compared with DEGEE indicating the likely importance of –OH to cyclization pathway. This also confirms that m/z 73 is not associated with carbonyl, which can both be formed with and without –OH. DPGBE has two $–CH_3$ on $–(OCH_2CH_2)_2–$OH which might hinder the cyclization pathway. It is also possible that the cyclization structure in DPGBE is formed with additional $–CH_3$ on the ring consistent with fragments of $C_4H_7O_2^+$ observed at m/z 87. Further gas phase product analysis in Section 7.3.3.2 indicates the possibility of ring formation during oxidation of DPGBE. A smaller fraction of m/z 73 while a larger fraction of m/z 61 ($C_2H_5O^+$) is formed during the oxidation of 13D2P and 33D1P suggesting cyclization is less favored than carbonyl formation compared with DEGEE. This implies that the location of –OH determinates the branching ratio between different oxidation pathways. Additionally, ethers with longer R- in the end of carbon bond (DEGBE and DPGBE) have higher carbon number fragments such as m/z 57 ($C_4H_9^+$ and $C_3H_5O^+$) and m/z 71($C_4H_7O^+$).

Therefore, the presence of –OH determines the possibility of cylcization nand the location of –OH determines branching ratio of cylization pathway.

7.3.3.2 Representative peaks in gas phase

Gas phase product composition is measured by SIFT-MS by relying on a soft chemical ionisation process that minimizes fragmentation of the molecular peak. SIFT-MS utilizes three ion sources (H_3O^+, NO^+ and O_2^+) to provide multiple fingerprints for the same compound and facilitate the identification of isomer species. For example, ketone and aldehyde may show the same peak from H_3O^+ ionization (M+1) but show different peaks in NO^+ ionization (ketone: M-1; aldehyde: M+30, M stands for the molecular weight of the compound) (Španěl, et al., 1997). The following discussion shows m/z of mass spectrum peak from different ions as (m/z_{H3O+}, m/z_{NO+} (, m/z_{O2+})) in which the subscript refers to the ion source. The m/z peak from O_2^+ may not be presented since the high ionization energy of O_2^+ leads to a large amount of fragment peaks instead of molecular peaks. Peaks associated with formate and aldehyde formation are observed during the oxidation of all ether precursors (Fig. S7.5), consistent with previous studies (Tuazon, et al., 1998; Geiger and Becker, 1999). A typical mass spectrum of gas phase products formed from the oxidation of DEGEE is presented in Fig. 7.6b. Products such as glycol monoformate (91,120) and glycolaldehyde C_2H_4O (61, 90) are observed during the oxidation of DEGEE. Cyclic products are found to form from the oxidation of selectethers. An m/z 75 in H_3O^+ mass spectrum indicates compounds with formula of $C_3H_6O_2$ while formate and aldehyde are observed in NO^+ mass spectrum as m/z 104 and cyclic ethers are observed at m/z 73. Therefore, (75, 73) indicates the formation of cyclic ether such as 1,3-dioxolane, which is found during the oxidation of DEGME, DEGEE and DEGBE. An m/z 75 in H_3O^+ mass spectrum in EGDEE and 13D2P are most related to ethyl formate formation accompanied

by the high m/z 104 signal rather than m/z 73. 1,3-dioxolane might also be formed during the oxidation of DPGBE and 33D1P since there is no significant signal at m/z 104 (Table 7.2). M_p-2 (M_p denotes major m/z peaks from precursor) is also considered as an important cyclic structure when it is formed in both H_3O^+ and NO^+ mass spectrum. A two hydrogen loss from the ether precursor is consistent with either formation of aldehyde substituting for –OH (M_p+29) or the cyclization involving –OH (M_p-2). M_p-2 peaks observed for DEGEE and DEGBE oxidation are a combination of aldehyde and cyclic ether formation. However, cyclic ether largely contributes to M_p-2 peaks during the oxidation of DPGBE and 13D2P. Insignificant (M_p-2, M_p-2) compared with (M_p-2, M_p+29) suggests that cyclization without fragmentation is less favored than aldehyde formation during the oxidation of DEGME. It is reasonable that M_p-2 peaks are not observed from the oxidation products of EGDEE due to the lack of –OH structure. Peaks from cyclization products (M_p-2, M_p-2) are also observed during the oxidation of 33D1P. Overall, cyclization products are indicated by SIFT-MS during the oxidation of all ethers with –OH function group.

7.3.3 Influence of NO on SOA formation from ethers

SOA formation from the photooxidation of ethers under low NO conditions (initial NO=15-25 ppb) are investigated (Table 7.1) to evalute the impact of NO on RO_2, HO_2 and therefore SOA formation from the photooxidation of ethers, especially compared with H_2O_2 only experiments. Larger amounts of SOA (>2 $\mu g \cdot m^{-3}$) is formed during the oxidation of DEGEE, DEGBE and DEGME (Fig. 7.7a) than that formed during the oxidation of EGDEE and DPGBE (0.01~1$\mu g \cdot m^{-3}$). No significant correlations are observed between

SOA formation and kinetic reaction rate, final NO concentration and hydrocarbon consumption. This result suggests that less SOA mass is formed form ethers under NO only conditions compared with H_2O_2 only conditions since NO leads to higher RO_2+NO reaction and therefore lowers the overall RO_2+ HO_2 reaction which determines SOA formation. More important, the extent of inhibition impact of NO on SOA formation from ethers depends on molecular structure. It is noted that, under NO only condition, SOA formation remains significant from ethers with $–(OCH_2CH_2)_2–OH$. The higher abundance of m/z 73 and lower m/z 61 in SOA during the photooxidation of DEGEE under NO only condition (Fig. S7.2a, Table 7.3) compared with under H_2O_2 only conditions (Fig. 7.6a) highlights the greater importance of cyclization to SOA formation under NO only conditions. There is much less SOA formed under the NO only condition than H_2O_2 only condition during the oxidation of DPGBE, when $–CH_3$ is added to $–(OCH_2CH_2)_2–OH$ structure, and EGDEE without –OH in ether structure. This suggests that certain mechanisms, such as cyclization, associated with $–(OCH_2CH_2)_2$ – OH leads to the formation of low volatility products and protects the molecular from fragmentation during further oxidation. Insignificant SOA is formed during the photooxidation of 13D2P and 33D1P, which forms >20 $\mu g \cdot m^{-3}$ SOA under H_2O_2 only conditions. It is possibly due to cyclization being less favored during the oxidation of 13D2P and 33D1P (Section 7.3.3.1) and the higher extent of oxidation required for 13D2P and 33D1P to form SOA (Section 7.3.2.2 and 7.3.2.3) is limited by initial NO. Fig 7.7a suggests that SOA formation under low NO conditions relies more on $–(OCH_2CH_2)_2–OH$ structure than under H_2O_2 only conditions. NO decreases the extent of oxidation by reacting with peroxide radical and

hence SOA formation depends more on the cyclization pathway to protect the molecule from fragmentation during further oxidation.

7.3.4 The relationship between oxidation and SOA formation

SOA formation during the photooxidation of DEGEE under different oxidation conditions are studied (NO only, H_2O_2 only and H_2O_2-NO; Table 7.1, Fig. 7.7b). The two-product model (Odum, et al., 1996) is used to compare the SOA yield under similar mass loadings (Fig. S7.3). The SOA yield of DEGEE under different conditions shows a trend of $yield_{NO\ only} > yield_{H2O2} > yield_{H2O2\text{-}NO,}$ inversely correlating with ·OH concentration and extent of oxidation. Italso implies that less low volatility products is formed with the presence of H_2O_2 (Fig. S7.3, $\alpha_1=0$ in two product model fitting of SOA yield under DEGEE+ H_2O_2 and DEGEE+ H_2O_2-NO conditions). This suggests that further oxidation of ether forms more volatile compounds.

Chemical bulk compositions of SOA formed from DEGEE under different conditions show an oxidation trend of $OSc_{,NO\ only}$ (-0.82±0.20)< $OSc_{,H2O2}$ (-0.29±0.03)<$OSc_{,H2O2\text{-}NO}$ (-0.21±0.03). It is noted that SOA formation under NO only conditions is associated with a large change in H/C with only a slight change in O/C, indicating the importance of cyclization H loss (Fig. 7.8). A significant O/C increase with insignificant H/C decrease in SOA formed in presence of H_2O_2 relative to SOA formed under NO only condition. This suggests carbonyl formation (hydrogen loss and oxygen gain) is more important in the oxidation of ether with H_2O_2. Further, it indicates that the cyclization enhances SOA yield more than carbonyl formation since higher SOA yield is observed in NO only conditions

compared with SOA yield in presence of H_2O_2. SOA formed under NO-H_2O_2 condition leads to higher OS_c, H/C and O/C than that under H_2O_2 only conditions. This agrees with the finding that NO could enhance ·OH concentration (Chapter 2) and therefore enhance the overall extent of oxidation. The further oxidation and lower SOA yield under NO-H_2O_2 conditions than that under H_2O_2 only conditions confirm that further oxidation of ether lead to more volatile products. The SOA difference (insignificant) in f_{CO2}^+vs f_{C2H3O}^+ (Fig. S7.4) during ether oxidation under three different conditions agrees with the oxidation trend inferred from the elemental ratio trend.

The differences among SOA composition are further explored by comparing the representative peaks in the mass spectrum of HR-TOF-AMS (Table 7.3). Lower fraction of m/z 73 is observed in SOA formed in presence of H_2O_2 only than that under NO only condition. This suggests that the cyclization is less important to SOA formation in presence of H_2O_2 when the level of oxidation is higher than that under the NO only condition. Insignificant m/z 61(carbonyl fragment) and a small fraction of m/z 87(carbonyl fragment) is found in SOA formed in the absence of H_2O_2. This confirms that carbonyl formation is less favored under lower levels of oxidation. It is also found the SOA formed in presence of NO and H_2O_2 shows a combination of representative peaks under NO only and H_2O_2 only condition. The extent of oxidation under H_2O_2-NO condition is expected to be higher than that under H_2O_2 only conditions. The higher fraction of m/z 73 in SOA formed under H_2O_2-NO condition than that under H_2O_2 condition suggests that the contribution of cyclization to SOA formation dose not linearly decrease with the extent of oxidation. Further, it implies that NO determines the oxidation mechanism of DEGEE leading to the

formation of cyclic compounds.

7.4 Discussion

The oxidation mechanism of representative glycol ether (DEGEE) is proposed in Fig. S7.5. The volatilities of most compounds proposed are not sufficiently low to contribute to SOA formation (Table S7.2). Further oxidation, such as oligomerization, is expected to form compounds with sufficient low voaltiltiy to partition into aerosol phase. One possible oligomerization pathway is associated with carbonyl compounds, possibly by aldol condensation (Jang, et al., 2002; Tolocka, et al., 2004).

The formation of cyclic products during ether oxidation is demonstrated in this work. Cyclic products prevent the C–C and C–O from breaking during oxidation reducing fragmentation. Cyclization in ethers is determined by the presence of $–(OCH_2CH_2)_2–OH$ in ether precursor. The cyclization pathway is critically important to SOA formation when the level of oxidation is low such as under NO only conditions. Higher level of oxidation form higher SOA mass concentration while forming more fragmentation products leading to lower SOA yield. SOA yield increases with the fraction of cyclic compounds formed and decreases with the extent of oxidation during the photooxidation of ether. This suggests that the formation of cyclic structure is more important to SOA formation from ethers under ambient atmospheric conditions, which has a lower level of oxidation compared with chamber experiments. Therefore, the contribution of ethers with $–(OCH_2CH_2)_2–OH$ is much more important than ether without it.

The assumption that oxidized products have the same number of carbons as precursor is

not perfect due to the fragmentation and possibly oligomerization that occurs during the oxidation process. However, it dose minimize the discrepancy in elemental ratio resulting from the difference in oxygen to aliphatic carbon in the ether precursor. Therefore, to analyze SOA chemical composition on a precursor carbon number normalized basis (*O/M* and -Δ*(H/M)*) instead of a mole basis provides insigt to the oxidation potential of different compounds and the role of different functional group in SOA formation. The finding that O/M is approximately 4 in SOA formed from ethers studied is similar to the observation that O/R is ~4 in SOA formed from aromatic hydrocarbons (Chapter 5). The similarity in the oxidation of precursors to form SOA is likely to exist in other group of precursor species with similar functional group. This method relates the SOA chemical composition with precursor molecular structure, which may contribute to the estimation of SOA formation from known VOCs. It is valuable to apply the precursor structure based elemental ratio analysis method into the investigation of SOA formation from other groups of VOCs.

Summarily, the molecular structure is important to SOA formation from the photooxidation of ethers. The presence and location of –OH structure in ether determinates SOA formation from ethers. Cyclic products are formed in gas and particle phase during with the presence of –OH structure in ether. The structure, –(OCH_2CH_2) –OH, determines SOA formation from glycol ethers in presence of NO_X. Further oxidation of glycol ethers lowers SOA yields by producing more fragmental products

7.5 Atmospheric Implication

The oxidation of ether is a combination of carbonyl formation, cyclization and

fragmentation. Similar oxidation mechanisms are demonstrated among those ethers forming significant amounts of SOA. The molecular structure of ethers determine the branching ratio among carbonyl formation, cyclization and fragmentation. Cyclization is found to be an important mechanism during the oxidation of ethers and become critical to SOA formation when the oxidation level is more comparable to ambient. Cyclization is affected by the presence and location of –OH in the carbon bond of ethers and –$(OCH_2CH_2)_2$–OH structure is found to readily form cyclization products. Therefore, we consider DEGEE and DEGBE as two dominating ethers that contribute to SOA formation under atmospheric conditions. The total emissions are from DEGBE 2.04 TPD and DEGEE 1.23 TPD (Cocker, et al., 2014). It is estimated that the SOA formation from the two glycol ethers is 0.215 TPD in California State by assuming ambient organic concentration of ~10 $\mu g \cdot m^{-3}$ (Jimenez, et al., 2009) and predicting SOA yield based on two product model of DEGEE+NO (0.066). Mobile sources contribute to 85.3 TPD PM2.5 in California (California Air Resource Board) and thereby approximately 25.6 TPD assuming organic aerosol accounts for 30% of PM 2.5 (Jimenez, et al., 2009). Therefore, the contribution of glycol ethers to anthropogenic SOA is about 1% of that from mobile sources.

7.6 Reference

Aiken, A. C., DeCarlo, P. F. and Jimenez, J. L.: Elemental analysis of organic species with electron ionization high-resolution mass spectrometry, Anal. Chem., 79(21), 8350-8358, 2007.

Aiken, A. C., DeCarlo, P. F., Kroll, J. H., Worsnop, D. R., Huffman, J. A., Docherty, K. S., Ulbrich, I. M., Mohr, C., Kimmel, J. R., Sueper, D., Sun, Y., Zhang, Q., Trimborn, A., Northway, M., Ziemann, P. J., Canagaratna, M. R., Onasch, T. B., Alfarra, M. R., Prevot, A. S. H., Dommen, J., Duplissy, J., Metzger, A., Baltensperger, U. and Jimenez, J. H.: O/C and OM/OC ratios of primary, secondary, and ambient organic aerosols with high-resolution time-of-flight aerosol mass spectrometry, Environ. Sci. Technol., 42(12), 4478-4485, 2008.

Aschmann, S. M., and Atkinson, R.: Kinetics of the gas‐phase reactions of the OH radical with selected glycol ethers, glycols, and alcohols, Int. J. Chem. Kineti., 30, 533-540, 1998.

Aschmann, S. M., and Atkinson, R.: Products of the gas-phase reactions of the OH radical with n-butyl methyl ether and 2-isopropoxyethanol: Reactions of ROC(O)< radicals, Int. J. Chem. Kineti., 31, 501-513, 10.1002/(sici)1097-4601(1999)31:7<501::aid-kin5>3.0.co;2-h, 1999.

Canagaratna, M. R., Jayne, J. T., Jimenez, J. L., Allan, J. D., Alfarra, M. R., Zhang, Q., Onasch, T. B., Drewnick, F., Coe, H., Middlebrook, A., Delia, A., Williams, L. R., Trimborn, A. M., Northway, M. J., DeCarlo, P. F., Kolb, C. E., Davidovits, P. and Worsnop D. R.: Chemical and microphysical characterization of ambient aerosols with the aerodyne aerosol mass spectrometer, Mass. Spectrom. Rev., 26(2), 185-222, 2007.

California Air Resource Board, Almanac Emission Projection Data 2012 Estimated Annual Average Emissions, http://www.arb.ca.gov/app/emsinv/2013/emseic1_query.php?F_DIV=-4&F_YR=2012&F_SEASON=A&SP=2013&F_AREA=CA.

Chew, A. A., Atkinson, R., and Aschmann, S. M.: Kinetics of the gas-phase reactions of NO_3 radicals with a series of alcohols, glycol ethers, ethers and chloroalkenes, J. Chem. Soc. Faraday T., 94, 1083-1089, 1998.

Chhabra, P. S., Ng, N. L., Canagaratna, M. R., Corrigan, A. L., Russell, L. M., Worsnop, D. R., Flagan, R. C. and Seinfeld, J. H.: Elemental composition and oxidation of chamber organic aerosol, Atmos. Chem. Phys., 11(17), 8827-8845, 2011.

Choi, H., Schmidbauer, N., Spengler, J., and Bornehag, C.-G.: Sources of propylene glycol and glycol ethers in air at home, Int. J. Environ. Res. Public Health, 7, 4213-4237, 2010.

Cocker III, D. R.., Flagan, R. C. and Seinfeld, J. H.: State-of-the-art chamber facility for studying atmospheric aerosol chemistry, Environ. Sci. Technol., 35(12), 2594-2601, 2001.

Collins, E., Sidebottom, H. W., Wenger, J. C., Calvé, S. L., Mellouki, A., LeBras, G., Villenave, E., and Wirtz, K.: The influence of reaction conditions on the photooxidation of diisopropyl ether, J. Photoch. Photobio. A., 176, 86-97, 2005.

Cooper, S. D., Raymer, J. H., Pellizzari, E., and Thomas, K. W.: The identification of polar organic compounds found in consumer products and their toxicological properties, J. Expo. Anal. Env. Epid., 5, 57-75, 1995.

Cocker III, D. R., Li, L., Price, J. D., Kacarab, M., Chen, C-L.: Review of VOC Emissions Inventory for consumer products and architectural coatings for potential alternative fate and availability corrections, Consumer Specialty Products Association Report, 2014.

DeCarlo, P. F., Kimmel, J. R., Trimborn, A., Northway, M. J., Jayne, J. T., Aiken, A. C., Gonin, M., Fuhrer, K., Horvath, T., Docherty, K. S., Worsnop, D. R. and Jimenez, J. L.: Field-deployable, high-resolution, time-of-flight aerosol mass spectrometer. Anal. Chem., 78(24), 8281-8289, 2006.

Eberhard, J., MüLler, C., Stocker, D. W., and Kerr, J. A.: The photo-oxidation of diethyl ether in smog chamber experiments simulating tropospheric conditions: Product studies and proposed mechanism, Int. J. Chem. Kineti., 25, 639-649, 1993.

Environmental Protection Agency United States: Toxics Release Inventory-List of Toxic Chemicals within the Glycol Ethers Category, 2000.

Espada, C., and Shepson, P. B.: The production of organic nitrates from atmospheric oxidation of ethers and glycol ethers, Int. J. Chem. Kineti., 37, 686-699, 2005.

Farina, S. C., Adams, P. J., and Pandis, S. N.: Modeling global secondary organic aerosol formation and processing with the volatility basis set: Implications for anthropogenic secondary organic aerosol. J. Geophys. Res.-Atmos., 115(D9), 2010.

Fromme, H., Nitschke, L., Boehmer, S., Kiranoglu, M., and Göen, T.: Exposure of German residents to ethylene and propylene glycol ethers in general and after cleaning scenarios, Chemosphere, 90, 2714-2721, 2013.

Geiger, H., and Becker, K.: Degradation mechanisms of dimethoxymethane and dimethoxyethane in the presence of NOx, Atmos. Environ., 33, 2883-2891, 1999.

Gibson, W., Keller, P., Foltz, D., and Harvey, G.: Diethylene glycol mono butyl ether concentrations in room air from application of cleaner formulations to hard surfaces, J. Expo. Anal. Env. Epid., 1, 369-383, 1991.

Heald, C. L., Kroll, J. H., Jimenez, J. L., Docherty, K. S., DeCarlo, P. F., Aiken, A. C., Chen, Q., Martin, S. T., Farmer, D. K., and Artaxo, P.: A simplified description of the evolution of organic aerosol composition in the atmosphere, Geophys. Res. Lett, 37(8), 2010.

Jang, M., Czoschke, N. M., Lee, S., and Kamens, R. M.: Heterogeneous atmospheric aerosol production by acid-catalyzed particle-phase reactions, Science, 298(5594), 814-817, 2002.

Jenkin, M. E., Hayman, G. D., Wallington, T. J., Hurley, M. D., Ball, J. C., Nielsen, O. J., and Ellermann, T.: Kinetic and mechanistic study of the self-reaction of methoxymethylperoxy radicals at room temperature, J. Phys. Chem., 97, 11712-11723, 1993.

Jimenez, J. L., Canagaratna, M. R., Donahue, N. M., Prevot, A. S. H., Zhang, Q., Kroll, J. H., DeCarlo, P. F., Allan, J. D., Coe, H., Ng, N. L., Aiken, A. C., Docherty, K. S., Ulbrich, I. M., Grieshop, A. P., Robinson, A. L., Duplissy, J., Smith, J. D., Wilson, K. R., Lanz, V. A., Hueglin, C., Sun, Y. L., Tian, J., Laaksonen, A., Raatikainen, T., Rautiainen, J., Vaattovaara, P., Ehn, M., Kulmala, M., Tomlinson, J. M., Collins, D. R., Cubison, M. J., Dunlea1, E., J., Huffman, J. A., Onasch, T. B., Alfarra, M. R., Williams, P. I., Bower, K., Kondo, Y., Schneider, J., Drewnick, F., Borrmann, S., Weimer, S.,, Demerjian, K., Salcedo, D., Cottrell, L., Griffin, R., Takami, A., Miyoshi, T., Hatakeyama, S., Shimono, A., Sun, J. Y., Zhang, Y. M., Dzepina, K., Kimmel, J. R., Sueper, D., J. Jayne, T., Herndon, S. C., Trimborn, A. M., Williams, L. R., Wood, E. C., Middlebrook, A. M., Kolb C. E., Baltensperger, U. and Worsnop D. R.: Evolution of organic aerosols in the atmosphere, Science, 326(5959), 1525-1529, 2009.

Johnson, D., and Andino, J. M.: Laboratory studies of the ·OH-initiated photooxidation of ethyl-n-butyl ether and di-n-butyl ether, Int. J. Chem. Kineti., 33, 328-341, 2001.

Malanca, F. E., Fraire, J. C., and Argüello, G. A.: Kinetics and reaction mechanism in the oxidation of ethyl formate in the presence of NO_2: Atmospheric implications, J. Photoch. Photobio. A., 204, 75-81, 2009.

Mellouki, A., Teton, S., and Le Bras, G.: Kinetics of OH radical reactions with a series of ethers, Int. J. Chem. Kineti., 27, 791-805, 1995.

Mellouki, A., Le Bras, G., and Sidebottom, H.: Kinetics and mechanisms of the oxidation of oxygenated organic compounds in the gas phase, Chem. Rev., 103, 5077-5096, 2003.

Nazaroff, W. W., and Weschler, C. J.: Cleaning products and air fresheners: exposure to primary and secondary air pollutants, Atmos. Environ., 38, 2841-2865, 2004.

Odum, J. R., Hoffmann, T., Bowman, F., Collins, D., Flagan, R. C., and Seinfeld, J. H.: Gas/particle partitioning and secondary organic aerosol yields, Environ. Sci. Technol., 30, 2580-2585, 1996.

Orlando, J. J.: The atmospheric oxidation of diethyl ether: chemistry of the C_2H_5–O–CH ($O^{\cdot}$) CH_3 radical between 218 and 335 K, Phys. Chem. Chem. Phys., 9, 4189-4199, 2007.

Pankow, J. F., and Asher, W. E.: SIMPOL. 1: a simple group contribution method for predicting vapor pressures and enthalpies of vaporization of multifunctional organic compounds, Atmos. Chem. Phys., 8, 2773-2796, 2008.

Platz, J., Sehested, J., Nielsen, O., and Wallington, T.: Atmospheric chemistry of trimethoxymethane, $(CH_3O)_3CH$; Laboratory studies, J. Phys. Chem. A., 103, 2632-2640, 1999.

Porter, E., Wenger, J., Treacy, J., Sidebottom, H., Mellouki, A., Téton, S., and LeBras, G.: Kinetic studies on the reactions of hydroxyl radicals with diethers and hydroxyethers, J. Phys. Chem. A.,, 101, 5770-5775, 1997.

Pye, H. O., and Seinfeld, J. H.: A global perspective on aerosol from low-volatility organic compounds, Atmos. Chem. Phys., 10, 4377-4401, 2010.

Sehested, J., Møgelberg, T., Wallington, T., Kaiser, E., and Nielsen, O.: Dimethyl ether oxidation: Kinetics and mechanism of the CH_3OCH_2+ O_2 reaction at 296 K and 0.38-940 torr total pressure, J. Phys. Chem., 100, 17218-17225, 1996.

Singer, B. C., Destaillats, H., Hodgson, A. T., and Nazaroff, W. W.: Cleaning products and air fresheners: emissions and resulting concentrations of glycol ethers and terpenoids, Indoor Air, 16, 179-191, 2006.

Španěl, P., Ji, Y., and Smith, D.: SIFT studies of the reactions of H_3O^+, NO^+ and O_2^+ with a series of aldehydes and ketones, Int. J. Mass. Spectrom., 165, 25-37, 1997.

Stemmler, K., Mengon, W., and Kerr, J. A.: OH radical initiated photooxidation of 2-ethoxyethanol under laboratory conditions related to the troposphere: Product studies and proposed mechanism, Environ. Sci. Technol., 30, 3385-3391, 1996.

Tolocka, M. P., Jang, M., Ginter, J. M., Cox, F. J., Kamens, R. M., and Johnston, M. V.: Formation of oligomers in secondary organic aerosol, Environ. Sci. Technol., 38, 1428-1434, 2004.

Tommaso, S. D., Rotureau, P., Crescenzi, O., and Adamo, C.: Oxidation mechanism of diethyl ether: a complex process for a simple molecule, Phys. Chem. Chem. Phys., 13, 14636-14645, 2011.

Tuazon, E. C., Carter, W. P., Aschmann, S. M., and Atkinson, R.: Products of the gas‐phase reaction of methyl tert‐butyl ether with the OH radical in the presence of NOx, Int. J. Chem. Kineti., 23, 1003-1015, 1991.

Tuazon, E. C., Aschmann, S. M., and Atkinson, R.: Products of the gas-phase reactions of the OH radical with 1-methoxy-2-propanol and 2-butoxyethanol, Environ. Sci. Technol., 32, 3336-3345, 1998.

Võ, U.-U. T., and Morris, M. P.: Nonvolatile, semivolatile, or volatile: Redefining volatile for volatile organic compounds, J. Air. Waste. Manage., 64, 661-669, 2014.

Wallington, T. J., and Japar, S. M.: Atmospheric chemistry of diethyl ether and ethyl tert-butyl ether, Environ. Sci. Technol., 25, 410-415, 1991.

Wenger, J., Porter, E., Collins, E., Treacy, J., and Sidebottom, H.: Mechanisms for the chlorine atom initiated oxidation of dimethoxymethane and 1, 2-dimethoxyethane in the presence of NO_x, Chemosphere, 38, 1197-1204, 1999.

Wieslander, G., and Norbäck, D.: A field study on clinical signs and symptoms in cleaners at floor polish removal and application in a Swedish hospital, Int. Arch. Occ. Env. Hea., 83, 585-591, 2010a.

Wieslander, G., and Norbäck, D.: Ocular symptoms, tear film stability, nasal patency, and biomarkers in nasal lavage in indoor painters in relation to emissions from water-based paint, Int. Arch. Occ. Env. Hea., 83, 733-741, 2010b.

Zhu, J., Cao, X.-L., and Beauchamp, R.: Determination of 2-butoxyethanol emissions from selected consumer products and its application in assessment of inhalation exposure associated with cleaning tasks, Environ. Int., 26, 589-597, 2001.

7.7 Tables and Figures

Table 7.1 Experimental Conditions

Compound[1]	Run ID	$Ether_i$[2] ppb	NO_i ppb	$NO_{x,i}$ ppb	M_0 $\mu g \cdot m^{-3}$	Ether reacted %	Yield
			H_2O_2 only[3]				
DEGEE	1986B	40	-	-	33.0	97.88%	0.1090
DEGEE	1991A	40	-	-	48.3	92.87%	0.1737
DEGEE	2058A	80	-	-	18.9	77.16%	0.0384
DEGBE	1999A	40	-	-	154	95.51%	0.1815*
DEGBE	2063B	80	-	-	177	100.00%	0.3545
DEGME	2148A	160			2.10	60.00%	0.0045
EGDEE	1991B	40	-	-	7.50	100.00%	0.0388
EGDEE	2007A	80	-	-	10.3	100.00%	0.0268
EGDEE	2148B	80	-	-	4.40	91.00%	0.0124
EGDEE	2154A	160	-	-	13.5	85.25%	0.0206
1,2-Dimethoxyethane	1993B	160	-	-	0.10	82.15%	0.0001
12M2MP	2007B	80	-	-	2.30	100.00%	0.0065
DEGDME	2048A	80	-	-	0.10	100.00%	0.0003
DPGBE	2051B	80	-	-	77.7	100.00%	0.1274
DPGBE	2152A	160	-	-	131	81.53%	0.1303
13D2P	2123A	80	-	-	29.2	100.00%	0.0606
33D1P	2124A	80	-	-	38.9	100.00%	0.0808
			Low NO				
DEGEE	1923B	40	20.9	22.4	9.10	72.40%	0.0663
DEGEE	1985A	80	23.5	24.4	2.70	50.32%	0.0105
DEGEE	1993A	40	25.1	26.4	3.90	57.73%	0.0246
DEGBE	1925B	40	22.1	22.5	12.6	79.09%	0.0607
DEGBE	1926A	80	22.6	23.3	7.70	48.67%	0.0302
DEGBE	1986A	40	26.0	26.8	2.00	55.47%	0.0224
DEGME	1925A	80	22.0	22.6	12.4	99.86%	0.0317
EGDEE	1923A	80	21.2	22.6	0.60	62.31%	0.0024
EGDEE	2154B	160	14.9	1.73	0.00	N/A	0.0000
1,2-Dimethoxyethane	1926B	160	22.8	23.2	0.00	43.75%	0.0000
DEGDME	1974B	80	22.4	25.8	0.00	37.50%	0.0000
DPGBE	1985B	80	23.8	24.6	1.0	50.00%	0.0031

DPGBE	2055A	40	20.8	21.6	0.0	N/A	0.0000
DPGBE	2152B	160	15.4	1.12	0.0	N/A	0.0000
12M2MP	1999B	80	23.7	24.9	0.0	44.13%	0.0001
13D2P	2123B	80	17.0	17.3	0.0	N/A	0.0000
33D1P	2124B	80	21.1	22.0	0.0	N/A	0.0000
			H_2O_2[3]+NO				
DEGEE	2058B	80	9.77	10.3	44.3	100.00%	0.0695
DEGEE	2059A	80	25.8	27.1	39.9	100.00%	0.0528
DEGEE	2059B	80	41.6	43.3	26.8	100.00%	0.0355
DEGBE	2063A	80	27.1	28.5	151.3	92.88%	0.3261

Note: 1- DEGEE: Diethylene glycol ethyl ether; DEGBE: Diethylene glycol butyl ether; DEGME: Diethylene glycol methyl ether; EGDEE: Ethylene glycol diethyl ether；12M2MP: 1-(2-Methoxyethoxy)-2-methyl-2-propanol; DEGDME: Diethylene glycol dimethyl ether; DPGBE: Di(propylene glycol) butyl ether; 13D2P: 1,3-Diethoxy-2-propanol; 33D1P: 3,3-Diethoxy-1-propanol; 2-Initial target ether concentration; 3-H_2O_2 and H_2O_2+NO_x experiment all injected 1ppm H_2O_2; N/A: data not available. *Ehter concentration is based on measurement.

Table 7.2 Representative particle (HR-TOF-AMS) and gas (SIFT-MS) phase peaks in SOA formed from ether photooxidation

	Particle phase		Gas phase				
m/z	73	47/61/89	75	73	104	M_p-2	M_p+29
	Fragment		SIFT Ion Source				
	$C_3H_5O_2^+$	$C_nH_{2n+1}O_2^+$	(H_3O^+)	(NO^+)	(NO^+)	(H_3O^+&NO^+)	(NO^+)
DEGME	✓	✓	✓	✓	✓	-	✓
DEGEE	✓	✓	✓	✓	✓	✓	✓
DEGBE	✓	✓	✓	✓	✓	✓	✓
EGDEE	-	✓	✓	*	✓	-	-
DPGBE	-	✓	✓	*	-	✓	-
13D2P	-	✓	✓	*	✓	✓	-
33D1P	-	✓	*	✓	-	✓	*

Note: ✓ : newly formed during the oxidation of ethers; * : Covered by high precursor peaks; - :Not observed. M_p: major m/z peaks from precursor

Table 7.3 Representative HR-TOF-AMS peaks from DEGEE oxidation under different conditions

Oxidation Condition	m/z 73 $C_3H_5O_2^+$	m/z 61 $C_2H_3O_2^+$	m/z 87 $C_4H_7O_2^+$
H_2O_2	1.18%	2.47%	-
NO	4.7%	-	0.80%
H_2O_2 + NO	2.44%	2.31%	0.84%

Note: -: not significant

Diethylene glycol ethyl ether (DEGEE)

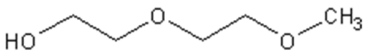

Diethylene glycol methyl ether (DEGME)

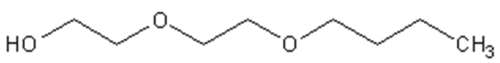

Diethylene glycol butyl ether (DEGBE)

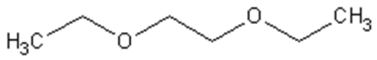

Ethylene glycol diethyl ether (EGDEE)

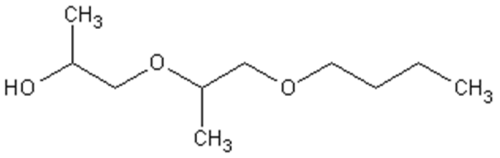

Di(propylene glycol) butyl ether (DPGBE)

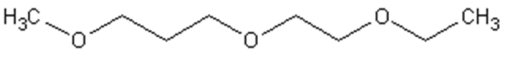

Diethylene glycol dimethyl ether (DEGDME)

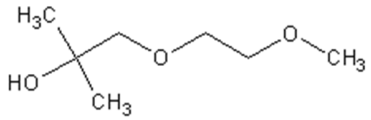

1-(2-Methoxyethoxy)-2-metyhl-2-propanol (12M2MP)

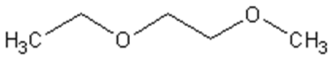

1, 2-Dimethoxyethane

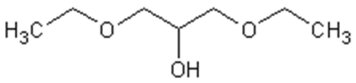

1,3-Diethoxy-2-propanol (13D2P)

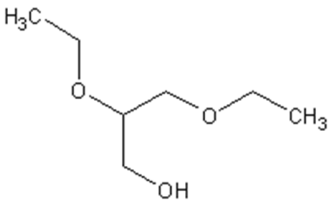

3,3-Diethoxy-1-propanol (33D1P)

Figure 7.1 Molecular structure of ethers investigated

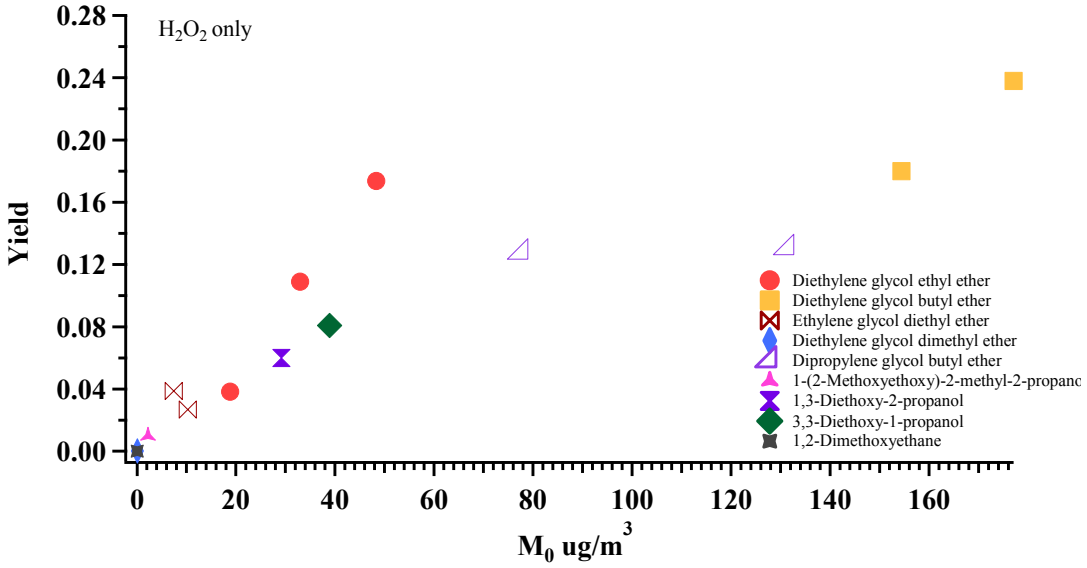

Figure 7.2 SOA yield from glycol ethers and relative ethers in absence of NO_x (Diethylene glycol concentration is based on measurement).

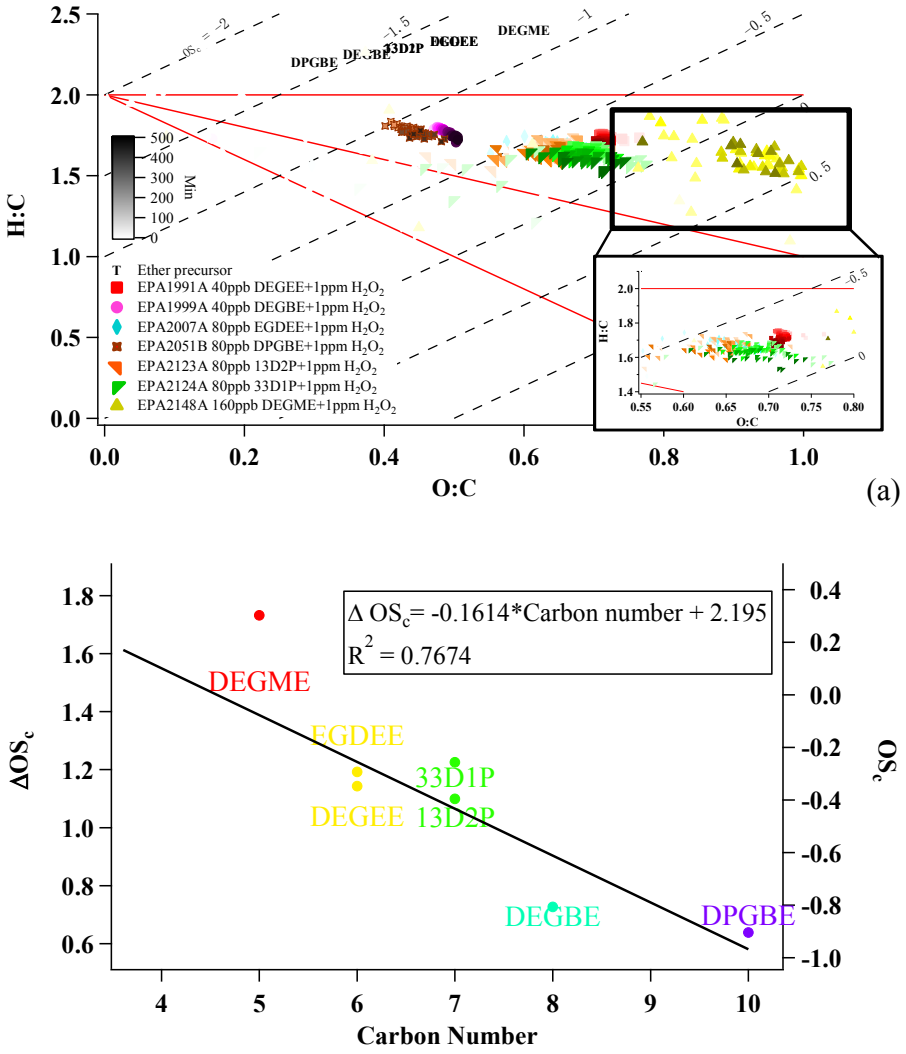

Figure 7.3 Elemental ratios of SOA formed from glycol ethers and relative ethers in absence of NO_x: a) H/C vs O/C (colored by photooxidation time, ether precursor location is marked by specie name in black text); b) OS_c vs. Carbon Number and OS_c vs. Carbon Number (text-OS_c, Solid cycle OS_c; colored by carbon number, black line is a linear fitting curve for OS_c and carbon number relationship).

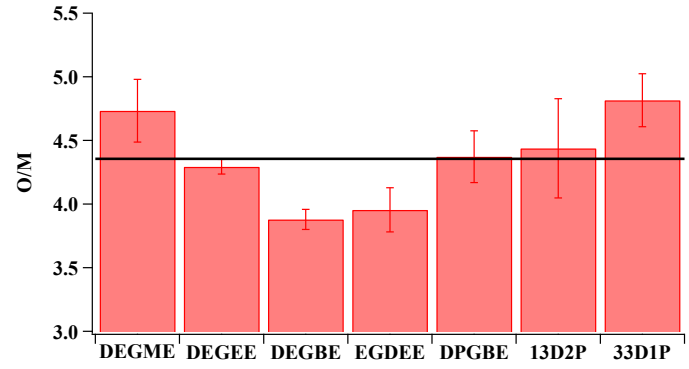

(a)

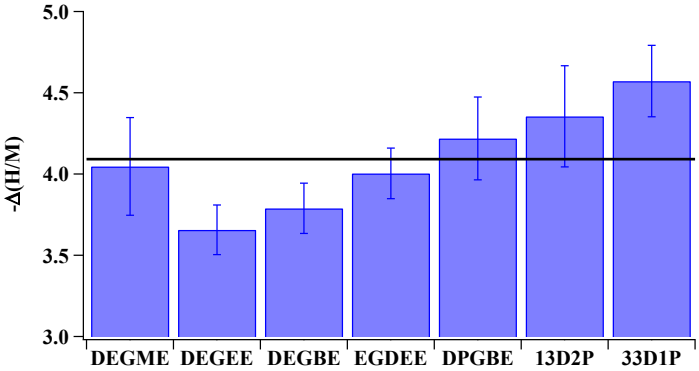

(b)

Figure 7.4Molecular based chemical composition of SOA formed during the oxidation of glycol ethers and relative ethers in absence of NO_x: a) O/M; b) (H/M). Horizontal black lines are average O/M and –Delta(H/M) of SOA formed from ethers listed in graphs.

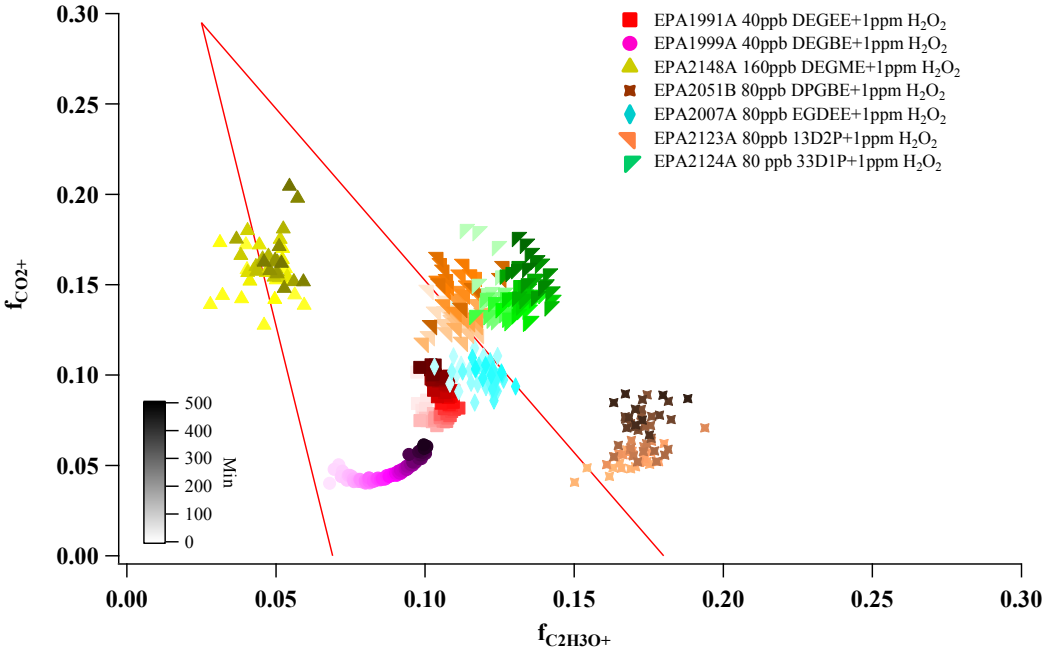

Figure 7.5. f_{CO2}^{+}vs f_{C2H3O}^{+} of SOA formed from glycol ethers and relative ethers in absence of NO_x (colored from light to dark by photooxidation time)

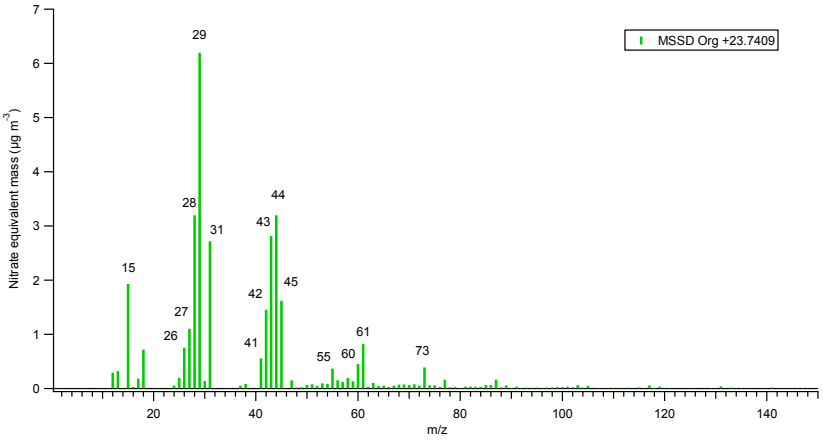

(a)

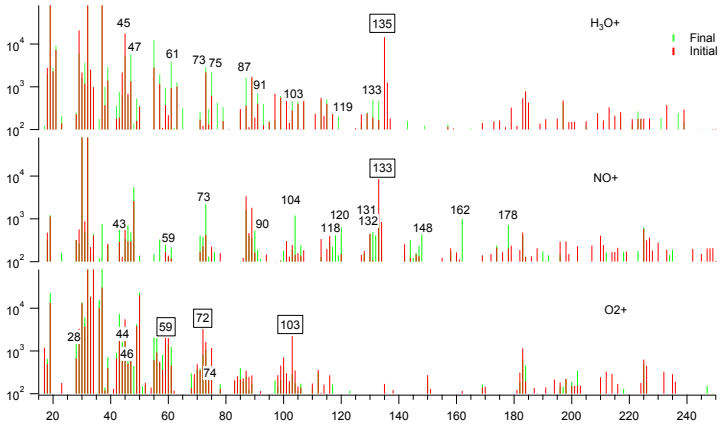

(b)

Figure 7.6 Particle phase (a) and gas phase (b) mass spectrum during the phtooxidaiotn of DEGEE in absence of NO_x (1991A). Top, middle and bottom panel in (b) stands for mass spectrum ionized by H_3O^+, NO^+ and O_2^+ correspondingly. (Final mass spectrum is showed as green bars underneath initial mass spectrum showed as red bas. The boxed m/z is the major peaks in ether precursors.)

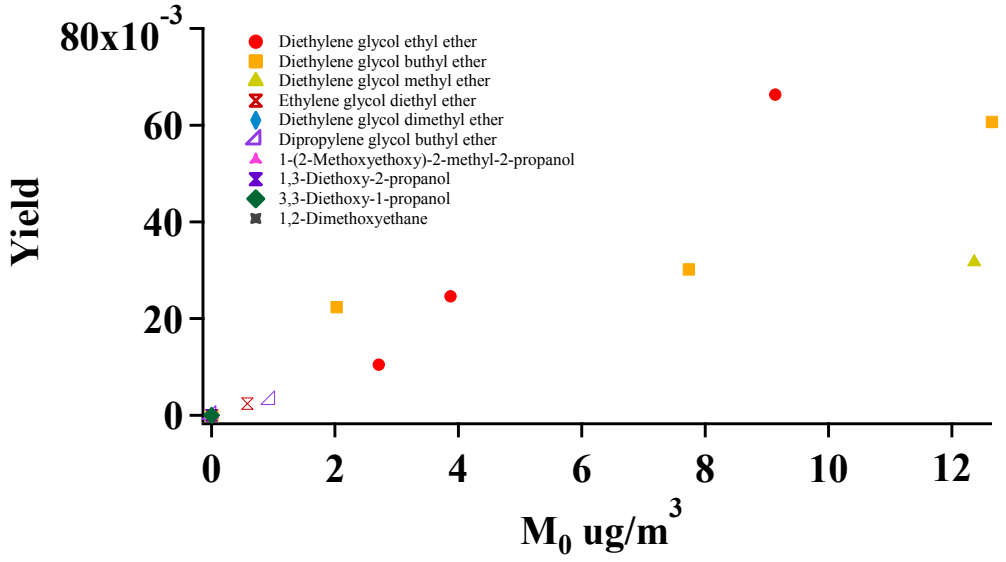

(a)

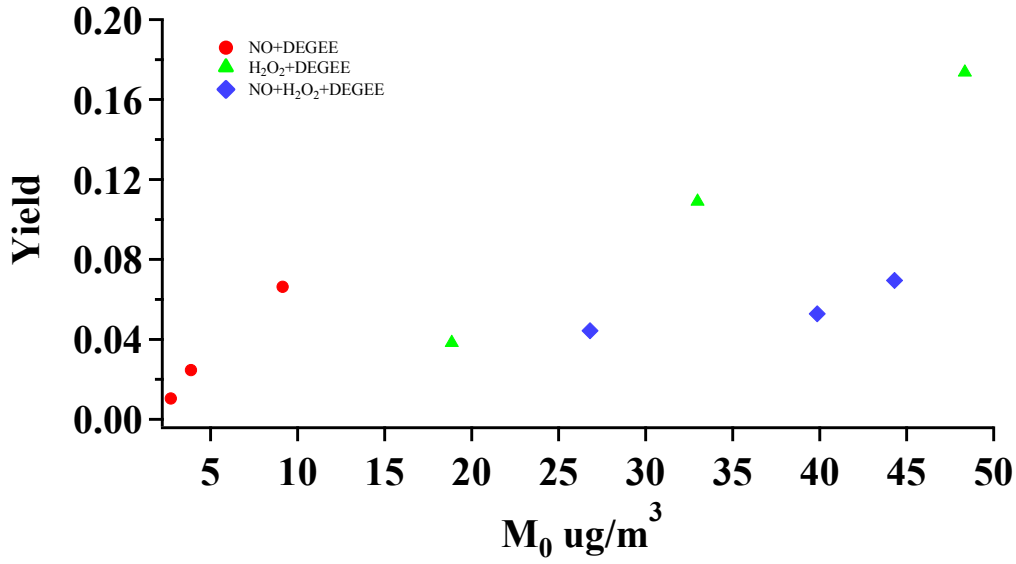

Figure 7.7 Comparison of SOA yield during the photooxidation of a) ethers under low NO_x conditions b) from DEGEE under different reactivity.

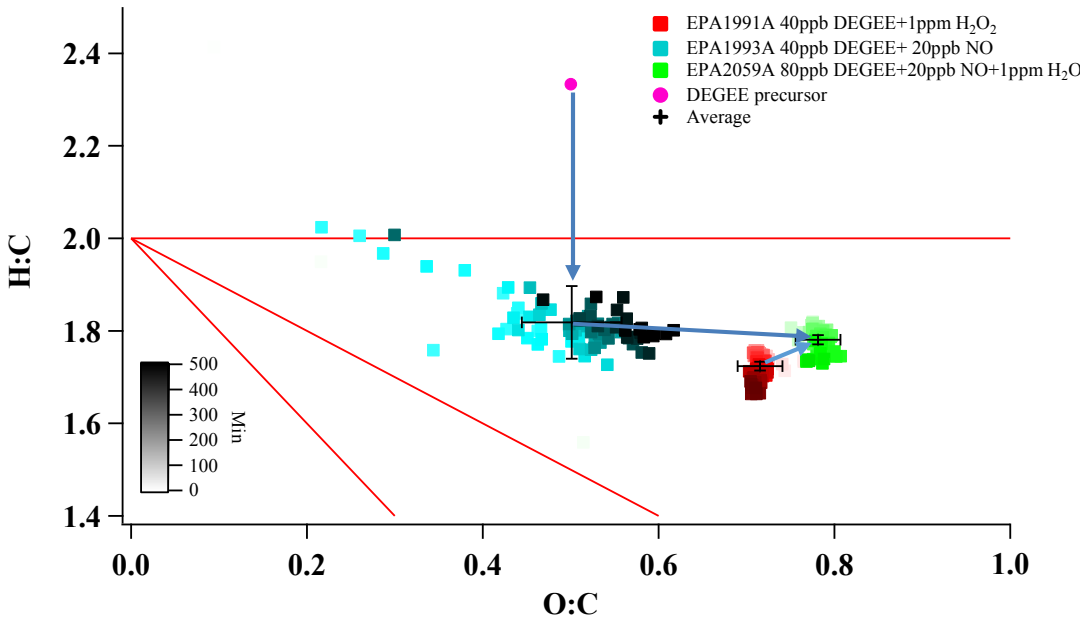

Figure 7.8 H/C vs O/C of SOA formed from DEGEE under different reactivity

8. Summary of Dissertation

This study provides insights into the prediction of SOA formation from anthropogenic VOCs. In this work, the importance of molecular structure, NO_x missing ratios and OH exposure to SOA formation is emphasized. New approaches and methods are developed in this study to improve the understanding of SOA formation. This work starts from laboratory chamber work and is further polished by novel analysis approaches. Important SOA formation mechanisms are proposed, especially when new methods are applied. This work is based on but not limited to the selected anthropogenic precursors. The ultimate goal of this work is to improve model predictions through improved mechanistic understandings. Further studies are recommended to generaize the approaches and methods provided in this work to additional SOA precursors.

Chapter 2 presents instantaneous NO effects on SOA formation from m-xylene under different atmospheric activities. $[HO_2\cdot]/[RO_2\cdot]$ shows a strong correlation with SOA yields in addition to $[\cdot OH]/[HO_2\cdot]$, $[\cdot OH]$, $[HO_2\cdot]$ and $[RO_2\cdot]$. A two-edged NO effect on SOA formation is found in this study indicating that NO could promote SOA formation from $RO_2\cdot$ and $HO_2\cdot$ at low concentration (<5 ppb) with sufficient hydrocarbon (HC/NO > 400) present. Further experiments and analyses are needed to more precisely define the boundary condition for NO promotion of SOA formation from other hydrocarbon precursors.

Chapter 3 reveals the role of methyl group number on SOA formation from aromatic hydrocarbons photooxidation under atmospherically relevant NO_x conditions. A

generally decreasing trend is found in the SOA mass yield and the carbon-number averaged oxidation level with increasing number of methyl groups. SOA physical properties agree with yield and oxidation results. The proposed methyl group dilution effect is then applied successfully to the predict SOA elemental ratio. This chapter demonstrates that the addition of methyl group substitutes to aromatic precursors decreases the oxidation of aromatic hydrocarbon to less volatile compounds.

Chapter 4 probes the impact of alkyl substitute number, location, carbon chain length and branching structure on SOA formation from aromatic hydrocarbons under atmospherically relevant NO_x conditions. The oxidation of aromatic hydrocarbons is promoted in aromatics with ortho position alkyl substitutes and suppressed in aromatics with para position alkyl substitutes. Meta position alkyl substitutes on aromatic ring lead to a lower extend of aromatic hydrocarbon oxidation since meta alkyl substitutes are more readily participate into aerosol phase products than ortho and para.

Chapter 5 generalized the SOA formation form aromatic hydrocarbons by developing new data analysis approaches. The ring normalized SOA yield analyzes SOA yield data on a mole basis or functional group (aromatic ring) basis of SOA precursors, instead of mass basis. Ring normalized SOA yield of all aromatic hydrocarbons is similar to SOA mass based yield of benzene. A similar amount of oxygen added per aromatic precursor ring for all aromatic hydrocarbons studied. This chapter indicates that the aromatic ring structure is more important than alkyl substitute to aromatic hydrocarbon oxidation.

Chapter 6 provides the reliable evidence for the difference in oxidation between alkyl substitute and aromatic ring carbon during the photooxidation of aromatic hydrocarbons. Methyl carbon is much less oxidized than aromatic ring carbon observed in the particle phase from the photooxidation of xylenes. Methyl carbon contributes less to the particle phase products than gas phase products according to the decrease in $^{13}C/^{12}C$ from ^{13}C labeled SOA precursor formula to SOA composition and corresponding mass balance. Therefore, it is confirmed that methyl group in xylenes exert little impact on SOA formation.

Chapter 7 discussed the contribution of new anthropogenic SOA precursors, glycol ethers, to global SOA formation. The relationship between SOA yield and molecular structure is discussed. Detailed products are identified by using gas phase and particle phase mass spectrometry (SIFT-MS and HR-TOF-AMS). Cyclization associated with –OH is found to be the most significant parmaters associated wtih SOA formation from glycol ethers.